JOINT TRANSPORTATION
RESEARCH PROGRAM
INDIANA DEPARTMENT OF TRANSPORTATION
AND PURDUE UNIVERSITY

CPT-Based Geotechnical Design Manual, Volume I: CPT Interpretation—Estimation of Soil Properties

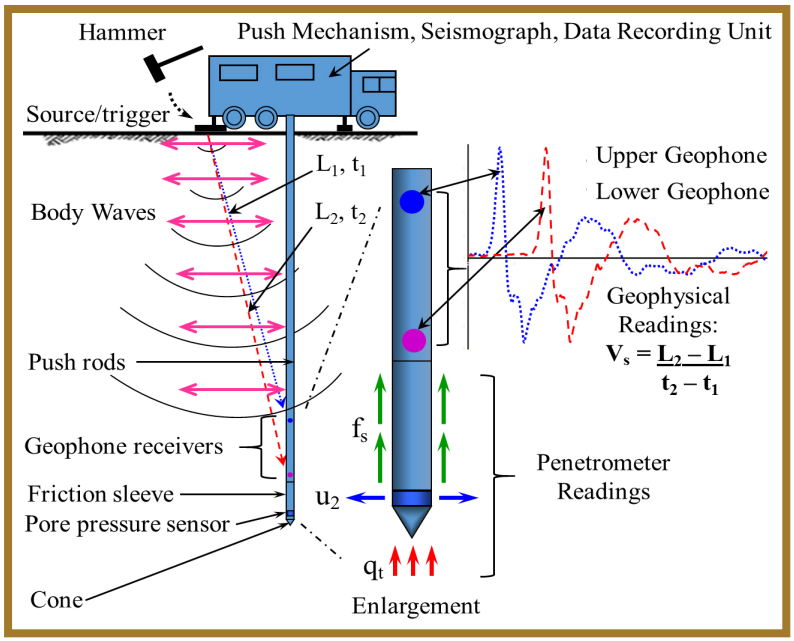

Fawad Niazi

SPR-4108 • Report Number: FHWA/IN/JTRP-2021/22 • DOI: 10.5703/1288284317346

RECOMMENDED CITATION

Niazi, F. (2021). *CPT-based geotechnical design manual, Volume 1: CPT interpretation—Estimation of soil properties* (Joint Transportation Research Program Publication No. FHWA/IN/JTRP-2021/22). West Lafayette, IN: Purdue University. https://doi.org/10.5703/1288284317346

AUTHORS

Fawad Niazi, PhD
Assistant Professor of Civil Engineering
Department of Civil and Mechanical Engineering
Purdue University Fort Wayne
(260) 481-0324
niazif@pfw.edu
Corresponding Author

JOINT TRANSPORTATION RESEARCH PROGRAM

The Joint Transportation Research Program serves as a vehicle for INDOT collaboration with higher education institutions and industry in Indiana to facilitate innovation that results in continuous improvement in the planning, design, construction, operation, management and economic efficiency of the Indiana transportation infrastructure. https://engineering.purdue.edu/JTRP/index_html

Published reports of the Joint Transportation Research Program are available at http://docs.lib.purdue.edu/jtrp/.

NOTICE

COVER IMAGE

The cover image was adapted from the following sources.

Mayne, P. W. (2007). *Cone penetration testing–A synthesis of highway practice* (NCHRP Synthesis 368). Transportation Research Board.

Niazi, F. S. (2014). *Static axial pile foundation response using seismic piezocone data* [Doctoral dissertation, Georgia Institute of Technology].

TECHNICAL REPORT DOCUMENTATION PAGE

1. Report No. FHWA/IN/JTRP-2021/22	**2. Government Accession No.**	**3. Recipient's Catalog No.**
4. Title and Subtitle CPT-Based Geotechnical Design Manual, Volume 1: CPT Interpretation—Estimation of Soil Properties		**5. Report Date** June 2021 **6. Performing Organization Code**
7. Author(s) Fawad Niazi		**8. Performing Organization Report No.** FHWA/IN/JTRP-2021/22
9. Performing Organization Name and Address Joint Transportation Research Program Hall for Discovery and Learning Research (DLR), Suite 204 207 S. Martin Jischke Drive West Lafayette, IN 47907		**10. Work Unit No.** **11. Contract or Grant No.** SPR-4108
12. Sponsoring Agency Name and Address Indiana Department of Transportation (SPR) State Office Building 100 North Senate Avenue Indianapolis, IN 46204		**13. Type of Report and Period Covered** Final Report **14. Sponsoring Agency Code**

15. Supplementary Notes

Conducted in cooperation with the U.S. Department of Transportation, Federal Highway Administration.

16. Abstract

This manual provides guidance on how to use the cone penetration test (CPT) for site investigation and foundation design. The manual has been organized into three volumes. Volume 1 covers the execution of CPT-based site investigations and presents a comprehensive literature review of CPT-based soil behavior type (SBT) charts and estimation of soil variables from CPT results. Volume 2 covers the methods and equations needed for CPT data interpretation and foundation design in different soil types, while Volume 3 includes several example problems (based on instrumented case histories) with detailed, step-by-step calculations to demonstrate the application of the design methods. The methods included in the manual are current, reliable, and demonstrably the best available for Indiana geology based on extensive CPT research carried out during the past two decades. The design of shallow and pile foundations in the manual is based on the load and resistance factor design (LRFD) framework. The manual also indicates areas of low reliability and limited knowledge, which can be used as indicators for future research.

17. Key Words cone penetration test, soil behavior type, shallow foundation, pile foundation, load and resistance factor design	**18. Distribution Statement** No restrictions. This document is available through the National Technical Information Service, Springfield, VA 22161.

19. Security Classif. (of this report) Unclassified	**20. Security Classif. (of this page)** Unclassified	**21. No. of Pages** 195 including appendices	**22. Price**

Form DOT F 1700.7 (8-72) Reproduction of completed page authorized

EXECUTIVE SUMMARY

Introduction

This manual provides guidance on how to use the cone penetration test (CPT) for site investigation and foundation design. The manual has been organized into three volumes.

Volume I covers the execution of CPT-based site investigations, a comprehensive literature review of CPT-based soil behavior type (SBT) charts, and several correlations for estimation of a soil variable of interest from CPT results. The volume has been organized into two chapters. Chapter 1 details the components of a CPT system, types of CPT equipment, testing procedures and precautions, maintenance of CPT equipment, and planning and execution of a CPT-based site investigation. Chapter 2 presents a compilation of correlations for the estimation of a soil variable of interest from CPT data, and also presents a comprehensive review of the chronological development of the SBT classification systems that have advanced during the past 55 years of CPT history.

Volume II covers the methods and equations needed for CPT data interpretation and foundation design in different soil types. The volume has been organized into four chapters. Chapter 1 provides an introduction to the manual. Chapter 2 presents an overview of Indiana geology, the typical CPT and soil profiles found in Indiana, and the influence of these profiles on CPT-based site variability assessment. Chapter 3 details the methods for the estimation of limit bearing capacity and settlement of shallow foundations from CPT data. Chapter 4 describes the methods for estimation of limit unit shaft resistance and ultimate unit base resistance of displacement, non-displacement, and partial displacement piles and pile groups from CPT data. The design of both shallow and pile foundations is based on the load and resistance factor design (LRFD) framework.

Volume III contains several example problems (based on case histories) with detailed, step-by-step calculations to demonstrate the application of the CPT-based foundation design methods covered in Volume II. The volume has been organized into three chapters. Chapter 1 includes example problems for the estimation of optimal spacing between CPT soundings performed in line and distributed in two dimensions using CPT data obtained from the Sagamore Parkway Bridge construction site in Lafayette, Indiana. Chapter 2 contains example problems for the estimation of limit bearing capacity and settlement of shallow foundations using CPT data reported in literature for sites in the US, UK, and Australia. Chapter 3 includes example problems for the estimation of limit unit shaft resistance and ultimate unit base resistance of displacement, non-displacement, and partial displacement piles using CPT data obtained from three sites in Indiana. The predicted foundation load capacities and settlements were found to be in agreement with the measured load test data reported for these sites.

Findings

Not applicable.

Implementation

The *CPT-Based Geotechnical Design Manual* can be used to train new employees and to facilitate interaction between INDOT engineers, industry, and consultants. Specific implementation items for each volume are listed below.

Volume I

A spreadsheet for the estimation of fundamental soil variables from CPT results was developed. INDOT engineers can use the spreadsheet on a routine basis to interpret CPT data, generate an SBT profile, and obtain the depth profile of a soil property of interest.

Volumes II and III

Spreadsheets for the estimation of optimal spacing between CPT soundings and CPT-based design of shallow and pile foundations were developed. INDOT engineers can use the spreadsheets on a routine basis for the design of transportation infrastructure projects in Indiana.

A relationship between cone resistance q_c, corrected SPT blow count N_{60}, and mean particle size D_{50} was developed using data reported by Robertson et al. (1983) and data obtained from 15 sites in Indiana. The relationship can be used to obtain an estimate of q_c for use in a CPT-based foundation design method when only SPT blow counts are available for a site.

A relationship between critical-state friction angle ϕ_c, mean particle size D_{50}, coefficient of uniformity C_U, and particle roundness R was developed using test data reported for 23 clean silica sands in the literature. In the absence of direct shear or triaxial compression test results, the relationship can be used to obtain an estimate of ϕ_c for poorly-graded, clean silica sands with D_{50}, C_U, and R values ranging from 0.15–2.68 mm (0.006–0.105 in.), 1.2–3.1, and 0.3–0.8, respectively.

CONTENTS

LIST OF TABLES

LIST OF FIGURES

LIST OF ABBREVIATIONS AND SYMBOLS

a' = in-situ attraction = c' cot(ϕ_p')

a^* = stress exponent that depends on the σ'_{vp}

A and B are empirical constants for determining V_{s1} based on Robertson and Fear (1995)

a_c = penetrometer probe radius (= 1.78 cm for a 10 cm^2 cone and 2.20 for a 15 cm^2 size)

a_n = cone net area ratio = A_n/A_c

A_c = projected cone cross-sectional area

A_n = cross-sectional area of the load cell behind the cone

a_q = cone factor by Agaiby and Mayne (2018) for determining rigidity index = $(U^* - 1)/Q_t = (u_2 - \sigma_v)/(q_t - \sigma_v)$

B_q = normalized pore pressure parameter ratio = $\Delta u_2/q_{t\text{-}net} = (u_2 - u_0)/(q_t - \sigma_v)$

b_x = compressibility constant for determining relative density according to Jamiolkowski et al. (2001)

c' = effective cohesion intercept

c^* = variable stress exponent based on the "Stress Focus" concept for SBT classification by Olsen and Mitchell (1995)

C_0 and C_2 are soil constants for determining relative density based on Robertson and Cabal (2014), equal to 15.7 and 2.41, respectively

C_c = virgin compression index of the soil material

CCT = calibration chamber test

c_h = coefficient of horizontal consolidation

CK_0UC = Triaxial compression test

CPT = cone penetration test

CPTu = piezocone penetration test

C_Q = overburden correction = $(p_A/\sigma'_v)^n$ for determining V_s according to Karray et al. (2011) with a maximum value of 2, and the exponent n is typically equal to 0.5

C_s = swelling index of the soil material

c_v = coefficient of vertical consolidation

D' = constrained modulus of soil

d = penetrometer diameter (= 3.57 cm for the standard 10 cm^2 cone, and 4.37 cm for 15 cm^2 cone

D_{50} = mean grain size

D_R = relative density

DSS = direct simple shear mode of testing

E' = drained Young's modulus

e_0 = in situ void ratio of soil

f and g are constants by Fahey and Carter (1993) for determining the modulus reduction factor depending on soil type and stress history

FC = fines content

FR = friction ratio = f_s/q_c (based on the measured cone resistance) or f_s/q_t (based on the corrected cone resistance)

F_R = normalized friction ratio = $f_s/q_{t,net} = f_s/(q_t - \sigma_v)$

FR_n = modified normalized friction ratio for Olsen and Malone (1988) SBT classification chart = $(f_s/q_c)/[1/(\sigma'_v)^{(1\ -\ n)}]$

FS = factor of safety

f_s = sleeve resistance

f_{s1} = normalized sleeve resistance for Olsen (1984) SBT classification chart = f_s/σ'_v

G = shear modulus

G_0 = small strain shear modulus = $\rho_m V_s^2$

g_a = gravitational acceleration constant = 9.8 m/s^2

G_s = specific gravity of the soil

I^*_G = modified rigidity index for Robertson (2016) SBT classification chart = $G_0/(q_t - \sigma_v)$

$I_{B(R16)}$ = SBT classification index for Robertson (2016) SBT classification chart =

100 (Q_{tn} + 10) [70 + Q_{tn} F_R(%)]

$I_{c(R\&W98)}$ = SBT classification index based on Robertson and Wride (1998) chart = $\sqrt{[3.47 - logQ_{tn}]^2 + [1.22 + LogF_R]^2}$

$I_{c(J\&B06)}$= SBT classification index based on Jefferies and Been (2006) chart = $\sqrt{\{3 - log[Q_t(1 - B_q) + 1]\}^2 + [1.5 + 1.3(LogF_R)]^2}$
(note: the range of values differ from $I_{c(J\&D93)}$)

$I_{c(J\&D93)}$= SBT classification index based on Jefferies and Davies (1993) chart= $\sqrt{\{3 - log[Q_t(1 - B_q)]\}^2 + [1.5 + 1.3(LogF_R)]^2}$
(note: the range of values differ from $I_{c(J\&B06)}$)

I_G = rigidity index = G_0/q_t

I_R = undrained rigidity index = G/s_u

$I_{R(50)}$ = undrained I_R of the clay (taken at 50% of strength)

K = empirical factor for conversion of u_1 pore pressure readings to equivalent u_2

k^* = preconsolidation cone factor

K_0 = lateral stress coefficient = σ'_h/σ'_v

K_c = correction factor for $Q_{tn,cs}$

K_D = constrained modulus number

K_E = Young's modulus number

K_G = small-strain shear modulus number

k_h = coefficient of permeability (hydraulic conductivity) in horizontal direction

k_v = coefficient of permeability (hydraulic conductivity) in vertical direction

LOC = lightly overconsolidated

M = frictional parameter in Cambridge q–p′ space = 6sinϕ'/(3-sinϕ')

M^* = gradient for determining c_h based on Teh (1987) approach, which corresponds to the theoretical curve for a given probe geometry and porous filter element location

m = measured gradient of the initial linear dissipation for determining c_h based on Teh (1987) approach $\left[\sqrt{(time)}\, units\right]$

m' = yield stress exponent for determining σ'_{vp} based on Mayne (2013)

m^* = stress exponent for determining G_0 based on Tanaka and Tanaka (1998) and Mayne (2007b)

m_q = cone resistance depth ratio = $\Delta q_t/\Delta z \approx q_t/z$

n = stress normalization exponent = $0.381\, I_{c(R\&W98)} + 0.05\dfrac{\sigma'_v}{p_A} - 0.15$ where n $\leq$ 1.0

NC = normally consolidated

N_{ke} = bearing factor

N_{kt} = cone bearing factor

N_m = cone resistance number = $q_{t,net}/(\sigma'_v + a') = (q_t - \sigma_v)/(\sigma'_v + a')$

$N_{\Delta u}$ = pore pressure bearing factor

OC = overconsolidated

OCR = overconsolidation ratio = σ'_{vp}/σ'_v

p_A = reference stress of 1 atmosphere = 1 bar = 100 kPa

PI = plasticity index

PPD = pore pressure difference = $(u_1 - u_2)/u_0$

$PPSV$ = normalized pore pressure difference = $(u_1 - u_2)/\sigma'_v$

q = applied stress in determining modulus reduction factor

q/q_{max} = mobilized strength of soil in determining modulus reduction factor

Q_A = aging factor for determining relative density based on Kulhawy and Mayne (1990) = 1.2 + 0.05 log(t/100), where t = time in years

Q_{c^*} = compressibility factor for determining relative density according to Kulhawy and Mayne (1990)

q_c = measure cone resistance

Q_c = normalized net measured cone resistance = $(q_c - \sigma_v)/(\sigma'_v)^{c^*}$

$q_{c,net}$ = net measured cone resistance = $q_c - \sigma'_v$

q_{c1} = normalized cone resistance = q_c/σ'_v

$q_{c1N\ (Andrus\ et\ al.\ 07)}$ = normalized corrected cone resistance according to Andrus et al. (2007)

= $(q_c/p_A)(p_A/\sigma'_v)^n$; n = 0.5 for clean sands and 1.0 for clays

Q_{cn} = measured cone resistance normalized for overburden pressure = $(q_c/p_A)/(\sigma'_v/p_A)^{0.5}$

q_{cn} = normalized measured cone resistance = $q_c/(\sigma'_v)^n$

q_E = effective cone resistance = $q_t - u_2$

q_{max} = ultimate or failure stress in determining modulus reduction factor

Q_{OCR} = overconsolidation factor used in determining relative density according to Kulhawy and Mayne (1990) = $OCR^{0.18}$

q_t = corrected cone resistance = $q_c + u_2\ (1 - a_n)$

Q_t = normalized net corrected cone resistance = $q_{t,net}/\sigma'_v = (q_t - \sigma_v)/\sigma'_v$

$q_{t,net}$ = net corrected cone resistance = $q_t - \sigma_v$

Q_{t1} = corrected cone resistance normalized for overburden pressure = $(q_t/p_A)/(\sigma'_v/p_A)^{0.5}$

$q_{t1N(H\&M06)}$ = normalized corrected cone resistance according to Hegazy and Mayne (2006) = $(q_t/p_A)(p_A/\sigma'_v)^{0.5}$ for $I_{C(R\&W98)} < 2.6$, and $(q_t/p_A)(p_A/\sigma'_v)^{0.75}$ for $I_{C(R\&W98)} > 2.6$

Q_{tn} = normalized net corrected cone resistance = $(q_{t,net}/p_A)(p_A/\sigma'_v)^n = [(q_t - \sigma_v)/p_A](p_A/\sigma'_v)^n$

$Q_{tn,cs}$ = clean sand equivalent normalized cone resistance = $K_c\ Q_{tn}$

SCE-CSSM = spherical cavity expansion-critical state soil mechanics

SCPT = seismic cone penetration test

SCPTu = seismic piezocone test

S_t = soil sensitivity = $s_{u(peak)}/s_{u(remolded)}$

s_u = undrained shear strength

$s_{u(peak)}$ = peak undrained shear strength

$s_{u(remolded)}$ = remolded undrained shear strength

t = time in years

T^*_{50} = time factors for 50% consolidation = 0.118 and 0.245 respectively for type 1 (midface, u_1) and type 2 filter elements (shoulder position, u_2)

t_{50} = measured time for 50% dissipation of excess pore pressure in a dissipation test from CPTu

U^* = normalized pore pressure = $(u_2 - u_0)/\sigma'_v$

u_0 = hydrostatic pore pressure = $(z - z_w)\gamma_w$

u_1 = apex or mid-face pore pressure recorded during penetration of piezocone

u_2 = type 2 pore pressure reading recorded at the shoulder (behind the cone) during penetration of piezocone

U_2 = normalized excess shoulder pore pressure = $\Delta u_2/\sigma'_v = (u_2 - u_0)/(\sigma_v - u_0)$

V_s = shear wave velocity

V_{s1} = stress-normalized shear wave velocity = $V_s/(\sigma'_v/p_A)^{0.25}$

w = water content

z = depth below the ground surface

z_i = thickness of the i-th soil layer

z_w = depth of the ground water table

Δu = excess pore pressure measured from the piezocone penetrometer ($\Delta u_2 = u_2 - u_0$) or ($\Delta u_1 = u_1 - u_0$) depending on the location of the filter element

α_D = empirical scaling factor that depends on soil type, confining stress level, OCR, soil plasticity and natural water content (w) for determining constrained modulus, D'

$\alpha_{D'\text{-}G0}$ = empirical scaling factor for converting G_0 to D'

α_E = Young's modulus factor

α_G = shear modulus factor

α_{vs} = shear-wave velocity cone factor = $10^{(0.55\ Ic(R\&W98)\ +\ 1.68)}$ when $I_{c(R\&W98)} < 2.6$

ϕ' = friction angle of soil

$\phi_{cs} = \phi'_{cv}$ = critical-state friction angle = critical state friction angle

ϕ'_p = peak friction angle

γ_{mi} = total unit weight of the i-th soil layer

γ_d = dry unit weight of the soil

γ_m = total unit weight of the soil

γ_{sat} = saturated unit weight of the soil

γ_w = unit weight of water = 9.81 kN/m^3 = 62.4 pcf

Λ = plastic volumetric strain potential = 1 - C_s/C_c

ρ_m = total mass density of soil = γ_m/g_a

σ'_h = effective horizontal stress = $\sigma_h - u_0 = K_0(\sigma'_v)$

σ'_v = effective vertical overburden stress = $\sigma_v - u_0$

σ_v = total vertical overburden stress = $\Sigma(\gamma_{mi} \bullet Z_i)$

σ'_{vp} = effective preconsolidation stress

τ = applied shear stress

τ_{max} = ultimate shear stress at failure

ψ = soil state parameter

1. CPT-BASED SITE INVESTIGATIONS

1.1 Historical Development of CPT

Penetration testing involves pushing and driving a system comprising a metal cone and series of rods into the ground and recording the mobilized resistance to penetration. The idea of pushing rods into the ground to determine the strength of subsurface soil is a very old one. It can be traced back to Collin (1846/1956) who used a Vicat-type needle of certain diameter and weight to estimate the strengths of different clays with varying consistency (Sanglerat, 1972).

Penetration testing evolved from the need for acquiring data on subsurface soils that were not obtainable by any other means. Early versions of soundings were developed in the 1920s by the Swedish and Danish State Railways. Significant improvements in penetration techniques were made around 1930 with the development of the dynamic penetration test methods in the United States and the static penetration test methods in Europe (Barentsen, 1936). Cone penetration tests were first introduced in 1932 in the Netherlands. A gas pipe of 19 mm (0.75 in.) inner diameter was used; inside this, a 15-mm (0.6 in.)-diameter metal rod with a conical tip attached to its front could move freely up and down. Both the outer pipe and the inner rod with the 10 cm^2 (1.55 $in.^2$) cone (Figure 1.1) were pushed down. The cone resistance, measured on a manometer, was corrected by subtracting the weight of the inner rod (Lunne et al., 1997). The method has been referred to as the static penetration test, quasi-static penetration test, Dutch cone penetration, Dutch static cone penetration test, and Dutch deep sounding test. The term quasi-static is used because the penetrometer is advanced into the ground at a constant speed rather than being subjected to truly static loading conditions (Broms & Flodin, 1990; Sanglerat, 1972).

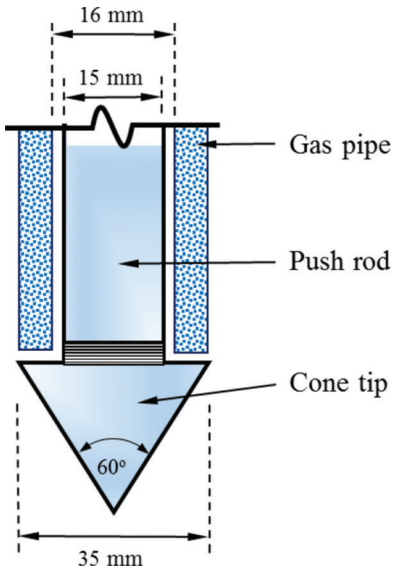

Figure 1.1 Early Dutch mechanical cone (after Sanglerat, 1972).

Tests on the first manually operated 10-tonne cone penetrometer rig were conducted in 1935 by the Delft Soil Mechanics Laboratory (Van de Graaf & Vermeiden, 1988). The initial design of the apparatus was then modified by the introduction of a mantle to prevent the ingress of soil particles between the cone and the push rods (Figure 1.2). A friction sleeve was introduced later to measure local side friction over a short length near the cone point, as shown in Figure 1.3 (Begemann, 1953, 1965). According to Sanglerat (1972) and Broms and Flodin (1990), other mechanical cone penetrometers with somewhat different features were also developed in Belgium, Sweden, Germany, France, and Russia. Hydraulic jacks and piston systems were extensively introduced in France in the 1950s and 1960s, such as L. Parez and The Centre Experimental du Batiment et des Travaux Publics (CEBTP). The oil pressure line transmitted the pressure to manometers located at the ground surface allowing continuous readings of cone resistance (Sanglerat, 1972).

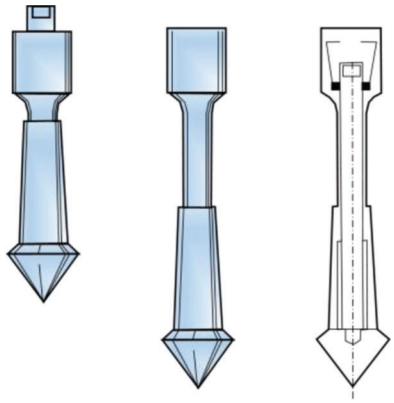

Figure 1.2 Dutch mechanical cone penetrometer with a conical mantle (after Sanglerat, 1972).

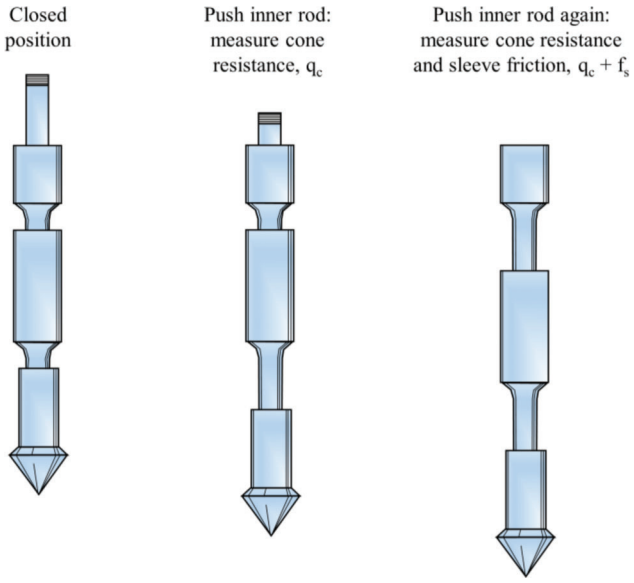

Figure 1.3 Begemann type cone with friction sleeve.

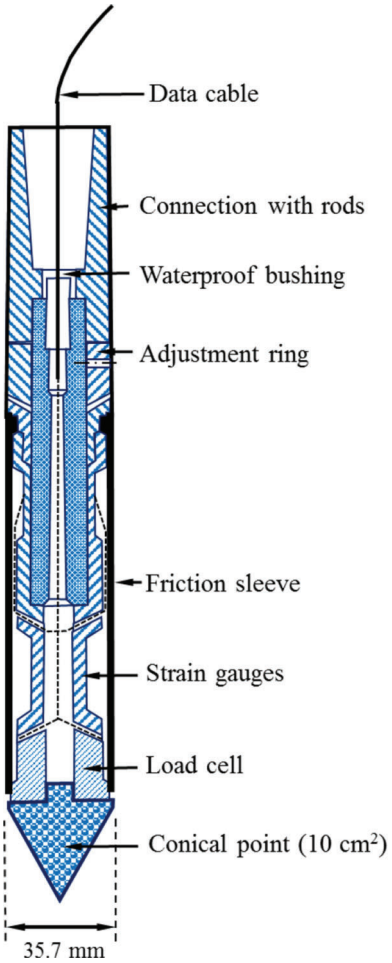

Figure 1.4 Schematic of Fugro electrical friction cone (after de Ruiter, 1971).

To improve the quality of the data, particularly in soft soils and highly stratified materials, an electronic cone penetrometer was introduced in Berlin during the late 1940s, where signals were transmitted to the ground surface through a data cable placed inside the hollow penetrometer rods. Noticeable early developments in the use of electronic cone penetrometers include the works by Delft Soil Mechanics Laboratory (DSML) in 1957, Dutch State Research Institute and Fugro in 1965 (Figure 1.4), and de Ruiter in 1971. The main improvements of the electric penetrometer relative to the mechanical cone penetrometers include the following (Muhs, 1978).

1. Elimination of possibly erroneous interpretation of test results due to the friction between inner rods and outer tubes.
2. Continuous penetration at a standard rate without the need for alternative movements of different parts of the penetrometer, thus preventing undesirable soil movements from influencing cone resistance.
3. Simpler and more reliable electrical measurement of cone resistance allowing for continuous measuring and recording of test results.
4. Possibility of using sensitive load cells for collecting accurate readings in soft soils.
5. Use of an electrical inclinometer to monitor deviations of the penetrometer from the vertical position during the test.

Further enhancements to the measurements obtained from penetrometers were made by the Norwegian Geotechnical Institute (NGI) in 1974 and Schmertmann (1974) when the electrical piezometer was added for the measurement of penetration pore pressures. Torstensson (1975) in Sweden and Wissa et al. (1975) in the USA developed electric piezometer probes to measure pore pressures during penetration as well as dissipation of pore pressures during pauses in penetration, thus enhancing the potential for detecting thin permeable seams embedded in clay layers. Schmertmann (1978b) evaluated the liquefaction potential of sands by using a Wissa-type piezoelectric probe. Baligh et al. (1980) suggested that the pore pressure data, when combined with the CPT data, could provide a promising method for soil identification and estimation of overconsolidation in a clay deposit. To determine the efficacy of the measurement results, various locations of the piezometer filter on the cone tip and rod were explored by researchers (Baligh et al., 1981; Campanella & Robertson, 1981; Jones et al., 1981; Muromachi, 1981; de Ruiter, 1981; Tumay et al., 1981). A large variety of piezocones have been developed since then. However, for practical purposes, pore pressures are typically measured at one location, which is just behind the cone face. With the measurement of pore pressures, it became apparent that it was necessary to correct the cone resistance for pore pressure effects, as detailed later.

An inclinometer was incorporated to detect deviations from verticality and thus offer a warning to the user against excessive slope and/or buckling problems (Van de Graaf & Jekel, 1982). Geophones and/or accelerometers were added to cone penetrometers to measure compression (P) and shear (S) wave velocities for estimation of small-strain shear modulus G_0 and constrained modulus M_0. This modern version of the CPT, termed seismic piezocone penetration test (SCPTu), was originally developed at the University of British Columbia (UBC) (Campanella et al., 1986; Robertson et al., 1986). Figure 1.5(a) shows the internal schematic of the seismic piezocone and Figure 1.5(b) shows the principles of the downhole seismic cone survey technique. Baldi et al. (1988) used a system consisting of two CPT trucks, one with a source cone and the other with a receiver cone, to carry out crosshole seismic piezocone penetration tests, as shown in Figure 1.6.

Due to the influence of electronics, which has greatly enhanced the accuracy of measurements, the CPT is steadily becoming the preferred penetration test for site investigation. Since the introduction of the electronic cone, many additional sensors, such as temperature, pressuremeter, camera (visible light), radioisotope (gamma/neutron), electrical resistivity/conductivity, dielectric, pH, oxygen exchange (redox), laser/ultraviolet-induced fluorescence, have been added to the cone (Robertson & Cabal, 2012). According to Mitchell (1988) and Robertson (2009), the reasons for the

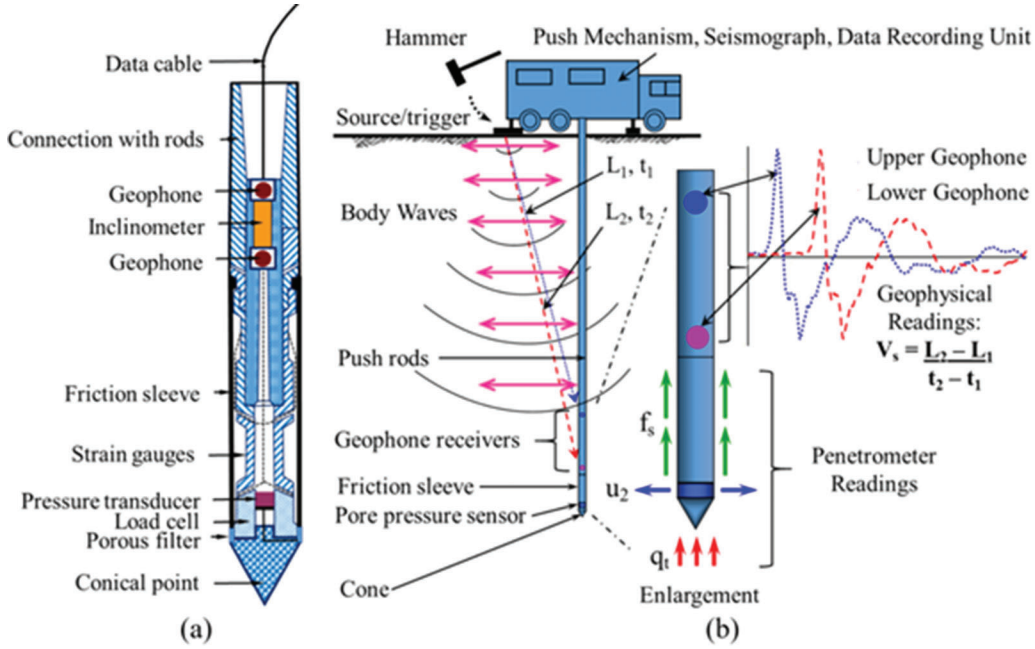

Figure 1.5 Seismic piezocone test: (a) internal schematic of penetrometer, and (b) procedure for downhole survey technique (adapted from Mayne, 2007a; Niazi, 2014).

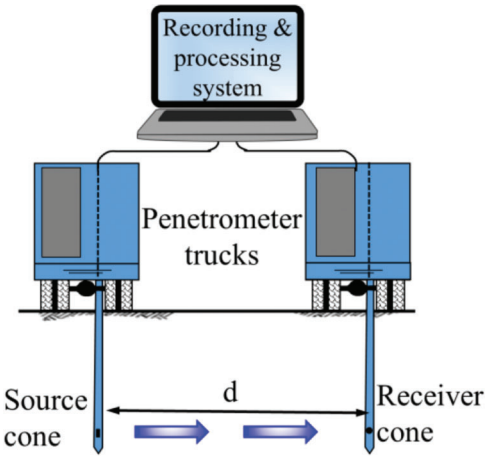

Figure 1.6 Schematic of crosshole seismic piezocone test (Baldi et al., 1988).

dominance of the CPT over other *in situ* tests are: (1) the test is simple to perform and relatively economical, (2) it is fast and repeatable, with continuous records with depth obtained, (3) results are interpretable on both empirical and analytical bases, i.e., it has a strong theoretical background, (4) both the cone and the friction sleeve can be instrumented with sensors, and (5) a large experience base is now available.

1.2 Components and Types of CPT Systems

The components of a modern CPT system are the following.

1. An electrical penetrometer.
2. A thrust mechanism with reaction arrangements—hydraulic pushing system with extension rods for deeper penetrations, anchors or deadweight.
3. Equipment for data acquisition and recording, including a cable or transmission device and a depth recorder.

Some of these items were introduced in the previous section; these will be presented in some detail herein. For the older mechanical CPT systems, standard guidelines as per ASTM D3441 (Subcommittee D18.02, 2016) are valid. The information presented below has been summarized from various sources in the literature (Briaud & Miran, 1992; IRTP, 1999; Jamiolkowski et al., 1985; Lunne et al., 1997; Mayne, 2007a; Robertson & Cabal, 2012; Robertson & Campanella, 1985; Subcommittee D18.02, 2012).

1.2.1 Electrical Seismic Piezocone Penetrometers

The standard piezocone test equipment consists of a 60° apex conical tip with a 35.7 mm (1.4 in.) base diameter (i.e., 10 cm^2 or 1.55 $in.^2$ base cross-sectional area A_c) and a 134-mm- (5.3 in.)-long friction sleeve with a surface area A_s of 150 cm^2 (23.25 $in.^2$) located above the cone. In general, penetrometers are fabricated from tool-grade steel material, although others made of stainless steel are also known to be available. The tip and sleeve elements are detachable and thus can be replaced in case of wear or damage.

The cone resistance q_c and sleeve resistance f_s are derived from the measurements of electrical strain gauge load cells. Figure 1.7 shows three different arrangements of load cells used by the cone manufacturing industry: (1) cone resistance and sleeve resistance are measured

separately by two independent load cells both in compression, (2) the same arrangement as the previous one, except that the sleeve resistance load cell acts in tension, and (3) the sleeve resistance load cell, in compression, records the summation of loads corresponding to both the cone and sleeve resistances; the sleeve resistance is thus obtained from the difference in load measured by the cone and sleeve load cells (this arrangement is sometimes referred to as the subtraction cone).

The pore pressure u is measured using a saturated filter element connected through a portal cavity to a pressure transducer housed within the penetrometer (Figure 1.5a). It is common practice to replace the pore filter after each sounding with either a disposable plastic ring type or a reusable sintered metal or ceramic type. The reusable types can be cleaned in an ultrasonic bath. A balance is required between high permeability of the porous filter to maintain a fast response time and low permeability to have high air entry resistance to maintain saturation. The fluid used for saturation should have low compressibility and viscosity, and the pressure transducer should have rigid to low compliance.

The location of the porous filter element is not standardized. Based on the type of soil being tested, the porous filter is usually located either at the apex or midface (Type 1), giving u_1 readings, or at the shoulder, i.e., behind the cone face (Type 2), giving u_2 readings, or behind the friction sleeve (Type 3), giving u_3 readings. Piezocones that measure pore pressures at two or three locations are termed dual element or triple element piezocones, respectively (Figure 1.8). The standard location of the pore pressure transducer is the Type 2 (u_2) position because it allows for the correction of q_c to total cone resistance q_t, as detailed in Section 1.2.2. However, in highly stratified or heavily overconsolidated and stiff, fissured clays, the dilative tendency of the soil can cause a pore water suction effect at the u_2 location, which can lead to the desaturation of the pore pressure measuring system. Consequently, inconsistent data in the form of sluggish pore pressure response can be recorded, including negative readings. In such cases, the Type 1 (u_1) location can provide a more effective and robust piezocone penetration test profiling capability (Mayne, 2007a; Peuchen et al., 2010; Sully & Campanella, 1994; Sully et al., 1999). The use of the Type 3 (u_3) location and the multi-element piezocone are least common and beyond standard practice. They have mostly been used in research related to the pore pressure distribution based on the response of the soil to changes in stress state during the advancement of the probe. The use of the Type 3 piezocone can be beneficial in soft, fine-grained soil deposits, where pore pressures are proportionately large compared to the sleeve resistance, or when the end areas of the sleeve are significantly different (see Section 1.2.2 for more details). Table 1.1 provides general recommendations for selecting the type of piezocone penetrometer based on the type of soil being tested.

As stated earlier, the SCPTu requires additional sensors including a geophone/accelerometer within the penetrometer above the friction sleeve, a memory oscilloscope, and an impulse source with a trigger for the oscilloscope at the ground surface. The source may consist of a beam in contact with the ground surface for shear wave generation, or a flat plate, a normal impact on which compression waves can be generated into the ground. As shown in Figure 1.5(b), a shear wave is generated by horizontally striking a hammer on the source beam in the direction of the beam's long axis. The beam is made to stay in contact with the ground under the weight of the CPT rig. Either the beam or the hammer carries an electronic trigger that records the initiation time of the wave. The wave's arrival time is noted at the geophone, which is integrated into the advancing penetrometer. Adding more than one geophone, spaced 0.5–1.0 m (1.64–3.28 ft) apart, provides

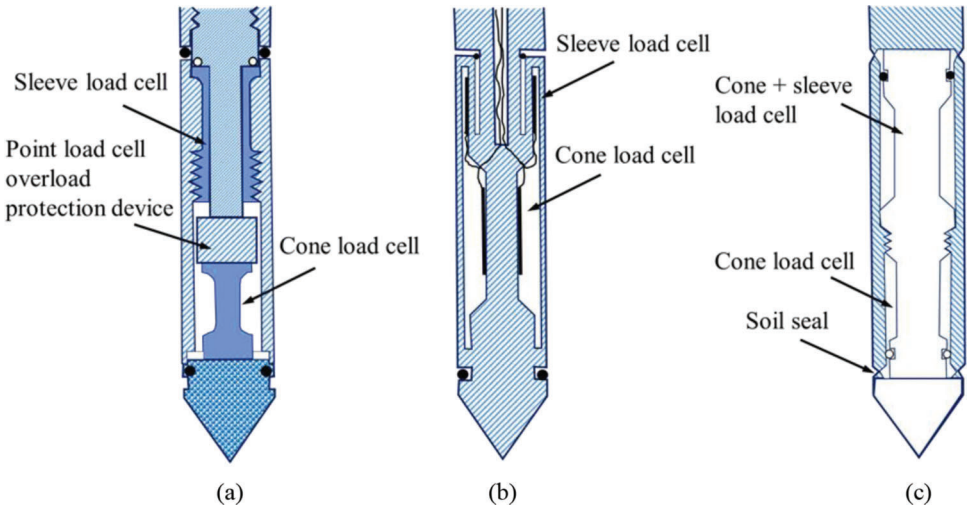

Figure 1.7 Cross-sections of cone penetrometers with different load cell schemes: (a) independent cone resistance and sleeve resistance load cells in compression, (b) cone resistance load cell in compression and sleeve resistance load cell in tension, and (c) subtraction cone penetrometer (adapted from Lunne et al., 1997).

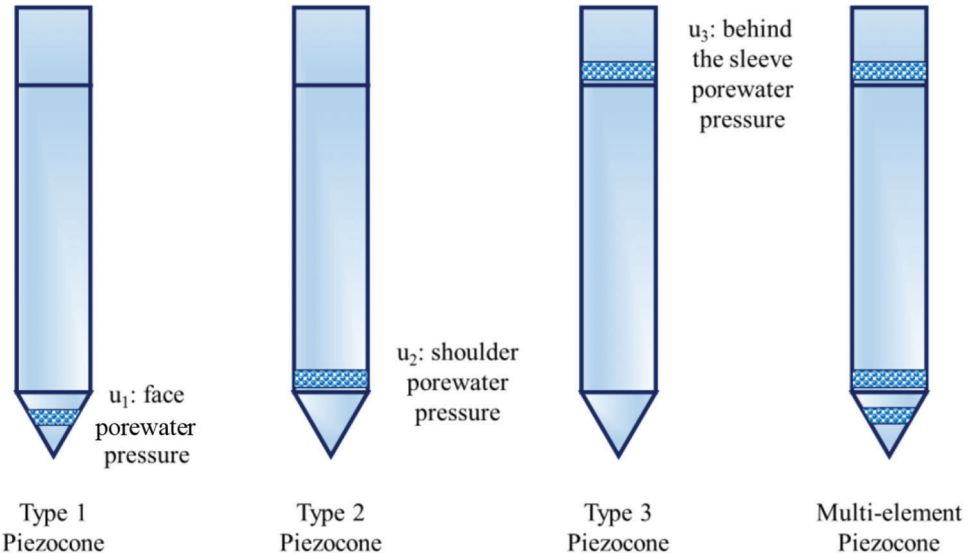

Figure 1.8 Types of piezocone penetrometers.

TABLE 1.1
General recommendations for selecting the type of piezocone penetrometer based on soil type and state

Type of Piezocone Penetrometer	Soil Type and State	Remarks	Source
Type 1	Highly stratified soils, heavily overconsolidated clays and silts, stiff fissured clays, dense fine sand	—	Lunne et al. (1997); Peuchen et al. (2010)
Type 2	Normally consolidated to lightly overconsolidated intact soft clays, loose compressible silts, loose to medium dense fine sand	—	Robertson et al. (1986)
Type 3	Soft fine-grained deposits where pore pressures are proportionately large compared to measured sleeve resistance or when end areas of sleeve are significantly different	For applying correction to the measured sleeve resistance (recorded in combination with Type 2)	Lunne et al. (1997), Robertson et al. (1986)

superior data because the true-interval downhole testing can be implemented, as shown in Figure 1.5(b).

For monitoring changes in temperature during CPT operation and for controlling potential zero shift in cone resistance measurements, the CPT apparatus incorporates a temperature probe in the penetrometer. In addition, the inclinometer can detect deviations from the vertical due to the cone being deflected by boulders, the effect of sloping soil layers, improper alignment of the rods and/or pushing system and buckling of the rods.

Cone penetrometers come in other sizes as well, i.e., with cone base areas A_c of 2 cm^2 (0.3 $in.^2$) (miniature cone), 15 cm^2 (2.325 $in.^2$), and 40 cm^2 (6.2 $in.^2$) (large cone). Miniature cones are useful to detect thin layers, whereas large cones are indicated for use in gravelly soils. However, the use of such non-standard penetrometer sizes needs to be done with the correct understanding of size effects (related to cone diameter-to-particle size ratios) on the data retrieved (Almeida & Parry, 1985; De Beer, 1963; de Lima & Tumay, 1991; Lunne, 1976; Lunne & Powell, 1992; Lunne et al., 1996; Muromachi, 1981; Power & Geise, 1995; Powell & Quarterman, 1988; Tani & Craig, 1995). Lunne et al. (1997) concluded that penetrometers with cone base areas ranging from 5 cm^2 (0.775 $in.^2$) to 15 cm^2 (2.325 $in.^2$) will give similar cone resistance values in most geomaterials.

Although the 10 cm^2 (1.55 $in.^2$) cone is considered to be standard for profiling the subsurface, there are some advantages associated with the use of larger size penetrometers, such as the 15 cm^2 (2.325 $in.^2$) cone. Because of the larger size of the penetrometer, compared to the diameter of routine extension rods (= 35.7 mm or 1.4 in.), a larger hole is created behind the advancing penetrometer, resulting in reduced friction along the following rods during pushing. Additional sensors, if needed, can also be fitted conveniently on a larger penetrometer. While using the standard 10 cm^2 (1.55 $in.^2$) penetrometer, the friction between the upper rods and the surrounding soil can be reduced by merely

adding a welded ring (to develop an enlarged hole) at the connection of the first rod with the penetrometer. This can also be accomplished by using an expanded coupling behind the penetrometer. This arrangement has the benefit of housing additional sensors, such as multiple-axes accelerometers, to receive shear waves polarized in different directions as well as compression waves (Figure 1.9).

1.2.2 Penetration Readings

The cone resistance q_c is the ratio of the axial force F_c measured by the cone load cell to the cone base area A_c. Due to the internal configuration of the penetrometer, the pore pressure acts not only on the shoulder area behind the cone but also on the ends of the friction sleeve; this is commonly referred to as the unequal area effect. It influences the stresses measured from both the cone and the friction sleeve, particularly in intact clays and silts where higher pore pressures are expected to develop during cone penetration. To account for this effect, the measured cone resistance q_c is corrected via the following expression:

$$q_t = q_c + u_2(1 - a_n) \qquad \text{(Eq. 1.1)}$$

where q_t = corrected cone resistance (sometimes, also called as corrected, total cone resistance), and a_n = net area ratio, which is equal to the ratio of the cross-sectional area A_n of the load cell to the projected cross-sectional area A_c of the cone base. Thus, the determination of q_t requires pore pressures to be measured at the shoulder (u_2) position (Figure 1.8) and calibration of the penetrometer in a triaxial vessel/chamber to obtain the value of a_n. Typically, the values of a_n lie between 0.55 and 0.90 for most penetrometers. Values of a_n smaller than 0.38 are also possible, but such penetrometers should be used sparingly, especially in very soft fine-grained soils. The penetration pore pressure u_2 in clean sands, dense to hard geomaterials, and dry soils is close to the hydrostatic pore pressure u_0, and thus the value of q_t is approximately equal to that of q_c. Equation 1.1 is most relevant to soft, fine-grained, saturated soils, where pore pressures can be quite large relative to the cone resistance.

Sleeve resistance f_s is the ratio of the shear force F_s acting along the cylindrical friction sleeve located above the cone tip to the sleeve surface area A_s. As stated earlier, the friction sleeve has "end areas" that are exposed to pore pressure, and thus the measured sleeve resistance will also be influenced by pore pressure

Figure 1.9 Extension rod with expanded coupling, capable of housing 3 accelerometers (courtesy of A.P. van den Berg, n.d).

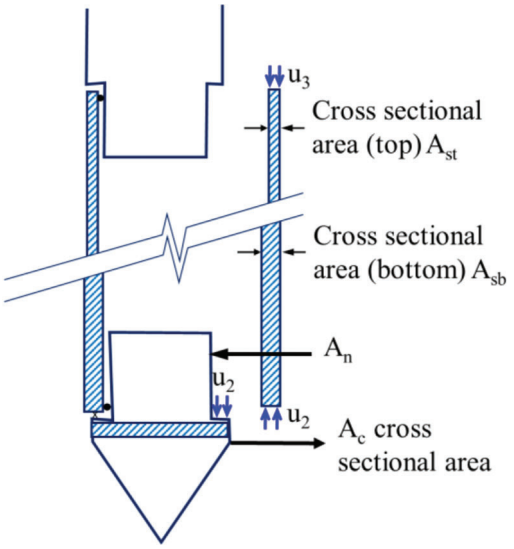

Figure 1.10 Pore pressure effects on CPT parameters (adapted from Robertson & Cabal, 2012).

effects (Figure 1.10). The pore pressures generated during cone penetration are different at the upper end (u_3) and lower end (u_2) of the sleeve. The corrected sleeve resistance f_t can be determined from the following expression:

$$f_t = f_s - \frac{(u_2 A_{sb} - u_3 A_{st})}{A_s} \qquad \text{(Eq. 1.2)}$$

where A_{sb} and A_{st} = cross-sectional areas at the bottom and top of the sleeve, respectively, and A_s = surface area of the sleeve. It is, however, not common practice to measure the value of u_3, thus making it difficult to apply this correction to the sleeve resistance. This correction can be reduced by having equal end areas (i.e., $A_{sb} = A_{st}$).

As stated earlier, the location of the pore pressure sensor is not standardized. However, according to the International Society of Soil Mechanics and Geotechnical Engineering (ISSMGE) reference test procedure (IRTP, 1999), the preferred location is just behind the cone face (u_2) due to the following advantages: (1) the filter element is less susceptible to damage and wear, (2) the measurements are less affected by the compressibility of the filter element, (3) the measured pore pressures can be directly used to correct the cone resistance, and (4) the pore pressures measured during a dissipation test are less influenced by the test procedure.

1.2.3 Driving Components

The penetrometer is driven into the ground up to the desired depth of investigation using standard hollow extension rods (or tubes) (typically 1-m (3.3 ft)-long and 35.7 mm (1.4 in.) outer diameter) constructed from high-tensile steel and a drill rig with hydraulic jacking and reaction systems. For stiffer subsurface materials, larger diameter (44 mm or 1.73 in.[2]) cone rods are

recommended. The signals obtained from the instrumented penetrometer are transmitted to a data acquisition system at the ground surface via electronic cables through the hollow extension rods (Figure 1.11a). These extension rods have special tapered threads for connections, as shown in Figure 1.11(b). Typically, each rod is pushed downwards for a stroke equal to its length, and the hydraulic ram is then retracted for the next rod stroke. The hydraulic load is transferred either by a thrust head on top of the push rods or by a clamping system that works by friction on the outside of the upper rod (Figure 1.12).

In most cases, the drill rigs used for cone penetration testing are custom-built for this purpose. However, the push-down arrangement of conventional drill rigs is also known to have been employed with appropriate coupling arrangements, as shown in Figure 1.13. These arrangements vary based on the site location, i.e., on-land/highway, off-road for remote access, and over-water. Accordingly, the systems can be either truck-, trailer-, track-, all-weather vehicle-mounted, towed, or even portable ones, as shown in Figure 1.14 and Figure 1.15. The track-type and all-terrain rubber-tire vehicle-mounted systems can be used for sites that are hard to access by conventional wheeled trucks. The

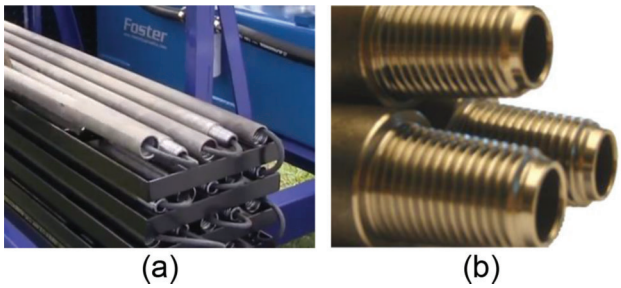

Figure 1.11 CPT rods: (a) electronic cable passing through the extension rods (courtesy of Vertek, n.d), and (b) standard tapered threads for rod connections (courtesy of Geosoft Sp. z o.o., n.d).

Figure 1.12 CPT hydraulic ram, clamping, and thrust system (courtesy of Vertek, n.d).

thrust capacity of the hydraulic pushing system ranges from 20 to 200 kN (4.5 to 45 kips), but sometimes even beyond, depending on the stiffness of the subsurface soil tested. Land-based rigs are commonly mounted in heavy-duty trucks with the deadweight representing the capacity of the rig. The power needed for the hydraulic jacking system is usually supplied by the truck's engine, and additional reactions can be acquired with screw anchors. The CPT system is designed such that the penetrometer and the extension rods are pushed through the centroid of the mass to ensure verticality. The rear cabin enclosure of the truck provides adequate space for all the electronics related to data acquisition and recording to be properly stored, as shown in Figure 1.16.

1.2.4 Data Acquisition and Logging System

The first important component of the subsurface data is the correct recording of depths during the advancement of the penetrometer. Typical depth loggers consist of depth wheel, spooled wire, displacement transducer, and gears. Whichever depth registration system is employed, it should always be referenced to either the ground surface or a stable platform and be fully independent of the thrust system to avoid its displacement during the advancement of the cone and the rods. The resolution of the depth measurements should be consistent with the depth intervals of the penetrometer readings. These requirements necessitate redundancy or alternative checks for the depth measurements. The simplest check is to record either the number of 1-m- (3.3 ft) long extension rods used during penetration, or the length of the marked/graduated data cable advanced through the rods. Figure 1.17 shows the internal schematic of a simple depth registration system and some actual depth loggers.

It is common in the newer electric cone penetrometers to have a simple slope sensor incorporated in their design to measure the verticality of a sounding. This is important to avoid damage to the equipment due to excessive deflections or inclinations, which are commonplace for deep soundings in stratified soils. Figure 1.18 highlights the importance of an inclinometer, and thus the verticality of the sounding, on the cone resistance profile.

A relatively complex system of data collection and recording is warranted for multi-channel seismic piezocone penetrometers. As stated previously, the data from the leading penetrometer is transmitted to the ground surface via a cable pre-threaded down the extension rods. The cable, along with a power supply source, provides the required voltage or current to the penetrometer. The 10-pin type standard cables are used to transmit and record data for at least 5 separate channels. Enhanced systems of up to 32 wires are also employed; however, these come at the cost of thinner and more fragile wires to allow housing within the rods.

In some of the modern penetrometers, acoustic or infrared transmission of signals may also be used to facilitate easier handling of the rods. (since no cable is

Figure 1.13 Advancement of penetrometer and extension rods using a conventional drill rig at a site located near Franklin, NC, USA.

Figure 1.14 Cone penetrometer rigs: (a) truck-mounted rig (ConeTec Inc., n.d.), (b) track-mounted CPT rig with closed cabin for data acquisition and recording (ConeTec Inc., n.d.), (c) and (d) front-mounted CPT rigs with ground anchors (Vertek, n.d.), (e) portable CPT rig (Geomil Equipment B.V., n.d.), and (f) towed CPT rig (Vertek, n.d).

Figure 1.15 Near-shore and off-shore CPT rigs (courtesy of A.P. van den Berg, n.d).

Figure 1.16 Inside view of various CPT truck rigs (courtesy of A.P. van den Berg, n.d).

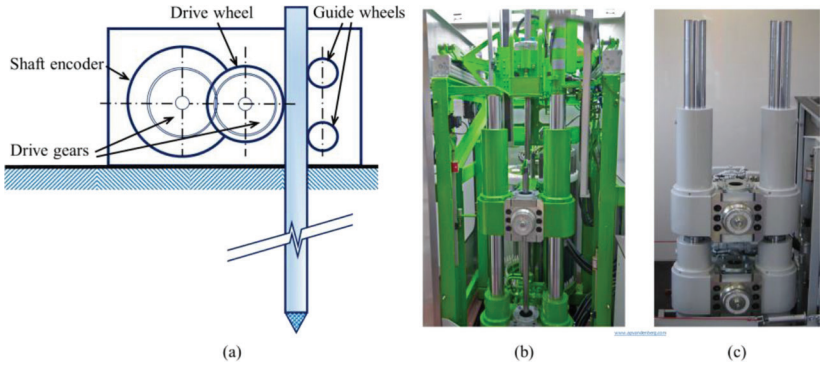

Figure 1.17 (a) Schematic of a depth registration system (adapted from Lunne et al., 1997), (b and c) built-in depth loggers as part of the overall CPT system (courtesy of A.P. van den Berg, n.d).

required). When using infrared and acoustic transmissions, special receivers are required at the top of the rods to capture and decipher the signals for digital output. Some systems, commonly known as memory cone, allow the data to be stored within the penetrometer so that it can be retrieved and synthesized after the test. Such systems have the advantage of eliminating the need for a cable, however, they have some major disadvantages as well: (1) the data cannot be collected, reviewed, and synthesized in real-time, and (2) damage to any of the sensors and excessive deflection or inclination of the rods cannot be detected during testing. Therefore, such wireless systems are generally reserved for special applications (e.g., offshore site investigations).

With regard to data acquisition, electric penetrometer systems include analog to digital converters for convenient computerized monitoring and logging. Proprietary programs are also available, whereby, complete

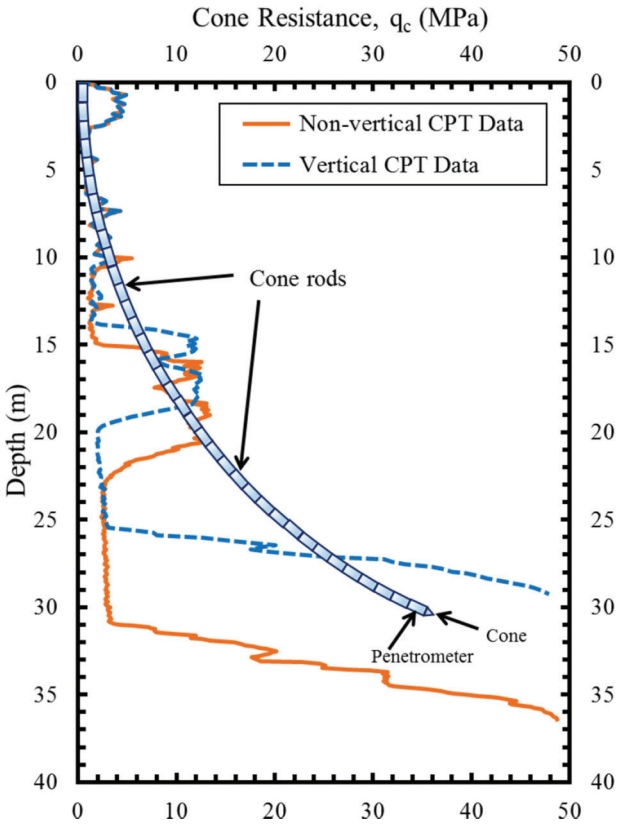

Figure 1.18 Comparison of curved and vertical cone resistance profiles (adapted from de Ruiter, 1981).

post-processing can be done in the field. To improve the data quality, digital cone penetrometers may also include amplification systems that significantly increase the number of channels that can be measured.

1.3 Test Procedure and Data Interpretation

ASTM D5778 (Subcommittee D18.02, 2012) and the International Reference Test Procedure (IRTP, 1999) provide complete details of the steps involved in implementing subsurface investigations using electronic friction cone and piezocone penetration testing. Therefore, these standards should be taken as reference, deviations from which may lead to non-representative results. A summary of the recommended procedures is presented herein, whereas aspects related to the preparation prior to advancing the penetrometer, all the related precautions before, during and after testing, and maintenance of the equipment will be discussed in the following section.

1.3.1 Data Recording During CPT Sounding

Normally, in an electric piezocone sounding, the cone resistance q_c, sleeve resistance f_s, and penetration pore pressure response at one or more of the three locations (u_1 and/or u_2 and/or u_3) are measured. Temperature and inclination are also noted simultaneously as the penetrometer is pushed into the ground. As the penetrometer advances into the ground, there is a break at every 1 m (3.3 ft) of penetration to allow the addition of the next extension rod at the top. This break inherently offers an opportunity to perform a pore pressure dissipation test at that depth before the advancement can resume for the next 1 m (3.3 ft) penetration. Furthermore, with the use of the SCPTu, these intermittent breaks also offer the desired time for the measurement and profiling of the downhole shear wave velocity V_s.

All the penetrometer readings when analyzed together, provide an accurate and useful indication of the subsurface conditions at the site (including stratigraphy) and can be used to define the bearing strata and estimate the likely type, size, and depth of the foundation elements of a structure. The penetration pore pressure readings, however, are particularly useful for the correction of cone resistance values in saturated clays and silts and the assessment of hydraulic conductivity and consolidation rate in slow-draining soils. Moreover, the downhole shear wave velocity V_s, which relates to the small-strain shear modulus G_0 via elasticity theory (i.e., $G_0 = \rho_m V_s^2$, where ρ_m = mass density of soil), offers essential input for many geotechnical engineering problems, such as analyses of embankments and slopes, settlements of shallow and deep foundations, deformations around excavations, ground-surface motions from earthquake excitation, behavior of foundations for vibrating equipment and offshore structures during wave loading, and ground improvement studies. Figure 1.19 shows the depth profiles of q_t, f_s, u_2, and V_s obtained from SCPTu sounding performed at Canon Plant site in Newport News, VA, USA with soil conditions similar to those found in Indiana. The friction ratio FR (= f_s/q_t), which is a derived parameter, will be discussed in Chapter 2.

1.3.2 Penetration Rate

The standard push rate for a CPT sounding using a 10 cm^2 penetrometer is 20 mm/s $\pm$ 5 mm/s. For this rate to be maintained, the hydraulic system should be able to adjust the applied pressure based on the resistance encountered to the push. The push rate is applied in 1 m (3.3 ft) increments, which corresponds to the length of each extension rod. Extra vigilance is mandatory to determine the actual push rate when a CPT system is coupled with conventional drill rigs. In that case, additional recording of the time taken for each penetration segment has to be ensured. Further discussion on penetration rate effects is included in Section 1.3.5 and in Chapter 2.

1.3.3 Data Collection Frequency

For the standard rate of penetration, the typical frequency with which the penetrometer readings are obtained varies between 20 and 100 readings per meter-(3.3 ft) depth, which corresponds to depth intervals of

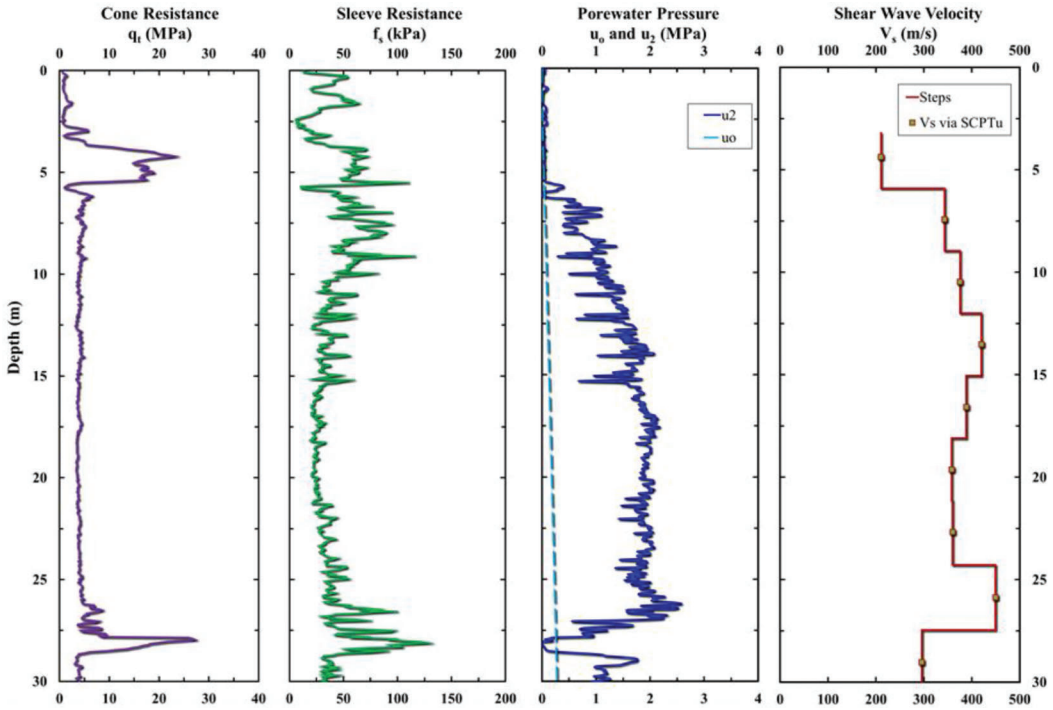

Figure 1.19 Results obtained from SCPTu sounding performed at Canon Plant, Newport News, VA, USA (Norfolk formation (silts, sands, and clays) over Yorktown formation (stiff sandy clay)).

5 cm (2 in.) and 1 cm (0.4 in.), respectively. At this rate, and accounting for the 1 m (3.3 ft) penetration intervals needed for adding the extension rods, a 50-m-(164 ft)-deep CPT sounding can be completed in about 2 to 3 hours.

1.3.4 Pore Pressure Response Based on the Soil Behavior (Dilative vs. Contractive)

The pore pressure distribution with the advancement of cone recorded at different filter locations has been studied by many researchers (e.g., Houlsby & Teh, 1988; Levadoux & Baligh, 1986; Lunne et al., 1996; Robertson et al., 1986; Whittle & Aubeny, 1991). These findings were summarized by Robertson et al. (1986) as shown in Figure 1.20.

In most cases, the largest pore pressures are measured in the zone ahead of the advancing cone where the compressive stresses are at a peak. The cylindrical zone immediately behind the cone experiences partial relief of the normal stress. However, the soil in both these zones continues to be subjected to large shear stresses. Resultantly, the stresses that dominate the pore pressure response in these two zones are: normal stresses below the cone, and shear stresses along the friction sleeve. Furthermore, in saturated soils, increase in normal stresses leads to positive pore pressures. However, depending on the dilatancy properties, the mobilized shear stress in the soil can induce either positive or negative pore pressures. Accordingly, the contractive (or compressible) nature of soft, normally consolidated (*NC*) to moderately overconsolidated (*OC*) fine-grained soils (undrained response) results in positive pore pressures, both on the cone and along the cylindrical shaft. In contrast, in dilative soils, like dense silts and sands and heavily overconsolidated clays, larger positive excess pore pressures develop on the cone, whereas very low or even negative pore pressures develop along the friction sleeve. For such dilative soils, type 1 piezocone (u_1) with porous filter element placed midface on the cone can provide more effective and robust pore pressure profiling. However, to apply correction to the measured cone resistance (q_c) reading, u_2 data (i.e., from a corresponding filter element placed behind the cone) is required.

1.3.5 u_1 vs. u_2 Readings and Empirical Conversions

Penetrometers, which can provide both u_1 and u_2 measurements simultaneously are not employed in standard practice. However, conversion factors can be used to estimate u_2. Cone users who record the pore pressure on the cone tip (i.e., u_1 type CPTu) have suggested factors to adjust the measured pore pressures to those that are assumed to exist immediately behind the tip (u_2). The assumed ratio of the pore pressure on the face to that behind the tip (u_1/u_2) is generally taken to be about 1.2 (i.e., the pore pressure on the face is assumed to be 20% larger than that immediately behind the tip). Measurements made by many cone users around the world (Campanella et al., 1982; Jamiolkowski et al., 1985) have shown that the ratio of 1.2 is generally only true for soft, normally consolidated clays.

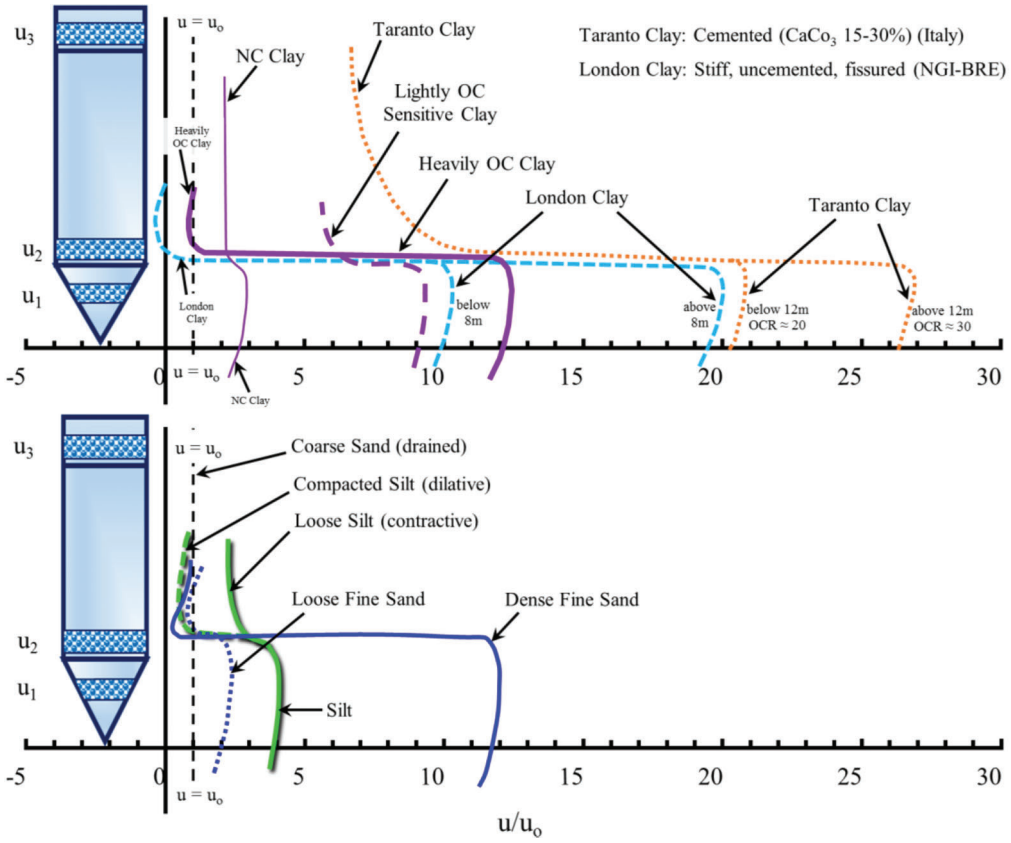

Figure 1.20 Typical measured pore pressure distribution in saturated soils during CPTu based on field measurements (adapted from Robertson et al., 1986).

TABLE 1.2
Empirical values of *K* for adjustment of pore pressures (after Senneset et al., 1989)

	Filter Location	
Soil Type	**Cone Face, Mid-Height**	**Cone Tip**
Normally consolidated clays	0.6–0.8	0.7–0.9
Slightly overconsolidated, sensitive clays	0.5–0.7	0.6–0.8
Heavily overconsolidated clays	0–0.3	0.1–0.3
Loose, compressible silts	0.5–0.6	0.5–0.7
Dilatant, dense silts	0–0.2	0.1–0.3
Loose, silty sands	0.2–0.4	0.5–0.6

Sandven et al. (1988) and Senneset et al. (1989) proposed the following expression to correlate u_1 *pore pressure to* u_2*:*

$$K = \frac{(u_2 - u_o)}{(u_1 - u_o)} \qquad \text{(Eq. 1.3)}$$

where u_o = hydrostatic pore pressure; K is the adjustment factor, primarily a function of soil type and its properties, and the exact location of the u_1 filter element on the cone. Senneset et al. (1989) presented a summary of empirical K factor as shown in Table 1.2.

Sandven (1990) proposed K values for selected soil behavior type (SBT) (see Appendix A for details on SBT). Peuchen et al. (2010) expanded the idea to all the Robertson (1990) SBT zones and presented the following general expression for estimating K values:

$$K = 0.91\, e^{\left(-0.09\, Q_t^{0.47}\right)} \left[\frac{1}{1 + F_R\left(0.17 + 0.061 (Q_t - 21.6)^{1/3}\right)} - e^{-2F_R} \right] \qquad \text{(Eq. 1.4)}$$

where Q_t = normalized corrected net cone resistance = $q_{t,net}/\sigma_v' = (q_t - \sigma_v)/\sigma_v'$; F_R (%) = normalized sleeve friction = $(f_s/q_{t,net})\ 100 = [f_s/(q_t - \sigma_v)]\ 100$.

Chen and Mayne (1994) distinguished the approximate magnitudes of u_1 for pore pressures measured at

the cone face (u_{1f}) from those measured at the apex (u_{1t}) and concluded a relationship of $u_{1t}/u_{1f} \approx 0.861$ using database from 7 clays (1 < overconsolidation ratio < 80). Using data from 53 different intact clay sites, they also proposed the relationship between u_2 and u_1: $u_2/u_1 \approx 0.742$.

1.3.6 Pore Pressure Dissipation Test

As the penetrometer advances into the ground in increments, excess pore pressure Δu is generated around the cone, particularly in saturated soils below the groundwater table. During the pause in penetration, (for adding the extension rods), these excess pore pressures tend to fall back toward the hydrostatic pore pressure (u_0) condition. This phenomenon is evident in Figure 1.19, where the u_2 readings tend to fall back to the hydrostatic u_0 at almost regular depth intervals. Thus, the measured pore pressures $u_{measured}$ at any time during and after cone penetration are the summation of the transient excess and hydrostatic pore pressures (i.e., $u_{measured} = \Delta u + u_0$). Dissipation testing involves the real-time monitoring of the transient pore pressures $u_{measured}$ as they decay while the advancement of the cone has been temporarily halted. Although the rod breaks provide an opportunity for conducting the pore pressure dissipation test, it may not be practically feasible to do so at every 1 m (3.3 ft) increment of penetration. Therefore, the test can be performed at reasonable depth intervals to determine the desired characteristics of different soil layers at the site; these aspects are detailed further in Chapter 2.

1.3.7 Data Interpretation vis-à-vis Drainage Conditions

With reference to the standard rate of cone penetration (20 ± 5 mm/s), the broad ends of the spectrum of soil classification, i.e., clean sand and pure clay can be given simple treatment as drained and undrained, respectively. Relating it to the perceptible measure of hydraulic conductivity k, the standard rate of penetration is expected to yield an undrained response for soils with $k \leq 10^{-6}$ cm/s, (clayey soils) a partially drained response for soils with 10^{-6} cm/s $< k < 10^{-3}$ cm/s (silty soils), and a drained response for soils with $k > 10^{-3}$ cm/s (essentially sands and gravels) (Bugno & McNeilan, 1985). The cone penetration rate, which controls the drainage condition within the soil being penetrated, gains greater significance, especially while interpreting CPT and CPTu data in pure silts as well as mixed soil types (silty clay, silty sand, clayey sand, clayey silt, sandy silt, sandy clay, and non-textbook types of geomaterials). It also becomes relevant when determining the soil parameters appropriate for the drainage condition applicable to different design problems. In other words, the correlations between cone penetration tests and laboratory tests (such as for shear strength) are affected by the shorter time to failure in CPT/CPTu than in, for example, a triaxial test. Therefore, consideration of variation from the standard penetration rate can produce the important required change in the drainage and the ensuing applications.

In ideal situation, the penetration rate should be dictated by or adjusted based on the drainage characteristics (such as hydraulic conductivity, k, and the coefficient of consolidation, c_v) of the soil being penetrated. Although, these parameters can be obtained from the dissipation test, they are not readily available for the entire subsurface profile prior to the penetration testing, making it hard to decide and vary the penetration rate as cone advances through the ground in a multi-layered stratum. It should also be noted that permeability varies by orders of magnitude, and therefore, it may require changes in the rate of penetration by orders of magnitude as well. Such large variations in the penetration rate are difficult to achieve (DeJong et al., 2013; Lunne et al., 1997).

Using variable rate testing during CPTu advancement, numerous researchers have studied rate effects on variety of soil deposits. Such attempts have helped delineation of drained, partially drained, and undrained regions of the soil response to penetration. Bemben and Myers (1974) concluded that in clays up to a penetration velocity (v) of about 0.5 mm/s drained conditions apply, while that above 50 mm/s, undrained conditions exist. They also observed that in clays the cone resistance (q_c) varies with the rate of penetration, being minimum at about 2 mm/s (within a total range of 0.2 and 200 mm/s). Similar observations were recorded by Roy et al. (1982) for sensitive, soft, slightly overconsolidated silty clay. Danziger and Lunne (2012) conjectured that the minimum q_c occurs at different rates for different types of clays depending on variations in overconsolidation, plasticity index, clay content, water content etc.

The results of CPTu testing in sands by Dayal and Allen (1975), Te Kamp (1982), Rocha Filho (1982), and Juran and Tumay (1989) summarized that there is little effect on the cone resistance for penetration rates a little slower than the standard, while for non-standard higher rates, increased q_c may be noticed, primarily due to dilatancy effects and higher negative pore pressures.

For assessing partial consolidation (alias partial drainage) effects, Finnie and Randolph (1994), and Randolph (2004) proposed a normalized penetration velocity (V) as a function of cone velocity (v), penetrometer diameter (D), and vertical coefficient of consolidation (c_v): $V = v\,D/c_v$. Accordingly, the rate effects can be studied by plotting the normalized cone resistance and pore pressure readings against normalized penetration velocities (V) for variable cone velocities (v). Many researchers have utilized such formulations to generate plots for demarcating the drainage boundaries (undrained, partially drained, and fully drained) for different soils (e.g., DeJong et al., 2013; Finnie & Randolph, 1994; Kim et al., 2008, Lehane et al., 2009, Randolph, 2004, Schneider et al., 2007, 2008). Sample results are presented in Figure 1.21, whereas findings regarding drainage con-

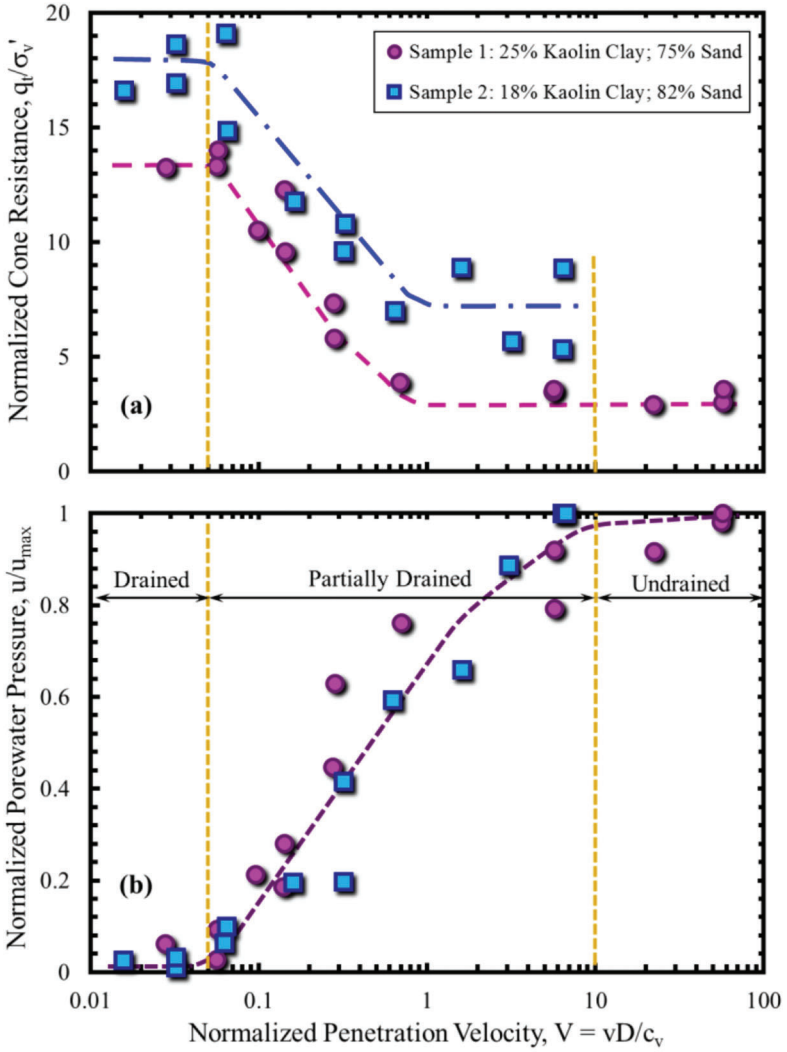

Figure 1.21 Variation of: (a) normalized cone resistance and (b) normalized excess pore pressure with normalized penetration velocity (adapted from Kim et al., 2008).

siderations vis-à-vis penetration rate are summarized in Table 1.3.

During penetration of cone, the appropriate "operational" coefficient of consolidation for use in the calculation of normalized penetration velocity (V) typically adopted is the one in vertical direction (i.e., c_v). DeJong et al. (2013) indicated that the pore pressure dissipation is believed to primarily occur horizontally, resulting in the horizontal coefficient of consolidation (c_h) to control the rate of dissipation more than the vertical coefficient of consolidation (c_v). Accordingly, they utilized a variant dimensionless penetration velocity V ($= vD/c_h$) in their study on the drainage condition vis-à-vis penetration rate. They also reported that the penetration rates required for undrained and drained conditions are proportional to the c_h, and two orders of magnitude change in penetration rate is generally required to move from one limiting condition to another, (i.e., from drained to undrained, or from undrained to drained). The penetration rate to be selected will depend not only on the desired measurement of interest for design (i.e., drained or undrained resistance), but also the capability of the equipment.

DeJong et al. (2013) proposed the following practical implementation strategies and considerations for the on-site assessment of drainage conditions during standard-rate testing and modification to obtain drained or undrained penetrometer measurements.

- A continuous cone sounding should be performed at the standard 20 mm/s rate complete with pore pressure dissipation tests at select locations.
- The hydrostatic pore pressure (u_0) should be determined based on either the ground water elevation or by completion of a pore pressure dissipation test to the hydrostatic pressure.
- With u_0 known, the dissipation tests must only last ~200 seconds. This is enough time to determine if partial drainage occurred during penetration.
- If the time to achieve 50% dissipation (t_{50}) > 100 seconds, undrained conditions exist during penetration and

TABLE 1.3
Recommendations for drainage considerations vis-à-vis penetration rate

Penetration Rate	Soil Type	Measurement Quantity	Drainage Behavior/ Soil Type	Source	Remarks
Standard (20 mm/s ± 5)	Clayey soils	$k \leq 10^{-6}$ cm/s	Undrained	Bugno & McNeilan (1985)	–
	Most silts and mixed soils	$10^{-6} < k < 10^{-3}$ cm/s	Partially drained		
	Essentially sands	$k > 10^{-3}$ cm/s	Drained		
Variable	Clays and silty clays	$V > 30$	Undrained	Finnie & Randolph (1994); Randolph (2004)	V based on c_v
		$0.01 \leq V \leq 30$	Partially drained		
		$V < 0.01$	Drained		
Variable	Clays and silty clays	$V > 30$	Undrained	Schneider et al. (2007)	V based on c_v
		$0.3 \leq V \leq 30$	Partially drained		
		$V < 0.3$	Drained		
Standard (20 mm/s ± 5)	Clays and silty clays	$c_v < 1.1 \times 10^{-5}$ m^2/s	Undrained	Schneider et al. (2008)	–
		3.2×10^{-3} m^2/s $< c_v < 1.1 \times 10^{-5}$ m^2/s	Partially drained		
		$c_v > 3.2 \times 10^{-3}$ m^2/s	Drained		
Variable	Kaolinitic clays ($1 \leq$ OCR ≤ 5)	$V > 15$	Undrained	Lehane et al. (2009)	V based on c_v
		$0.05 \leq V \leq 15$	Partially drained		
		$V < 0.05$	Drained		
Variable	Saturated clayey soils	$V > 10$	Undrained	Kim et al. (2008)	V based on c_v
		$0.05 \leq V \leq 10$	Partially drained		
		$V < 0.05$	Drained		
Standard (20 mm/s ± 5)	Saturated clayey soils	$c_v < 7.1 \times 10^{-5}$ m^2/s	Undrained	Kim et al. (2008)	–
		1.4×10^{-2} m^2/s $< c_v < 7.1 \times 10^{-5}$ m^2/s	Partially drained		
		$c_v > 1.4 \times 10^{-2}$ m^2/s	Drained		
Variable	Saturated clayey soils	$V > 30$	Undrained	DeJong et al. (2013)	V based on c_h
		$0.3 \leq V \leq 30$	Partially drained		
		$V < 0.3$	Drained		
Standard (20 mm/s ± 5)	General application to all soils	$t_{50} > 100$ s ($c_h < 3 \times 10^{-5}$ m^2/s)	Undrained	DeJong et al. (2013)	–
		$t_{50} < 100$ s	Partially drained		
		$u_2 = u_o$ ($c_h > 3 \times 10^{-3}$ m^2/s)	Drained		

Note: k = hydraulic conductivity; V = normalized penetration velocity = vD/c_v or vD/c_h; v = penetration rate (or velocity) of cone; d = penetrometer diameter; c_v = vertical coefficient of consolidation; c_h = horizontal coefficient of consolidation; t_{50} = time to achieve 50% dissipation in a piezocone dissipation test; u_2 = type 2 pore pressure reading recorded at the shoulder (behind the cone) during penetration of piezocone and u_o = hydrostatic pore pressure reading.

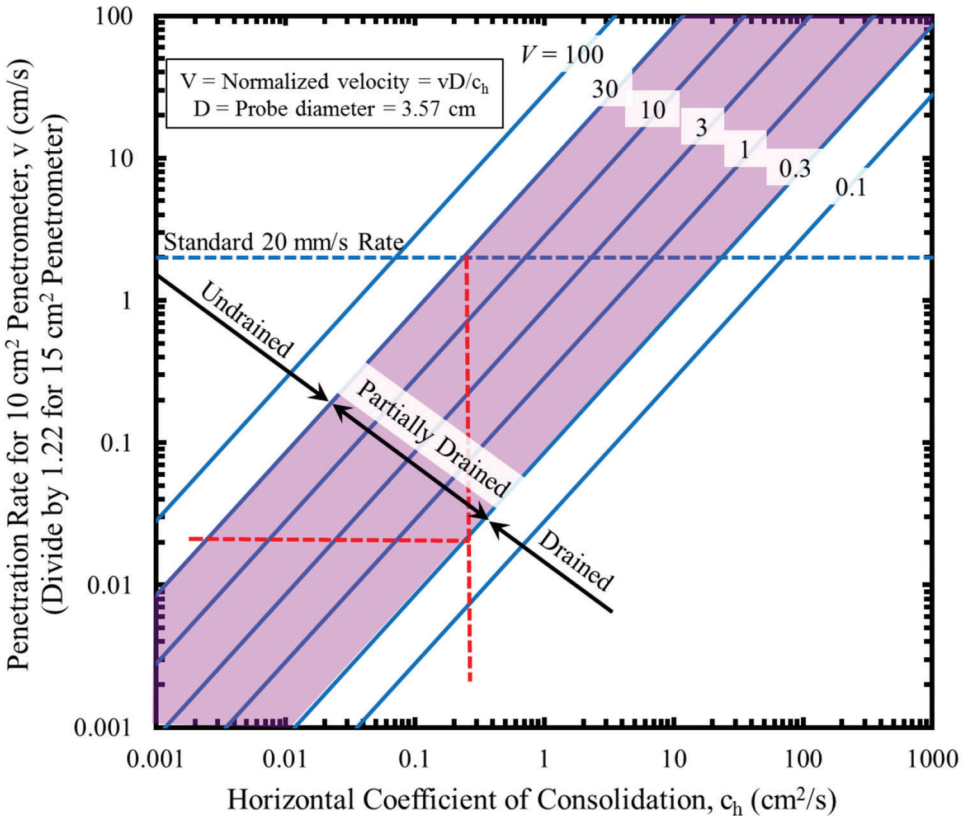

Figure 1.22 Chart presenting the relationship between coefficient of consolidation, penetration velocity, and normalized velocity (adapted from DeJong et al., 2013).

c_h is less than about 3×10^{-5} m^2/s; if $t_{50} < 100$ seconds, intermediate conditions exist with partial drainage.

- Fully drained conditions exist when u_2 is equal to the hydrostatic water pressure (u_o) and $c_h > 3 \times 10^{-3}$ m^2/s (also see Section 2.3.14 for c_h, and t_{50}).
- It should be noted that shorter dissipation tests naturally occur at rod breaks (due to the pause in penetration) and therefore can be easily performed at each 1-m interval.
- If the conditions thus evaluated are partially drained, and the results desired are either drained or undrained, then the penetration rate required to develop desired drainage conditions should be estimated in the field.
- Figure 1.22 presents a simplified chart developed by DeJong et al. (2013) to allow this estimation for 10 cm^2 and 15 cm^2 cone penetrometers. For understanding simple use of this chart, consider a soil with t_{50} (determined from the dissipation test at the standard rate of 20 mm/s with a 10 cm^2 cone penetrometer) barely at 100 seconds; it will likely have c_h in close proximity of 3×10^{-5} m^2/s. (i.e., on the border of undrained and partially drained). As shown in Figure 1.22 with red-dashed lines, for this soil to exhibit fully drained behavior, the penetration rate (or velocity) of cone must not exceed 0.02 cm/s.
- "Twitch" (variable velocities) tests can also be employed using the equipment mentioned above to systematically reduced the velocity (in either one-half or full log cycles, e.g., v = 20, 2, 0.2, 0.002 cm/s or v = 100, 30, 10, 3, 1 cm/s) following short penetration increments of 4 cone diameters (Chung et al., 2006; DeJong et al., 2010; 2013; House et al., 2001).
- During such testing, the magnitude of horizontal and vertical spatial variability of the soil is a concern. The difficulty associated with extraction of the influence of partial drainage during cone penetration given the spatial variability can be moderately mitigated by employing the four-step procedure of site variability rating (*SVR*) using the vertical and horizontal site variability indices (*VVI* and *HVI*, respectively) developed by Salgado et al. (2015). Accordingly, if the *SVR* assessment results in either low horizontal variability and low vertical variability (*LL*) or medium horizontal variability and low vertical variability (*ML*) or low horizontal variability and medium vertical variability (*LM*), a second sounding should be performed with twitch tests at select intervals (four twitch intervals per 1 m are practical), with additional data above and below the 1 m twitch interval at the standard rate of 20 mm/s. If *SVR* results in either high horizontal variability and high vertical variability (*HH*) or medium horizontal variability and high vertical variability (*MH*) or high horizontal variability and medium vertical variability (*HM*), then the twitch interval length should be increase during slow penetrations in subsequent soundings as time allows. As the variability of a deposit increases, it can take considerably more data (soundings) to obtain reliable statistics on partial drainage effects in a specific stratum.

1.3.8 Shear Wave Testing

At the 1 m (3.3 ft) rod breaks, a vertically propagated and horizontally polarized downhole shear wave is generated from the ground surface with the help of a

hammer and a crossbeam. The travel time of this wave is recorded upon arrival at the test elevation via one or more velocity transducers (geophones/accelerometers)-placed within the penetrometer to determine the shear wave velocity V_s. This method is advantageous over the crosshole method of V_s measurement, as shown in Figure 1.6, because only one hole is needed, and the test can be performed during the course of a regular CPT. As such, the test was introduced in Section 1.1, and a schematic of the test was shown in Figure 1.5.

The simplest arrangement commonly used for this test is that of a single velocity transducer fitted within the penetrometer. However, this does not provide the most precise measurement of the downhole shear wave velocity V_s, especially if the axis of the geophone/accelerometer within the penetrometer is not parallel to the orientation of the source wave. Even if the cone is placed in such a way at the start of the CPT sounding that the required parallelism of the geophone/accelerometer to the surface source generator is ensured, it is quite possible that the penetrometer may rotate when successive extension rods are being attached during its advancement. To overcome this problem, the use of two or more geophones/accelerometers located at two different elevations within the penetrometer is recommended (Figure 1.5). Biaxial geophones placed at the same elevation can improve the results further, whereas triaxial geophone arrays provide a third (vertical) component that can collect additional information, i.e., shallow compression wave arrivals (*P*-waves) to determine the compressive wave velocity V_p.

The original method for determining the arrival time of a shear wave at each geophone elevation is to record the first noticeable crossover point resulting from the arrival of a pair of oppositely directed source wavelets, (commonly referred to as the left and right-strike), as shown in Figure 1.23. Modern equipment, such as the AutoSeis, offers convenience in terms of time-and effort-saving and repeatability by generating automatic frequent waves from the ground surface at the set intervals that can be post-processed in computer programs employing the cross-correlation method of matching the waveforms from consecutive depth intervals (Figure 1.24).

1.4 Preparations, Calibrations, Maintenance, and Precautions

The actions required for preparing, calibrating, and maintaining the penetrometer are well documented in official standards, such as ASTM D5778 (Subcommittee D18.02, 2012) and IRTP (1999), which should be considered as authority. In the following subsections, these aspects are summarily covered along with other important precautions that must be ensured for the successful execution of a CPT sounding.

1.4.1 Zero-Load Readings for Temperature Effects

Although modern penetrometers have a high degree of accuracy and precision and some means for compensating temperature variations, there is still a probability of a certain degree of sensitivity of the sensors to these changes. It is, therefore, important for tracking purposes to note the zero-load readings of all the sensors. These readings should be noted both before and after each CPT sounding.

1.4.2 Calibration and Maintenance

Each and every CPT system, including all its components, experiences wear and deterioration with constant and frequent use. This is likely to influence data recording and retrieval. It is, therefore, important to follow a program that consists of regular calibration checks and maintenance. This should be dictated by the precision of the zero-load readings, frequency of use, storage arrangements, and the scale of each project. Typically, no calibration check of the load cells is required if the zero-load readings of the sensors remain stable and within the manufacturer's recommended range. However, for major and important projects requiring frequent use of the CPT, calibration checks should be carried out not only before and after the project, but functional checks, such as recording and evaluating the zero-load measurements (baseline readings), should also be a routine matter throughout the duration of use of the CPT system.

The desired calibration checks for the penetrometer sensors can be performed in-house in a simple sealed calibration chamber/vessel; the schematic of such a vessel is shown in Figure 1.25. It is designed to contain the penetrometer, which is suspended so that no dead loads are applied to the cone or friction sleeve, and to apply an all-round air or fluid pressure. Readings can be recorded for q_c, f_s, and u_2 as the pressure in the vessel is increased incrementally. The desired calibration can be performed by plotting the recorded readings versus the applied vessel pressure. This also helps determine

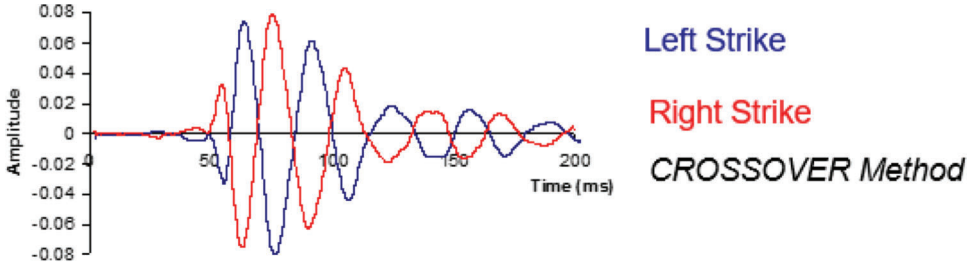

Figure 1.23 Crossover method for determining the arrival time of a shear wave.

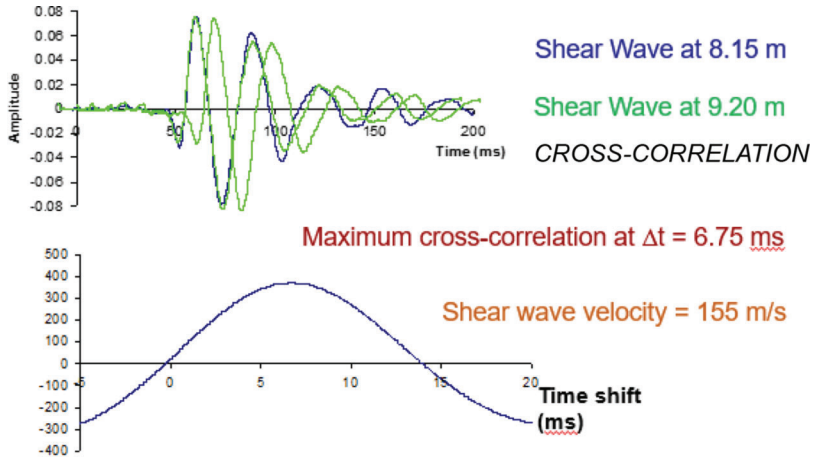

Figure 1.24 Example of the cross-correlation method for determining shear wave velocity.

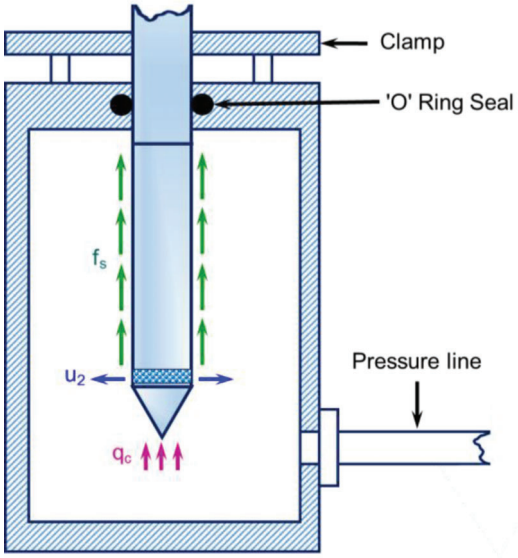

Figure 1.25 Schematic of vessel for calibrating pressure sensors, q_c, f_s, and u_2, and for determining the net area ratio a_n (adapted from Mulabdic et al., 1990).

the net area ratio a_n needed in the correction of cone resistance readings from q_c to q_t. Figure 1.26 shows sample results from such tests. Note that the q_c, f_s, and u_2 readings are generated and measured simultaneously in response to the increasing vessel pressure. Calibrations should be done with all O-ring seals in-place, thus replicating the actual testing, and by using high-quality, reference sensors/transducers that are checked periodically. Similarly, to examine the complete system, the original cable and data acquisition system used in the field should also be employed during the calibration.

The cone tip and sleeve should be replaced if they are damaged or excessively worn. As a guideline, for a rate of 12,000 m (7.46 mi) of cone penetration per year, the cone tip and sleeve should be replaced at least twice per year. Note that the use of the CPT in coarse-grained soils, such as sand and gravel, will require more frequent replacement of the cone tip and sleeve. Table 1.4 summarizes the recommended checks, calibrations, recalibrations, and maintenance frequency for the CPT equipment. Following these recommendations ensures the desired accuracy and precision of the system to last for the life of the equipment.

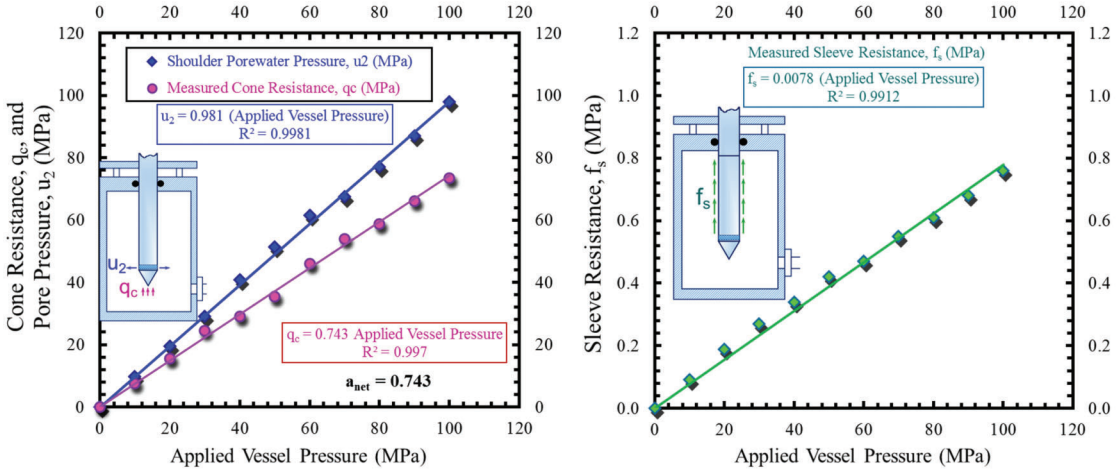

Figure 1.26 Sample results from the pressurized vessel for calibration of q_c, f_s, and u_2 sensors and net area ratio determination.

TABLE 1.4
Summary of recommended calibration checks and maintenance frequency for a CPT system (after Robertson & Cabal, 2012)

	Type of Maintenance								
Frequency	Wear	O-Ring Seals	Push-Rods	Pore Pressure Filter	Calibrations	Computer	Cone	Zero-Load	Cables
Start of project	√	√		√					√
Start of test	√		√	√				√	
End of test								√	
End of day		√							
Once a month	√		√			√	√		√
Every 3 months					√				

1.4.3 Saturation of Piezo Filter Elements

Since porous plastic is relatively inexpensive, convenient to use, and frequently disposed-off/replaced, it is the most common material of the filter elements, particularly when used in the Type 2 piezocone (for u_2 readings). For Type 1 piezocones (u_1 readings), a ceramic filter is preferred because it is more rigid to withstand abrasive forces along the face of the cone. The ceramic filters are reusable in multiple soundings after cleaning.

To obtain high-quality pore pressure data from a piezocone test, the measurement system must be leakproof and have the desired full saturation. Thus, not only does the filter element have to be fully saturated both before and during the test, but also the cavity between the filter element and the pressure transducer, as well as that housing the transducer itself. De-aired water, silicon oil, or glycerin is used for saturation for a period of about 24 hours. Of the three saturating fluids, glycerin is the most preferred one. For perfect saturation, the tip could be screwed into the cylindrical portion of the penetrometer while it is submerged in the saturating fluid kept within a chamber designed for such purposes. Between the initial saturation and start of the test, the front of the penetrometer should be housed in a light rubber membrane containing the saturation fluid so that the membrane automatically ruptures during the initial push into the ground.

When using the piezocone, it may be necessary to pre-drill and fill the hole with water up to the elevation of the groundwater table to ensure that the saturation of the piezo element is maintained. This may also necessitate the use of a casing based on the soil types encountered at the site.

1.4.4 Testing in Gravelly Material

Pre-drilling is often required at sites containing soils that are too difficult for the cone to penetrate. This is done to avoid damage to the penetrometer from excessive loads. Subsurface geomaterials made of gravelly soils should always be pre-bored. In some instances, pre-drilling may be replaced by making a hole through the upper harder material using a solid dummy probe whose diameter is greater than that of the actual penetrometer.

1.4.5 Standards for Employment of Inclinometers

As stated previously, inclinometers are important to ensure that the readings collected during a CPT sounding correspond to the correct depths. The standard push rods can afford about 1° of deflection per meter length without undergoing noticeable damage. A deflection exceeding 5° per meter length can damage the penetrometer and the rods due to excessive bending. Based on the tolerable error in the recorded depth, some allowance may still be affordable, and thus an inclinometer may be omitted up to a certain penetration depth. For most CPT operations, the maximum allowable depth without an inclinometer is about 15 m (49.2 ft). For deeper soundings, inclinations should be continuously noted so that the required corrections can be made to the depth records. Additionally, when sudden deflections are confirmed, penetration should be stopped immediately to avoid any permanent damage to the penetrometer and the rods.

1.4.6 Additional Corrections to Depth Records

An important consideration warranting attention is the fact that each sensor in the penetrometer practically advances at a slightly different depth (see Figure 1.4, Figure 1.5 and Figure 1.7). Therefore, appropriate corrections should be routinely implemented to the single depth value being recorded for each set of q_c, f_s, u_2, and V_s readings.

1.4.7 Practice for Post-CPT Sounding Treatment of Test Site

Depending on the site conditions and project requirements, the procedure for closing the hole created by a CPT sounding is established by the local governing agencies. The main purpose behind the closure of the hole is to minimize the short- and long-term damage and/or contamination due to water and contaminant ingress. The holes can either be filled with pea gravel/sand or bentonite slurry/lean grout made from Portland cement using a simple surface pour method (or through

tremic pipes) or grouted during the withdrawal of special CPT systems.

1.5 CPT Soundings as Part of Overall Site Investigation

Every geotechnical project requires a site-specific investigation to collect data regarding the subsurface conditions. This is because the ground conditions beneath a given property location are unique and totally different when compared to another property location. Therefore, site investigations must be undertaken to determine the underlying strata, their depth and thickness, groundwater conditions, types of geomaterials, and the associated engineering parameters needed for geotechnical design.

Conventional site exploration programs have been accomplished using traditional rotary drilling methods to create boreholes in order to obtain small split-spoon drive samples. Additional information can be gained from the use of geophysical techniques and/or deployment of *in situ* probes to measure specific soil parameters. These include vane shear testing (VST) in clay layers for estimation of undrained shear strength, pressuremeter testing (PMT) for modulus determination, packer testing (PKT) for measuring hydraulic conductivity, and crosshole testing (CHT) to evaluate shear wave velocity, which is used in seismicity studies and dynamic analyses. The borings are also used to extract "undisturbed" thin-walled tube samples that are transported to the laboratory for testing in consolidometers, triaxial cells, permeameters, direct shear boxes, and resonant column apparatuses. However, laboratory testing can take weeks, sometimes months, to obtain information about the compressibility, hydraulic conductivity, shear strength, and stiffness characteristics of each soil layer at the site.

Although such an elaborate program can produce the necessary information regarding geostratification and soil engineering properties, it does so at great cost and time. In fact, the full suite of field testing, geophysics, and laboratory testing is so expensive and of such long duration that a program of this level can only be afforded on relatively large-scale projects with substantial budgets and lengthy schedules. For small- to medium-size geotechnical projects, the economies of time and money restrict the amount of exploration and testing that can be afforded, even though the engineering analyses demand a thorough knowledge regarding the site-specific geomaterials present below the ground. In those instances, the budgets for many investigations are cut back so severely that insufficient information is usually obtained. A common occurrence is the utilization of a single measurement, such as the SPT blow count, but the consequence is that undue conservatism is adopted in design to offset the poor quality and low reliability of the data, thereby producing foundation solutions that are unnecessarily expensive for the construction of new facilities.

An alternative to conventional exploration practices is to use direct-push technologies, particularly the cone penetrometer test (CPT) and its various derivatives, such as the piezocone test (CPTu), the seismic piezocone test (SCPTu), and the inclusion of monitored dissipations of pore pressures with time at select depths. Moreover, the penetration test data are recorded digitally, continuously, and directly to a computer for immediate post-processing so that on-site decisions can either be made instantly by the geotechnical engineer or sent by wireless transmission immediately to the main office for review and consideration. It is, however, important to understand that despite the myriad of advantages provided by the CPT and its derivatives, most large-scale infrastructure projects will always require an integrated approach toward subsurface investigations. This integration includes geological mapping, conventional boring and sampling for laboratory validation of important soil properties, geophysical testing, and *in situ* probing via alternative direct-push tools, of which the CPT is the most versatile.

1.6 Summary

In this chapter, a brief historical background of the development of the CPT is provided. This is followed by an explanation of the various components of the modern SCPTu system, the standards for testing procedures, and the basics of data interpretation. The need for proper maintenance of the penetrometer, calibration of the sensors within the penetrometer, and important precautions are discussed to ensure the quality performance of CPT systems throughout their design life and the desired accuracy and precision of the test data. Finally, the applicability and relevance of the CPT system within the overall program of site investigations are discussed.

This chapter does not serve as a specification document. By nature, even a specification document cannot be absolutely prescriptive. With the essentials of the equipment components, testing procedures, calibration, maintenance, and precautions for good CPT implementation covered in this chapter, it is up to the engineer responsible for the test to tailor the document to the specific needs of the project and make decisions regarding the precision desired in the test data and the accuracy in estimation of geotechnical design parameters from CPT results.

2. ESTIMATION OF SOIL VARIABLES FROM CPT RESULTS

2.1 Overview

Since the introduction of cone penetration test in geotechnical engineering practice, its use has grown to a wide variety of applications including estimation of bearing capacity, design of shallow and deep foundations, walls and embankments, assessment of ground improvement and soil liquefaction, as well as a variety of geo-environmental applications. However, site characterization including simple visual interpretation of the subsurface soil profiles from the CPT data to more detailed stratigraphic logging and preliminary evaluation of geotechnical properties and parameters are still the primary purposes of the CPT.

Included in this chapter are the recommended formats for presentation of CPT/CPTu/SCPT data, their interpretations towards determining the subsurface stratigraphy (i.e., identification of geomaterials, layering, and formal classification based on well-established systems of soil behavior type), and of soil properties and parameters using well-established correlations. To benefit from the information provided in this chapter, it is important to have also reviewed the relevant information presented in Chapter 1.

This chapter has been organized in a manner that each subsection presents interpretations for a particular geotechnical engineering parameter. Each subsection includes limited selective yet mandatory description, and discussions regarding source data and the applicability of each correlation presented therein. For convenience in the use of information presented in this chapter, a comprehensive summary table is included at the end of each subsection, which provides the following information.

- Sets of correlative expressions for the variety of soil types.
- References to figure numbers of the applicable graphs and charts of that subsection or of this chapter.
- Information regarding source geomaterials and the types of CPT equipment used in developing those expressions.
- References to the original sources of respective methods or correlations.
- Comprehensive explanations of every symbol presented in each individual summary table along with mathematical expressions for their calculations.

Each table has been developed as an all-encompassing and stand-alone information source for convenient use towards estimating the geotechnical design parameter presented therein. However, the significant descriptive sets of information offered in each subsection preceding those summary tables are mandatory to be reviewed for the correct use of those interpretive methods, correlations, expressions, and graphs for estimating various parameters. It may also be noted that in many cases multiple correlations are presented for evaluating the same parameter and for the same soil type. This required redundancy for an indirect investigation method like CPT is considered useful to obtain a probable range of values. Convergence of those separate evaluations offers confidence in the interpretations, whereas contrast signifies the need for additional investigations.

The following is a list of the comprehensive summary tables from each subsection detailing its respective soil parameter.

- Void ratio: Table 2.3 (Subsection 2.3.1)
- State parameter: Table 2.4 (Subsection 2.3.2)
- Unit weight: Table 2.5 (Subsection 2.3.3)
- Shear wave velocity: Table 2.7 (Subsection 2.3.4)
- Relative density of coarse-grained soils: Table 2.8 (Subsection 2.3.5)
- Effective stress friction angle: Table 2.9 (Subsection 2.3.6)
- Stress history, including preconsolidation stress and overconsolidation ratio: Table 2.10 (Subsection 2.3.7)
- Rigidity index: Table 2.11 (Subsection 2.3.8)
- Geostatic lateral stress: Table 2.12 (Subsection 2.3.9)
- Undrained shear strength including peak and remolded strengths, and sensitivity of fine-grained soils: Table 2.14 (Subsection 2.3.10)
- Soil stiffness, including Young's, Shear, Constrained Moduli, and modulus reduction schemes: Table 2.17 (Subsection 2.3.13)
- Coefficient of consolidation: Table 2.20 (Subsection 2.3.14)
- Coefficient of permeability (hydraulic conductivity): Table 2.24 (Subsection 2.3.15)

In addition, a variety of CPT-based Soil Behavior Type (SBT) classification systems (charts and tables) are presented in Appendix A to this Chapter. The need for including these many SBT charts and tables develops from the fact that many soil variables are directly correlated to different SBT systems. Such correlations are presented in their respective subsections. For easy reference to the relevant SBT systems, the figure and table numbers of such graphs and tables from Appendix A are also included in the summary tables. Review of this appendix is, therefore, also considered valuable for convenient use of this chapter.

Finally, as part of this manual, a Microsoft Excel spreadsheet solution has been prepared for direct implementation of the correlations presented in different subsections (and in the tables listed above). The graphs or charts presented in this chapter are also available in digitized format in Microsoft Excel. This offers convenience in interpretations during the post-processing phase of the CPT data towards retrieving information of the subsurface profiles and evaluating various geotechnical engineering parameters required for range of design problems. A deliberate effort has been made to redraw and develop each graph and chart with all the relevant information in order to minimize the need for referring to the applicable details from the respective sections. The procedural steps for convenient use of the Excel spreadsheet solution are given in Appendix B.

2.2 Geostratification

2.2.1 Data Presentation

Since CPT data are logged at a nearly continuous rate during penetration of the probe, proper presentation of the recorded readings can provide good insight into the subsurface soil profile including changes in the strata and delineation of the soil layers. A preferred approach is to present multiple readings of cone resistance, sleeve resistance and pore pressure on independently plotted side-by-side graphs with those data shown on their respective abscissa axes while consistent depths (or elevations) on the ordinate axes. Here, the corrected cone resistance should always be preferred over the measured value for reasons explained in Chapter 1. It is also helpful to plot the profile of hydrostatic pore pressure (u_0) on the graph of the CPTu measured pore pressure. This is possible if two conditions are satisfied: (1) depth to the ground water table (z_w) is known, and (2) the ground water regime is established as an unconfined aquifer. In this case, the u_0 can be calculated from: $u_0 = (z - z_w)\,\gamma_w$, where z = depth in question, γ_w = unit weight of water = 9.81 kN/m^3 = 62.4 pcf. Another plot of an important CPT parameter, i.e., the friction ratio [$FR = f_s/q_t$ (%)], is often useful in geostratification. This parameter is often used as a simple index to identify soil type.

Selection of appropriate scales and units while plotting the data is another important consideration for easier post-processing and interpretations. Typically, cone resistance measurements are few orders of magnitude greater than the sleeve resistance. The same could be true for CPTu measured pore pressures in clayey soils. Thus, in SI units, cone resistance (q_c, q_t) and pore pressure (u_1 or u_2 and u_0) data are better presented in either megapascals (MPa) or kilopascals (kPa) (1 MPA = 1,000 kPa = 1,000 kN/m^2) and sleeve resistance (f_s) is commonly presented in kPa, while depth (z) in meters. In English Engineering units, cone resistance (q_c, q_t) and pore pressure (u_1 or u_2 and u_0) may be expressed in the units of kilopound per square foot (ksf) or tons per square foot (tsf– US short), sleeve resistance (f_s) in pound per square foot, (psf) or kilopound per square foot (ksf), and the depth in feet. Here the appropriate units' conversions must be employed with due care.

Examples of data presentation are given in numerous figures presented in Chapter 1, and in Figure 2.1.

2.2.2 First Order Interpretation of CPTu Data for Geostratigraphic Evaluation

Before a comprehensive CPT based soil classification system is adopted for formal geostratigraphic profiling, it is possible to perform simple visual interpretations from well-presented graphs of the sounding measurements. However, in order to accomplish such deciphering of the stratigraphic information, it is important to understand the behavior of different types of soils and the ground water to loading introduced by penetration of a CPT or CPTu probe, and the response recorded via its different sensing elements (i.e., the cone, the sleeve, and the porous filter). It should also be noted that the real soil behavior is very complex and challenging to precisely comprehend via a simple soil model. Therefore, due care and experienced judgement must be applied in fully interpreting the CPT data. The following sections provide observations gathered from aggregated previous experience (e.g., Gillespie, 1990; Huntsman et al., 1986; Jefferies et al., 1987; Lunne et al., 1996; 1997; Mayne et al., 1990; Mayne, 2005; 2007a; Robertson et al., 1986; Robertson, 2009; 2016; Schmertmann, 1978b; 1991; Treadwell, 1976).

2.2.2.1 General

- The general hierarchy of the magnitudes of CPT measurements falls along the following order: $q_t > f_s$, $q_t > u$, and $u_1 > u_2 > u_3$.
- The pore pressures generally do not vary significantly along the friction sleeve. Therefore, equal end area friction sleeve should record as approximately equal to f_s.
- The measured pore pressures depend on the position of the filter element. It develops in response to the soil type being penetrated in the immediate area of the sensing filter element. Therefore, during interpretation and post-processing of the measured data, the due consideration must be given to the location of the filter element.
- Besides the position of the filter element, the pore pressures also rely on the ground water level. At depths above that level, pore pressures vary with capillarity, moisture, degree of saturation, among other factors, and should be interpreted with care.
- The measurement of sleeve resistance (f_s) is often less accurate and less reliable than the cone resistance, particularly in soft fine-grained soils.
- The cone resistance, sleeve resistance and pore pressure readings, all tend to increase with increasing depth, primarily due to increasing overburden stress.
- The in-situ horizontal effective stress (σ_h'), which is an indirect indicator of the geologic stress history of the soil deposit, has a dominant effect on the cone resistance and friction resistance.
- The compressibility of soils can significantly influence the cone resistance and friction resistance. Cementation between particles, which is more likely in older soil deposits, reduces compressibility and thereby increases cone resistance.

2.2.2.2 Clay

- The measured values of cone resistance in clays are low (typically, $q_t < 5$ MPa) and indicative of undrained soil response due to low permeability.
- In intact clays below the ground water table, the u_2 values are considerably higher than hydrostatic ($u_2 > u_0$). Soft to medium stiff clays can give very high pore pressures.
- For intact clays, the ratio u_2/u_0 increases with the stiffness according to the following approximate trend.
  - Soft clays: u_2/u_0 may be around $\approx 3 \pm$
  - Medium stiff to stiff clays: $u_2/u_0 \approx 10 \pm$
  - Very hard clays: $u_2/u_0 \geq 30$

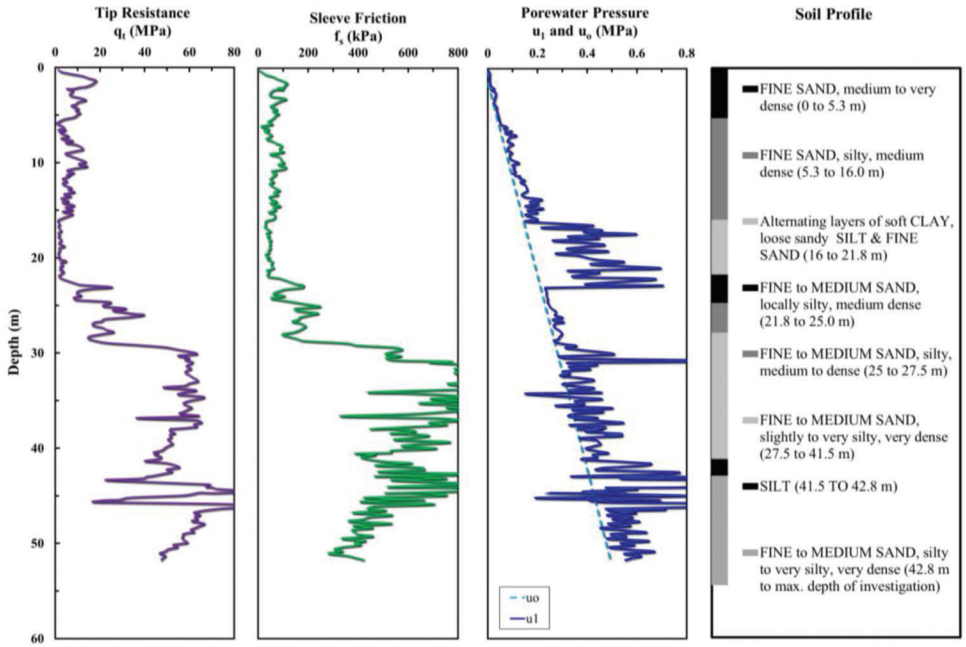

(a)

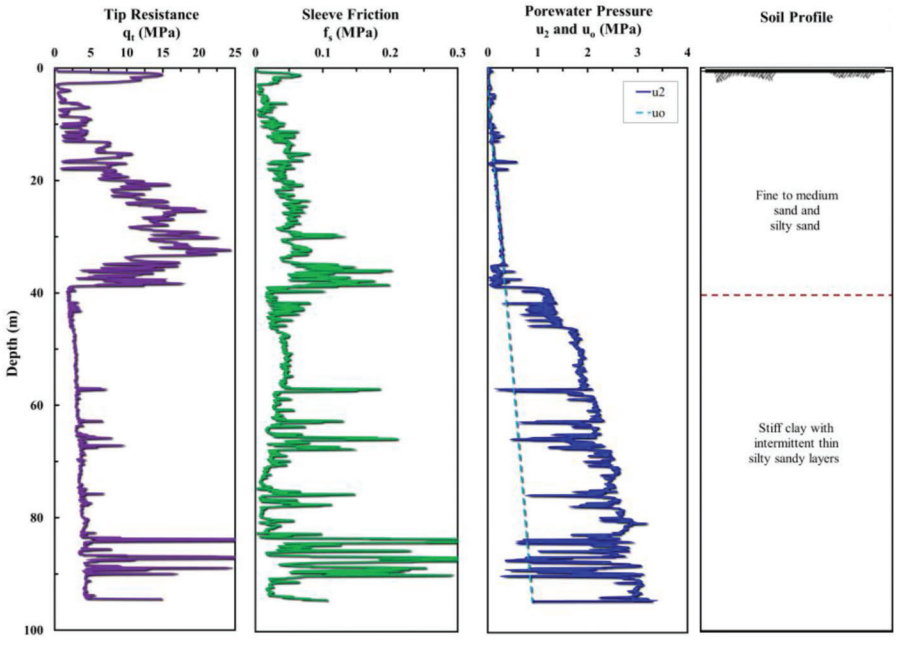

(b)

Figure 2.1 Continued.

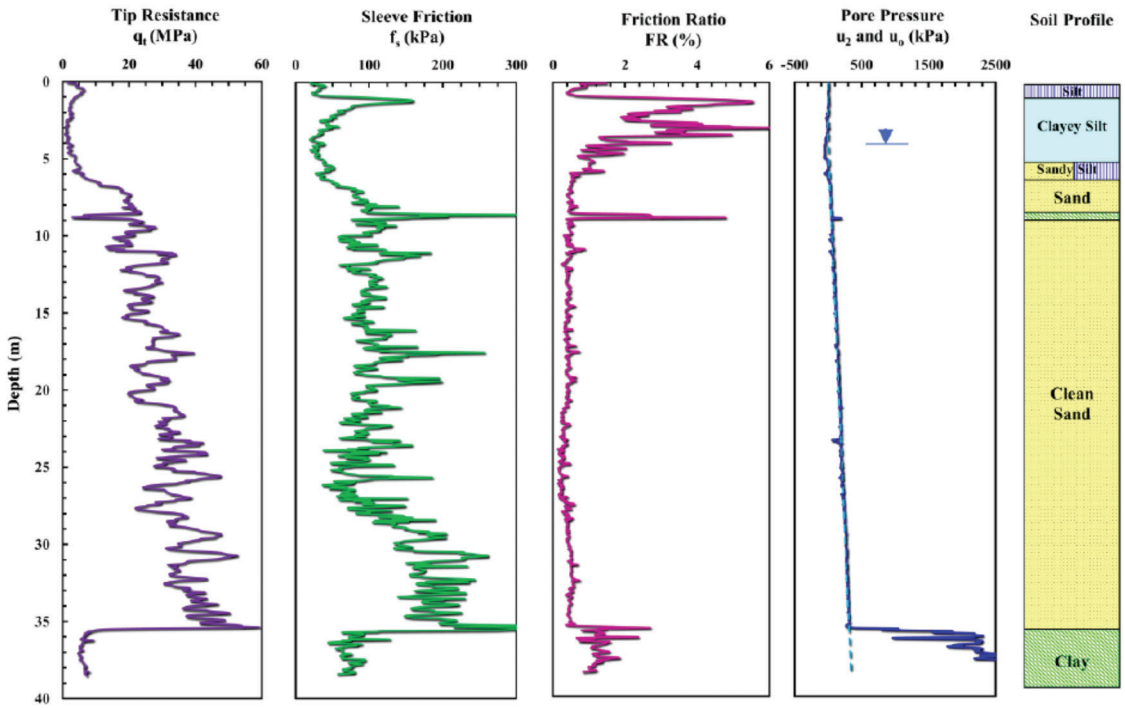

(c)

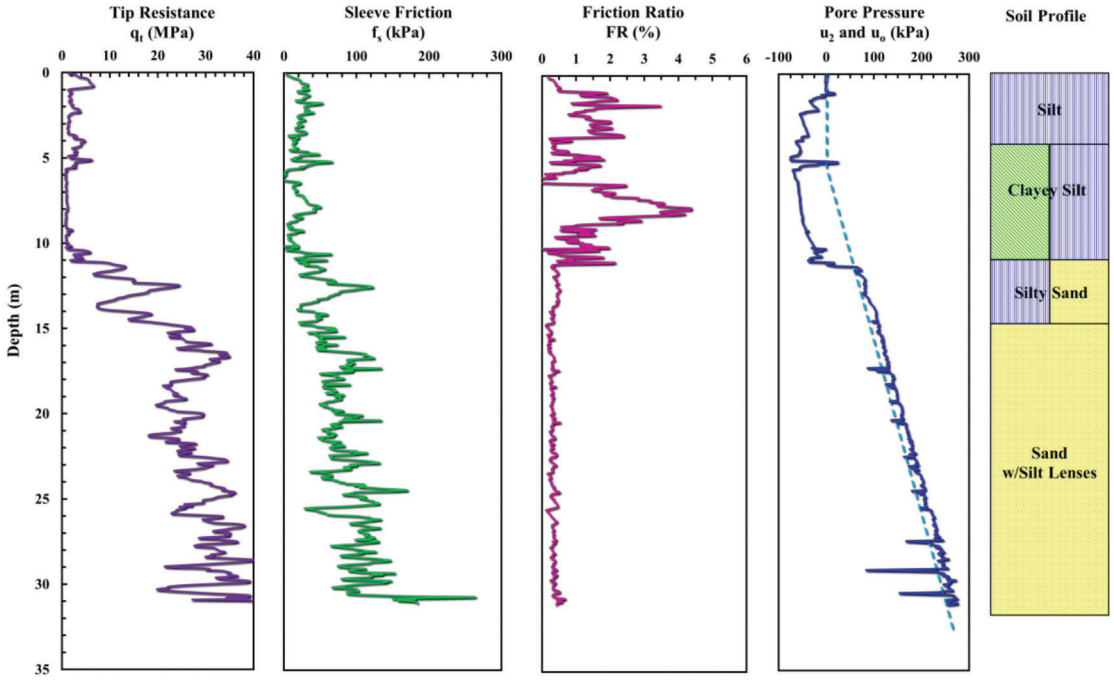

(d)

Figure 2.1 Continued.

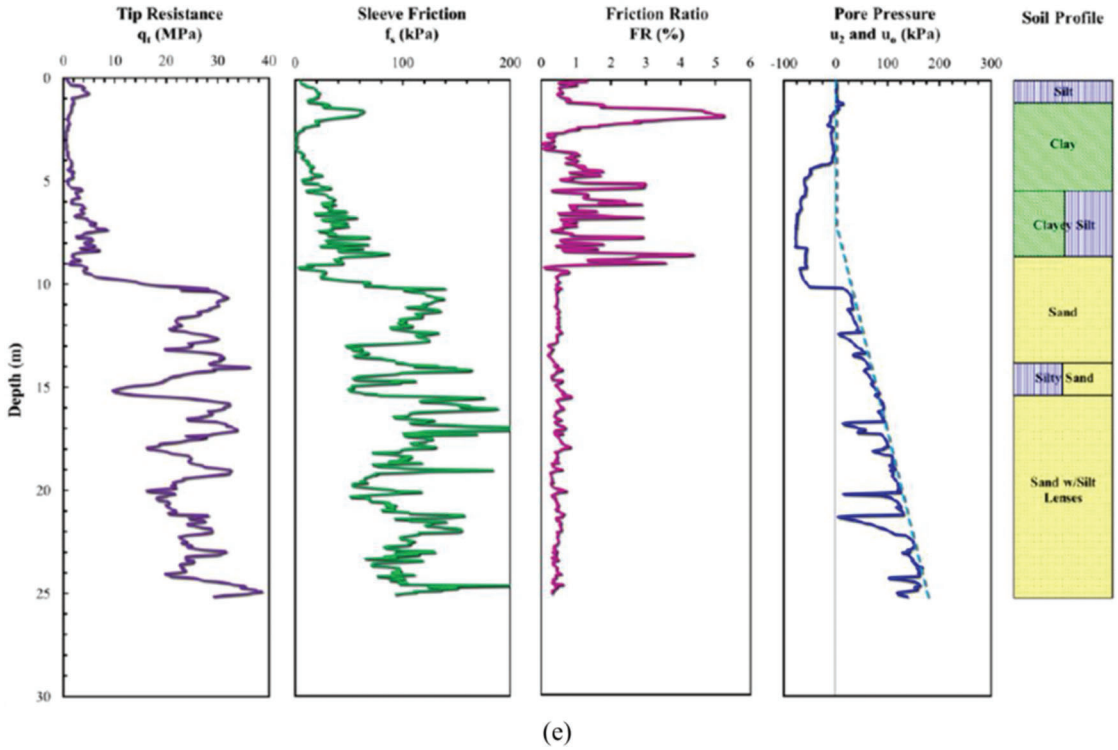

Figure 2.1 CPTu sounding and soil profile: (a) EURIPIDES Test Site, Eemshaven, Netherlands (Niazi et al., 2010b), (b) Golden Ears Bridge South Bank Site, British Columbia, Canada (Niazi et al., 2010a), (c) Bugg-40 test site in Blytheville, AR (Schneider & Mayne, 1999), (d) 3MS617 test site in Blytheville, AR (Schneider & Mayne, 1999), (e) Johnson Farm test site in Southeast, MO (Schneider & Mayne, 1999).

- In very stiff, heavily overconsolidated fissured clays, zero and even negative u_2 pore pressures could be observed.
- For type 1 piezocones, fissured clays can be identified by a low ratio $u_1/q_t < 0.4$. The intact clays exhibit characteristic ratios on the order of $u_1/q_t > 0.7$.
- In clays of low sensitivity, the friction ratios (FR) are typically $> 4\%$.
- In soft sensitive to quick clays, the friction ratio can be quite low, approaching zero in some instances.

2.2.2.3 Silt

- Silts that behave in contractive manner at large strain can produce high positive u_2 pore pressures.
- Silts that behave in dilative manner at large strain can result in low or negative u_2 pore pressures.
- In clayey silts of low sensitivity, the friction ratio (FR) is typically $> 4\%$.

2.2.2.4 Sand

- The measured values of cone resistance in sands are high (typically, $q_t > 5$ MPa), exhibiting the drained strength conditions due to higher permeability.
- In clean saturated sands below the ground water table, the u_2 values are near hydrostatic ($u_2 \approx u_0$).
- Very dense fine or silty sands can give very low or negative u_2 pore pressures.
- In clean quartz sands to siliceous sands, the friction ratios are typically low: $FR < 1\%$.
- Highly compressible sands tend to have low cone resistance and, in some cases, high friction ratio (FR) values, as high as 3%.
- The incompressible quartz sands can have friction ratio (FR) of about 0.5%.

2.2.2.5 Geostratigraphic evaluation from normalized CPTu parameter. In addition to the use of simple measurements of CPTu (i.e., q_t, f_s, and u_2), guidelines are also available for evaluating soil type using an alternate normalized set of parameters as summarized in Table 2.1.

2.2.2.6 Sample soundings and soil profiles. Figure 2.1 illustrates five examples of CPTu soundings and soil profiles obtained at different worldwide sites. It may be specifically noted that the sounding from the first site used type 1 piezocone with filter element at the cone location (u_1 readings), whereas, for the remaining sites, type 2 piezocone with filter element behind the cone (u_2 readings) were employed. The detailed soil profiles shown in the figures, as confirmed from the borings at these respective sites, validate the general and specific observations and rules of thumb outlined above. One important observation that needs due attention is the frequent spikes within the profiles of three readings,

TABLE 2.1
Guidelines for evaluating soil type from normalized CPTu parameters (after Mayne 2005)

Soil Behavior Type	Normalized Cone Stress, $Q_t = q_{t,net}/\sigma'_v = (q_t - \sigma_v)/\sigma'_v$	Normalized Excess Pore Pressure, $U_i = \Delta u/\sigma'_v = (u_{measured} - u_0)/\sigma'_v$	Normalized Friction, $F_R = f_s/q_{t,net} = f_s/(q_t - \sigma_v)$
Clean sand	$Q_t > 40$	$\Delta u/\sigma'_v \approx 0$	$< 1\%$
Intact clay	$Q_t < 20$	$\Delta u_1/\sigma'_v > 3$	Often
		$\Delta u_2/\sigma'_v > 3$	$F_R > 4\%$ but
			$F_R < 2\%$ for
			$S_t > 4$
Fissure clay	$20 < Q_t < 40$	$\Delta u_1/\sigma'_v > 10$	Generally
		$\Delta u_2/\sigma'_v < 0$	$F_R > 4\%$

Note: q_t = corrected cone resistance = $q_c + u_2 (1 - a_n)$; q_c = measured cone resistance; u_2 = shoulder (behind the cone) pore pressure recorded during penetration of piezocone; a_n = cone net area ratio = A_n/A_c; A_n = cross-sectional area of the load cell behind the cone; A_c = projected cone cross-sectional area; Δu = excess pore pressure measured from the piezocone penetrometer = ($\Delta u_2 = u_2 - u_0$) or ($\Delta u_1 = u_1 - u_0$) depending on the location of the filter element; u_1 = apex or mid-face pore pressure recorded during penetration of piezocone; σ'_v = effective vertical overburden stress = $\sigma_v - u_0$; σ_v = total vertical overburden stress = $\Sigma(\gamma_{mi} \bullet z_i)$; γ_{mi} = total unit weight of the i-th soil layer; z_i = thickness of the i-th soil layer; u_0 = hydrostatic pore pressure = $\gamma_w (z - z_w)$; γ_w = unit weight of water; z = depth below the ground surface; z_w = depth of the ground water table; f_s = sleeve resistance; $q_{t,net}$ = net corrected cone resistance = $q_t - \sigma_v$; $U_2 = (u_2 - u_0)/(\sigma_v - u_0)$; Q_t = normalized net corrected cone resistance = $q_{t,net}/\sigma'_v$; F_R = normalized friction ratio = $f_s/q_{t,net}$; CPTu = piezocone penetration test; S_t = soil sensitivity = $s_{u(peak)}/s_{u(remolded)}$.

especially the pore pressure profiles. Two of the physical processes that possibly lead to such readings are: (1) rod breaks when additional one-meter rods are added for the next one-meter penetration allows excess pore pressures to partly dissipate before the penetration is resumed, and (2) presence of thin sand lenses and seams. Therefore, the first order interpretation of the soil profile must be done keeping these additional possibilities into consideration as well. However, all three profiles (i.e., q_t, f_s, u_i, and FR) must be studied together for a bigger picture instead of making their separate assessments.

2.2.2.7 Special considerations

- Due to the possible loss of saturation of the pore pressure element, the "u" measurements for onshore testing are not always accurate and/or repeatable. Indeed, in an onshore sounding, the water table is generally found few to several meters below the ground surface. Therefore, the penetrometer is often required to advance through dry ground before reaching saturated soil. If the dry layer is either clay or dense silty sand, the suction in the unsaturated soil can be sufficient to de-saturate the pore pressure element. Therefore, interpretations of the pore pressure readings from an onshore sounding must be done keeping the q_t, f_s, and the ground water table into consideration.
- The CPTu pore pressure measurements are mostly reliable in offshore setting due to high ambient water pressure that ensures full saturation.
- The cone resistance is influenced by the geomaterial ahead of and behind the penetrating probe. It implies that the advancing cone can detect a change in material type before it reaches the new material, and it continues to feel the effect of the preceding material even when it has penetrated into the new material. Hence, the CPT will not always truly measure the correct mechanical properties in thinly interbedded materials.
- The space surrounding the cone in which it detects an interface increases with the hardness of the material. In materials with softer consistency, the influence zone can be of a low order of twice the cone diameters. In contrast, in very stiff soils this zone can extend as wide and as deep as about 20 cone diameters. Hence, the cone resistance can fully mobilize with much ease within a thin layer of soft soil, representing the true value, compared to that of a thin layer of stiff soil. For instance, while using a standard cone (35.7 mm base diameter, and 10 cm^2 base cross-sectional area), a soft layer thinner than 100 mm can be easily detected by the cone resistance recorded, whereas for the same cone a stiff layer may have to be as thick as $>$ 700 mm for the measured cone resistance to give its true representation. Therefore, sufficient judgement and care must be employed, especially while interpreting cone resistance in a thin stiff clay or a sand layer sandwiched between two adjacent soft clay layers.
- The drainage characteristics of thin layers are also very important for identification of thin layers in sand, silt or clay in a thick body of clay or sand. The response time for a fully saturated piezocone is usually sufficiently fast to observe pore pressure changes for very thin layers ($<$5 mm). Whether or not such thick layers are observed in practice depends on the response of the soil to the advancing cone, the data recording frequency (i.e., depth interval of the data), and the location of the filter.
- The sleeve load cells measure the average frictional resistance along a larger interface between the sleeve and the surrounding soil (i.e., 145.8 cm^2 for a standard 10 cm^2 cone). Therefore, it tends to smooth out the effects of thin layers.
- Besides the suction effects as a cause of negative pore pressures in stiff fissured clays and dense to very dense sands, another plausible explanation is the occurrence of stones (such as in clay till). When the piezocone hits a stone, the stone is pushed aside, and a cavity is formed which creates low pressure or suction recorded as negative on the pore pressure transducer.

2.2.3 CPT-Based Soil Behavior Type Classification Systems

The most common soil classification system used by geotechnical engineers across the world, including

North America, is the one based on textural and physical properties (particle size analysis and plasticity) (e.g., Unified Soil Classification System (USCS)). It is, however, important to understand that the classification systems based on the soil behavior (commonly termed as soil behavior type, SBT classification), such as those derived from CPT, are superior compared to the traditional textural-based systems since they represent the natural in-situ response of the soil to loading with much less disturbance to the soil samples. The traditional system relies on basic index properties measured on remolded samples, leading to considerable uncertainties. Robertson (2009) illustrated with numerous examples that the CPT-based SBT may not always agree with traditional USCS-based soil types and that the biggest difference is likely to occur in mixed soil types (i.e., sand mixtures and silt mixtures).

Fortunately, geotechnical engineers are ultimately interested in the response of soil to loading (alias, soil behavior), rather than classifying it based on the grain-size distribution and plasticity properties only, although knowledge of both is helpful. Realizing the importance of data derived from the soil behavior, many researchers, with the help of extensive world-wide CPT, CPTu, and SCPT soundings, have attempted to develop formal system of classifying the soils and towards delineating the subsurface strata. These include charts/graphs and tables that offer direct method of site-specific soil profiling. For the best use of different methods, it is considered important to understand how these formulations have evolved with increasing understanding of the soil behavior in response to cone penetration.

Appendix A to this chapter presents a comprehensive review of the chronological development of the soil behavior type (SBT) classification systems advanced during the past 55 years of CPT history. A total of 31 methods have been presented along with their respective charts, tables, and significant information regarding their formulation, source data, type of cone, whether each method was an extension of the earlier one(s), and the uniqueness of each method from the previous formats. Since SBT classification system has been one of the most researched areas in the realm of CPT interpretations, and since many of the correlations presented in the later sections of this chapter are founded on these classification systems, a full review of Appendix A is highly recommended for use of this manual in applications. A concise tabulated summary of these methods is given in Table 2.2.

2.2.3.1 Recommendations for the selection of appropriate SBT classification scheme. In general, the soil behavior type response obtained from CPT, CPTu, or SCPT sounding can lead to interpretation of the soil type different from its traditional classification based on grain-size distribution and soil plasticity. However, such interpretation together with other in-situ strength testing, index and basic laboratory testing on selective sampling and conservative design is considered appropriate for a low- to moderate-risk project.

With availability of such a large number of classification schemes, the choice and selection of the most suitable SBT charts is often challenging. In this regard, more recent recommendations based on DeJong et al. (2013), Ganju et al. (2017), Jaeger et al. (2010), Robertson (2016), Salgado et al. (2015), and Schneider et al. (2012) are aggregated below.

- Since the soil behavior can be complex, multiple CPT-based measurements should be applied for improved classification. Classification based on only two measurements (q_t and f_s) are more appropriate for predominately silica-based, young, uncemented soil, while for fine-grained soils, those with three measurements (q_t, f_s, and u_2) provide improved interpretation. Ideally, it should be based on four measurements (q_t, f_s, u_2, and shear wave velocity, V_s) since this allows identification of possible microstructure.
- The charts that present normalized parameters lead to better in-situ soil behavioral interpretations. Since soils are essentially frictional and both strength and stiffness increase with depth, normalized parameters are more consistent with in situ soil behavior.
- The Q_{tn} and F_r charts are useful in the absence of high-quality penetration pore pressure data.
- The Q_{tn} vs. U_2 chart can be helpful in fine-grained soils where CPT penetration is essentially undrained.
- Dissipation tests in both fine-grained soils (with partial dissipation to t_{50} only) and coarse-grained layers (with 100% rapid and cost-effective dissipation) are valuable and recommended (where possible), for the correct determination of the equilibrium pore pressure (u_0).
- In consideration of the geologic history of the deposit, the charts based on Q_{tn} and F_r provide reliable classification for uncemented young soils that are predominately silica-based (e.g., Holocene to Pleistocene age).
- In unfamiliar areas, additional information from the knowledge of local geology, drilling and sampling, or variable rate penetration tests allow for the local calibration of Q_{tn} and F_r soil classification charts.
- The SBT charts should be used in conjunction with the traditional textural-based classification system from the soil samples. The behavioral response reflected in the CPT measurements and the textural characteristics are linked, particularly in soils with little or no microstructure.
- If V_s (and the derivative G_0) data are available from SCPT, the proposed Q_{tn} vs. I_G chart should be used to evaluate the approximate degree of microstructure in a deposit with supporting evidence from the local geology. Here, $I_G = G_0/q_t$ is the small-strain rigidity index.
- The normalized SBT charts are generally not best suited for soils with significant microstructure {i.e., when $K^*_G >$ 330, where K^*_G is the normalized small-strain rigidity index $= [G_o/(q_t - \sigma_v)](Q_{tn})^{0.75}$}.
- Since the SBT charts were developed using data from standard penetration rate (20 mm/s), they are not appropriate for other penetration rates.
- For identification of thin soil layers within a stratigraphic profile, the algorithms proposed by Salgado et al. (2015) and Ganju et al. (2017) are quite useful.
- Sampling and testing are particularly recommended for verification of soil type in intermediate soils.

TABLE 2.2
Summary of SBT classification frameworks

Source	Type of Penetrometer	Site Locations and Soil Types	Presentation Format	Figure/Table	Remarks
Begemann (1965)	Dutch mechanical friction cone penetrometer	250 soundings in Dutch Soil	q_c (arithmetic) ordinate vs. f_s (arithmetic) abscissa	Figure A.1	–
			q_c (logarithmic) ordinate vs. FR (%) (logarithmic) abscissa	Figure A.2	Modified chart by Douglas & Olsen (1981)
Schmertmann (1969)	Dutch mechanical friction CPT	20 soundings in N-Central Florida	Tabulated interpretations	Table A.1	Also recorded in Schmertmann (1966; 1967)
Sanglerat et al. (1974)	Andina mechanical friction CPT (80 mm diameter)	Several hundred soundings in Rhône-Alps region of France, the Netherlands, Taiwan (formerly Formosa) and Indonesia	q_c (logarithmic) ordinate vs. FR (%) (arithmetic) abscissa	Figure A.3	Data analyzed at the Ecole Centrale of Lyons
Schmertmann (1978b)	Dutch mechanical friction CPT	CPT soundings in North-Central Florida	q_c (logarithmic) ordinate vs. FR (%) (arithmetic) abscissa	Figure A.4	
			q_c (logarithmic) ordinate vs. f_s (logarithmic) abscissa	Figure A.5	Modified chart by Fellenius & Eslami (2000)
Searle (1979)	Dutch static penetration friction jacket tests	Schmertmann data plus assortment of data from worldwide case histories	q_c (logarithmic) ordinate vs. FR (%) (logarithmic) abscissa	Figure A.6	The chart also provides solutions for estimation of φ', D_R and c_u
Douglas & Olsen (1981)	Electric friction CPT (10 cm^2)	Several sites in California, Oklahoma, Utah, Arizona, and Nevada	q_c (logarithmic) ordinate vs. FR (%) (arithmetic) abscissa	Figure A.7	
Jones et al. (1981)	Electric CPTu (10 cm^2)	Mine tailings and natural normally consolidated materials (soft, highly plastic clays to dense medium grained sands)	$\Delta u_2/u_0$ (arithmetic) ordinate vs. $q_{c,net}/\sigma_v$ (arithmetic) abscissa	Figure A.8	Study on mine tailing characterization
Jones & Rust (1982)	Electric CPTu (10 cm^2)	Mine tailings and natural normally consolidated materials (soft, highly plastic clays to dense medium grained sands)	Δu_2 (arithmetic) ordinate vs. $q_{c,net}$ (arithmetic) abscissa	Figure A.9	Study on mine tailing characterization
			Δu_2 (arithmetic) ordinate vs. $q_{c,net}$ (logarithmic) abscissa	Figure A.10	Scale adjustment by Vermeulen & Rust (1995)
Vos (1982)	Electric friction CPT (10 cm^2)	CPT soundings in Dutch soils	Tabulated interpretations	Table A.2	
Olsen (1984)	Electric friction CPT (10 cm^2)	Large scale laboratory chamber tests on fine to coarse sands, and soil mixtures	q_{cn} (logarithmic scale) ordinate vs. f_{s1} (logarithmic) abscissa	Figure A.11	Chart developed in reference to the analysis of liquefaction potential
Senneset & Janbu (1985); Senneset et al. (1989)	Electric CPTu (10 cm^2)	Data from three marine sediment deposits in North Sea, Lake Mjøsa and Trondheim, Norway	Tabulated interpretations based on N_m and B_q	Table A.3 & Figure A.12	Theoretical solution verified with data from three sites of marine deposit
			q_t (arithmetic scale) ordinate vs. B_q (arithmetic scale) abscissa	Figure A.13	

Continued

TABLE 2.2
(Continued)

Source	Type of Penetrometer	Site Locations and Soil Types	Presentation Format	Figure/Table	Remarks
Tumay (1985)	Variety of electric CPT and CPTu including different apex angles, cross-sectional areas, & cone types ($q_c + f_s$, $q_c + u_1$, $q_c + u_2$, $q_c + f_s + u_1$)	Data from twelve sites in Louisiana, USA	q_c (logarithmic) ordinate vs. FR (%) (arithmetic) abscissa	Figure A.14	Additional data from the earlier studies by Douglas & Olsen (1981) and Schmertmann (1978b) including sites in California, Oklahoma, Utah, Arizona, and Nevada in the USA
Olsen & Farr (1986)	Electric friction CPT (10 cm^2)	Several sites in California, Oklahoma, Utah, Arizona, and Nevada	q_c (logarithmic) ordinate vs. FR (%) (arithmetic) abscissa	Figure A.15	A modified version of Douglas & Olsen (1981) SBT chart
Robertson et al. (1986)	Variety of electric friction CPTu developed by Fugro, Hogentogler, Geotech & UBC, & pore pressure measured at different locations (u_1; u_2; $u_1 + u_2$; $u_1 + u_2 + u_3$)	Data of soundings from sites mainly near Vancouver, British Columbia, Canada and few others throughout the world	q_t (logarithmic) ordinate vs. FR (%) (arithmetic) abscissa	Figure A.16a	Charts best applicable for depth (z) shallower than 30 m; for $z > 30$ m, use normalize cone resistance q_{t1}: $q_t/(\sigma'_v)^{0.7}$
			q_t (logarithmic) ordinate vs. B_q (arithmetic scale) abscissa	Figure A.16b	
Olsen & Malone (1988)	Electric friction CPT (10 cm^2)	Field and large-scale laboratory chamber CPT data	q_{cn} (logarithmic) ordinate vs. FR_n (%) (logarithmic) abscissa	Figure A.17	Data from Douglas & Olsen (1981), Olsen (1984), Schmertmann (1978b)
Robertson (1990)	Electric CPTu (10 cm^2)	Data of soundings from across the world	Q_t (logarithmic) ordinate vs. F_R (%) (logarithmic) abscissa	Figure A.18a	Data from mostly onshore sites < 30 m deep (most data from Robertson et al., 1986)
			Q_t (logarithmic) ordinate vs. B_q (logarithmic) abscissa	Figure A.18b	Data from mostly onshore sites < 30 m deep
Jefferies & Davies (1991)	Electric CPTu (10 cm^2)	Data from offshore sites in Canadian Beaufort Shelf consisting of very stiffer silty clay sediments	Q_t $(1 - B_q)$ (logarithmic) ordinate vs. F_R (%) (logarithmic) abscissa	Figure A.19	Improvement of Robertson (1990) chart
Robertson (1991)	Electric CPTu (10 cm^2)	Data from Robertson (1986; 1990) and Jefferies and Davies (1991)	Q_t (logarithmic) ordinate vs. B_q (logarithmic) abscissa	Figure A.20	Onshore and offshore applications
Larsson & Mulabdic (1991)	Electric CPTu (10 cm^2)	Data from soundings in Swedish clays, Norway, and UK	$q_{t,net}$ (arithmetic) ordinate vs. B_q (arithmetic) abscissa	Figure A.21	The chart was originally developed of estimation of the unit weight of soil
Jefferies & Davies (1993)	Electric CPTu (10 cm^2)	Data from offshore sites in Canadian Beaufort Shelf consisting of very stiffer silty clay sediments	Q_t $(1 - B_q)$ (logarithmic) ordinate vs. F_R (%) (logarithmic) abscissa	Table A.4 & Figure A.22	A continuum approach of fitting an equation for $I_{c(J\&D93)}$ to the trend of SBT
Olsen & Mitchell (1995)	Electric friction CPT (10 cm^2)	Extensive field and large-scale laboratory chamber CPT data	Q_c (logarithmic) ordinate vs. FR (%) (logarithmic) abscissa	Figure A.23	Improvement of Olsen and Malone (1988) SBT chart

Continued

TABLE 2.2
(Continued)

Source	Type of Penetrometer	Site Locations and Soil Types	Presentation Format	Figure/Table	Remarks
Robertson & Fear (1995)	Electric SCPT	Data from across the world	Q_t (logarithmic) ordinate vs. I_G (logarithmic) abscissa	Figure A.24	Developed to include unusual soils (cemented & aged), compressible sands, and clays with low and high void ratios
Eslami & Fellenius (1997)	Mechanical and electric CPT and CPTu	Data from 20 worldwide sites in Australia, Belgium, Brazil, Canada, France, Iraq, Italy, Japan, the Netherlands, Norway, Taiwan, UK, USA, and Yugoslavia	q_E (logarithmic) ordinate vs. f_s (logarithmic) abscissa	Figure A.25	One-half of the cases are from CPTu. Non-CPTu tests are from sandy soils and were used with the assumption that u_2 values are approximately equal to u_0.
Robertson & Wride (1998)	Electric CPTu (10 cm^2)	Data from across the world	Q_{tn} (logarithmic) ordinate vs. F_R (%) (logarithmic) abscissa	Table A.5 & Figure A.26	A continuum approach of fitting an equation for $I_{c(R\&W98)}$ to the trend of SBT
Ramsey (2002)	Electric CPTu (10 cm^2 and 15 cm^2) with pore pressure measurements at different locations (u_1, u_2, u_1+u_2)	Database from Quaternary soils in the North, Norwegian and Irish Seas (excluding soils in zones 1 and 2)	Q_t (logarithmic) ordinate vs. F_R (%) (logarithmic) abscissa Q_t (logarithmic) ordinate vs. B_q (logarithmic) abscissa	Figure A.27a Figure A.27b	Reliability in zones 1 & 2 is tentative only; for non-calcareous Quaternary & Tertiary soils; Q_t - B_q chart identifies thin secondary layers & inclusions within primary soil type; Q_t - B_q chart unreliable for gravel inclusions within clay
Jefferies & Been (2006)	Electric CPTu (10 cm^2)	Same data as for Jefferies and Davies (1998)	Q_t $(1 - B_q) + 1$ (logarithmic) ordinate vs. F_R (%) (logarithmic) abscissa	Table A.6 and Figure A.28	To account for soft sensitive clays where B_q greater than 1.0
Schneider et al. (2008)	Electric CPTu (10 cm^2 and 15 cm^2) with pore pressure measurements at different locations (u_1, u_2, u_1+u_2)	Database of clay, sand, silt, and varietal clay sites from Australia, Bangladesh, Canada, Sweden, and the Netherlands, North Sea, Norway, UK, USA	Q_t (logarithmic) ordinate vs. U_2 (logarithmic) abscissa Q_t (logarithmic) ordinate vs. U_2 (arithmetic) abscissa Q_t (logarithmic) ordinate vs. B_q (arithmetic) abscissa	Figure A.29a Figure A.29b Figure A.29c	Q_t vs. B_q space tends to provide detail for separating clay behavior, whereas Q_t vs. U_2 space is more useful for identifying sands, silts and clays, or soil type
Robertson (2009)	Electric CPTu (10 cm^2)	Data same as Robertson (1990; 1991)	Q_{tn} (logarithmic) ordinate vs. F_R (%) (logarithmic) abscissa	Figure A.30	Stress normalization exponent, $n = 0.381\ [I_{c(R\&W98)}] + 0.05\ (\sigma'_v/p_A) - 0.15 \leq 1.0$
Schneider et al. (2012)	Electric CPTu (10 cm^2 and 15 cm^2) with pore pressure measurements at different locations (u_1, u_2, u_1+u_2)	Database of clay, sand, silt, and varietal clay sites from Australia, Bangladesh, Canada, Ireland, Italy, Sweden, and the Netherlands, North Sea, Norway, UK, USA	Q_t (logarithmic) ordinate vs. F_R (%) (logarithmic) abscissa Q_t (logarithmic) ordinate vs. U_2 (arithmetic) abscissa	Figure A.31a Figure A.31b	Slight modification of soil types within selected zones from Schneider et al. (2008)
Salgado et al. (2015); Ganju et al. (2017)	Tumay (1985) database	Tumay (1985) database	q_c/p_A (logarithmic) ordinate vs. FR (%) (arithmetic) abscissa	Figure A.32	Modified Tumay chart
	Robertson (1990) database	Robertson (1990) database	Q_t (logarithmic) ordinate vs. F_R (%) (logarithmic) abscissa	Figure A.33	Modified Robertson chart

Continued

TABLE 2.2
(Continued)

Source	Type of Penetrometer	Site Locations and Soil Types	Presentation Format	Figure/Table	Remarks
Robertson (2016)	Electric cones of either 500, 1,000, or 1,500 mm^2 area at the standard penetration rate of 20 mm/s.		Q_{tn} (logarithmic) ordinate vs. I^*_G (logarithmic) abscissa	Figure A.34	
			Q_{tn} (logarithmic) ordinate vs. F_R (%) & Q_{tn} (logarithmic) ordinate vs. f_{s1} (logarithmic) abscissa	Figure A.35a & A.35b, & Table A.7	
			Q_t (logarithmic) ordinate vs. U_2 (arithmetic) abscissa	Figure A.36, & Table A.8	
Le Doan (2019)	CPT based analytical approach	For normally consolidated reconstituted or recent deposit	Based on $I_{c(R\&W98)}$ and Q_{tn}		F_R is not required for this method

Note: q_c = measured cone resistance; f_s = sleeve resistance; u_1 = apex or mid-face pore pressure recorded during penetration of piezocone; u_2 = shoulder (behind the cone) pore pressure recorded during penetration of piezocone; Δu_2 = excess pore pressure recorded at the shoulder during penetration of piezocone = $u_2 - u_0$; u_0 = hydrostatic pore pressure = $\gamma_w (z - z_w)$; γ_w = unit weight of water; z = depth below the ground surface; z_w = depth of the ground water table; $q_{c,net}$ = net measured cone resistance = $q_c - \sigma_v$; σ_v = total vertical overburden stress = $\Sigma(\gamma_{mi} \bullet z_i)$; γ_{mi} = total unit weight of the i-th soil layer; z_i = thickness of the i-th soil layer; n = stress normalization exponent; f_{s1} = normalized sleeve friction = f_s/σ'_v; CPT = cone penetration test; CPTu = piezocone penetration test; q_t = corrected cone resistance = $q_c + u_2 (1 - a_n)$; a_n = cone net area ratio = A_n/A_c; A_n = cross-sectional area of the load cell behind the cone; A_c = projected cone cross-sectional area; q_{cn} = normalized measured cone resistance = $q_c/(\sigma'_v)^n$; σ'_v = effective vertical overburden stress = $\sigma_v - u_0$; $N_m = q_{t,net}/(\sigma'_v + a)$; a = in-situ attraction; $q_{t,net}$ = net corrected cone resistance = $q_t - \sigma_v$; Q_{tn} = normalized net corrected cone resistance = $[(q_t - \sigma_v)/p_A](p_A/\sigma'_v)^n$; F_R = normalized friction ratio = $f_s/(q_t - \sigma_v)$; FR_n = modified normalized friction ratio = $(f_s/q_c)/[1/(\sigma'_v)^{(1-n)}]$; I_G = rigidity index = G_0/q_t; I^*_G = modified rigidity index = $G_0/(q_t - \sigma_v)$; G_0 = small strain shear modulus = $\rho_m V_s^2$; ρ_m = total mass density of soil = γ_m/g_a; g_a = gravitational constant = 9.81 m/s^2; V_s = shear wave velocity; q_E = effective cone resistance = $q_t - u_2$; Q_c = normalized net measured cone resistance = $(q_c - \sigma_v)/(\sigma'_v)^c$; c^* = variable stress exponent based on the "Stress Focus" concept (by Olsen and Mitchell, 1995); U_2 = normalized excess shoulder pore pressure = $(u_2 - u_0)/\sigma'_v$; p_A = reference atmospheric pressure = 100 kPa; FR = friction ratio = fs/qc (based on the measured cone resistance) or f_s/q_t (based on the corrected cone resistance); $B_q = \Delta u_2/q_{t,net} = (u_2 - u_0)/q_{t,net}$; Qt = normalized net corrected cone resistance = $q_{t,net}/\sigma'_v = (q_t - \sigma_v)/\sigma'_v$.

2.3 Interpretation of Soil Parameters

Soils are complex materials with diverse mineralogical compositions, and geologic origins that have experienced the evolving environmental and climatic conditions during their formation processes. Accordingly, their non-linear stress-strain-strength response is fairly complicated based on stress history, dimensional anisotropy, drainage regime and characteristics, presence of structures due to ageing and cementation, and fissuring etc., with yet an additional aspects of strain rate of loading. Mayne et al. (2009) provided a comprehensive list of parameters that have been defined by the geoengineering profession to completely portray the soil behavior. These parameters fall under three categories (indices, state, and mechanical properties and parameters) as outlined below.

The index parameters provide a measure of the compositional makeup and components of the soil mass. They include the following.

- Origin
- Geological Age
- Grain Sizes
- Mineralogy
- Plasticity
- Shape
- Sphericity/roughness
- Angularity
- Packing limits (e_{max} and e_{min})

The state parameters represent the packing arrangement and stress reflecting the long-term geostatic conditions. These are sometimes denoted by symbol accompanied by a subscript "0" representing the initial state prior to loading. They include the following.

- Void ratio, e_0
- State parameter, ψ
- Unit weight, γ_m
- Relative density, D_R
- Vertical stress, σ_v
- Hydrostatic pore pressure, u_0
- Degree of saturation, S
- Geostatic lateral stress coefficient, $K_0 = \sigma_h'/\sigma_v'$
- Cementation
- Intact or fissured

The mechanical type of material parameters and properties that the deformations behavior and stability of the soils upon loading. Examples of such parameters include the following.

- Hydraulic conductivity (or permeability) represented by its coefficient k_v, k_h.
- Compressibility (recompression index (C_r), yield stress ratio (σ_y', YSR), preconsolidation ratio (σ_{vp}', OCR), coefficient of consolidation (c_v), virgin compression (C_c), swelling index (C_s)).
- Stiffness {shear stiffness ($G_0 = G_{max}$), shear modulus (G), elastic modulus (E), constrained modulus (D'), Poisson's ratio (ν), non-linearity [G/G_0 versus shear strain (γ_s)]}.
- Strength (drained and undrained. shear strength (τ_{max}), Peak (s_u, c', ϕ'), post-peak, remolded/softened/critical state, residual, cyclic).

The ideal approach for a comprehensive site characterization would require a detailed program of drilling, boring, sampling, in-situ testing, geophysics, and laboratory testing. From a practical perspective, most geotechnical projects do not have the desired time and money to perform such extensive series of investigations. CPT, with its modern variants (CPTu and SCPTu), provide extensive subsurface information, and thereby offer a unique opportunity to assess values for a suite of soil engineering parameters commonly used in geotechnical analysis and design.

In this section, a review of methodologies and correlations is presented towards the evaluation and assigning of values for geomaterial parameters. In nearly all cases, multiple sets of correlations/expressions/methodologies are summarized herein, realizing in some cases that redundancy occurs when two or more readings are used to interpret the same parameter. Redundancy in many cases is good in helping to home in on a probable range of values, if separate evaluations tend to show convergence. In contrast, discrepancies and conflicts in the various interpretations from the different expressions should be considered a "red flag." In such cases, the geotechnical practitioner might wish to request additional laboratory and/or in-situ testing to help resolve these difficulties and explain the contrasts.

2.3.1 Initial Void Ratio

A preliminary estimate of initial void ratio (e_0) is necessary for unit weight determinations needed for evaluating the magnitude of overburden stress. Mayne and Rix (1995) compiled a database of 31 clay sites including intact and fissured clays with varied plasticity characteristics ($8 < PI < 300$), sensitivities ($2 < S_t < 200+$), overconsolidation stress states ($1 < OCR < 100+$), and void ratio ($0.4 < e_0 < 11$). By using the data from intact clays only, a correlation between V_s, q_t' and e_0 was developed (also see Figure 2.2). Inversion of that equation allows for the evaluation of e_0 from independent measurements of V_s and q_t from SCPT in intact clays:

$$e_0 = 68 q_t^{0.818} V_s^{-1.88} \qquad \text{(Eq. 2.1)}$$

where, q_t is in kPa and V_s is in m/sec. This equation provides approximate and immediate estimation of e_o in clays where values are not normally known a priori.

Burns and Mayne (1996) developed another relationship via multiple regression analyses on a worldwide database of shear wave velocity:

$$e_0 = 120.9 V_s^{-1.0} z^{0.22} \qquad \text{(Eq. 2.2)}$$

where, V_s is in m/s and depth z is in m, as presented in Figure 2.3.

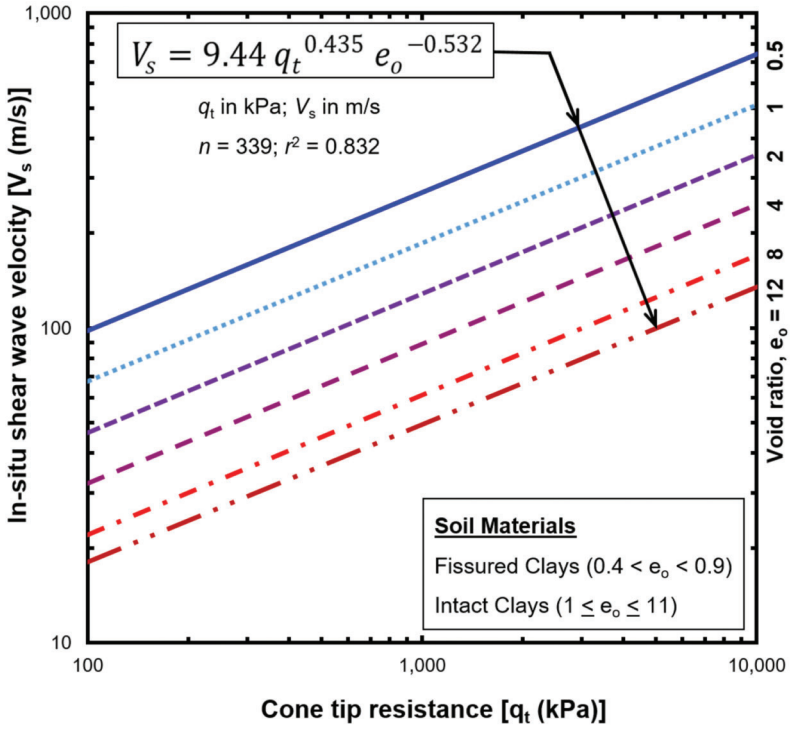

Figure 2.2 Shear wave velocity versus cone tip-resistance correlations in clays (adapted from Mayne & Rix, 1995).

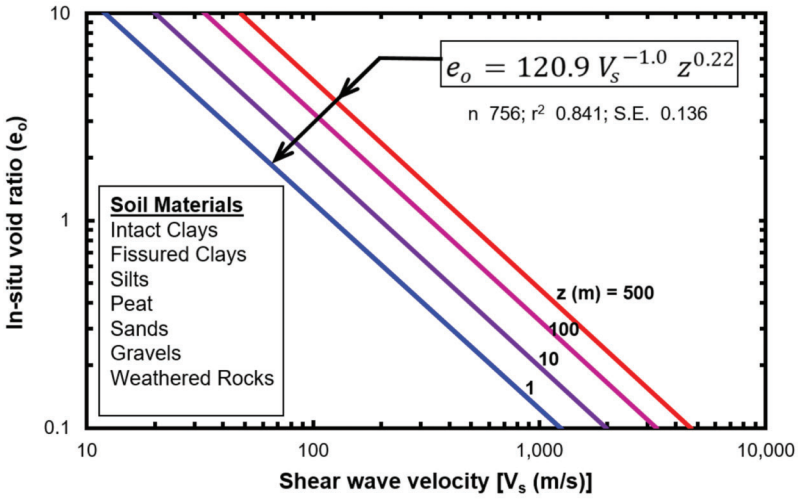

Figure 2.3 First-order void ratio estimates from shear wave velocity (adapted from Burns & Mayne, 1996).

Figure 2.4 shows the relationship between stress normalized shear wave velocity (V_{s1}) and void ratio (e_0) for a wide range of freshly deposited uncemented sand samples in the laboratory (Robertson & Fear, 1995). They approximated this relationship in the form of the following correlation:

$$V_{s1} = (A - Be_0)K_0^{0.125} \qquad \text{(Eq. 2.3)}$$

where $V_{s1} = V_s\,(p_A/\sigma_v')^{0.25}$, A and B are empirical constants, $K_0 = \sigma_h'/\sigma_v'$ = lateral stress coefficient, and p_A = 1 bar = 100 kPa. It should be noted that this linear relationship is limited to a certain range of void ratios. The constants A and B can be developed for site specific conditions, or an average value could be adopted from the database shown in Figure 2.4 as a first order approximation. It should however be used if other condition (K_o, V_s etc.) match to those of the database.

An alternative trend using effective overburden stress (σ_v' in kPa) gave (Mayne, 2005):

$$e_0 = 139.4\ V_s^{-1.08}\sigma_v'^{0.181} \qquad \text{(Eq. 2.4)}$$

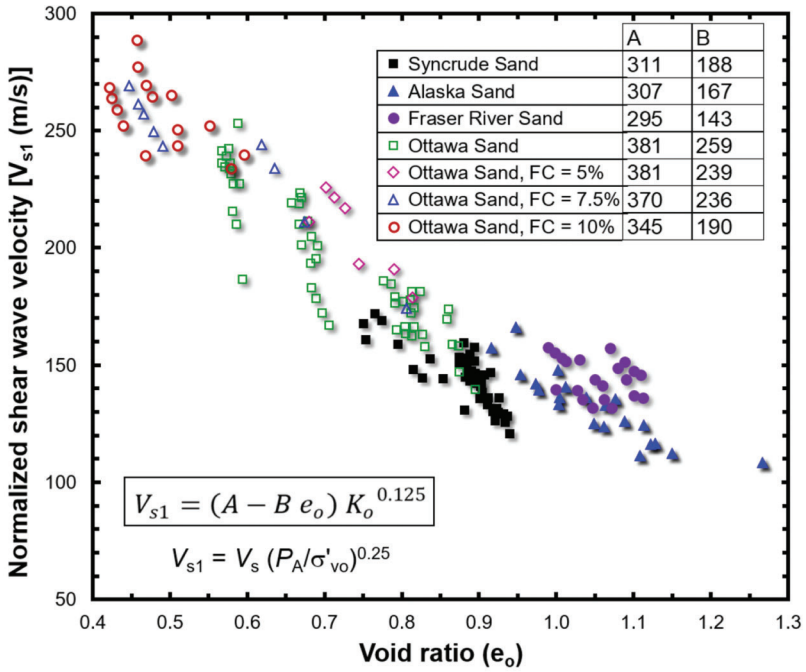

Figure 2.4 Normalized shear wave velocity with void ratio for a range of uncemented sands (adapted from Robertson & Fear, 1995).

TABLE 2.3
Summary of selected correlations between initial void ratio and shear wave velocity from SCPT

Soil Type and General Data Information	Relationship	Reference
A database of 30 intact clay sites with varied plasticity characteristics ($8 < PI < 300$), sensitivities ($2 < S_t < 200+$), overconsolidation stress states ($1 < OCR < 100+$), and void ratio ($0.4 < e_o < 11$)	e_0=68 [q_t (kPa)]$^{0.818}$ [V_s (m/s)]$^{-1.88}$ (also see Figure 2.2)	Mayne & Rix (1995)
Intact and fissured clays, silts, peat, sands, gravel, weathered and intact rocks	e_0=120.9 [V_s (m/s)]$^{-1.0}$ z (m)$^{0.22}$ (also see Figure 2.3)	Burns & Mayne (1996)
Wide range of freshly deposited uncemented sand samples (including Syncrude, Alaska, Fraser River, and Ottawa sites with varying fines content) tested in the laboratory	V_{s1} (kPa)=[A (m/s)–B (m/s) e_0] $K_o^{0.125}$ (also see Figure 2.4)	Robertson & Fear (1995)
Wide range of soils	e_0=139.4 [V_s (kPa)]$^{-1.08}$ [σ'_v(kPa)]$^{0.181}$	Mayne (2005)

Note: e_0 = in-situ void ratio; q_t = corrected cone resistance = $q_c + u_2\ (1 - a_n)$; q_c = measured cone resistance; u_2 = shoulder (behind the cone) pore pressure recorded during penetration of piezocone; a_n = cone net area ratio = A_n/A_c; A_n = cross-sectional area of the load cell behind the cone; A_c = projected cone cross-sectional area; V_s = shear wave velocity; z = depth below the ground surface; $V_{s1} = V_s\ (p_A/\sigma'_v)^{0.25}$; A and B are empirical constants, $K_0 = \sigma'_h/\sigma'_v$ = lateral stress coefficient, and p_A = 1 bar = 100 kPa; σ'_v = effective vertical overburden stress = $\sigma_v - u_0$; σ_v = total vertical overburden stress = $\Sigma(\gamma_{mi} \bullet z_i)$; γ_{mi} = total unit weight of the i-th soil layer; z_i = thickness of the i-th soil layer.

Table 2.3 provides a concise summary of different SCPT-based relationships for estimating e_o.

2.3.2 State Parameter

A parameter applicable fundamentally to coarse-grained (sandy) soils and commonly termed as the soil state parameter (ψ) is defined as the difference between the current void ratio, e and the void ratio at critical state e_{cs}, at the same mean effective stress. It is an important parameter primarily used in assessment of liquefaction potential at a site, yet other significant uses such as estimation of the frictional strength of sandy soils cannot be undermined. The problem of evaluating the state parameter from CPT response is complex and depends on several other soil parameter, including the in-situ horizontal effective stress (σ'_h), in-situ shear stiffness (G_0), shear strength, compressibility and plastic hardening (e.g., Jefferies & Been, 2006).

Accordingly, to Jefferies and Been (2006), a combination of in-situ tests (for σ'_h and G_0) and laboratory tests on reconstituted samples (for shear strength, compressibility and plastic hardening), duly assisted by numerical modeling must be performed for high-risk projects. However, there is a need for simpler estimate of soil state for low-risk projects and in the preliminary screening for high-risk projects. In this regard, Plewes et al. (1992) and Jefferies and Been (2006) provided a means for approximate estimation of soil state using the normalized SBT charts by Jefferies and Davies (1991)

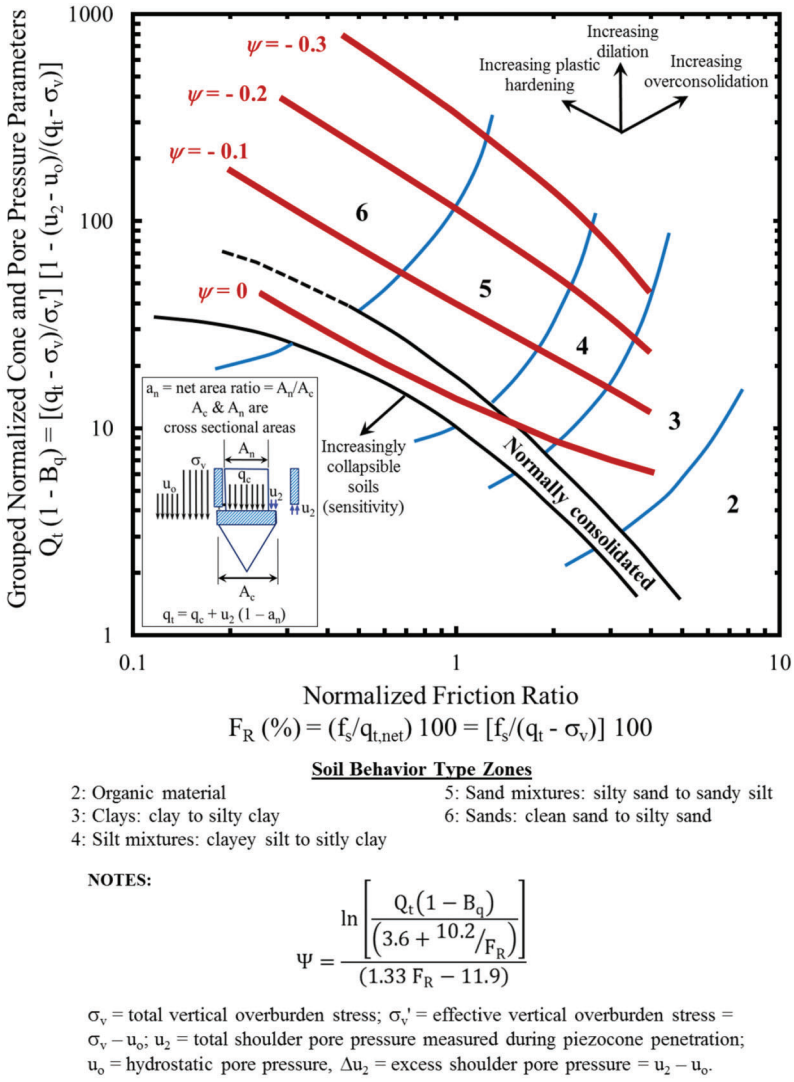

Figure 2.5 Jefferies and Davies (1991) SBT chart with approximate contours of soil state parameter (adapted from Plewes et al., 1992).

(see Figure 2.5) and Jefferies and Been (2006) (see Figure 2.6). The contours of state parameter (ψ) shown in these figures are derived from the following two equations, respectively:

$$\Psi = \frac{\ln\left[\frac{Q_t(1-B_q)}{(3.6+10.2/F_R)}\right]}{(1.33\,F_R - 11.9)} \qquad \text{(Eq. 2.5)}$$

$$\Psi = \frac{\ln\left[\frac{Q_t(1-B_q)+1}{(3.6+10.2/F_R)}\right]}{(1.33\,F_R - 11.9)} \qquad \text{(Eq. 2.6)}$$

where, Q_t = normalized net corrected cone resistance = $(q_t - \sigma_v)/\sigma_v'$; $B_q = \Delta u_2/(q_t - \sigma_v)$; Δu_2 = excess pore pressure recorded at the shoulder during penetration of piezocone = $u_2 - u_0$, and F_R = normalized friction ratio = $f_s/(q_t - \sigma_v)$. It is important to note that these contours are considered approximate since stress state and plastic hardening (not incorporated in these correlations) will also influence the estimate of in-situ soil state in the coarse-grained region of the chart and soil sensitivity for fine-grained soils.

Owing to the lack of accuracy and reliability of Jefferies and Been (2006) normalized parameter [Q_t (1 – B_q) +1] for soft clay highlighted by Robertson (2009), he developed contours of state parameter (ψ) based on the updated SBTn $Q_{tn} - F_R$ chart for uncemented, Holocene-age soils (see Figure 2.7).

Robertson (2010b,c) suggested a simplified and approximate relationship between ψ and the clean sand equivalent normalized cone resistance, $Q_{tn,cs,}$ as follows.

$$\Psi = 0.56 - 0.33\,\log(Q_{tn,cs}) \qquad \text{(Eq. 2.7)}$$

where $Q_{tn,cs}$ is based on a correction factor, K_c, suggested by Robertson and Wride (1998) for silty sand to an equivalent clean sand value using the following equation:

$$Q_{tn,cs} = K_c\, Q_{tn} \qquad \text{(Eq. 2.8)}$$

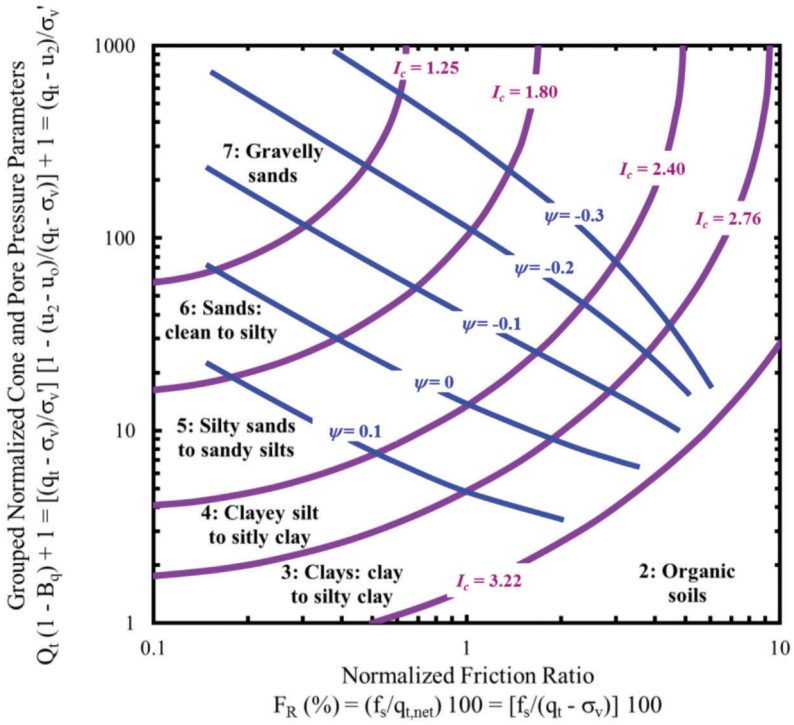

Possible Type of Soil	Zone	CPTu Index, $I_{c(J\&B06)}$
Gravelly sands	7	$I_{c(J\&B06)} < 1.25$
Sands: clean sand to silty sand	6	$1.25 < I_{c(J\&B06)} < 1.80$
Sand mixtures: silty sand to sandy silt	5	$1.80 < I_{c(J\&B06)} < 2.40$
Silt mixtures: clayey silt to silty clay	4	$2.40 < I_{c(J\&B06)} < 2.76$
Clays	3	$2.76 < I_{c(J\&B06)} < 3.22$
Organic soils	2	$I_{c(J\&B06)} > 3.22$

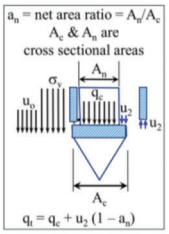

NOTES:

$$I_{c(J\&B06)} = \sqrt{\{3 - \log[Q_t(1 - B_q) + 1]\}^2 + [1.5 + 1.3(\log F_R)]^2}$$

$$\psi = \frac{\ln\left[\frac{Q_t(1 - B_q) + 1}{\left(3.6 + \frac{10.2}{F_R}\right)}\right]}{(1.33\, F_R - 11.9)}$$

σ_v = total vertical overburden stress; σ_v' = effective vertical overburden stress = $\sigma_v - u_o$; u_2 = total shoulder pore pressure measured during piezocone penetration; u_o = hydrostatic pore pressure, Δu_2 = excess shoulder pore pressure = $u_2 - u_o$.

Figure 2.6 SBT chart with approximate contours of soil state parameter (adapted from Jefferies & Been, 2006).

where K_c is a function of grain characteristics (including influence of fines content, mineralogy, and plasticity) of the soil that can be estimated using $I_{c(R\&W98)}$ as follows.

$$K_c = 1.0 \; if \; I_{c(R\&W98)} \leq 1.64 \qquad \text{(Eq. 2.9)}$$

$$K_c = -\,0.403\, I_{c(R\&W98)}{}^4 + 5.581\, I_{c(R\&W98)}{}^3 - 21.63\, I_{c(R\&W98)}{}^2 + 33.75\, I_{c(R\&W98)} - 17.88 \quad if \quad I_{c(R\&W98)} > 1.64 \qquad \text{(Eq. 2.10)}$$

$$K_c = 1.0 \quad if \quad 1.64 < I_{c(R\&W98)} < 2.36 \text{ and } F_R < 0.5\% \qquad \text{(Eq. 2.11)}$$

Figure 2.8 shows the contours of the equivalent clean sand cone resistance, $Q_{tn,cs}$, on the CPT SBTn chart, while Figure 2.9 shows recommended K_c. Table 2.4 provides a summary of different CPT- and CPTu-based relationships for estimating ψ.

2.3.3 Unit weight

The calculation of overburden stresses requires the total unit weight of soil (γ_m). This initial state parameter is also needed in the conversion of shear wave velocity (V_s) to small-strain shear modulus (G_0). The total unit weight relates to the more fundamental mass density (ρ_m):

$$\gamma_m = \rho_m \, g_a \qquad \text{(Eq. 2.12)}$$

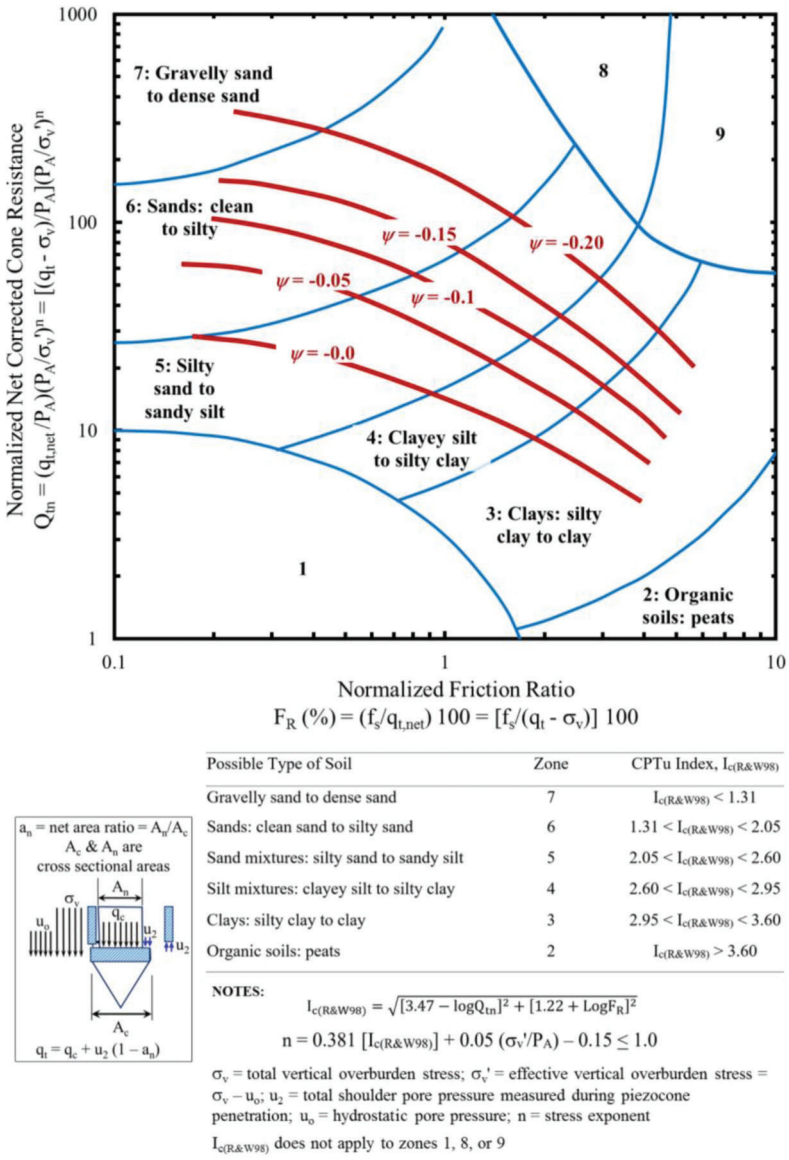

Possible Type of Soil	Zone	CPTu Index, $I_{c(R\&W98)}$
Gravelly sand to dense sand	7	$I_{c(R\&W98)} < 1.31$
Sands: clean sand to silty sand	6	$1.31 < I_{c(R\&W98)} < 2.05$
Sand mixtures: silty sand to sandy silt	5	$2.05 < I_{c(R\&W98)} < 2.60$
Silt mixtures: clayey silt to silty clay	4	$2.60 < I_{c(R\&W98)} < 2.95$
Clays: silty clay to clay	3	$2.95 < I_{c(R\&W98)} < 3.60$
Organic soils: peats	2	$I_{c(R\&W98)} > 3.60$

NOTES:

$$I_{c(R\&W98)} = \sqrt{[3.47 - \log Q_{tn}]^2 + [1.22 + \log F_R]^2}$$

$$n = 0.381\,[I_{c(R\&W98)}] + 0.05\,(\sigma_v'/P_A) - 0.15 \leq 1.0$$

σ_v = total vertical overburden stress; σ_v' = effective vertical overburden stress = $\sigma_v - u_o$; u_2 = total shoulder pore pressure measured during piezocone penetration; u_o = hydrostatic pore pressure; n = stress exponent

$I_{c(R\&W98)}$ does not apply to zones 1, 8, or 9

Figure 2.7 Contours of estimated state parameter (ψ) on normalized SBTn Q_{tn}–F_R chart for uncemented Holocene-age sandy soils (adapted from Robertson, 2009).

where g_a = gravitational constant (= 9.8 m/s^2 = 32.2 ft/s^2).

Soil phase relationships provide information about the initial state of the soil. One primary identity is:

$$G_s\, w_n = S\, e_0 \qquad \text{(Eq. 2.13)}$$

where G_s = specific gravity of soil solids (for "normal" soils: G_s = 2.70 ± 0.1), w_n = natural water content, S = degree of saturation, and e_0 = initial void ratio. A second identity for the general case of total unit weight is:

$$\gamma_m = \left[\frac{(1 + w_n)}{(1 + e_o)}\right] G_s\, \gamma_w \qquad \text{(Eq. 2.14)}$$

where γ_w = unit weight of water = 9.8 kN/m^3 = 62.4 pcf for freshwater. Depending on the w_n and S, two boundary cases are commonly taken in soil mechanics: (a) dry soil (with w_n = 0); and (b) fully saturated soil with S = 1. Accordingly,

$$\text{Dry unit weight: } \gamma_d = \left[\frac{G_s\, \gamma_w}{(1 + e_o)}\right] \qquad \text{(Eq. 2.15)}$$

$$\text{Saturated unit weight: } \gamma_{sat} = \left[\frac{(G_s + e_o)}{(1 + e_o)}\right] \gamma_w \qquad \text{(Eq. 2.16)}$$

Thus, the hierarchy for assignment of unit weights would be: $\gamma_d \leq \gamma_m \leq \gamma_{sat}$. For soils above the groundwater

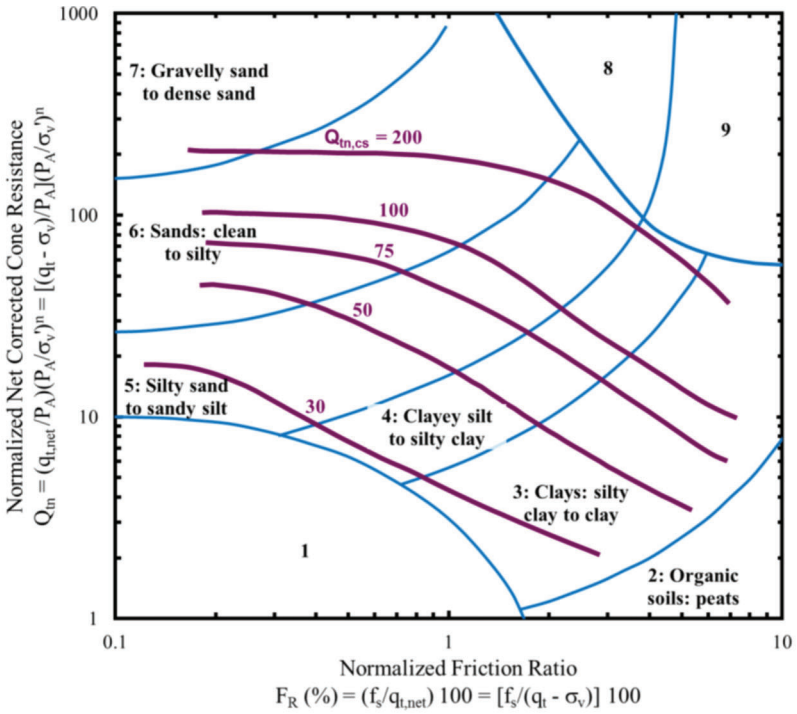

Possible Type of Soil	Zone	CPTu Index, $I_{c(R\&W98)}$
Gravelly sand to dense sand	7	$I_{c(R\&W98)} < 1.31$
Sands: clean sand to silty sand	6	$1.31 < I_{c(R\&W98)} < 2.05$
Sand mixtures: silty sand to sandy silt	5	$2.05 < I_{c(R\&W98)} < 2.60$
Silt mixtures: clayey silt to silty clay	4	$2.60 < I_{c(R\&W98)} < 2.95$
Clays: silty clay to clay	3	$2.95 < I_{c(R\&W98)} < 3.60$
Organic soils: peats	2	$I_{c(R\&W98)} > 3.60$

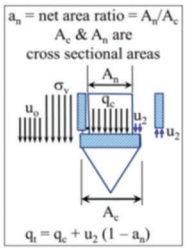

NOTES:

$$I_{c(R\&W98)} = \sqrt{[3.47 - \log Q_{tn}]^2 + [1.22 + \log F_R]^2}$$

$$n = 0.381\,[I_{c(R\&W98)}] + 0.05\,(\sigma_v'/P_A) - 0.15 \leq 1.0$$

$$Q_{tn,cs} = K_c\, Q_{tn}$$

$$K_c = 1.0 \text{ if } I_{c(R\&W98)} \leq 1.64$$

$$K_c = 5.581\, I_{c(R\&W98)}^3 - 0.403\, I_{c(R\&W98)}^4 - 21.63\, I_{c(R\&W98)}^2 + 33.75\, I_{c(R\&W98)} - 17.88 \text{ if } I_{c(R\&W98)} > 1.64$$

$$K_c = 1.0 \text{ if } 1.64 < I_{c(R\&W98)} < 2.36 \text{ and } F_R < 0.5\%$$

σ_v = total vertical overburden stress; σ_v' = effective vertical overburden stress = $\sigma_v - u_o$; u_2 = total shoulder pore pressure measured during piezocone penetration; u_o = hydrostatic pore pressure; n = stress exponent; $Q_{tn,cs}$ = clean sand equivalent normalized cone resistance; K_c = correction factor = K_c(grain characteristics: fines content, minerology, and plasticity)

Figure 2.8 Contours of equivalent clean sand normalized cone resistance, $Q_{tn,cs,}$ by Robertson (2010b,c) based on corrections suggested by Robertson and Wride (1998) (adapted from Robertson, 2009).

table, γ_d would apply for no capillarity (e.g., clean sands), while if full capillarity exists (e.g., clays), then γ_{sat} would be appropriate. If the soil is partially saturated, the γ_m will depend on the ambient degree of saturation, likely a value that changes with the weather, humidity, and temperature. For soils below the water table, it is often taken that the γ_m is equal to the γ_{sat}. In some cases, calculations involve the effective unit weight ($\gamma' = \gamma_{sat} - \gamma_w$), also referred to as the buoyant unit weight or submerged unit weight.

Unit weights are best obtained by securing "undisturbed" samples (e.g., thin-walled Shelby tubes; piston samples) and weighing a known volume of soil. When this is not feasible or possible, the CPT data offers means for estimating the γ_m. Numerous researchers have proposed relationships between γ_m and different CPT, CPTu, and SCPTu parameters for variety of soils. One such relationship by Larsson and Mulabdic (1991) is presented in Figure A.21. This is based on net corrected cone resistance ($q_{t,net} = q_t - \sigma_v$) and pore pressure parameter ratio [$B_q = \Delta u_2/q_{t,net} = (u_2 - u_0)/(q_t - \sigma_v)$], where the approximate range of unit weights are provided for different SBT zone. Obviously, with overburden stress (σ_v) being a component of both $q_{t,net}$ and B_q, this γ_m estimation requires an iterative process. Table 2.5 provides a summary of different CPT-based

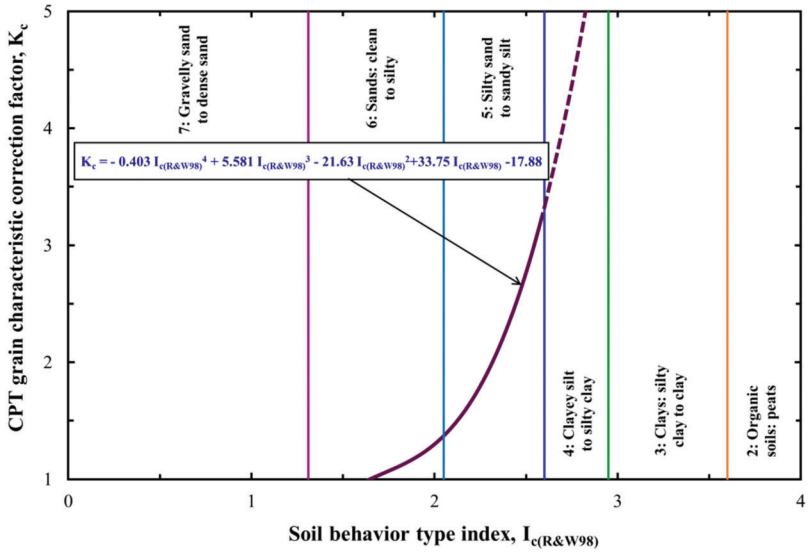

Figure 2.9 Recommended grain characteristic correction to obtain clean sand equivalent CPT penetration resistance in sandy soils (adapted from Robertson & Wride, 1998).

TABLE 2.4
Summary of selected correlations between soil state parameter and normalized CPT/CPTu parameters

Soil Type	Relationship	Reference
See Figure 2.5 for applicable soil zones and contours of the state parameter	$\Psi = \dfrac{\ln\left[\dfrac{Q_t(1-B_q)}{\left(3.6+{}^{10.2}/_{F_R}\right)}\right]}{(1.33\ F_R - 11.9)}$	Plewes et al. (1992)
See Figure 2.6 for applicable soil zones and contours of the state parameter	$\Psi = \dfrac{\ln\left[\dfrac{Q_t(1-B_q)+1}{\left(3.6+{}^{10.2}/_{F_R}\right)}\right]}{(1.33\ F_R - 11.9)}$	Jefferies & Been (2006)
Uncemented, Holocene-age soils; see Figure 2.7 for applicable soil zones and contours of the state parameter	See the contours of estimated state parameter (ψ) on normalized SBTn $Q_{tn} - F_R$ chart in Figure 2.7	Robertson (2009)
See Figures 2.8 and 2.9 for applicable soil zones and contours of $Q_{tn,cs}$ and K_c	$\Psi = 0.56 - 0.33\ \log(Q_{tn,cs})$ $Q_{tn,cs} = K_c\ Q_{tn}$ $K_c = 1.0\ \ if\ \ I_{c(R\&W98)} \le 1.64$ $K_c = 5.581\ I_{c(R\&W98)}^3 - 0.403\ I_{c(R\&W98)}^4 - 21.63\ I_{c(R\&W98)}^2 + 33.75\ I_{c(R\&W98)} - 17.88\ \ if\ \ I_{c(R\&W98)} > 1.64$ $K_c = 1.0\ \ if\ \ 1.64 < I_{c(R\&W98)} < 2.36$ *and* $F_R < 0.5\%$	Robertson (2010b, c); Robertson & Wride (1998)

Note: Q_t = normalized net corrected cone resistance = $(q_t - \sigma_v)/\sigma'_v$; q_t = corrected cone resistance = $q_c + u_2\ (1 - a_n)$; a_n = cone net area ratio = A_n/A_c; A_n = cross-sectional area of the load cell behind the cone; A_c = projected cone cross-sectional area; q_c = measured cone resistance; u_2 = shoulder (behind the cone) pore pressure recorded during penetration of piezocone; σ'_v = effective vertical overburden stress = $\sigma_v - u_0$; σ_v = total vertical overburden stress = $\Sigma(\gamma_{mi} \bullet z_i)$; γ_{mi} = total unit weight of the i-th soil layer; z_i = thickness of the i-th soil layer; u_0 = hydrostatic pore pressure = $\gamma_w\ (z - z_w)$; γ_w = unit weight of water; z = depth below the ground surface; z_w = depth of the ground water table; $B_q = \Delta u_2/q_{t,net}$; Δu_2 = excess pore pressure recorded at the shoulder during penetration of piezocone = $u_2 - u_0$; $q_{t,net}$ = net corrected cone resistance = $q_t - \sigma_v$; F_R = normalized friction ratio = $f_s/(q_t - \sigma_v)$; f_s = sleeve resistance; ψ = soil state parameter; Q_{tn} = normalized net corrected cone resistance = $[(q_t - \sigma_v)/p_A](p_A/\sigma'_v)^n$; n = stress normalization exponent; CPT = cone penetration test; CPTu = piezocone penetration test; p_A = atmospheric pressure = 1 bar = 100 kPa; $Q_{tn,cs}$ = clean sand equivalent normalized cone resistance; K_c = correction factor for $Q_{tn,cs}$; $I_{c(R\&W98)}$ = classification index = $\sqrt{[3.47 - logQ_{tn}]^2 + [1.22 + LogF_R]^2}$.

TABLE 2.5
Summary of selected CPT-based relationships for unit weight estimation

Soil Type	Relationship	Reference
General cases: all soil types	$\gamma_m\left(\frac{kN}{m^3}\right) = 26 - \frac{14}{1 + \{0.5\ log\ [f_s\ (kPa) + 1]\}^2}$	Mayne (2014)
General cases: all soil types	$\frac{\gamma_m}{\gamma_w} \approx 1.22 + 0.15\ ln\left[100\left(\frac{f_s}{p_A}\right) + 0.01\right]$	Mayne & Peuchen (2012); Mayne (2017)
Soft to firm *NC* to *LOC* clays	For $m_q < 80$, $\frac{\gamma_m}{\gamma_w} = 1 + 0.125\left(\frac{m_q}{\gamma_w}\right)$	Mayne & Peuchen (2012); Mayne (2017)
Soft to firm *NC* to *LOC* clays	For $m_q < 80$ kN/m^3, $\frac{\gamma_m}{\gamma_w} = 0.886\left(\frac{q_t}{p_A}\right)^{0.072}\left(1 + 0.125\ \frac{m_q}{\gamma_w}\right)$	Mayne & Peuchen (2012)
Stiff to hard *OC* clays	For $m_q > 80$ kN/m^3, $\gamma_m = 19 - 21.8$ kN/m^3 (intact); $18 - 20.7$ kN/m^3 (stiff fissured); $16.9 - 17.1$ kN/m^3 (carbonate fine grained) (also see Figure 2.10)	Mayne (2014)
General cases: all soil types	$\frac{\gamma_m}{\gamma_w} = 0.27\ [\log\ FR(\%)] + 0.36\left[\log\left(\frac{q_t}{p_A}\right)\right] + 1.236$ $\frac{\gamma_m}{\gamma_w} = \left\{0.27\ [\log\ FR(\%)] + 0.36\left[\log\left(\frac{q_t}{p_A}\right)\right] + 1.236\right\}\left(\frac{G_s}{2.65}\right)$	Robertson & Cabal (2014)
General cases: all soil types	$\gamma_m\left(\frac{kN}{m^3}\right) = 11.46 + 0.33\ log\ [z\ (m)] + 3.1\ log\ [f_s\ (kPa)] + 0.7\ log\ [q_t\ (kPa)]$	Mayne et al. (2010)
General cases: all soil types	$\gamma_m = 1.95\gamma_w\left(\frac{\sigma_v'}{p_A}\right)^{0.06}\left(\frac{f_s}{p_A}\right)^{0.06}$	Mayne et al. (2010)
Intact and fissured clays, peat, silts, sands, gravels and rocks	$\gamma_{sat} = 4.17\ ln\ (V_{s1} - 4.03)$	Mayne (2007b)
General cases: all soil types	$\gamma_m\left(\frac{kN}{m^3}\right) = 8.63\ log\ [V_s\ (m/s)] - 1.18\ log\ [z\ (m)] - 0.53$	Mayne (2005)
General cases: all soil types	$\gamma_m\left(\frac{kN}{m^3}\right) = 8.64\ log\ [V_s\ (m/s)] - 0.74\ log\ [\sigma_v'\ (kPa)] - 0.40$	Mayne et al. (2010)
Sands	$\gamma_d = 1.89\ log\ (Q_{t1}) + 11.8$	Mayne (2006b)
General cases: all soil types	$\gamma_{sat}\left(\frac{kN}{m^3}\right) = 8.32\ log\ [V_s\ (m/s)] + 1.61\ log\ [z\ (m)]$	Mayne (2006b)
General cases: all soil types	$\gamma_{sat}\left(\frac{kN}{m^3}\right) = 2.6\ log\ (f_s) + 15\ G_s - 26.5$	Mayne (2006b)
Different soil types	Based on $q_{t,net}$ and B_q (see Figure A.21)	Larsson & Mulabdic (1991)

Note: γ_m = total unit weight of the soil; f_s = sleeve resistance; γ_w = unit weight of water = 9.81 kN/m^3 = 62.4 pcf; p_A = reference atmospheric pressure = 100 kPa; γ_{sat} = saturated unit weight of the soil; $V_{s1} = V_s\ (p_A/\sigma_v')^{0.25}$; V_s = shear wave velocity; σ_v' = effective vertical overburden stress = $\sigma_v - u_0$; σ_v = total vertical overburden stress = $\Sigma(\gamma_{mi} \bullet z_i)$; m_q = cone resistance depth ratio = $\Delta q_t/\Delta z \approx q_t/z$; *NC* = normally consolidated; *LOC* = lightly overconsolidated; *OC* = overconsolidated; z = depth below the ground surface; q_t = corrected cone resistance = $q_c + u_2\ (1 - a_n)$; q_c = measured cone resistance; u_2 = shoulder (behind the cone) pore pressure recorded during penetration of piezocone; a_n = cone net area ratio = A_n/A_c; A_n = cross-sectional area of the load cell behind the cone; A_c = projected cone cross-sectional area; u_0 = hydrostatic pore pressure = $\gamma_w\ (z - z_w)$, where, z = depth in question; γ_w = unit weight of water = 9.81 kN/m^3 = 62.4 pcf; γ_d = dry unit weight of the soil; Q_{t1} = normalized tip resistance = $(q_t/p_A)/(\sigma_v'/p_A)^{0.5}$; FR = friction ratio = f_s/q_t; G_s = specific gravity of the soil; γ_{mi} = total unit weight of the i-th soil layer; z_i = thickness of the i-th soil layer; $q_{t,net}$ = net corrected cone resistance = $q_t - \sigma_v$; B_q = pore pressure parameter ratio = $\Delta u_2/q_{t,net} = (u_2 - u_0)/(q_t - \sigma_v)$.

relationships for estimating γ_m, γ_d, and γ_{sat}. The correlations that are based on the shear wave velocity (V_s) readings require seismic cone penetration test (SCPT), or seismic piezocone test (SCPTu). Preliminary approximate estimate of the unit weight may also be obtained using the SBT charts and the values for different soil types given in Table 2.6.

2.3.4 Shear Wave Velocity

The shear wave velocity (V_s) and small-strain shear [$\gamma_s < 10^{-4}$ (%)] modulus (G_0) are fundamental soil parameters, important in determining soil dynamic behavior and liquefaction susceptibility, as well as in static loading situations (Hegazy & Mayne, 2006). Values of G_0 are commonly determined from in situ V_s measurements using the following equation:

$$G_0 = \rho_m V_s^2 \qquad \text{(Eq. 2.17)}$$

where ρ_m = soil mass density.

If the shear wave velocity (V_s) measurements are not available via conventional test methods, those may be estimated from the CPT data, although this may incur additional uncertainties. A summary of selected correlations is presented in Table 2.7. Care and engineering judgment should be exercised when applying these relationships to sites with conditions different from their databases. Karray and Hussein (2018) offered the following general suggestions regarding applicability of selected V_s-q_t relationship:

- Relationships based on SBT index, $I_{c(R\&W98)}$ (e.g., Andrus et al., 2007, Hegazy & Mayne, 2006; Robertson; 2009) differ from other relationships, since $I_{c(R\&W98)}$ cannot provide predictions of soil grain size, but it rather estimates the mechanical behavior of the soils.
- Correlations solely between V_s and q_t or between V_s and F_R with independent parameters such as D_{50} to account for soil type are expected to provide more realistic trends that reflect the true soil behavior.

2.3.5 Relative Density of Clean Sands

The degree of packing of clean sands is often expressed in terms of relative density (D_R), or density index (I_D). The simple expression for determination of D_R (expressed in percent) is:

TABLE 2.6
Approximate unit weights for SBT zones by Robertson et al. (1986) for Figure A.16 (after Lunne et al., 1997)

Zone	Soil Behavior Type	Approximate Unit Weight (kN/m^3)
1	Sensitive fine grained	17.5
2	Organic material	12.5
3	Clay	17.5
4	Silty clay to clay	18.0
5	Clayey silt to silty clay	18.0
6	Sandy silt to clayey silt	18.0
7	Silty sand to sandy silt	18.5
8	Sand to silty sand	19.0
9	Sand	19.5
10	Gravelly sand to sand	20.0
11	Very stiff fine grained	20.5
12	Sand to clayey sand	19.0

$$D_R = \left(\frac{e_{max} - e_o}{e_{max} - e_{min}}\right) 100 \qquad \text{(Eq. 2.18)}$$

where e_{max} = the maximum possible void ratio (loosest state), e_{min} = the minimum void ratio (densest state), and e_0 = the current (in-situ) void ratio. The use of term "relative density" is normally restricted to sands with fines content $\leq$ 15%. There also exists relationship between the states of sand density, e.g., Cubrinovski and Ishihara (2002) suggested the following relationship based on several database of clean quartz sands:

$$e_{min} = 0.571\, e_{max} \qquad \text{(Eq. 2.19)}$$

Test procedures for determination of e_0, e_{min} and e_{max}, specified per the ASTM standards are not normally practical for production testing of sands, such as large fill placement for embankments, earth retaining structures, and hydraulically filled ground. The field compaction is controlled and verified using penetration tests.

Several correlations between D_R and particle grain characteristics have been proposed. The early findings of calibration chamber tests (CCT) and studies (e.g., Baldi et al., 1981; Robertson & Campanella, 1983; Schmertmann, 1978a) showed that the D_R for clean quartz sands correlates with the measured cone tip resistance ($q_t \approx q_c$) and effective vertical overburden stress (σ_v'), with additional effects caused by compressibility, stress history, lateral stress, and grain crushing factors. Robertson and Campanella (1983) concluded that sands with a high compressibility (that is, a sand with a large feldspar and/or mica content and/or angular grains) would have a lower cone resistance (q_c) than a sand at the same relative density (D_R) with a

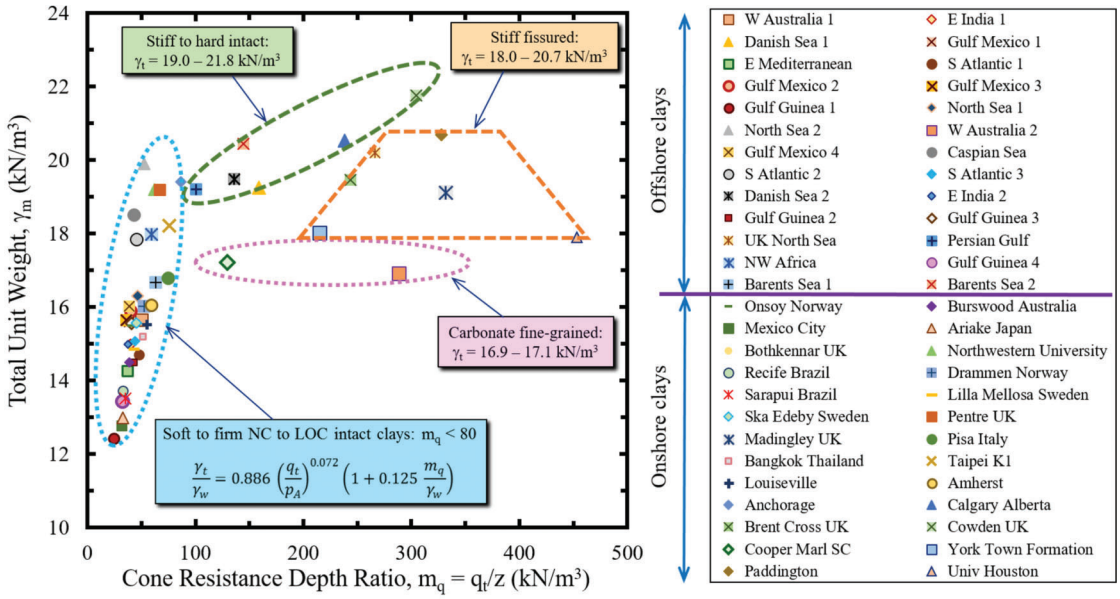

Figure 2.10 General trends between unit weight (γ_m) of stiff-hard overconsolidated clays and cone resistance depth ratio (m_q) (adapted from Mayne, 2014).

TABLE 2.7
Summary of selected correlations between shear wave velocity and CPT parameters

Soil Type and General Data Information	Relationship	Reference
CPT calibration chamber and V_s resonant column on uncemented unaged quartzitic sands from Ticino, Italy verified at Po River sand and Gioia Turo sand	$V_s(m/s) = 277\ [q_t\ (MPa)]^{0.13}[\sigma_v'\ (MPa)]^{0.27}$	Baldi et al. (1989)
CPT calibration chamber and resonant column on freshly deposited washed mortar sand, verified from three Holocene sand deposits in Imperial Valley of S. California	$\left[\frac{G_o\ (kPa)}{q_c\ (kPa)}\right] = \frac{1{,}634}{\left\{\frac{[q_c\ (kPa)]}{\sqrt{[\sigma_v'\ (kPa)]}}\right\}^{0.75}}$	Rix & Stokoe (1991)
Seismic CPT measurements on uncemented silica clean sand from the Fraser River Delta region of BC, Canada	$V_s(m/s) = 60.3\left\{\frac{[\sigma_v'\ (kPa)]}{[p_A\ (kPa)]}\right\}^{0.25}[q_{c1}\ (bars)]^{0.23}$	Robertson et al. (1992a)
Seismic CPT measurements on dirty sand (30% fines and carbonate shell) from a tailings sand site in Alaska	$V_s(m/s) = 135\ [q_c\ (MPa)]^{0.23}\left\{\frac{[\sigma_v'\ (kPa)]}{[p_A\ (kPa)]}\right\}^{0.135}$	Fear & Robertson (1995)
Generalized cases of soft to firm to stiff intact clays to fissured clay materials (see Figure 2.2)	$V_s(m/s) = 1.75\ [q_t\ (kPa)]^{0.627}$ $V_s(m/s) = 9.44\ [q_t\ (kPa)]^{0.627}e_o{}^{-0.532}$	Mayne & Rix (1995)
General cases: all soil types; use with caution for calcareous soils or diatomaceous clays or mudstones	$V_s(m/s) = \{10.1\ log[q_t\ (kPa)] - 11.4\}^{1.67}[FR(\%)]^{0.3}$	Hegazy & Mayne (1995)
Data from 24 sand sites; V_S measurements from SCPT, crosshole, downhole, or SASW tests)	$V_s(m/s) = 13.18\ [q_c\ (kPa)]^{0.192}[\sigma_v'\ (kPa)]^{0.179}$ $V_s(m/s) = 12.02\ [q_c\ (kPa)]^{0.319}[f_s\ (kPa)]^{-0.0466}$	Hegazy & Mayne (1995)
Data from 36 clay sites; V_s measurements from SCPT, crosshole, downhole, or SASW tests)	$V_s(m/s) = 14.13\ [q_c\ (kPa)]^{0.359}e_o{}^{-0.473}$ $V_s(m/s) = 3.18\ [q_c\ (kPa)]^{0.549}[f_s\ (kPa)]^{0.025}$	Hegazy & Mayne (1995)
General cases: all soil types	$V_s(m/s) = 118.8\ log\ [f_s\ (kPa)]$ $V_s(m/s) = 51.6\ ln\ [f_s\ (kPa)] + 18.5$	Mayne (2006a) Mayne (2007b)
Data from 73 sites representing sands, silts, clays, soil mixtures and mine tailings	$V_s(m/s) = 0.0831\ q_{t1N(H\&M06)}\left\{\frac{[\sigma_v'\ (kPa)]}{[p_A\ (kPa)]}\right\}^{0.25}e^{[1.786I_{c(R\&W98)}]}$	Hegazy & Mayne (2006)
72 data sets of Holocene sands	$V_s(m/s) = 16.5\ \left[q_{c1N(\text{Andrus et al., 07})}\right]^{0.411}\left\{\frac{[\sigma_v'\ (kPa)]}{[p_A\ (kPa)]}\right\}^{0.25}\left[I_{c(R\&W98)}\right]^{0.97}$	Andrus et al. (2007)
Coarse-grained soils (Holocene to Pleistocene age; mostly uncemented)	$V_s(m/s) = \sqrt{10^{[0.55I_{c(R\&W98)}+1.68]}[q_t\ (kPa) - \sigma_v\ (kPa)]\ p_A\ (kPa)}$ $V_{s1}(m/s) = \sqrt{\alpha_{vs}Q_{tn}}$ (also see Figure 2.11)	Robertson (2009)
Uncemented young silica sands	$V_s(m/s) = 125.5\left[q_cC_Q(MPa)\right]^{0.25}\left\{\frac{[\sigma_v'\ (kPa)]}{[p_A\ (kPa)]}\right\}^{0.25}[D_{50}(mm)]^{0.115}$	Karray et al. (2011)

Note: V_s = shear wave velocity; q_t = corrected cone resistance = $q_c + u_2\ (1 - a_n)$; q_c = measured cone resistance; u_2 = shoulder (behind the cone) pore pressure recorded during penetration of piezocone; a_n = cone net area ratio = A_n/A_c; A_n = cross-sectional area of the load cell behind the cone; A_c = projected cone cross-sectional area; e_0 = in-situ void ratio; σ_v' = effective vertical overburden stress = $\sigma_v - u_0$; σ_v = total vertical overburden stress = $\Sigma(\gamma_{mi} \bullet z_i)$; γ_{mi} = total unit weight of the i-th soil layer; z_i = thickness of the i-th soil layer; u_0 = hydrostatic pore pressure = $\gamma_w\ (z - z_w)$, where, z = depth in question; γ_w = unit weight of water = 9.81 kN/m^3 = 62.4 pcf; G_0 = small strain shear modulus = $\rho_m\ V_s{}^2$; ρ_m = soil mass density; p_A = reference atmospheric pressure = 100 kPa; q_{c1} = normalized cone resistance = q_c/σ_v'; FR = friction ratio = f_s/q_t; f_s = sleeve resistance; $q_{t1N(H\&M06)}$ = normalized corrected cone resistance according to Hegazy and Mayne (2006) = $(q_t/p_A)(p_A/\sigma_v')^{0.5}$ for $I_{C(R\&W98)} < 2.6$, and $(q_t/p_A)(p_A/\sigma_v')^{0.75}$ for $I_{C(R\&W98)} > 2.6$; $q_{c1N(\text{Andrus et al., 07})}$ = normalized corrected cone resistance according to Andrus et al. (2007) = $(q_c/p_A)(p_A/\sigma_v')^n$; n = 0.5 for clean sands and 1.0 for clays; $I_{c(R\&W98)} = \sqrt{[3.47 - logQ_{tn}]^2 + [1.22 + LogF_R]^2}$; $Q_{tn} = [(q_t - \sigma_v)/p_A](p_A/\sigma_v')^n$; $F_R = f_s/q_{t,net} = f_s/(q_t - \sigma_v)$; $V_{s1} = V_s\ (p_A/\sigma_v')^{0.25}$; α_{vs} = shear-wave velocity cone factor = $10^{(0.55\ Ic(R\&W98)\ +\ 1.68)}$ when $I_{c(R\&W98)} < 2.6$; C_Q = overburden correction = $(p_A/\sigma_v')^n$ with a maximum value of 2, and the exponent n is typically equal to 0.5; D_{50} = mean grain size.

lower compressibility (that is, a sand with very little feldspar and mica and rounded grains). Baldi et al. (1986) based on their CCTs on Ticino sand (a clean, uniform silica sand with sub-angular grains and moderate compressibility) recommended a relationship for estimating the relative density (D_R) from cone resistance (q_c). Robertson and Cabal (2014) presented the following modified normalized version of expression:

$$D_R(\%) = \left(\frac{1}{C_2}\right)\ln\left(\frac{Q_{cn}}{C_0}\right) \qquad \text{(Eq. 2.20)}$$

where C_0 and C_2 are soil constants, equal to 15.7 and 2.41, respectively for moderately compressible, normally consolidated, unaged and uncemented, predominantly quartz sands, Q_{cn} = normalized cone resistance, corrected for overburden pressure (more

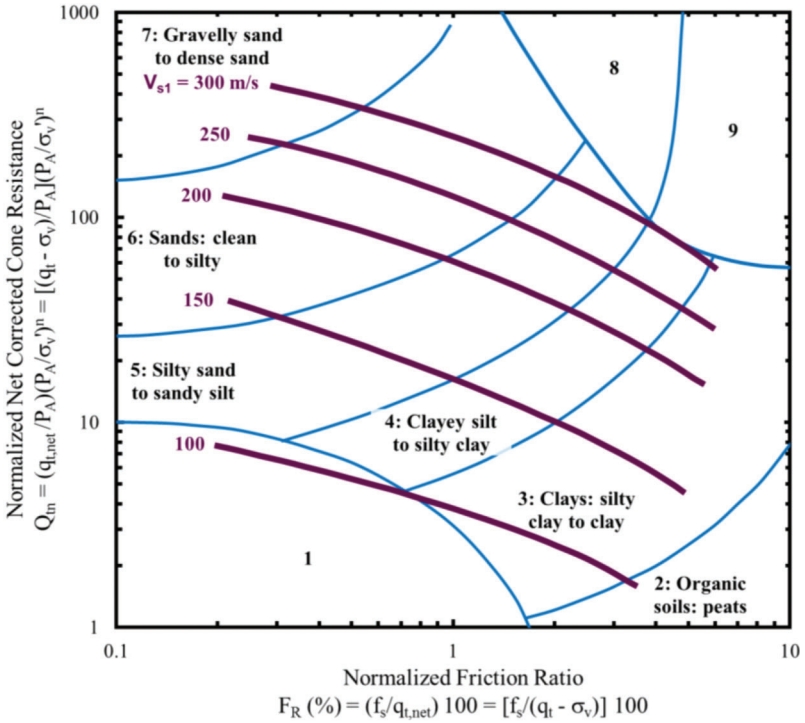

Figure 2.11 Contours of normalized shear-wave velocity, V_{s1} (thick lines), on normalized SBTn Q_{tn}-F_R chart for uncemented Holocene- and Pleistocene-age soils $V_{s1} = V_s\,(p_A/\sigma_v')^{0.25}$ (m/s) (adapted from Robertson, 2009).

recently defined as Q_{tn}, using net cone resistance, $q_{c,net}$) $= (q_c/p_A)/(\sigma_v'/p_A)^{0.5}$; p_A = reference stress of 100 kPa in the same units as q_c and σ_v'; q_c = cone resistance (more correctly, q_t).

A well-known published correlation shown in Figure 2.12, based on five series of CCTs on normally consolidated, uncemented, unaged, predominantly clean quartz sands, was proposed by Jamiolkowski et al. (1985). The average relationship from the database is given by:

$$D_R(\%) = -98 + 66 \log\left[\frac{q_c}{(\sigma_v')^{0.5}}\right] \qquad \text{(Eq. 2.21)}$$

Jamiolkowski et al. (1985) showed three lines corresponding to different sand compressibility: high, medium, and low. The relationship in Eq. 2.21 corresponds to medium compressibility sands.

Kulhawy and Mayne (1990) suggested a simpler formula for estimating relative density:

$$D_R{}^2(\%) = \frac{Q_{cn}}{305\, Q_{c^*}\, Q_{OCR}\, Q_A} \qquad \text{(Eq. 2.22)}$$

where Q_{cn} as defined above in Eq. 2.22, Q_{c*} = compressibility factor (0.91 for low compressibility: predominantly quartz sands, rounded grains with little or no fines; 1.00 for medium compressibility: quartz sand with some feldspar and/or several percent fines; 1.09 for high compressibility: high fines content, mica or other compressible minerals); Q_{OCR} = overconsolidation factor = $OCR^{0.18}$; Q_A = aging factor = 1.2 + 0.05 log(t/100); t = time in years.

The CCT results require a correction factor due to boundary effects and yielding of the flexible walls during testing. The chambers are limited in width compared to the natural sand deposits, and the q_c values differ from those of the true values corresponding to far-field conditions. Thus, the CCT-based correlations overestimate the actual D_R in the field. Jamiolkowski et al. (1985) recommended application of appropriate correction factor to the field measured q_c values before utilizing the CCT-based relationships. The available CCT correction factors for CPT have been developed based on several different approaches (1) statistical analyses involving varied size penetrometers in identical chamber deposits (Kulhawy & Mayne, 1990), (2) cavity expansion theory (Yu & Houlsby, 1991), and (3) numerical modeling (Salgado et al., 1998). In the statistical approach, the correction factor depends upon the relative sizes of the chamber diameter (D) and penetrometer diameter (d), such that:

$$\frac{q_{t(field)}}{q_{t(chamber)}} = \left\{\frac{\left[\left(D/d\right) - 1\right]}{70}\right\}^{0.005 D_R} \qquad \text{(Eq. 2.23)}$$

where D = chamber diameter; d = penetrometer diameter.

Since many users were apparently unaware of the need for this correction factor and simply used the

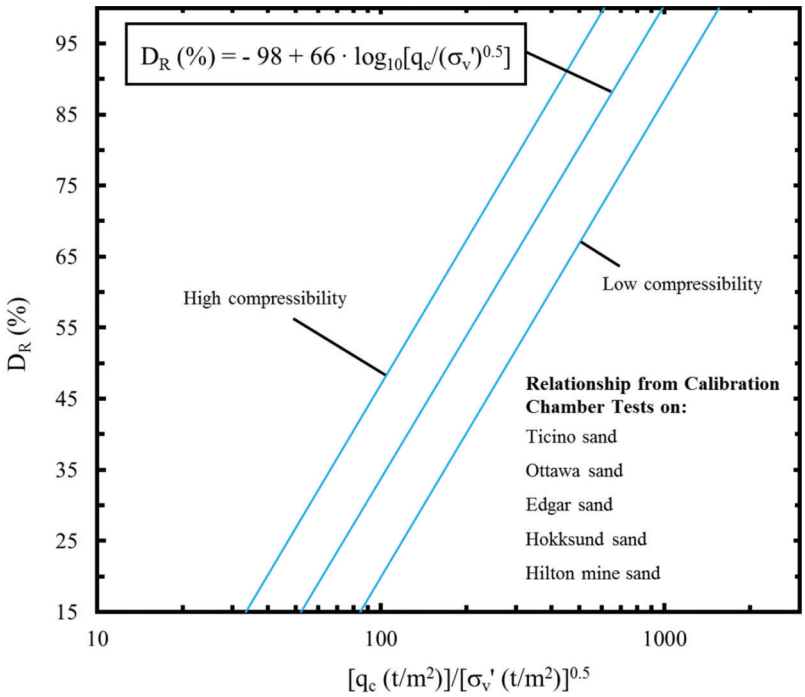

Figure 2.12 Relative density vs. normalized tip resistance relationship for normally consolidated, uncemented, unaged, predominantly quartz sands (after Jamiolkowski et al., 1985).

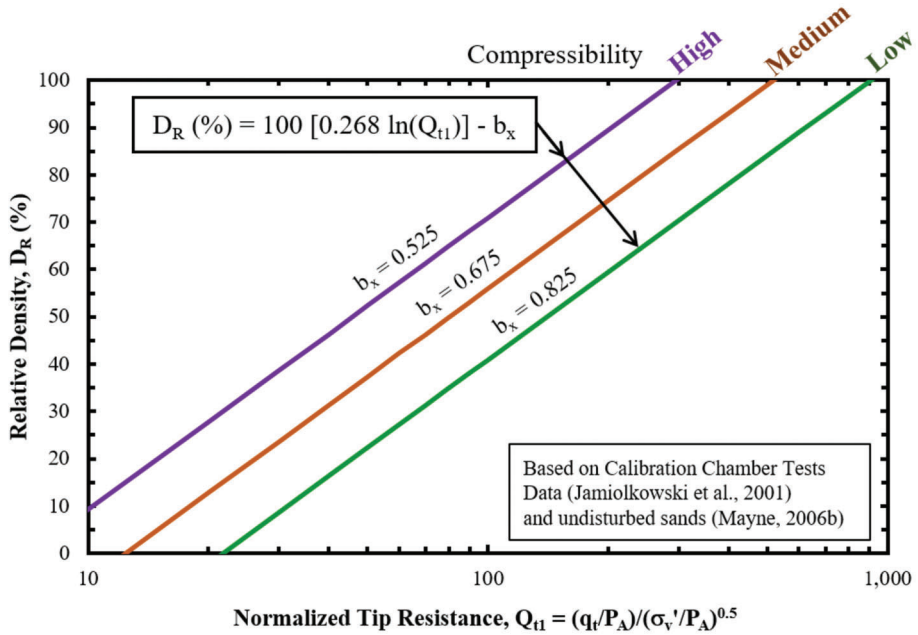

Figure 2.13 Relative density from stress-normalized cone tip resistance in clean *NC* sands where CPT calibration chamber test data corrected for limited *D*/*d* ratios (Jamiolkowski et al., 2001; undisturbed sands compiled by Mayne, 2006a).

laboratory curves directly, Jamiolkowski et al. (2001) reworked on the original database and incorporated appropriate corrections to account for the calibration chamber effects, leading to the following relationship:

$$D_R(\%) = 100\,[0.268\ln(Q_{t1}) - 0.625] \qquad \text{(Eq. 2.24)}$$

where $Q_{t1} = (q_t/p_A)/(\sigma_v'/p_A)^{0.5}$; p_A = reference stress of 1 atmosphere = 100 kPa.

To account for the compressibility in the above relationship, they modified it to the following form (also see Figure 2.13):

$$D_R(\%) = 100\,[0.268\ln(Q_{t1}) - b_x] \qquad \text{(Eq. 2.25)}$$

where the terms b_x represents the compressibility = 0.525 for high compressibility sand (mica sands, calcareous sands and carbonate sands), 0.675 for medium compressibility sand (siliceous sands with equal proportion of quartz and feldspar), and 0.825 for low compressibility sands (quartz sand, such as Ottawa sand).

Kulhawy and Mayne (1990) applied the same approach on overconsolidated sands, and thus Mayne (2006a) complied results on carbonate sands. Accordingly, for the average trend presented in Eq. 4.25, the effect of overconsolidation ratio (OCR) on D_R may be approximated by:

$$b_x \approx 0.675 OCR^{0.2} \qquad \text{(Eq. 2.26)}$$

Lunne et al. (1997) indicated that the CCTs have shown that q_c is controlled by sand density, in-situ vertical and horizontal effective stress and sand compressibility.

Salgado and Prezzi (2007) and Salgado (2008) proposed an expression to estimate D_R of sand from cone resistance. This expression allows a tighter estimation of D_R from q_c, with D_R determinable to within 10% if the input parameters are realistically used,

$$D_R(\%) = \frac{\left[\ln\left(q_c/p_A\right) - 0.4947 - 0.1041\phi_{cs} - 0.841\ln\left(\sigma_h'/p_A\right)\right]}{\left[0.0264 - 0.0002\phi_{cs} - 0.0047\ln\left(\sigma_h'/p_A\right)\right]} \leq 100\% \qquad \text{(Eq. 2.27)}$$

where σ_h' = horizontal effective stress; ϕ_{cs} = critical-state friction angle; other parameters are the same as defined in Eq. 2.27. Presented in Figure 2.14 are the charts by Salgado and Prezzi (2007) for ϕ_{cs} = 29° through 36°, showing the relationships between q_c, σ_h' and D_R. Based on data from Salgado et al. (1997) Figure 2.15 further illustrates the trends in terms of normalized lateral effective stress (σ_h'/p_A) vs. normalized cone resistance (q_c/p_A) for four relative density ranges between 20% and 100%. These were based on the CPTs performed in calibration chambers on sands with varying properties.

Mayne (2014) proposed the following linear relationship for the relative density of calcareous-carbonate sands based on the data from six sources:

$$D_R(\%) = 0.87\, Q_{t1} \qquad \text{(Eq. 2.28)}$$

where $Q_{t1} = (q_t/p_A)/(\sigma_v'/p_A)^{0.5}$; p_A = reference stress of 1 atmosphere = 100 kPa. This trend is independent of the calcite content ($CaCO_3$ (%) between 42 and 98).

Table 2.8 provides a summary of well-known relationships for estimating the relative density (D_R) of sands. In employing any of this correlation, care must be exercised in interbedded deposits where the cone resistance may not have reached the full value within a thin layer. This table also presents an older correlation based on the Searle (1979) SBT classification chart presented earlier.

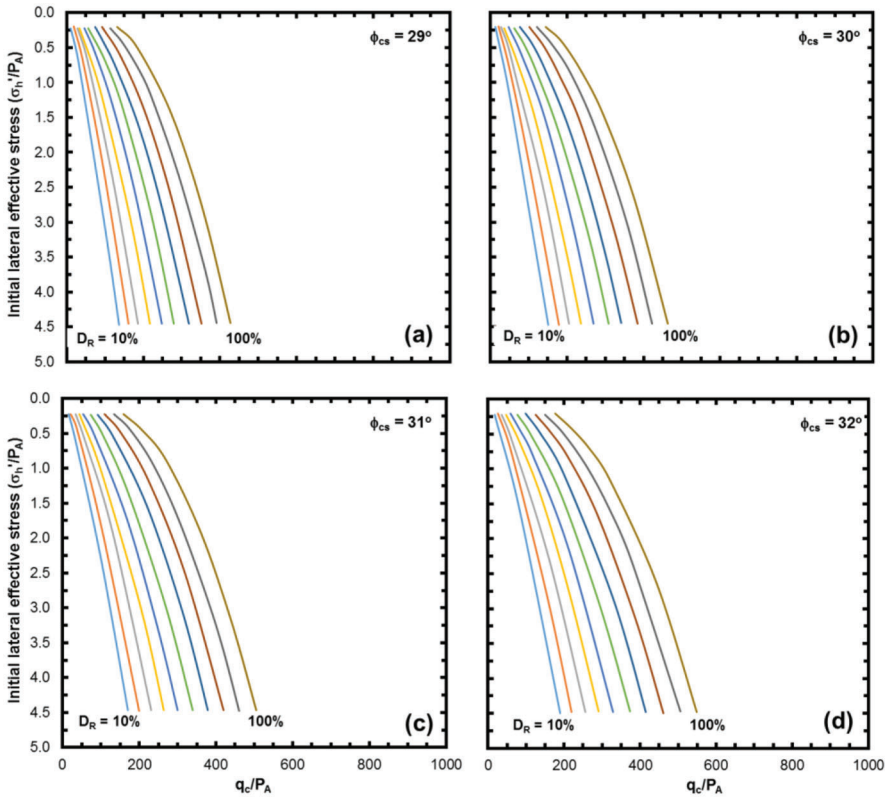

Figure 2.14 Continued.

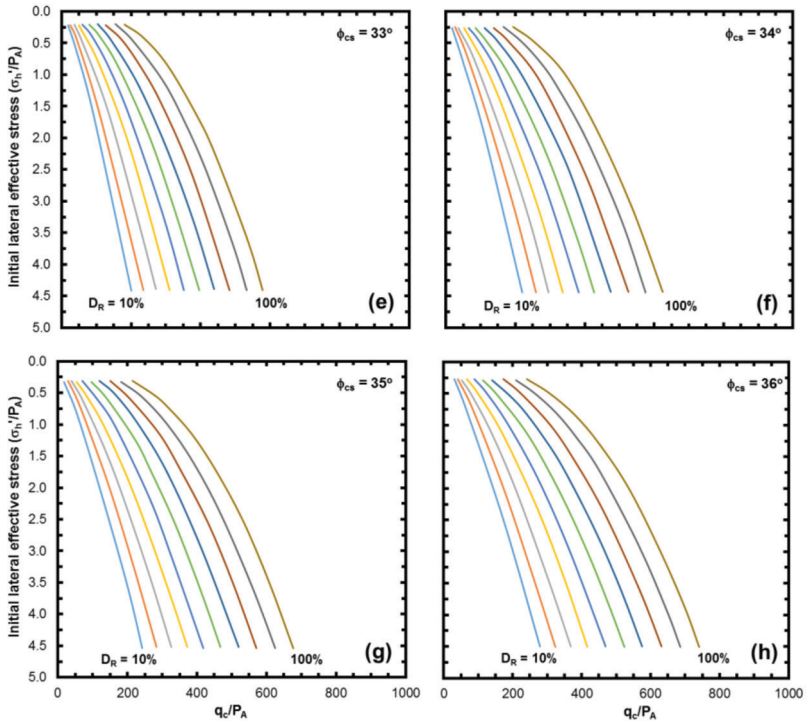

Figure 2.14 Cone resistance charts, calculated for typical intrinsic variables for silica sand and ϕ_{cs} values of (a) 29°, (b) 30°, (c) 31°, (d) 32°, (e) 33°, (f) 34°, (g) 35°, and (h) 36° (after Salgado et al., 1997).

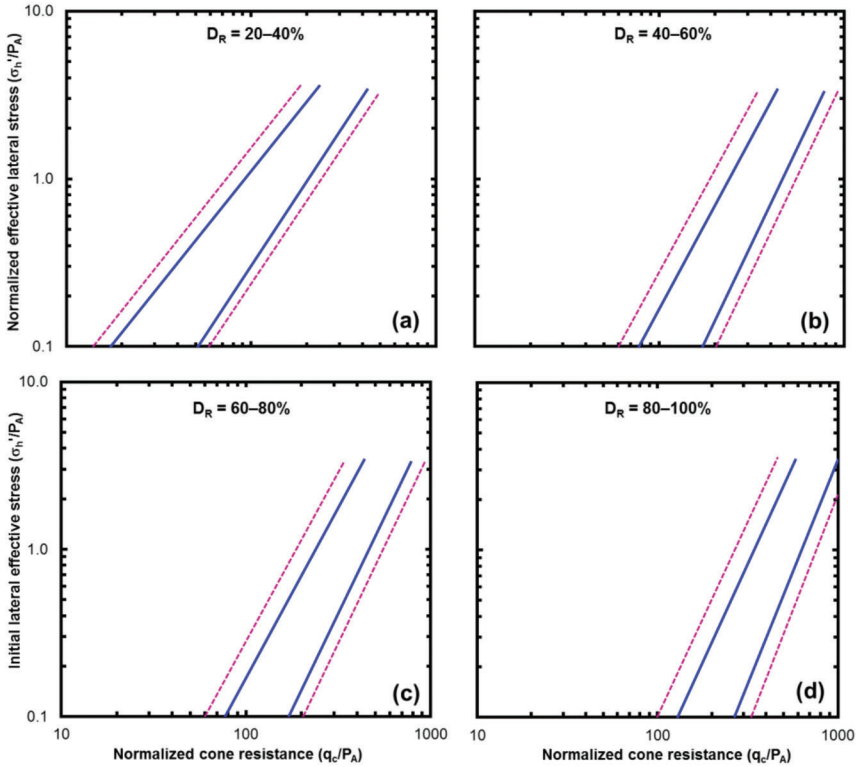

Figure 2.15 Cone resistance versus relative density from CPTs performed in calibration chamber tests on sands with various properties for (a) D_R = 20%–40%, (b) D_R = 40%–60%, (c) D_R = 60%–80%, and (d) D_R = 80%–100%. The solid blue lines represent a range of calculated q_c values for the test sands using Eq. 4.27, and the dashed purple lines, 80% and 120% of these calculated q_c values (after Salgado et al., 1997; actual data that fits well within these bounds are not shown).

TABLE 2.8
Summary of selected solutions for estimating relative density from CPT parameters

Soil Type and General Data Information	Relationship	Reference
Developed based on the SBT classification chart by Searle (1979) presented in Figure A.6	$D_R(\%) = 43 \log [1.33\, q_c\ (MPa)\, FR\ (\%)]$	Searle (1979)
CCTs on Ticino sand (clean, normally consolidated, unaged and uncemented, uniform silica sand with sub-angular grains and moderate compressibility, predominantly quartz sands)	$D_R(\%) = \left(\frac{1}{C_2}\right) \ln\left(\frac{Q_{cn}}{C_0}\right) 100$	Baldi et al. (1986); Robertson & Cabal (2014)
CCTs on Ticino sand, Ottawa sand, Edgar sand, Hokksund sand, and Hilton mine sand (normally consolidated, uncemented, unaged, predominantly quartz sands)	$D_R(\%) = -98 + 66 \log\left[\frac{q_c}{(\sigma_v')^{0.5}}\right]$	Jamiolkowski et al. (1985)
Sands including: (1) low compressibility, predominantly quartz sands, rounded grains with little or no fines; (2) medium compressibility: quartz sand with some feldspar and/or several percent fines; (3) high compressibility: high fines content, mica or other compressible minerals	$D_R{}^2(\%) = \frac{Q_{cn}}{305 Q_c\ Q_{OCR}\ Q_A}$; Q_c = 0.91 for low compressibility sands, 1.00 for medium compressibility sands, and 1.09 for high compressibility sands	Kulhawy & Mayne (1990)
Jamiolkowski et al. (1985) data including: high compressibility sand (mica sands, calcareous sands and carbonate sands), medium compressibility sand (siliceous sands with equal proportion of quartz and feldspar), and low compressibility sands (quartz sand, such a Ottawa sand)	$D_R(\%) = 100\, [0.268\ \ln (Q_{t1}) - b_x]$; b_x = 0.525 for high compressibility sand, 0.675 for medium compressibility sand, and 0.825 for low compressibility sands	Jamiolkowski et al. (2001)
Jamiolkowski et al. (1985) data along with additional overconsolidated carbonate sands	$D_R(\%) = 100\, [0.268\ \ln (Q_{t1}) - b_x]$ with $b_x \approx 0.675\ OCR^{0.2}$ (this applies to mean trend or medium compressibility sands)	Mayne (2006b)
CCTs on Hokksund sand, Monterey sand, Ottawa sand, Toyoura sand, Ticino sand with ϕ_{cs} ranging from 26.0 to 37.0 degrees; expression developed by employing rigorous cavity expansion analysis (also see Figures 2.14 and 2.15)	$D_R(\%) = \frac{\left[\ln\left(q_c/p_A\right) - 0.4947 - 0.1041\ \phi_{cs} - 0.841\ \ln\left(\sigma_h'/p_A\right)\right]}{\left[0.0264 - 0.0002\ \phi_{cs} - 0.0047\ \ln\left(\sigma_h'/p_A\right)\right]} \le 100\%$	Salgado (2008); Salgado & Prezzi (2007); Salgado et al. (1997)
CCTs on carbonate sands [Quiou] (France), Dogs Bay (Ireland), Ewa (Hawaii), Kingfish (Australia), Kenya (Africa), Keju (S. Korea)]	$D_R(\%) = 0.87\ Q_{t1}$	Mayne (2014)

Note: D_R = relative density; q_c = measured cone resistance (more correctly, q_t); q_t = corrected cone resistance = $q_c + u_2\,(1 - a_n)$; u_2 = shoulder (behind the cone) pore pressure recorded during penetration of piezocone; a_n = cone net area ratio = A_n/A_c; A_n = cross-sectional area of the load cell behind the cone; A_c = projected cone cross-sectional area; FR = friction ratio = f_s/q_t; f_s = sleeve resistance; C_0 and C_2 are soil constants, equal to 15.7 and 2.41, respectively; σ_v' = effective vertical overburden stress = $\sigma_v - u_0$; σ_v = total vertical overburden stress = $\Sigma(\gamma_{mi} \bullet z_i)$; γ_{mi} = total unit weight of the i-th soil layer; z_i = thickness of the i-th soil layer; u_0 = hydrostatic pore pressure = $\gamma_w\,(z - z_w)$, where, z = depth in question; γ_w = unit weight of water = 9.81 kN/m^3 = 62.4 pcf; Q_{cn} = normalized cone resistance, corrected for overburden pressure (more recently defined as Q_{tn}, using net cone resistance, $q_{c,net}$) = $(q_c/p_A)/(\sigma_v'/p_A)^{0.5}$; p_A = reference stress of 1 atmosphere = 100 kPa in the same units as q_c and σ_v'; Q_{t1} = $(q_t/p_A)/(\sigma_v'/p_A)^{0.5}$; σ_{vp}' = preconsolidation stress; Q_{c*} = compressibility factor; Q_{OCR} = overconsolidation factor = $OCR^{0.18}$; Q_A = aging factor = 1.2 + 0.05 • log(t/100); t = time in years; b_x represents the compressibility constant; OCR = overconsolidation ratio = σ_{vp}'/σ_v'; σ_h' = effective horizontal stress = $\sigma_h - u_0$ = $(K_0)(\sigma_v')$; K_0 = lateral stress coefficient; ϕ_{cs} = critical-state friction angle.

2.3.6 Effective Stress Friction Angle

2.3.6.1 Sands. The drained (effective stress) friction angle (ϕ') of soils is a fundamental property that controls much of its behavioral response to loading and initial stress state. The ϕ' of sands (also termed angle of internal friction) represents the strength of the material in stability analyses and is often required to assess the coefficient of lateral stress (K_0), footing bearing capacity, pile end-bearing resistance, and side resistance in deep foundations. In terms of the commonly adopted Mohr-Coulomb strength criterion, the shear strength (τ_{max}) is expressed:

$$\tau = c' + \sigma_n' \tan \phi' \qquad \text{(Eq. 2.29)}$$

where c' = effective cohesion intercept (generally: $c' = 0$ for unbonded geomaterials). In most cases, the normal stress can be taken equal to the effective vertical stress: $\sigma_n' = \sigma_v'$.

The peak friction angle (ϕ_p') of sands is composed of two components: (1) a basic frictional value (designated ϕ_{cs}' for critical state) that is due to particle grain shape, compressibility characteristics and mineralogy; and (2) a dilatancy effect (quantified by ψ_d, the dilatancy angle) which reflects the relative packing of particles (e_0 or D_R) and ambient stress level (σ_v'). The two components combine to produce a peak friction angle:

$$\phi_p' \approx \phi_{cs}' + \psi_d' \qquad \text{(Eq. 2.30)}$$

Mayne (2014) summarized from the work by Bolton (1986), Salgado et al. (2000) and Jamiolkowski et al. (2001) that the characteristic values of ϕ_{cs}' are on the order of 32° for quartz sands, 33° for silty quartz sands with up to 20% fines content, 34° for siliceous sands (approximately half quartz-half feldspar), 39° for calcareous sands, and 40° for feldsparic sands. The friction angle also depends upon the mode of testing (i.e., plane strain vs. triaxial) and direction of loading (compression vs. extension).

Significant advances have been made in the development of theories to model the cone penetration process in sands. For the assessment of ϕ_p' of sands from CPT, the following are several approaches.

- Dilatancy framework where Q_{t1} provides the input value of D_R (Bolton, 1986).
- Inverse bearing capacity, such as from cavity expansion (CE) or limit plasticity theories (Schnaid, 2009; Yu & Mitchell, 1998).
- Numerical simulation by finite elements, finite differences, and/or discrete elements (e.g., Salgado et al., 1998).
- Estimating the dilatancy angle (ψ_d') from CPT relationships (Tokimatsu et al., 1995).
- State parameter relationships (Jefferies & Been, 2006).
- Direct CPT methods (Lunne et al., 1997; Mayne, 2006a).

Because of the difficulties in procuring intact samples of natural sands, many early approaches were either referenced to or based on reconstituted samples where small triaxial specimens were prepared at similar relative densities and confining stress levels to those of larger CCTs subjected to CPTs. Empirical correlations based on calibration chamber test results and field results are still the most popular methods for estimation of the friction angle.

Robertson and Campanella (1983) suggested a correlation to estimate the peak friction angle (ϕ_p') for uncemented, unaged, moderately compressible, predominately quartz sands based on CCT results. For sands of higher compressibility (i.e., carbonate sands or sands with high mica content), the method tends to predict low friction angles:

$$\tan \phi_p' = \frac{1}{2.68}\left[\log\left(\frac{q_c}{\sigma_v'}\right) + 0.29\right] \qquad \text{(Eq. 2.31)}$$

Kulhawy and Mayne (1990) developed the following expression on the basis CPT CCT high quality data on clean rounded, uncemented quartz sands that have been corrected for boundary effects and stress-normalized:

$$\phi_p'(degrees) = 17.6^\circ + 11.0 \log Q_{t1} \qquad \text{(Eq. 2.32)}$$

where $Q_{t1} = (q_t/p_A)/(\sigma_v'/p_A)^{0.5}$.

The methods of reconstitution in CCTs, however, were not standardized by then (including pluviation, compaction, vibration, sedimentation, moist tamping, slurry). Furthermore, the CPT data were not corrected for boundary conditions from limited size chambers (i.e., D/d ratio). Towards an improved solution, a database of 17 sands was compiled from special undisturbed samples of clean sands (Mayne, 2006). These samples, obtained via expensive in-place one-dimensional freezing and then careful thawing were sheared in triaxial apparatuses to failure to derive ϕ_p' corresponding to undisturbed intact sands. The sites for these sands were subjected to SPT, CPT, and V_s measurements, as well as other laboratory and field tests. The sand types in the database include natural sands, natural alluvial sands, natural coarse sands, tailings, and hydraulic fills from sites in Asia, Europe, and North America.

Jefferies and Been (2006) showed a strong link between state parameter (ψ) and the peak friction angle (ϕ_p') for a wide range of sands:

$$\phi_p'(degrees) = \phi_{cv}'(degrees) - 48\Psi \qquad \text{(Eq. 2.33)}$$

where ϕ_{cv}' = constant volume (or critical state, ϕ_{cs}') friction angle depending on minerology (Bolton, 1986), typically about 33 degrees for quartz sands but can be as high as 40 degrees for feldspar and carbonate sands. Using the above link, Robertson and Cabal (2014) presented the relationship between normalized clean sand equivalent cone resistance ($Q_{tn,cs}$) and ϕ_p' becomes:

$$\phi_p'(degrees) = \phi_{cv}' + 15.84\,[\log Q_{tn,cs}] - 26.88 \qquad \text{(Eq. 2.34)}$$

where $Q_{tn,cs} = K_c \cdot Q_{tn}$, as defined in Section 2.3.2 above.

Using the average relationship between the state parameter (ψ) and peak friction angle (ϕ_p') suggested by Jefferies and Been (2006) and the contours of the state parameter shown in Figure 2.7, Robertson (2009)

generated approximate contours of the peak friction angle on the SBTn Q_{tn}–F_R chart, as shown in Figure 2.16.

Uzielli et al. (2013) performed evaluation of a database of triaxial compression tests on natural, marine, alluvial, and hydraulic fill sands from China, Japan, Canada, Norway, Italy, and N. Atlantic sites in terms of reliability and probabilistic considerations and presented the following deterministic expression (applicable domain: $Q_{t1} \geq 25$). These were all clean quartz to siliceous sands having trace to little fines content ($FC < 10\%$):

$$\phi_p'(degrees) = 25.0^\circ (Q_{t1})^{0.1} \qquad \text{(Eq. 2.35)}$$

For SCPTu soundings, an additional assessment of ϕ_p' is afforded from the shear wave velocity data (applicable domain: 125 m/s $\leq V_{s1} \leq$ 225):

$$\phi_p'(degrees) = 3.9^\circ [V_{s1}(m/s)]^{0.44} \qquad \text{(Eq. 2.36)}$$

where $V_{s1} = V_s/(\sigma_v'/p_A)^{0.25}$ = stress-normalized shear wave velocity.

2.3.6.2 Clays and silts. For fine-grained silty and clayey soils exhibiting excess pore pressures during penetration ($B_q > 0.1$), a limit plasticity solution for undrained penetration can be implemented towards the evaluation of ϕ' (Senneset et al., 1988; 1989). In this approach, a cone resistance number (N_m), also presented in Appendix A (Section A.1.10), is reproduced below:

$$N_m = \frac{(q_t - \sigma_v)}{(\sigma_v' - a')} = \frac{(N_q - 1)}{(1 + N_u B_q)} \qquad \text{(Eq. 2.37)}$$

where a' = in-situ attraction = $c'\cot(\phi_p')$ = attraction, $N_q = K_p \exp[(\pi\text{-}2\beta)\tan\phi']$ is the end-bearing factor, $K_p = (1 + \sin\phi')/(1 - \sin\phi')$ is the passive stress coefficient, β = angle of plastification ($-20^\circ < \beta < +20^\circ$) which defines the size of the failure zone beneath the tip, $N_u = 6\tan\phi'(1 + \tan\phi')$ is the pore bearing factor. The full solution allows for an interpretation of a paired set of c' and ϕ' for all soil types: sands, silts, clays, and mixed soils. For simplicity, it can be adopted that $\beta = 0$ (Terzaghi equation) and $c' = 0$, thereby resulting in the graphical form shown in Figure 2.17. It may also be noted that for $c' = a' = 0$, the parameter $N_m = Q_{t1}$.

Mayne (2005) devised an approximate algorithm for the NTH solution to allow a line-by-line analysis, easily handled by computer software or spreadsheets:

$$\phi_p'(degrees) = 29.5^\circ B_q^{\,0.121}[0.256 + 0.336 B_q + \log N_m] \qquad \text{(Eq. 2.38)}$$

which is applicable for the following ranges of parameters: $20^\circ \leq \phi_p' \leq 45^\circ$ and $0.1 \leq B_q \leq 1.0$. Mayne (2014) recommended restricted use of Eq. 2.38 to clays, silts, and mixed soils with low OCRs < 2.

Table 2.9 provides a summary of the above relationships for estimating the peak friction angle (ϕ_p') of sands, silts, clays and mixed soil types.

2.3.7 Stress History

The stress history is a significant measurement in soils as it affects important strength, stability, stiffness,

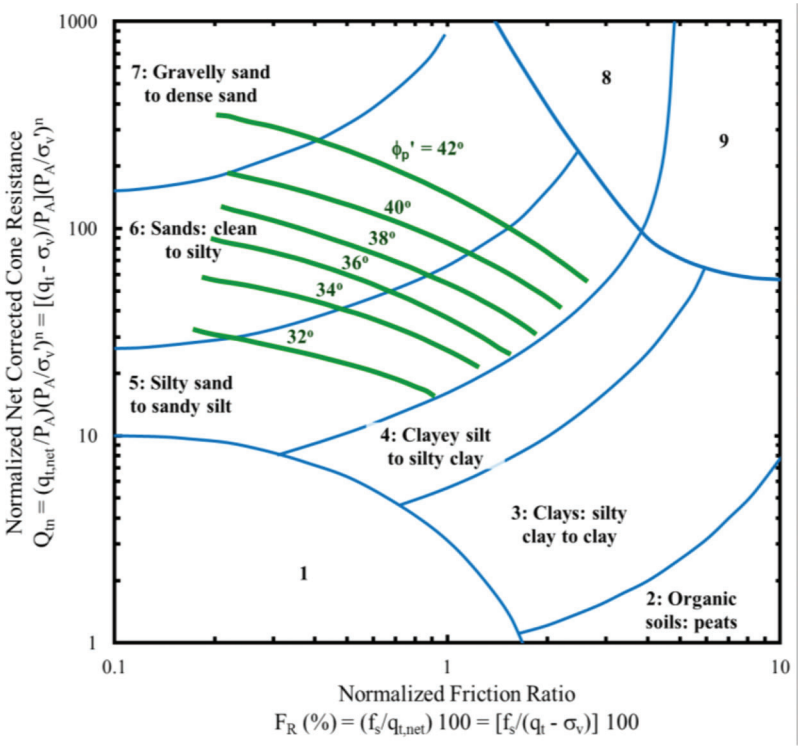

Figure 2.16 Contours of peak friction angle (ϕ_p'), (thick green lines) on normalized Q_{tn}-F_R chart for uncemented Holocene-age sandy soils (adapted from Robertson, 2009).

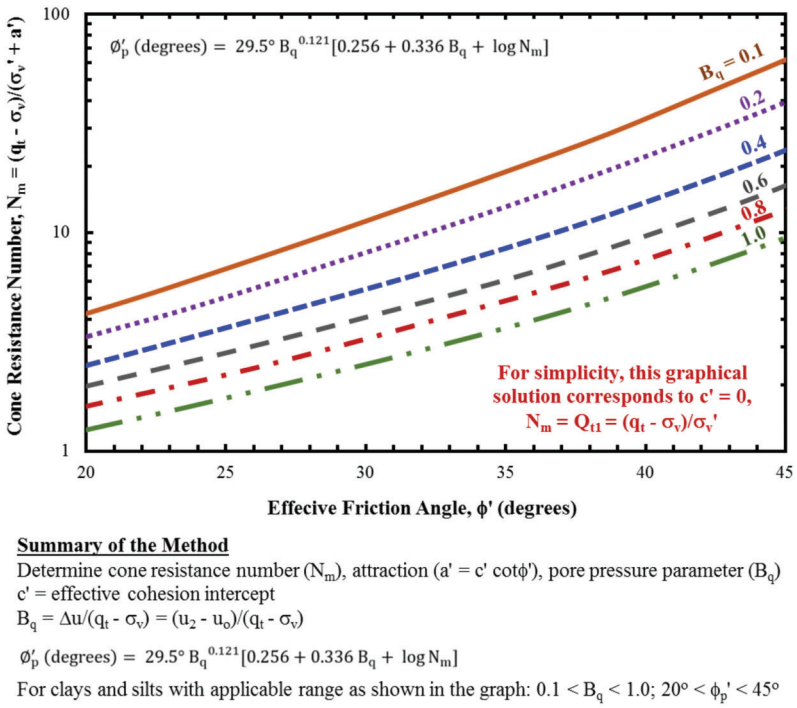

Figure 2.17 NTH method for evaluating effective friction angle in silts and clays (adapted from Mayne, 2007a).

deformational characteristics, and pore pressure response. The stress history of clays is conventionally determined using one-dimensional consolidation tests on undisturbed soil samples to assess the effective yield stress (σ_y') or effective preconsolidation stress ($\sigma_{vp}' = P_c'$), which is sometime also called as the maximum past effective stress ($\sigma_{v\text{-}max}'$). For silts and sands, this is more difficult to assess as undisturbed samples are difficult, expensive, and/or impossible to procure. Thus, stress history in these types of geomaterials generally must be evaluated by other means such as geologic evidence, captured embedded clay layers, groundwater, and ageing. Stress history also distinguishes the pore pressures generated during shear which can either be positive or negative, and the volumetric strain characteristics that can be contractive or dilative.

In terms of its most common occurrence, the mechanical removal of overburden stresses due to processes like erosion, glaciation, and excavation, the normalized and dimensionless form of stress history is termed as the overconsolidation ratio ($OCR = \sigma_{vp}'/\sigma_v'$). However, for cemented or aged soils, the OCR may represent the ratio of the effective yield stress and the present effective overburden stress ($YSR = \sigma_y'/\sigma_v'$). Hence when applying OCR to cemented or aged soil, caution must be exercised.

An alternative and relatively more convenient stress history parameter is the overconsolidation difference ($OCD = \sigma_{vp}' - \sigma_v'$) or the yield stress difference ($YSD = \sigma_y' - \sigma_v'$) as its value is generally constant at all elevations in the formation. This is in contrast to OCR or YSR that decreases with depth (Locat et al., 2003). In the case of soils with quasi-preconsolidation caused by repeated wetting-drying, ageing, groundwater variations, cementation, and freeze-thaw cycles, their representative OCD (or YSD) values are difficult to assess.

The evaluation of in-situ stress history from the results of cone penetration tests allows for an economical and expedient means to profile the stress history of clays, sands, and mixed soil types. In the subsections below, the evaluation methods for OCR and σ_{vp}' have been discussed based on the soil types.

2.3.7.1 Spherical cavity expansion theory and critical state soil mechanics solution for clays and silts. A hybrid solution derived from spherical cavity expansion theory and critical state soil mechanics (SCE-CSSM) was presented for clays and silts by Burns and Mayne (1998; 2002a), and Chen and Mayne (1994, 1996). Here, the overconsolidation ratio (OCR) is obtained using the following analytical solutions:

$$OCR = 2\left[\frac{\frac{q_t - \sigma_v}{\sigma_v'}}{M\left[\left(\frac{2}{3}\right)[\ln(I_R)+1] + \frac{\pi}{4} + \frac{1}{2}\right]}\right]^{(1/\Lambda)} \quad \text{(Eq. 2.39)}$$

$$OCR = 2\left[\frac{\frac{\Delta u_2}{\sigma_v'} - 1}{\left(\frac{2}{3}M\right)[\ln(I_R) - 1]}\right]^{(1/\Lambda)} \quad \text{(Eq. 2.40)}$$

$$OCR = 2\left[\frac{1}{1.95M + 1}\left(\frac{q_t - u_2}{\sigma_v'}\right)\right]^{(1/\Lambda)} \quad \text{(Eq. 2.41)}$$

TABLE 2.9
Summary of selected relationships between effective stress peak friction angle and CPT/CPTu parameters

Soil Type	Relationship	Reference
Derived from Searle (1979) SBT chart	$\phi'(degrees) = \frac{\log_{10} FR(\%) + \log_{10}[q_c\ (MPa)] - 2.87}{0.021\ \log_{10}[q_c\ (MPa)] - 0.88}$	Searle (1979)
Uncemented, unaged, moderately compressible, predominately quartz sands based on CPT in CCT results	$tan\phi'_p(degrees) = \frac{1}{2.68}\left[\log\left(\frac{q_c}{\sigma_v'}\right) + 0.29\right]$	Robertson & Campanella (1983)
Based on CPT in CCT on high quality samples of clean rounded, uncemented quartz sands that have been corrected for boundary effects and stress-normalized	$\phi'_p(degrees) = 17.6^\circ + 11.0\ \log\ Q_{t1}$	Kulhawy & Mayne (1990)
Wide range of sands, typically about 33° for quartz sands and as high as 40° for feldspar and carbonate sands	$\phi'_p(degrees) = \phi'_{cv} - 48\ \Psi$	Jefferies & Been (2006)
Uncemented Holocene-age sandy soils	Contours of peak friction angle (ϕ'_p) on normalized Q_{tn}-F_R chart shown in Figure 2.16	Robertson (2009)
Clean sand	$\phi'_p(degrees) = \phi'_{cv}(degrees) + 15.84\ [\log Q_{tn,cs}] - 26.88$	Robertson & Cabal (2014)
Database of triaxial compression tests on undisturbed samples of 16 natural, marine, alluvial, and hydraulic fill sand sites from China, Japan, Canada, Norway, Italy and N. Atlantic. These were clean quartz to siliceous sands having trace to little fines content (FC < 10%)	$\phi'_p(degrees) = 25.0^\circ\ (Q_{t1})^{0.1}$ $\phi'_p(degrees) = 3.9^\circ\ [V_{s1}(m/s)]^{0.44}$	Uzielli et al. (2013); Mayne (2014)
NTH solution for normally- to lightly-overconsolidated clays and silts (c′ = 0) with low OCRs < 2	$\phi'_p(degrees) = 29.5^\circ\ B_q^{0.121}\left[0.256 + 0.336\ B_q + \log\ N_m\right]$ (also see Figure 2.17)	Mayne (2005); Senneset et al. (1988; 1989)

Note: ϕ'_p = peak friction angle; q_c = measured cone resistance; σ'_v = effective vertical overburden stress = $\sigma_v - u_0$; σ_v = total vertical overburden stress = $\Sigma(\gamma_{mi} \bullet z_i)$; γ_{mi} = total unit weight of the i-th soil layer; z_i = thickness of the i-th soil layer; u_0 = hydrostatic pore pressure = $\gamma_w\,(z - z_w)$, where, z = depth in question, γ_w = unit weight of water = 9.81 kN/m^3 = 62.4 pcf; z = depth below the ground surface; z_w = depth of the ground water table; $Q_{t1} = (q_t/p_A)/(\sigma'_v/p_A)^{0.5}$; q_t = corrected cone resistance = $q_c + u_2\ (1 - a_n)$; a_n = cone net area ratio = A_n/A_c; A_n = cross-sectional area of the load cell behind the cone; A_c = projected cone cross-sectional area; u_2 = shoulder (behind the cone) pore pressure recorded during penetration of piezocone; p_A = atmospheric pressure = 1 bar = 100 kPa; ϕ'_{cv} = constant volume friction angle = critical state friction angle, ϕ'_{cs}; ψ = soil state parameter; $V_{s1} = V_s/(\sigma'_v/p_A)^{0.25}$ = stress-normalized shear wave velocity; $Q_{tn,cs}$ = clean sand equivalent normalized cone resistance = $K_c \cdot Q_{tn}$; K_c = correction factor for $Q_{tn,cs}$ (defined in Section 2.3.2); Q_{tn} = normalized net corrected cone resistance = $[(q_t - \sigma_v)/p_A](p_A/\sigma'_v)^n$; n = stress normalization exponent; FC = fines content; $B_q = \Delta u_2/q_{t,net}$; Δu_2 = excess pore pressure recorded at the shoulder during penetration of piezocone = $u_2 - u_0$; $q_{t,net}$ = net corrected cone resistance = $q_t - \sigma_v$; F_R = normalized friction ratio = $f_s/(q_t - \sigma_v)$; f_s = sleeve resistance; N_m = cone resistance number = $(q_t - \sigma_v)/(\sigma'_v + a')$; a' = in-situ attraction = $c'\cot(\phi'_p)$; c' = effective cohesion intercept. CPT = cone penetration test; CPTu = piezocone penetration test; CCT = calibration chamber test.

where $M = 6\sin\phi'/(3\text{-}\sin\phi')$ represents the frictional parameter in Cambridge q–p′ space; Λ = plastic volumetric strain potential = 1 - C_s/C_c; C_s = swelling index and C_c = virgin compression index of the soil material, I_R = rigidity index = G/s_u (discussed in Section 2.3.8); G = shear modulus; s_u = undrained shear strength; Δu_2 = measured excess pore pressure behind the tip during cone penetration = $u_2 - u_0$; u_2 = measured total pore pressure behind the tip during cone penetration. The ϕ' = friction angle of the soil, which can be evaluated using the NTH method (Senneset et al., 1988; 1989; see Section 2.3.6), else a default value of $\phi' \approx 30^\circ$ might be adopted, giving $M = 1.2$. A characteristic value of $\Lambda = 0.80$ applies to clays and silts of low to medium sensitivity, increasing to $\Lambda = 1$ for structured and sensitive soils (Jamiolkowski et al., 1985; Ladd & DeGroot, 2003; Larsson & Åhnberg, 2005).

For soft to firm clays, Baligh (1986) and Burns and Mayne (2002a) noted that the shear-component of pore pressures is small (< 20% of the total measured pore pressures). Thus, neglecting that component, Eq. 4.40 can be reduced without much error to the following:

$$OCR = 2\left[\frac{\Delta u_2/\sigma_v'}{\left(\frac{2}{3}M\right)[\ln(I_R)]}\right]^{(1/\Lambda)} \qquad \text{(Eq. 2.42)}$$

A first order approximation of the preconsolidation stress can be applied by assuming $\Lambda \approx 1$ to simplify the following expressions:

$$\sigma'_{vp} = \frac{(q_t - \sigma_v)}{M\left[\frac{1}{3}\ln(I_R) + 1\right]} \qquad \text{(Eq. 2.43)}$$

$$\sigma'_{vp} = \frac{(u_2 - u_o)}{\frac{M}{3}[\ln(I_R)]} \qquad \text{(Eq. 2.44)}$$

$$\sigma'_{vp} = \frac{(q_t - u_2)}{0.975\,M + 1/2} \qquad \text{(Eq. 2.45)}$$

2.3.7.2 Effective preconsolidation and yield stress in clays of low sensitivity and OCR. For intact inorganic clays (which are not fissured) of low sensitivity and low OCR (< 3), the SCE-CSSM expressions can be further simplified for practical use by adopting the characteristic values of $\phi' = 30^\circ$ and $I_R = 100$ (Kulhawy & Mayne, 1990; Mayne, 2001; 2005; 2007b; 2017):

$$\sigma'_{vp} = k^* q_{t,net} = k^*(q_t - \sigma_v) \qquad \text{(Eq. 2.46)}$$

where k is the preconsolidation cone factor with an average value of 0.33 and an expected range of 0.2 to 0.5. The higher values of k are recommended in aged, heavily overconsolidated clays. If previous experience is available in the same deposit, the values of k should be adjusted to reflect this experience and to provide a more reliable profile of the *OCR*. Other simplified correlations based on piezocone tests include the following (Mayne, 2007b; 2013):

$$\sigma'_{vp} = 0.54(u_2 - u_o) = 0.54\Delta u_2 \qquad \text{(Eq. 2.47)}$$

$$\sigma'_{vp} = 0.47(u_1 - u_o) = 0.47\Delta u_1 \qquad \text{(Eq. 2.48)}$$

$$\sigma'_{vp} = 0.60(q_t - u_2) = 0.60\, q_E \qquad \text{(Eq. 2.49)}$$

$$\sigma'_{vp} = 0.75(q_t - u_1) \qquad \text{(Eq. 2.50)}$$

Furthermore, the shear wave velocity (V_s) and its derivative small-strain shear modulus (G_0) from SCPT may also be used for estimating the preconsolidation stress via the following relationships (Mayne et al., 1998; Mayne, 2005; L'Heureux & Long, 2017, respectively):

$$\sigma'_{vp}(kPa) = 0.106[V_s(m/s)]^{1.47} \qquad \text{(Eq. 2.51)}$$

$$\frac{\sigma'_{vp}}{P_A} = \left(\frac{1}{158}\frac{G_o}{P_A}\right)^{0.8} \qquad \text{(Eq. 2.52)}$$

$$\sigma'_{vp}(kPa) = 0.0077\,[V_s(m/s)]^{2.01} \qquad \text{(Eq. 2.53)}$$

In the case of fissured clays, the above equations do not generally apply. Furthermore, if highly structured clays or geomaterials with significant quantities of "unusual" mineralogy exist (i.e., calcite, diatoms, etc.), these equations will require retuning based on that particular geologic formation attributes (Mayne, 2005).

2.3.7.3 Indirect method based on the undrained shear strength of clays. Lunne et al. (1997) discussed an indirect CPT/CPTu-based approach by combining the Schmertmann (1974; 1975), Andresen et al. (1979), and Brooker and Ireland (1965) correlations to present a procedure for estimating the *OCR* from the undrained shear strength, s_u, and the plasticity characteristics of the soil. It requires estimation of the normalized undrained shear strength (s_u/σ'_v) from CPT/CPTu-based correlations (see Section 2.3.10), and the measured or estimated plasticity index, PI, to be used along with Figure 2.18 to estimate the OCR. With PI unknown, an approximate value of $s_u/\sigma'_v = 0.3$ for normally consolidated (i.e., OCR = 1) clay may be adopted (this is an average value corresponding to that obtained from anisotropically consolidated undrained triaxial compression test).

2.3.7.4 Approximate method based on the q_t profile. Lunne et al. (1997) presented a simple method for identifying overconsolidated clays by plotting a theoretical band of $q_t = 2.5$ to 5.0 $\times$ σ'_v on the q_t vs. depth diagram that represents normally consolidated clays (see example shown in Figure 2.19). If the q_t profile plots within or close to that theoretical band, the clay is

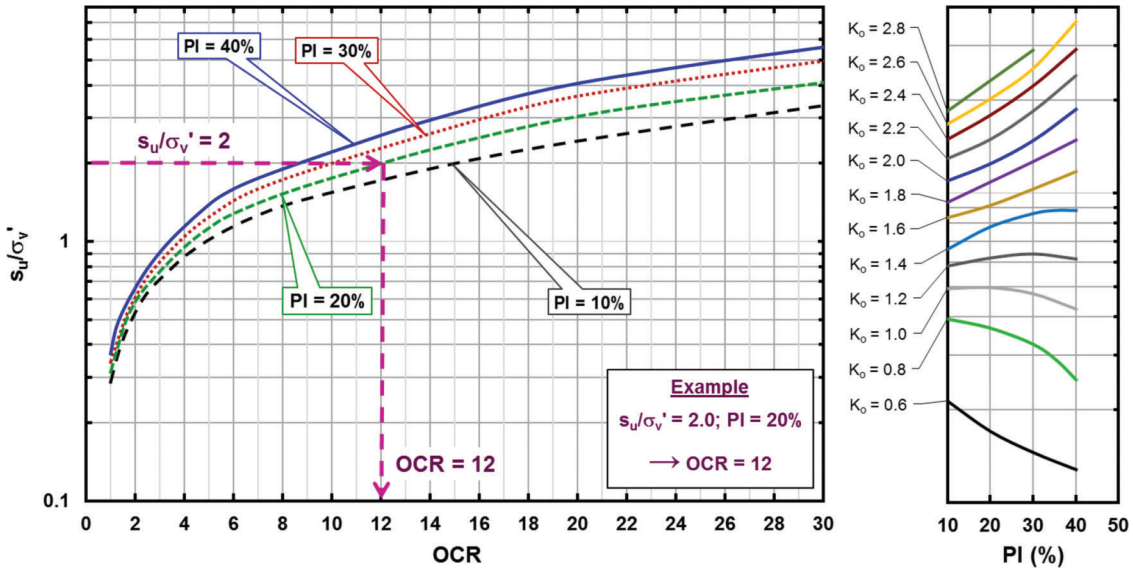

Figure 2.18 *OCR* and K_0 from s_u/σ'_v and *PI* (after Andresen et al., 1979; Brooker & Ireland, 1975).

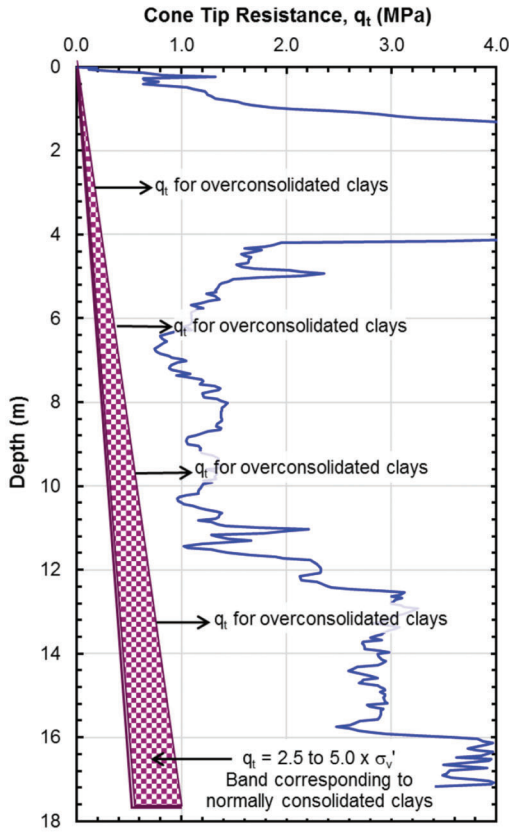

Figure 2.19 Example of approximate indication of *OCR* from q_t vs. depth from an overconsolidated North Sea Clay (after Powell et al., 1989).

likely to be normally consolidated. If q_t is significantly larger, the clay is likely to be overconsolidated.

2.3.7.5 Method based on pore pressure difference from CPTu. When, in a piezocone test, the pore pressures are measured both on the cone face and behind it, the normalized pore pressure difference, $PPD = (u_1 - u_2)/u_0$, can be used to estimate the *OCR* (applicable to soils with $OCR < 10$; Sully et al., 1988):

$$OCR = 0.66 + 1.43\,(PPD) \qquad \text{(Eq. 2.54)}$$

2.3.7.6 Preconsolidation in sandy soils. For sands, the evaluation of stress history by CPT is much more exlusive and less reliable. A methodology based on statistical analyses of chamber data is of the form (Mayne, 2001):

$$OCR = \left[\frac{0.192\left(\frac{q_t}{p_A}\right)^{0.22}}{(1-\sin\phi')\left(\frac{\sigma_v'}{p_A}\right)^{0.31}}\right]^{\left(\frac{1}{\sin\phi' - 0.27}\right)} \qquad \text{(Eq. 2.55)}$$

Mayne (2005) proposed the following expression that provides first order approximation of the effective preconsolidation stress from G_0 obtained of SCPT in mostly sandy soils. This relationship is based on the data from Holmen sand, Po River sand, and Piedmont residual fine sandy silts at the National Geotechnical Test Site (NGES) at Opelika, Alabama.

$$\sigma_{vp}'(kPa) = \left[\frac{G_o(kPa)}{50}\right]^{0.8} \qquad \text{(Eq. 2.56)}$$

2.3.7.7 General expression for sands, silts, clays, and mixed soils. For the general case of evaluating the preconsolidation stress of natural soils, including sands, silts, clays, and mixed soil types, Mayne and Brown (2003) presented the overall relationship based on SCPT sounding:

$$\sigma_{vp}'(kPa) = 0.101[G_o(kPa)]^{0.478}\left[\sigma_v'(kPa)\right]^{0.420}[p_A(kPa)]^{0.102} \qquad \text{(Eq. 2.57)}$$

For the general case, Mayne et al. (2009) offered another preliminary method that extends Eq. 4.46 to the form:

$$\sigma_{vp}' = 0.33(q_t - \sigma_v)^{m'}\left(\frac{p_A}{100}\right)^{1-m'} \qquad \text{(Eq. 2.58)}$$

where the exponent m' apparently increases with fines content and/or decreases with mean grain size. Based on available observations, the parameter $m' \approx 0.72$ in clean quartz sands, 0.8 in silty sands, up to $m' = 1.0$ in intact clays of low sensitivity and may even take on values of 1.1+ in fissured geomaterials.

Mayne (2013) utilized he CPT material index $I_{c(R\&W98)}$ as a means of identifying the magnitude of the parameter m' for general profiling of σ_{vp}' in homogeneous or heterogeneous deposits, as well as mixed soils and/or stratified formations (also see Figure 2.20):

$$m' = 1 - \frac{0.28}{1 + \left[\frac{I_{c(R\&W98)}}{2.65}\right]^{25}} \qquad \text{(Eq. 2.59)}$$

Caution is warranted towards application of these relationships in micaceous and cemented as well as uncemented carbonate sands.

2.3.7.8 Organic clays. Mayne and Agaiby (2019) noted from a review of CPTu data on different organic soils that when the three expressions presented as Eqs. 2.47 to 2.49 are used, unmatched profiles occur in the following hierarchal order and the geomaterials can be identified as organic soils:

$$0.53\,\Delta u_2 < 0.33\,q_{t,net} < 0.60\,q_E \qquad \text{(Eq. 2.60)}$$

Mayne and Agaiby (2019) also noted that this can be particularly helpful in identifying the presence of soft organic clays and peats, since there are cases where soil

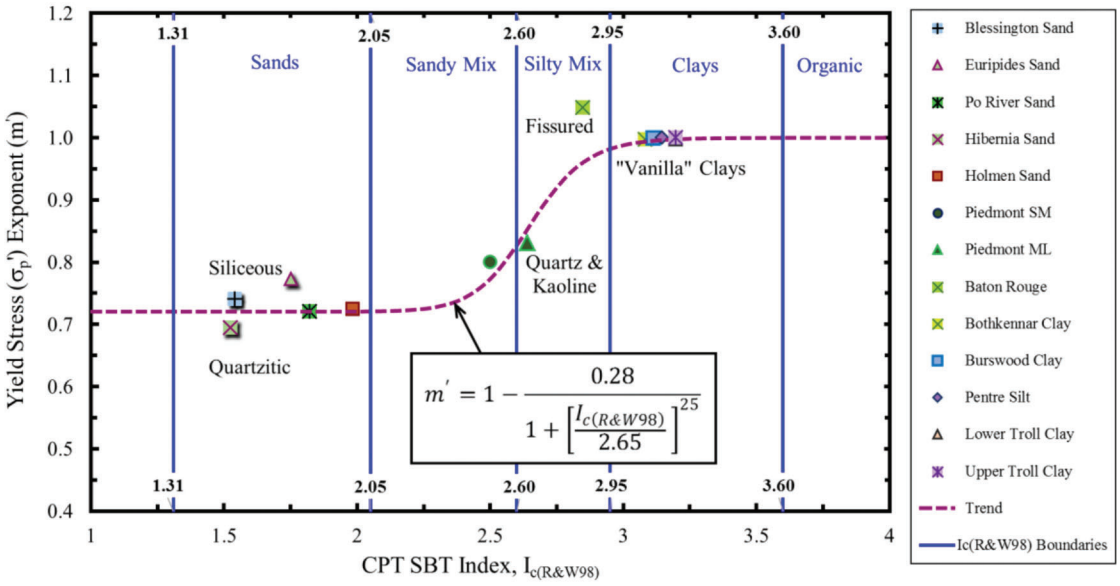

Figure 2.20 Observed approximate trend of yield stress (σ'_{vp}) exponent (m') with CPT SBT Material Index [$I_{c(R\&W98)}$] (adapted from Mayne, 2013).

behavioral charts do not correctly diagnose these types of geomaterials, instead often classify them as clays or silts. Once properly recognized, the yield stress of organic clays can be estimated from:

$$\sigma'_{vp} = 0.33\, q_{t,net}{}^{0.9} \qquad \text{(Eq. 2.61)}$$

Finally, where possible, the interpreted σ'_{vp} results should be cross-checked and validated with other information, including results from one-dimensional consolidation tests on high-quality undisturbed samples, geologic stress history reconstruction, and/or methods based on other in-situ tests.

Table 2.10 provides a summary of the sets of relationships for estimating stress history in terms of the OCR and σ_{vp}' (ϕ_p') of various soil types using data from CPT/CPTu/SCPT.

2.3.8 Rigidity Index

The rigidity index ($I_R = G/s_u$) is an important input parameter for geotechnical applications involving bearing capacity, pile driving, porewater pressure generation, and piezodissipations. The value of soil rigidity index is incorporated in various theories and analytical solutions involving cavity expansion, strain path method, and finite element analyses. For piezocone penetration into clays, the magnitude of undrained rigidity index is often needed in the interpretation of coefficient of consolidation (c_{vh}), its associated hydraulic conductivity (k), as well as the stress history (OCR, σ'_{vp}).

The rigidity index, I_R of the clay (also termed as the undrained rigidity index) can be estimated as (e.g., Burns & Mayne, 2002a):

$$I_R = \exp\left[\left(\frac{1.5}{M} + 2.925\right)\left(\frac{q_t - \sigma_v}{q_t - u_2}\right) - 2.925\right] \qquad \text{(Eq. 2.62)}$$

Mayne (2016) developed an expression for rigidity index of clays from spherical cavity expansion theory which is dependent on the CPTu normalize pore pressure parameter (B_q). The I_R expression is given by:

$$I_R = \exp\left[\frac{2.93 B_q}{(1 - B_q)}\right] \qquad \text{(Eq. 2.63)}$$

where $B_q = (u_2 - u_0)/(q_t - \sigma_v)$. Obtained I_R value can be restricted to the narrow range: $0.50 < B_q < 0.7$.

Agaiby and Mayne (2018) presented a direct CPTu solution for evaluating I_R by rearranging the SCE-CSSM solution:

$$I_R = \exp\left[\frac{1.5 + 2.925 M\left(\frac{U^* - 1}{Q_t}\right)}{M - M\left(\frac{U^* - 1}{Q_t}\right)}\right] \qquad \text{(Eq. 2.64)}$$

where $Q_t = (q_t - \sigma_v)/\sigma_v'$; U^* = normalized pore pressure = $(u_2 - u_0)/\sigma_v'$. Since the above expression is an exponential form, its use in a line-by-line post-processing of CPTu data results in highly variable profiles with depth. Therefore, Agaiby and Mayne (2018) highlighted the necessity of moving average for any practical use of this equation. They also presented a stable representation in the following format:

$$I_R = exp\left[\frac{1.5 + 2.925\, M\, a_q}{M(1 - a_q)}\right] \qquad \text{(Eq. 2.65)}$$

where $a_q = (U^* - 1)/Q_t = (u_2 - \sigma_v)/(q_t - \sigma_v)$. Hence, a_q can be determined as a single value for any clay deposit by taking the slope of a plot of the parameter ($U^* - 1$) versus Q_t, or alternatively taken as the slope of ($u_2 - \sigma_v$)

TABLE 2.10
Solutions for estimating stress history (OCR and σ'_{vp}) from CPT/CPTu/SCPT parameters

Soil Type	Relationship	Reference
Clays and silts (based on spherical cavity expansion and critical state soil mechanics, SCE-CSSM solution)	$OCR = 2\left[\frac{\frac{q_t-\sigma_v}{\sigma_v'}}{M\left[\left(\frac{2}{3}\right)[\ln(I_R)+1]+\frac{\pi}{4}+\frac{1}{2}\right]}\right]^{(1/\Lambda)}$ $OCR = 2\left[\frac{\frac{\Delta u_2}{\sigma_v'}-1}{\left(\frac{2}{3}M\right)[\ln(I_R)-1]}\right]^{(1/\Lambda)}$ $OCR = 2\left[\frac{1}{1.95\,M+1}\left(\frac{q_t-u_2}{\sigma_v'}\right)\right]^{(1/\Lambda)}$ $\sigma'_{vp} = \frac{(q_t-\sigma_v)}{M\left[\frac{1}{3}\ln(I_R)+1\right]}$ (assuming $\Lambda \approx 1$) $\sigma'_{vp} = \frac{(u_2-u_o)}{\frac{M}{3}[\ln(I_R)]}$ (assuming $\Lambda \approx 1$) $\sigma'_{vp} = \frac{(q_t-u_2)}{0.975\,M+1/2}$ (assuming $\Lambda \approx 1$)	Burns & Mayne (1998; 2002a); Chen & Mayne (1994; 1996); Keaveny & Mitchell (1986); Krage et al. (2014); Mayne (2009)
SCE-CSSM solution for soft to firm clays	$OCR = 2\left[\frac{\frac{\Delta u_2}{\sigma_v'}}{\left(\frac{2}{3}M\right)[\ln(I_R)]}\right]^{(1/\Lambda)}$	Baligh (1986); Burns & Mayne (2002a)
Intact inorganic clays (which are not fissured) of low sensitivity and low OCR, (<3) the SCE-CSSM expressions are simplified for practical use by adopting the characteristic values of $\phi' = 30^\circ$ and $I_R = 100$)	$\sigma_p{}' = k^*(q_t-\sigma_v) = k^* q_{t,net}$ $k^* = 0.33$ (average value, with a range of 0.2 to 0.5); higher values of k are recommended in aged, heavily overconsolidated clays. $\sigma'_{vp} = 0.54\,(u_2-u_0) = 0.54\,\Delta u_2$ $\sigma'_{vp} = 0.47\,(u_1-u_0) = 0.47\,\Delta u_1$ $\sigma'_{vp} = 0.60\,(q_t-u_2) = 0.60\,q_E$ $\sigma'_{vp} = 0.75\,(q_t-u_1)$	Kulhawy & Mayne, 1990; Mayne, 2001; 2005; 2007b; 2017
Intact clays (not fissured); adjustment are needed (based on particluar geologic formation attributes) particularly for highly structured clays and geomaterials with significant quantitites of unusual minerology (i.e., calcite, diatoms, etc.)	$\sigma'_{vp}\,(kPa) = 0.106\,[V_s\,(m/s)]^{1.47}$	Mayne et al. (1998)
Same as above	$\frac{\sigma'_{vp}}{p_A} = \left(\frac{1}{158}\cdot\frac{G_o}{p_A}\right)^{0.8}$	Mayne (2005)
Same as above	$\sigma'_{vp}\,(kPa) = 0.0077\,[V_s\,(m/s)]^{2.01}$	L'Heureux & Long (2017)
Indirect method based on the undrained shear strength and plasticity characteristics of clays	Chart based estimation method presented in Figure 2.18 (For PI unknown, adopt an approximate average value of $s_u/\sigma'_v = 0.3$ for NC clays)	Andresen et al. (1979); Brooker & Ireland (1965) Lunne et al. (1997); Schmertmann (1974; 1975);
Approximate method for clays	Based on measured q_t profile with a theoreical band representing $q_t = 2.5\,\sigma'_v$ to $5.0\,\sigma'_v$. If actual q_t profile falls within the theoreical band, the clay in NC; if it is significantly higher, the clay is OC (see Figure 2.19 as an example)	Powell et al. (1989)
Method based on CPTu tests with pore pressures measured at u_1 and u_2 locations, both (applicable to $OCR < 10$)	$OCR = 0.66 + 1.43(PPD)$	Sully et al. (1988)
For sands; methodology based on statistical analyses of chamber data	$OCR = \left[\frac{0.192\left(\frac{q_t}{p_A}\right)^{0.22}}{(1-sin\phi')\left(\frac{\sigma_v'}{p_A}\right)^{0.31}}\right]^{\left(\frac{1}{sin\varphi'-0.27}\right)}$	Mayne (2001)

Continued

TABLE 2.10
(Continued)

Soil Type	Relationship	Reference
Sandy soils (data from Holmen, Norway; Po River sand; and Piedmont residual fine sandy silts at the National Geotechnical Test Site (NGES) at Opelika, Alabama)	$\sigma'_{vp}\ (kPa) = \left[\frac{G_o\ (kPa)}{50}\right]^{0.8}$	Mayne (2005)
General for sand, silt, clays, and mixed soils	$\sigma'_{vp} = 0.33\ (q_t - \sigma_v)^{m'}\left(\frac{p_A}{100}\right)^{1-m'}$ m′ ≈ 0.72 in clean quartz sands, 0.8 in silty sands, 1.0 in intact clays of low sensitivity, and possible values of 1.1 + in fissured geomaterials Alternatively, m′ can be estimated based on the relationship shown in Figure 2.20: $m' = 1 - \frac{0.28}{1 + \left[\frac{I_{c(R\&W98)}}{2.65}\right]^{25}}$	Mayne (2009); Mayne (2013)
General for silt, clays, and mixed soils (based on SCPT or SCPTu)	$\sigma'_{vp}\ (kPa) = 0.101\ [G_o\ (kPa)]^{0.478}\left[\sigma_v'\ (kPa)\right]^{0.420}[p_A\ (kPa)]^{0.102}$	Mayne & Brown (2003)
Organic clays from CPTu	First estimate σ'_{vp} to confirm presence of organic clays using the following hierarchal order: $0.53\Delta u_2 < 0.33 q_{t,net} < 0.60 q_E$ Once properly recognized, the yield stress of organic clays may be estimated from: $\sigma'_{vp} = 0.33 q_{t,net}^{0.9}$	Mayne & Agaiby (2019)

Note: *OCR* = overconsolidation ratio; *OC* = overconsolidated; *PPD* = pore pressure difference = $(u_1 - u_2)/u_0$; CPTu = piezocone penetration test; SCPT = seismic cone penetration test; SCPTu = seismic piezocone test; SCE-CSSM = spherical cavity expansion-critical state soil mechanics; CCT = calibration chamber test; q_t = corrected cone resistance = $q_c + u_2\ (1 - a_n)$; a_n = cone net area ratio = A_n/A_c; A_n = cross-sectional area of the load cell behind the cone; A_c = projected cone cross-sectional area; u_2 = shoulder (behind the cone) pore pressure recorded during penetration of piezocone; q_c = measured cone resistance; σ'_v = effective vertical overburden stress = $\sigma_v - u_0$; σ_v = total vertical overburden stress = $\Sigma(\gamma_{mi} \bullet z_i)$; γ_{mi} = total unit weight of the i-th soil layer; z_i = thickness of the i-th soil layer; u_0 = hydrostatic pore pressure = $\gamma_w\ (z - z_w)$, where, z = depth in question, γ_w = unit weight of water = 9.81 kN/m^3 = 62.4 pcf; z_w = depth of the ground water table; M = 6sinφ'/(3-sinφ') represents the frictional parameter in Cambridge q–p′ space; φ' = friction angle; Λ = plastic volumetric strain potential = $1 - C_s/C_c$; C_s = swelling index and C_c = virgin compression index of the soil material, I_R = rigidity index = G/s_u; G = shear modulus; s_u = undrained shear strength; σ'_{vp} = preconsolidation stress; *PI* = plasticity index; *NC* = normally consolidated; G_0 = small strain shear modulus = $\rho_m\ V_s^2$; ρ_m = soil mass density; V_s = shear wave velocity; k^* = preconsolidation cone factor; Δu_2 = measured excess pore pressure behind the tip during cone penetration = $u_2 - u_0$; p_A = atmospheric pressure = 1 bar = 100 kPa; CPT = cone penetration test; $q_{t,net}$ = net corrected cone resistance = $q_t - \sigma_v$; m' = yield stress exponent; $I_{c(R\&W98)} = \sqrt{[3.47 - logQ_{tn}]^2 + [1.22 + LogF_R]^2}$; $Q_{tn} = [(q_t - \sigma_v)/p_A](p_A/\sigma'_v)^n$; F_R = normalized friction ratio = $f_s/(q_t - \sigma_v)$; f_s = sleeve resistance; q_E = effective cone resistance = $q_t - u_2$; z = depth below the ground surface.

versus $(q_t - \sigma_v)$. Using regression analyses, slightly different slope values for a_q are obtained.

Alternatively, I_R (taken at 50% of the ultimate strength) has been correlated to *OCR* and plasticity index (*PI*) of the clay and presented in graphical form by Keaveny and Mitchell (1986). This relationship can be approximated by the expression (Mayne, 2009):

$$I_{R(50)} \approx \frac{exp\left[\frac{137 - PI}{23}\right]}{\left\{1 + \ln\left[1 + \frac{(OCR - 1)^{3.2}}{26}\right]\right\}^{0.8}} \qquad \text{(Eq. 2.66)}$$

$I_{R(50)}$ can also be estimated from the following recent formulation developed by Krage et al. (2014), which requires small-strain shear modulus (G_0) assessment from the shear wave velocity (V_s):

$$I_{R(50)} = \frac{1.81\ G_0}{(q_t - \sigma_v)^{0.75}(\sigma_v')^{0.25}} \qquad \text{(Eq. 2.67)}$$

Table 2.11 provides a concise summary of the correlations for estimating the rigidity index (I_R) from CPTu/SCPT data.

2.3.9 Geostatic Lateral Stress

The geostatic horizontal stress state is represented by the at-rest coefficient K_0, where $K_0 = \sigma'_h/\sigma'_v$, and σ'_h = effective horizontal stress, which specifically applies to one-dimensional vertical loading under conditions of zero lateral strain (or horizontal) strain ($\varepsilon_h = 0$). The value of K_0 can be assessed directly using various in-situ tests (e.g., self-boring pressuremeter tests (SBPMT),

TABLE 2.11
Solutions for estimating rigidity index (I_R) from CPTu/SCPT data

Soil Type	Relationship	Reference
Clays and silts (based on spherical cavity expansion and critical state soil mechanics, SCE-CSSM solution)	$I_R = \exp\left[\left(\frac{1.5}{M}+2.925\right)\left(\frac{q_t-\sigma_v}{q_t-u_2}\right)-2.925\right]$ $I_R = \exp\left[\frac{2.93B_q}{(1-B_q)}\right]$ $I_R = \exp\left[\frac{1.5+2.925M\left(\frac{U^*-1}{Q_t}\right)}{M-M\left(\frac{U^*-1}{Q_t}\right)}\right]$ $I_R = \exp\left[\frac{1.5+2.925Ma_q}{M(1-a_q)}\right]$ $I_{R(50)} \approx \frac{\exp\left(\frac{137-PI}{23}\right)}{1+\ln\left[1+\frac{(OCR-1)^{3.2}}{26}\right]^{0.8}}$ $I_{R(50)} = \frac{1.81G_o}{(q_t-\sigma_v)^{0.75}(\sigma_v')^{0.25}}$	Agaiby & Mayne (2018); Burns & Mayne (2002a); Keaveny & Mitchell (1986); Krage et al. (2014); Mayne (2009); Mayne (2016)

Note: I_R = rigidity index = G/s_u; G = shear modulus; s_u = undrained shear strength; M = 6sin ϕ'/(3-sin ϕ') represents the frictional parameter in Cambridge q–p′ space; ϕ' = friction angle; q_t = corrected cone resistance = $q_c + u_2$ ($1 - a_n$); a_n = cone net area ratio = A_n/A_c; A_n = cross-sectional area of the load cell behind the cone; A_c = projected cone cross-sectional area; u_2 = shoulder (behind the cone) pore pressure recorded during penetration of piezocone; q_c = measured cone resistance; σ_v' = effective vertical overburden stress = $\sigma_v - u_0$; σ_v = total vertical overburden stress = $\Sigma(\gamma_{mi} \bullet z_i)$; γ_{mi} = total unit weight of the i-th soil layer; z_i = thickness of the i-th soil layer; u_0 = hydrostatic pore pressure = $\gamma_w (z - z_w)$, where, z = depth below the ground surface, γ_w = unit weight of water = 9.81 kN/m^3 = 62.4 pcf; z_w = depth of the ground water table; $B_q = (u_2 - u_0)/(q_t - \sigma_v)$; U^* = normalized pore pressure = $(u_2 - u_0)/\sigma_v'$; $a_q = (U^* - 1)/Q_t = (u_2 - \sigma_v)/(q_t - \sigma_v)$; $I_{R(50)} = I_R$ of the clay (taken at 50% of strength); PI = plasticity index; OCR = overconsolidation ratio; G_0 = small strain shear modulus = $\rho_m V_s^2$; ρ_m = soil mass density; V_s = shear wave velocity.

total stress cells (TSC), and paired sets of directional and polarized shear wave velocities, such as crosshole (CHT) and downhole (DHT) geophysics surveys). As such, there are no reliable methods for determination of σ_h' or K_0 from CPT/CPTu and therefore, no well-established direct relationship exists for the assessment of K_0 from the CPT data.

Based on theoretical, analytical, and empirical investigations on extensive laboratory data on clays, silts, sands, and gravels, Mayne and Kulhawy (1982), offered a solution in the form of following expression for uncemented sands and non-structured clays of low to medium sensitivity:

$$K_{0,OC} = K_{0,NC} OCR^{\sin\phi'} = (1 - \sin\phi') OCR^{\sin\phi'} \quad \text{(Eq. 2.68)}$$

where $K_{0,OC}$ corresponds to the overconsolidated horizontal stress coefficient, and $K_{0,NC}$ corresponds to the normally consolidated horizontal stress coefficient. It may be noted that the part of the above equation $K_{0,NC}$ = (1 – sin ϕ') was originally presented by Jaky. In implementation of the above solution, appropriate estimations of OCR and ϕ' from CPT data allows for a first order approximation of K_0, although with lesser reliability. This may generally apply to all soils.

In the absence of reliable friction angle of material, the first-order approximations are (Mayne, 2005):

$$\textit{For clays from TSC}: K_0 = 0.5\, OCR^{0.5} \quad \text{(Eq. 2.69)}$$

$$\textit{For clays from SBPMT}: K_0 = 0.47\, OCR^{0.53} \quad \text{(Eq. 2.70)}$$

$$\textit{For uncemented sand from PMT}: K_0 = 0.4\, OCR^{0.5} \quad \text{(Eq. 2.71)}$$

For highly structured soils, higher values of K_0 can be realized (e.g., Hamouche et al., 1995). In the case of a complex stress history that involves virgin loading-unloading-reloading, the following expression may apply (Schmidt, 1983):

$$K_0 = \frac{(1 - sin\,\phi')}{(OCR_{max} - 1)} \left[OCR_{max} - OCR + (OCR - 1)(OCR_{max})^{sin\,\phi'}\right] \quad \text{(Eq. 2.72)}$$

where OCR_{max} = the maximum applied overconsolidation ratio prior to loading (note: when $OCR = OCR_{max}$, Eq. 2.72 reduces to Eq. 2.68.

Although no direct methods are available to determine K_0 from CPT/CPTu data, approximate estimates can be made via the following recommended indirect methodologies. It should be noted that most of these methodologies are generally limited to mechanically overconsolidated soils.

2.3.9.1 Interpretation in fine-grained soils

2.3.9.1.1 Based on OCR. This method requires estimation of the undrained shear strength, s_u, from CPTu (see Section 2.3.10), and effective vertical stress, σ_v', using the unit weight data (see Section 2.3.3) for s_u/σ_v', or alternatively estimate OCR to make a first-order approximation of K_0 from Figure 2.18. This method requires knowledge of the plasticity index of the clay.

Based on the results from SBPMT, Kulhawy and Mayne (1990) offered an approach to estimate K_0 from CPT (see Figure 2.21). The results, however, indicate a considerable scatter in the data used for this correlation, and, therefore, must be used with caution.

$$K_0 = 0.1\left(\frac{q_t - \sigma_v}{\sigma_v'}\right) \qquad \text{(Eq. 2.73)}$$

2.3.9.1.2 Based on measured pore pressure difference. Sully and Campanella (1991) proposed that pore pressure distribution around the penetration cone is a function of in situ horizontal stress. They correlated the ratio of the difference in pore pressure measured to the effective overburden pressure [$PPSV = (u_1 - u_2)/\sigma_v'$)] with K_0 determined by other in situ tests. The correlation is shown in Figure 2.22.

It is evident that the approach by Sully and Campanella (1991) can be used only when pore pressures are measured at the two locations: either using a dual filter element or performing parallel soundings of piezocone with u_1 and u_2 measurements. This correlation, summarized below, should also be used only as a guide in view of the visible scatter in Figure 2.22.

$$K_o = 0.5 + 0.11PPSV = 0.5 + 0.11\left(\frac{u_1 - u_2}{\sigma_v'}\right) \qquad \text{(Eq. 2.74)}$$

2.3.9.1.3 Based on measured lateral stress and sleeve friction. Masood and Mitchell (1993) proposed a method to estimate K_0 from the measured sleeve friction (f_s) (see Figure 2.23). It requires knowledge of OCR. The correlation is highly dependent on the reliability of f_s measurement, and hence should be used sparingly.

2.3.9.2 Interpretation in coarse-grained soils

2.3.9.2.1 Based on OCR. A method based on the assessment of OCR from geological evidence or from neighboring clay layers may be used to derive K_0 from the following empirical correlation (Lunne et al., 1997):

$$\frac{K_{o(OC)}}{K_{o(NC)}} = OCR^m \qquad \text{(Eq. 2.75)}$$

where the subscripts "OC" and "NC" represent overconsolidated and normally consolidated sands, respectively; exponent m varies between 0.45 and 0.65, being

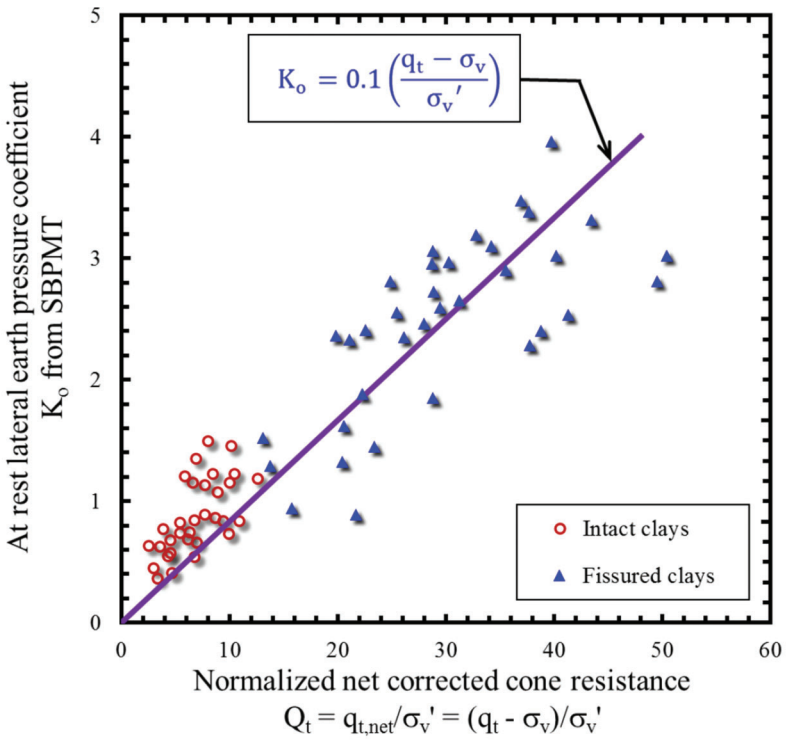

Figure 2.21 K_0 correlation of clays from CPTu data (adapted from Kulhawy & Mayne, 1990).

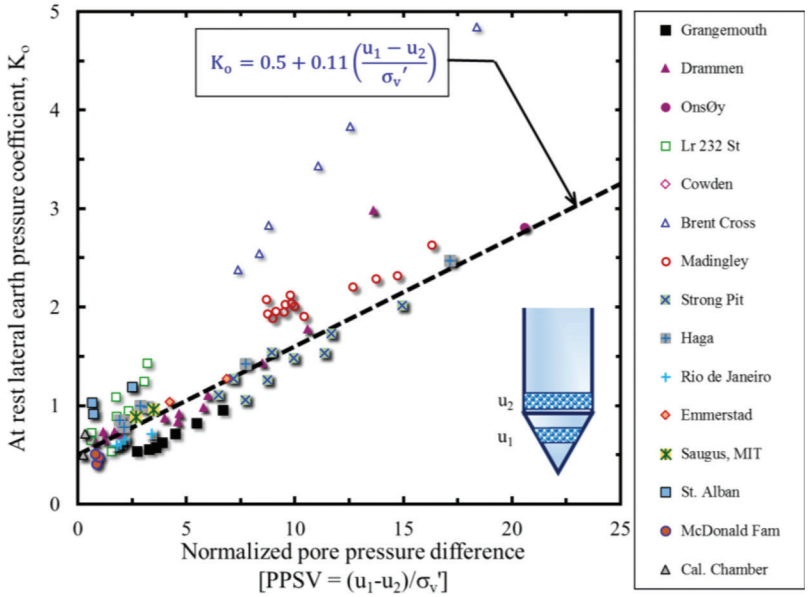

Figure 2.22 K_0 vs. normalized pore pressure difference PPSV (adapted from Sully & Campanella, 1991).

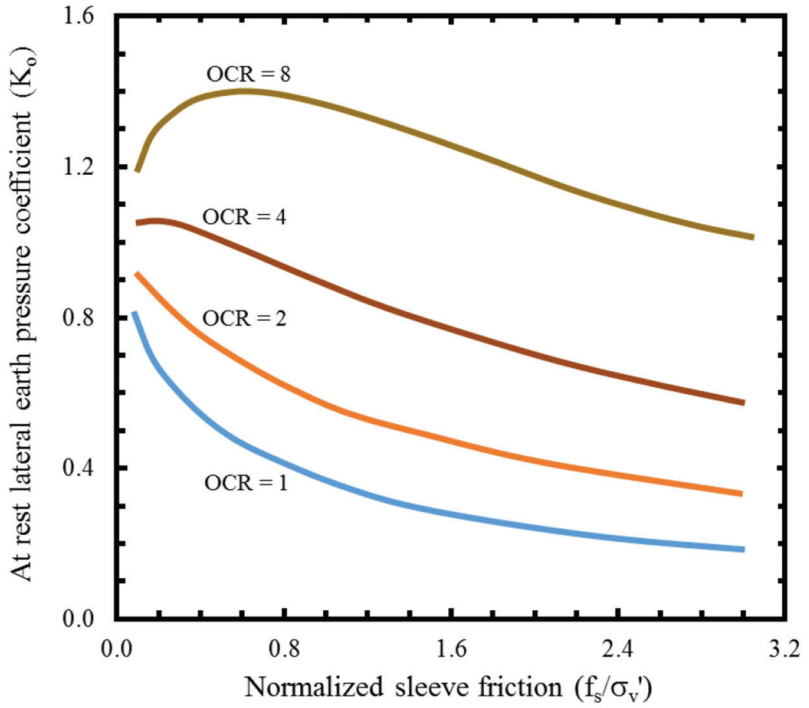

Figure 2.23 Relationship between f_s, *OCR*, and K_0 (adapted from Masood & Mitchell, 1993).

smaller for loose sand than for dense (Al-Hussaini & Townsend, 1975; Lunne & Christoffersen, 1983; Mayne & Kulhawy, 1982).

2.3.9.2.2 Based on sand density. Calibration chamber tests on Leighton Buzzard sand by Houlsby and Hitchman (1988) have demonstrated that cone resistance is controlled by density and horizontal stress (also see Figure 2.24):

$$\frac{q_c}{p_A} = A\left(\frac{\sigma_h'}{p_A}\right)^{0.6} \qquad \text{(Eq. 2.76)}$$

where A is a constant depending on sand density equal to 45 for the loose sand, 155 for the medium sand, and 230 for the dense sand. Thus, if the sand density can be evaluated, Eq. 2.76 has the potential to estimated σ_h'.

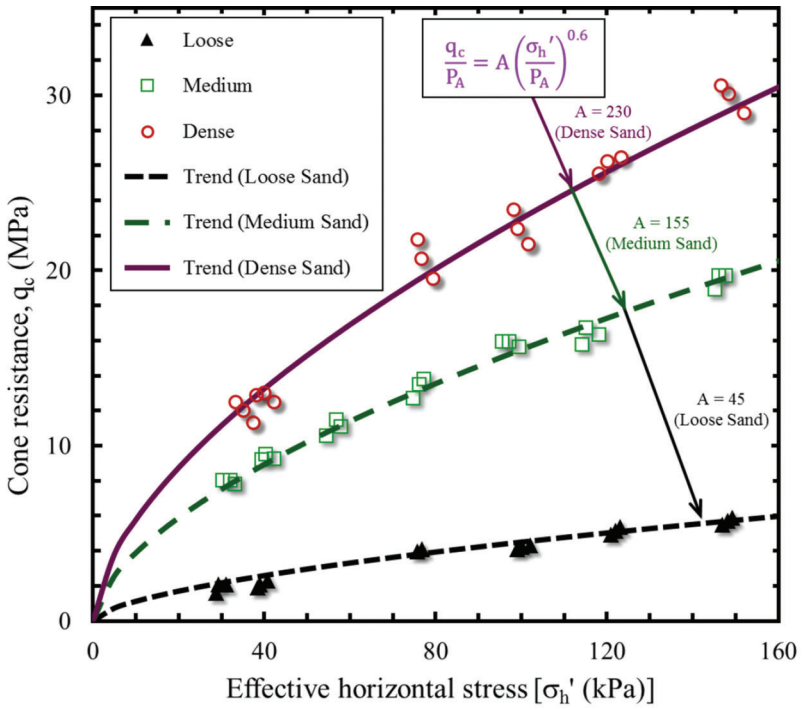

Figure 2.24 Cone tip resistance, q_c, versus effective horizontal stress, σ_h', for Leighton Buzzard sand (adapted from Houlsby & Hitchman, 1988).

Based on the calibration chamber data, Mayne (1991) also proposed the following expression for estimating K_0 based on cone resistance:

$$K_0 = \left(\frac{p_A}{\sigma_v'}\right)\left(\frac{q_c}{p_A}\right)^{1.6} \Bigg/ \left\{145\, exp\left[\left(\frac{\left(\frac{q_c}{p_A}\right)\Big/\left(\frac{\sigma_v'}{p_A}\right)^{0.5}}{12.2\, OCR^{0.18}}\right)^{0.5}\right]\right\} \quad \text{(Eq. 2.77)}$$

Mayne (2005) observed that the effective lateral (horizontal) stress applied in 26 series of calibration chamber test (CCT) programs affected the cone tip stress (q_c) more than effective vertical stress (σ_v'). Thus, the applied consolidation state used in CCTs is given by both lateral stress coefficient ($K_0 = K_c = \sigma_{hc}'/\sigma_{vc}'$) and overconsolidation ratio (OCR). The relationship in Eq. 2.77 incorporates this specific observation, and in its rearranged form below:

$$K_0 = 0.192\left(\frac{q_t}{p_A}\right)^{0.2}\left(\frac{\sigma_v'}{p_A}\right)^{-0.31} OCR^{0.27} \quad \text{(Eq. 2.78)}$$

These indirect methods and correlations for K_o estimation are summarized in Table 2.12.

2.3.10 Undrained Shear Strengths

The undrained shear strength ($s_u = c_u$), which represents the total stress strength of soil for geotechnical applications involving short term loading of clays and clayey silts, depends on the direction of loading, soil anisotropy, degree of drainage, loading direction, strain-rate, and stress history. Therefore, no single value of s_u exists (Lunne et al., 1997; Robertson & Cabal, 2014). From the most common types of undrained shear strength tests, experience has shown that the s_u of a soil in triaxial compression is larger than in direct simple shear than in triaxial extension [$s_{u(CKoUC)} > s_{u(DSS)} > s_{u(CKoUE)}$]. An example to demonstrate the influence of various test methods and loading modes for normally consolidated Boston Blue clay is presented in Table 2.13.

The applicable s_u to be used in the analysis, therefore, depends on the design problem, and hence the values of s_u reported must also include the information regarding the test method. Based on the hierarchy of the measured s_u given above, it is customary to consider the direct simple shear as the average undrained strength [$s_{u(DSS)} \approx s_{u(ave)}$].

It may be seen in Table 2.13 that the undrained shear strength is expressed in terms of its normalized state, i.e., undrained shear strength ratio (s_u/σ_v'). It is considered useful to express it in this form since it relates directly to overconsolidation ratio (OCR). If only a representative undrained strength is needed for analysis, the simple shear mode may be sufficient (Wroth, 1984). This may be useful if the geotechnical problem has not yet fully established since simple shear represents a middle value among the different modes, as shown above. In the simple shear, pure shear is applied to the specimens, whereas, in several available commercial systems, a direct simple shear (DSS) mode is a close approximation. The general expression for the undrained shear

TABLE 2.12
Summary of selected methods for indirect assessment of lateral earth pressure coefficient K_0 from CPT/CPTu parameters

Soil Type	Method/Relationship	Reference
Fine grained soils with information of *PI* and *OCR* known	Use Figure 2.18 (method requires estimation of s_u and σ_v' to find K_0 from graphical solution)	Andresen et al. (1979); Brooker & Ireland (1965)
Fine grained soils (12 intact and 5 fissure clays); based on the results of SBPMT	$K_0 = 0.1\left(\frac{q_t - \sigma_v}{\sigma_v'}\right)$ (also see Figure 2.21)	Kulhawy & Mayne (1990)
Based on CPTu data from 15 worldwide clay sites pore pressures were measured at two locations: either using a dual filter elements or performing parallel soundings of piezocone with u_1 and u_2 measurements	$K_0 = 0.5 + 0.11 PPSV = 0.5 + 0.11\left(\frac{u_1 - u_2}{\sigma_v'}\right)$ (also see Figure 2.22)	Sully & Campanella (1991)
For fine-grained soils with information of *OCR* known	Graphical solution based on normalized sleeve friction (f_s/σ_v') and *OCR* (see Figure 2.23)	Masood & Mitchell (1993)
For coarse-grained soils with OCR information obtained from geological evidence or from neighboring clay layers	$\frac{K_{0,OC}}{K_{0,NC}} = OCR^m$ m = 0.45 to 0.65 (smaller values for loose sand than dense sand) $K_{0,NC} = 1 - \sin\phi'$	Lunne et al. (1997)
Sands (based on relative density)	$\frac{q_c}{p_A} = A\left(\frac{\sigma_h'}{p_A}\right)^{0.6}$ A = 45 (loose sand), 155 (medium sand), and 230 (dense sand) (also see Figure 2.24)	Houlsby & Hitchman (1988)
Calibration chamber test data on sands	$K_0 = \left(\frac{p_A}{\sigma_v'}\right)\left(\frac{q_c}{p_A}\right)^{1.6} \Bigg/ \left\{145\, exp\left[\left(\frac{\left(\frac{q_c}{p_A}\right)\Big/\left(\frac{\sigma_v'}{p_A}\right)^{0.5}}{12.2\, OCR^{0.18}}\right)^{0.5}\right]\right\}$	Mayne (1991)
Calibration chamber test data on sands	$K_0 = 0.192\left(\frac{q_t}{p_A}\right)^{0.2}\left(\frac{\sigma_v'}{p_A}\right)^{-0.31} OCR^{0.27}$	Mayne (2005)

Note: *PI* = plasticity index; *OCR* = overconsolidation ratio; s_u = undrained shear strength; σ_v' = effective vertical overburden stress = $\sigma_v - u_0$; σ_v = total vertical overburden stress = $\Sigma(\gamma_{mi} \bullet z_i)$; γ_{mi} = total unit weight of the i-th soil layer; z_i = thickness of the i-th soil layer; u_0 = hydrostatic pore pressure = $\gamma_w (z - z_w)$; γ_w = unit weight of water; z = depth below the ground surface; z_w = depth of the ground water table; K_0 = lateral earth pressure coefficient; q_t = corrected cone resistance = $q_c + u_2 (1 - a_n)$; a_n = cone net area ratio = A_n/A_c; A_n = cross-sectional area of the load cell behind the cone; A_c = projected cone cross-sectional area; u_2 = shoulder (behind the cone) pore pressure recorded during penetration of piezocone; q_c = measured cone resistance; $PPSV = (u_1 - u_2)/\sigma_v'$ = normalized pore pressure difference; p_A = atmospheric pressure = 1 bar = 100 kPa; u_1 = apex or mid-face pore pressure recorded during penetration of piezocone; f_s = sleeve resistance; *OC* = overconsolidated; *NC* = normally consolidated; σ_h' = effective lateral (horizontal) stress; CPT = cone penetration test; CPTu = piezocone penetration test; CCT = calibration chamber test.

strength ratio corresponding to the SS or DSS modes for intact clays over a range of overconsolidation ratios is given by (Wroth & Houlsby, 1985):

$$\left(\frac{s_u}{\sigma_v'}\right)_{OC[DSS]} = \frac{1}{2} sin\,\phi' OCR^{\Lambda} \qquad \text{(Eq. 2.79)}$$

where Λ = plastic volumetric strain potential = 1 - C_s/C_c; C_s = swelling index and C_c = virgin compression index of the soil material.

The rational evaluation of s_u by piezocone is accomplished in a two-step procedure:

- Evaluation of *OCR* profile using the aforementioned relationships between σ_{vp}' and CPTu parameters, and ϕ' and CPTu parameters presented in the previous sections.
- Use of Eq. 2.79 to obtain a complementary suite of s_u profiles.

In the CSSM (critical state soil mechanics) version, Λ is taken to be 0.8 for many "vanilla" clays and Λ = 0.9 to 1 will be appropriate for structured and sensitive clays.

According to the MIT SHANSEP (stress history and normalized soil engineering parameters) approach, if unknown, default values may be adopted: ϕ' = 28° and Λ = 0.80. This would give (Ladd & DeGroot, 2003):

$$\text{SHANSEP}: \left(\frac{s_u}{\sigma_v'}\right)_{OC[DSS]} = 0.22\, OCR^{0.8} \qquad \text{(Eq. 2.80)}$$

Furthermore, in the case of soft lightly-overconsolidated (*LOC*) to normally consolidated (*NC*) soils (*OCRs* < 2), the expression can de-convolute to the following simple form (Mesri, 1975):

$$s_{uNC[DSS]} = 0.22\, \sigma_{vp}' \qquad \text{(Eq. 2.81)}$$

TABLE 2.13
Undrained shear strength ratios (s_u/σ_v') for normally consolidated Boston Blue clay (after Mayne, 2008; data from Ladd et al., 1980; Ladd, 1991; Whittle, 1993)

Test Method and Mode	Normalized Undrained Shear Strength (s_u/σ_v')
Self-boring pressuremeter tests (SBPMT)	0.42
Plane strain compression (PSC)	0.34
Triaxial compression (CK_0UC)	0.33
Unconsolidated undrained (UU)	0.275
Field vane shear test (FVST)	0.21
Direct simple shear (DSS)	0.20
Plane strain extension (PSE)	0.19
Triaxial extension (CK_0UE)	0.16
Unconfined compression (UC)	0.14

Note: s_u = undrained shear strength; σ_v' = effective vertical overburden stress = $\sigma_v - u_0$; σ_v = total vertical overburden stress = $\Sigma(\gamma_{mi} \bullet z_i)$; γ_{mi} = total unit weight of the i-th soil layer; z_i = thickness of the i-th soil layer; u_0 = hydrostatic pore pressure = $\gamma_w (z - z_w)$; γ_w = unit weight of water; z = depth below the ground surface; z_w = depth of the ground water table.

In summary, for intact clays, Eqs. 2.79, 2.80, and 2.81 offer a hierarchical approach to a consistent interpretation of an "average" undrained shear strength for fine-grained clays and silts. For fissured clays, the calculated undrained strengths should be reduced to one-half of those for intact geomaterials.

Since cone penetration is a complex phenomenon, the use of theoretical solutions requires making several simplifying assumptions as previously presented. Furthermore, theoretical solutions have limitations in modelling the real soil behavior under conditions of varying stress history, anisotropy, sensitivity, ageing and macrofabric. Empirical correlations are, therefore, generally preferred. The empirical approaches available for interpretation of s_u from CPT/CPTu data can be grouped under three main categories as discussed below. Other empirical approaches for estimating the remolded undrained shear strength [$s_{u(remolded)}$] and the sensitivity of clayey soils (S_t) from CPT parameters are also presented.

2.3.10.1 s_u Estimation using net cone resistance. When CPTu soundings reveal the presence of clay soils, the conventional practice is to directly evaluate the in-situ undrained shear strength (s_u) from the tip resistance. The classical route is to adopt an inverted (or rearranged) bearing capacity form, whereby:

$$s_u = \frac{q_{t,net}}{N_{kt}} = \frac{(q_t - \sigma_v)}{N_{kt}} \qquad \text{(Eq. 2.82)}$$

where N_{kt} is a bearing factor that depends upon the theory, (e.g., limit plasticity, cavity expansion) or numerical simulation method (e.g., strain path method, finite elements), as discussed by Konrad and Law (1987) and Yu and Mitchell (1998). In practice, this is most often the sole interpretation performed, using an assumed value for N_{kt}.

Common values for N_{kt} in soft intact clays are generally taken to be between 10 and 20, with an average of 14, yet are certainly mode dependent (Lunne et al., 1997). In fissured clays, N_{kt} factors have been reported in the range of 20 to 30, somewhat dependent upon the degree of fissuring (Powell & Quarterman, 1988). N_{kt} tends to increase with increasing plasticity and decrease with increasing soil sensitivity. Based on field observations, Robertson (2009) noted that N_{kt} is close to 14 for many insensitive fine-grained soils, and proposed a simplified approach to estimate peak undrained shear strength [$s_{u(peak)}$] ratio in direct simple shear mode:

$$\left[\frac{s_{u(peak)}}{\sigma_v'}\right]_{DSS} = \frac{Q_{tn}}{N_{kt}} \text{ (where preliminary } N_{kt} = 14) \qquad \text{(Eq. 2.83)}$$

If CPT pore pressure measurements are made, the normalized parameter B_q can also be used to estimate N_{kt}, as suggested Lunne et al. (1997) (see Figure 2.25), where N_{kt} values are in the range of 6–15. They noted an increase in N_{kt} with decreasing OCR. For comparison, the range corresponding to the data from Lunne et al. (1986) is also shown, giving on average, higher N_{kt} values with considerably more scatter (N_{kt} = 8.5 to 20). In very sensitive fine-grained soil, where $B_q \approx 1.0$, N_{kt} can be as low as 6. For deposits where little experience is available, estimate s_u using preliminary cone factor values (N_{kt}) from 14 to 16. For more conservative estimate, select a value close to the upper limit.

Mayne and Peuchen (2018) used a database involving 407 high-quality triaxial compression tests (CK_0UC) to review strengths from a wide variety of clays. The study considered a total 62 clays, categorized into five groups: soft offshore, soft-firm onshore, sensitive, overconsolidated, and fissured clays. The backfigured N_{kt} factors ranged from 8 to 25 and found to decrease with pore pressure ratio, B_q.

Mayne and Peuchen (2018) recommended a single N_{kt} for each clay group for use in preliminary studies: N_{kt} = 10 (sensitive clays); N_{kt} = 12 (normally consolidated to lightly overconsolidated soft-firm onshore clays); N_{kt} = 12.3 (normally consolidated to lightly overconsolidated offshore clays); N_{kt} = 14 (overconsolidated intact clays); and N_{kt} = 25 (overconsolidated fissured clays). They, however, noted a considerable range and variance for the specified N_{kt} within each group that could be associated with sample disturbance, clay mineralogy, fabric, organic content, and other variables. They also presented a continuous approximate function to assess N_{kt} based on B_q (which applies to $B_q > -0.1$):

$$N_{kt} = 10.5 - 4.6 \ \ln(B_q + 0.1) \qquad \text{(Eq. 2.84)}$$

2.3.10.2 s_u estimation using effective cone resistance. Senneset et al. (1982) and Campanella et al. (1982)

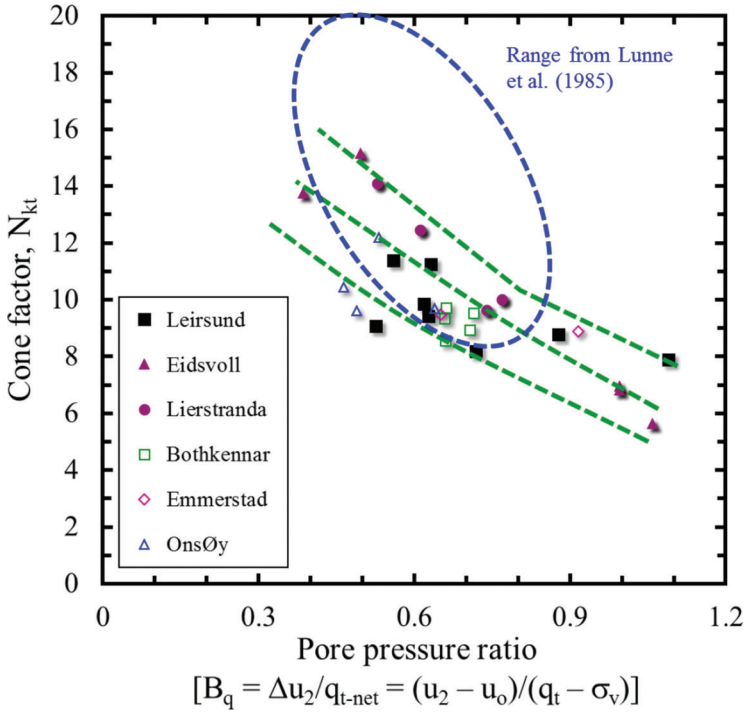

Figure 2.25 Cone factor N_{kt} versus B_q (adapted from Karlsrud et al., 1996; Lunne et al., 1997).

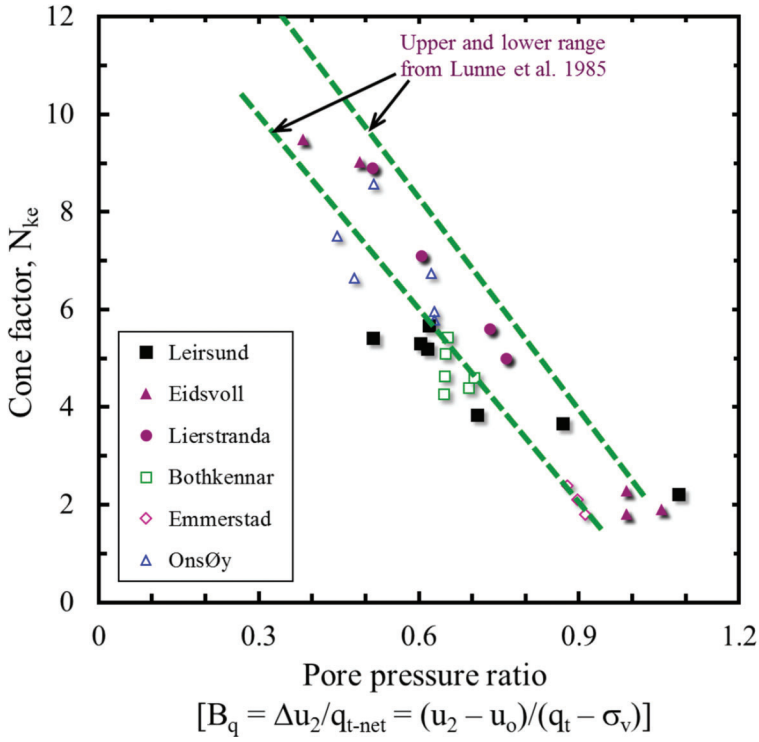

Figure 2.26 Cone factor N_{ke} versus B_q (after Karlsrud et al., 1996; Lunne et al., 1997).

suggested the use of effective cone resistance ($q_E = q_t - u_2$) to determine s_u:

$$s_u = \frac{q_E}{N_{ke}} = \frac{(q_t - u_2)}{N_{ke}} \qquad \text{(Eq. 2.85)}$$

where the bearing factor $N_{ke} = 9 \pm 3$. Karlsrud et al. (1996) developed a correlation between N_{ke} and B_q for normally to lightly overconsolidated clays (see Figure 2.26), and therefore, these should not be extrapolated to heavily overconsolidated deposits

where B_q is small or even negative (Powell et al., 1989). Lunne et al. (1997) noted that, in general, it is not recommended to estimate s_u using q_E. In soft normally consolidated clays, the total pore pressure generated behind cone is often approximately 90% or more of the measured cone resistance. A major disadvantage of using q_E to interpret s_u in such soils, therefore is the q_E is a very small quantity, sensitive to small errors in q_c or u measurements. In such soils use of excess pore pressure (Δu) to interpret s_u may therefore by more accurate.

2.3.10.3 s_u estimation using excess pore pressure. In reality, it is possible to independently evaluate a profile of s_u entirely from the excess pore pressure measurements (Δu). While this may be best handled by a mid-face element (designated u_1), the shoulder element (u_2) reading is usually more common (because u_2 is required in the correction of q_c to q_t). The expression for undrained strength here is given by:

$$s_u = \frac{\Delta u}{N_{\Delta u}} = \frac{(u_2 - u_o)}{N_{\Delta u}} \qquad \text{(Eq. 2.86)}$$

where $N_{\Delta u}$ = pore pressure bearing factor (Tavenas & Leroueil, 1987). $N_{\Delta u}$ is theoretically shown to vary between 2 and 20. For a more conservative estimate, select a value close to the upper limit. Lunne et al. (1986) found $N_{\Delta u}$ to correlate well with B_q and to vary between 3 and 12, for North Sea clays taking triaxial compression (CK_0UC) as the reference strength. Using s_u values from CK_0UC tests on block samples, Karlsrud et al. (1996) obtained $N_{\Delta u}$ values varying between 4 and 8 (see Figure 2.27). These correlations were derived for normally to lightly overconsolidated clays and should not be extrapolated to heavily overconsolidated deposits where B_q is small or negative (Powell et al., 1989).

2.3.10.4 s_u estimation using friction ratio and cone resistance. Lastly, since redundancy in the evaluation of s_u from alternative CPTu based relationships is likely to provide a basis for comparison and better assessment, another correlation by Searle (1979) is also presented below:

$$s_u(kPa) = 6.67\, FR\,(\%) q_t\,(MPa) \qquad \text{(Eq. 2.87)}$$

where FR = friction ratio (f_s/q_t).

For larger, moderate to high-risk projects, where high quality field and laboratory data may be available, site-specific correlations should be developed based on appropriate and reliable values of s_u. (Robertson, 2009).

2.3.10.5 Remolded s_u estimation. The measured sleeve resistance (f_s) can be considered as a remolded (or residual) undrained shear strength, $s_{u(remolded)}$, of clays

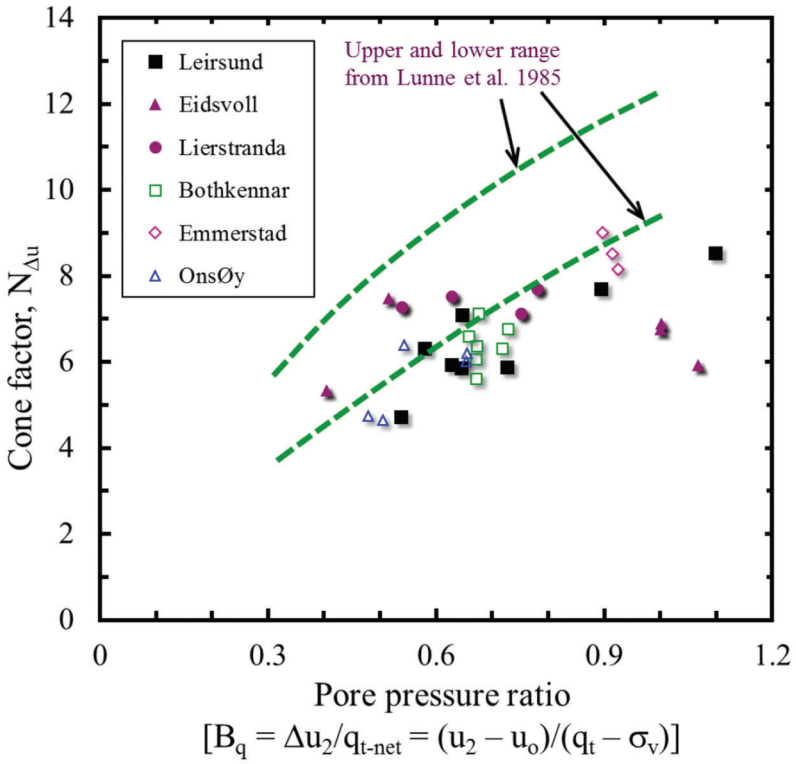

Figure 2.27 Cone factor $N_{\Delta u}$ versus B_q (after Karlsrud et al., 1996).

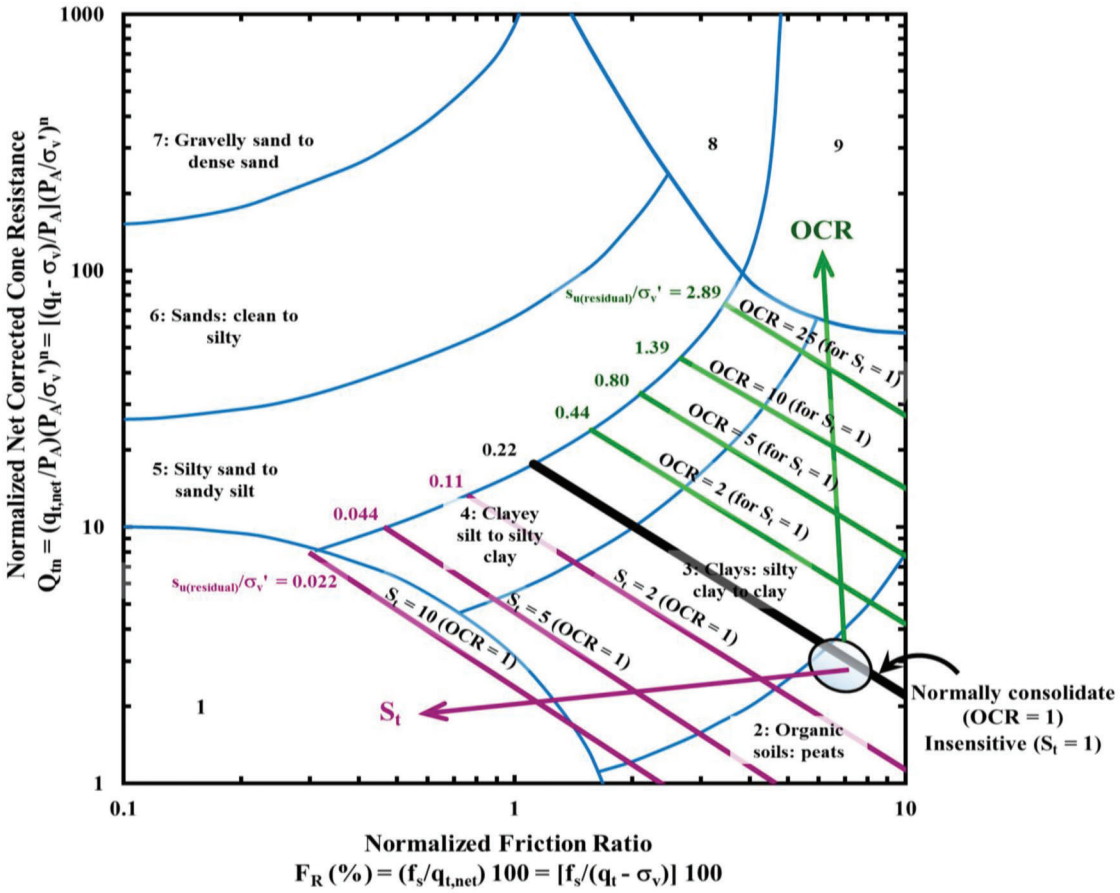

Figure 2.28 Contours of residual undrained shear strength ratio ($s_{u(remolded)}/\sigma_v'$) and trends in the *OCR* and soil sensitivity on normalized SBTn chart (adapted from Robertson, 2009).

(e.g., Gorman et al., 1975; Lunne et al., 1997), and expressed as:

$$s_{u(remolded)} = f_s \qquad \text{(Eq. 2.88)}$$

From the above relationship, the $s_{u(remolded)}$ can also be expressed as undrained shear strength ratio in terms of CPT normalized parameter as (e.g., Robertson, 2009):

$$\frac{s_{u(remolded)}}{\sigma_v'} = \frac{f_s}{\sigma_v'} = \frac{(F_R\, Q_{tn})}{100} \qquad \text{(Eq. 2.89)}$$

2.3.10.6 Clay sensitivity S_t estimation. While Eqs. 2.82 to 2.87 provide estimates of the peak strength of the clay (i.e., $s_u = s_{u(peak)}$), Eqs. 2.88 and 2.89 may serve as a lower bound in assessing the overall $s_{u(remolded)}$ profile. The CPTu can thus provide an approximate measure of clay sensitivity, defined as the ratio of peak shear strength to remolded shear strength at the same water content:

$$S_t = \frac{s_{u(peak)}}{s_{u(remolded)}} \qquad \text{(Eq. 2.90)}$$

Robertson (2009) noted that combining Eqs. 2.89 and 2.90, clay S_t can also be estimated using:

$$S_t = \frac{s_{u(peak)}}{s_{u(remolded)}} = \frac{7.1}{F_R} \qquad \text{(Eq. 2.91)}$$

where the value of constant varies from 5 to 10 with an average of about 7.1. Robertson (2009) also represented approximate contours of $s_{u(remolded)}/\sigma_v'$ on the normalized SBTn chart (see Figure 2.28) and emphasized that these contours should be used as a guide only. It may be seen in Figure 2.28 that for insensitive normally consolidated fine-grained soil, Q_{tn} values fall between 2 and 6, and stay close to $s_{u(remolded)}/\sigma_v' = 0.22$. With increasing sensitivity, the values for both N_{kt} and Q_{tn} decrease. Figure 2.28 also shows the contours of $s_{u(remolded)}/\sigma_v'$ for *NC* fine-grained soils (*OCR* = 1) with different S_t, and those for insensitive fine-grained soils (S_t = 1) with different *OCRs*.

A concise summary of the empirical and analytical approaches for the estimation of undrained shear strength (s_u), undrained shear strength ratio (s_u/σ_v'), remolded undrained shear strength [$s_{u(remolded)}$], and clay sensitivity (S_t) from CPT/CPTu parameters are presented in Table 2.14.

TABLE 2.14
Summary of the empirical and analytical approaches for estimation of undrained shear strength (s_u), undrained shear strength ratio (s_u/σ_v'), remolded undrained shear strength [$s_{u(remolded)}$], and clay sensitivity (S_t) from CPT/CPTu parameters

Soil Type	Method/Relationship	Reference
For intact clays over a range of overconsolidation ratios; requires estimates of ϕ', OCR and Λ that may be obtained from CPT/CPTu parameters	$\left(\frac{s_u}{\sigma_v'}\right)_{OC[DSS]} = \frac{1}{2} sin\phi' \ OCR^{\Lambda}$ For fissured clays, the estimated values should be reduced to one-half	Wroth & Houlsby (1985)
For intact clays, when estimates of ϕ' and Λ are not available; requires estimates of OCR that may be obtained from CPT/CPTu parameters	$\left(\frac{s_u}{\sigma_v'}\right)_{OC[DSS]} = 0.22 \ OCR^{0.8}$ (assume default values: $\phi' = 28^{\circ}$; $\Lambda = 0.8$) For fissured clays, the estimated values should be reduced to one-half	Ladd & DeGroot (2003)
Soft lightly-overconsolidated to normally consolidated soils ($OCRs < 2$); requires estimates of σ_{vp}' that may be obtained from CPT/CPTu parameters	$s_{uNC[DSS]} = 0.22 \ \sigma_p'$ For fissured clays, the estimated values should be reduced to one-half	Mesri (1975)
For fine-grained soils; requires estimate of γ_m for calculation of σ_v	$s_u = \frac{q_{t,net}}{N_{kt}} = \frac{(q_t - \sigma_v)}{N_{kt}}$ Common values for N_{kt} in soft intact clays are generally taken to be between 10 and 20, with an average of 14; in fissured clays, N_{kt} range from 20 to 30, dependent upon the degree of fissuring; use higher values for conservative estimates	Konrad & Law (1987); Yu & Mitchell (1998); Lunne et al. (1997); Powell & Quarterman (1988)
For insensitive fine-grained soils; requires estimate of γ_m for calculation of σ_v and σ_v' to calculate Q_{tn}	$\left[\frac{s_{u(peak)}}{\sigma_v'}\right]_{DSS} = \frac{Q_{tn}}{N_{kt}}$ (where preliminary $N_{kt} = 14$)	Robertson (2009)
For fine-grained soils where piezocone test (CPTu) data is available	$s_u = \frac{q_{t,net}}{N_{kt}} = \frac{(q_t - \sigma_v)}{N_{kt}}$ N_{kt} should be estimated from the normalized pore pressure parameter (B_q) using Figure 2.25; values in the range of 6–15 (Karlsrud et al., 1996); 8.5–20 (Lunne et al., 1986); in very sensitive fine-grained soil ($B_q \approx 1.0$) low as 6; for deposits where little experience, estimate s_u using preliminary N_{kt} from 14 to 16; for more conservative estimate, select a value close to the upper limit	Karlsrud et al. (1996); Lunne et al. (1986)
From a database involving 407 high-quality triaxial compression tests (CK_0UC) from a wide variety of clays. The study considered a total 62 clays, categorized into five groups: soft offshore, soft-firm onshore, sensitive, overconsolidated, and fissured clays	$s_u = \frac{q_{t,net}}{N_{kt}} = \frac{(q_t - \sigma_v)}{N_{kt}}$ $N_{kt} = 10.5–4.6 \ \mathrm{In}(B_q + 0.1)$ (applies to $B_q > -0.1$); Average N_{kt} = 10 (sensitive clays), 12 (NC-LOC soft-firm onshore clays), 12.3 (NC to LOC offshore clays), 14 (OC intact clays), 25 (OC fissured clays)	Mayne & Peuchen (2018)
For NC to lightly OC clays where piezocone test (CPTu) data is available	$s_u = \frac{q_E}{N_{ke}} = \frac{(q_t - u_2)}{N_{ke}}$ Use Figure 2.26 to estimate N_{ke} based on B_q; in general, it is not recommended to estimate s_u using q_E since in soft NC clays, the total pore pressure generated behind cone is often approximately 90% or more of q_c (here q_E is very small), and in such soils use Δu for better interpretation of s_u; also, do not extrapolate to heavily overconsolidated deposits where B_q is small or even negative	Karlsrud et al. (1996); Lunne et al. (1986); Powell et al. (1989); Tavenas & Leroueil (1987)
Based on CK_0UC tests on NC to lightly OC clays where piezocone test (CPTu) data is available	$s_u = \frac{\Delta u}{N_{\Delta u}} = \frac{(u_2 - u_o)}{N_{\Delta u}}$ Use Figure 2.27 to estimate $N_{\Delta u}$ based on B_q (it varies between 2 and 20 (3–12 for N. Sea clays (Lunne et al., 1986), and 4–8 (Karlsrud et al., 1996)) 6 and 8; do not extrapolate to heavily overconsolidated deposits where B_q is small or negative; for a conservative estimate, select a value close to the upper limit	Karlsrud et al. (1996); Lunne et al. (1986); Powell et al. (1989)
A generalized relationship for fine-grained soils	$s_u \ (kPa) = 6.67 FR(\%) \ q_t(MPa)$	Searle (1979)

Continued

TABLE 2.14
(Continued)

Soil Type	Method/Relationship	Reference
For estimation of remolded (residual) undrained shear strength of intact fine-grained soils	$S_u(remolded)=f_s$	Gorman et al. (1975); Lunne et al. (1997)
For estimation of remolded (residual) undrained shear strength of intact fine-grained soils	$\frac{s_{u(remolded)}}{\sigma_v'}=\frac{f_s}{\sigma_v'}=\frac{(F_R Q_{tn})}{100}$	Robertson (2009)
For *NC* to heavily *OC*, insensitive to highly sensitive fine-grained soils	$S_t=\frac{s_{u(peak)}}{s_{u(remolded)}}=\frac{7.1}{F_R}$ Use Figure 2.28 as a guide only for estimating S_t	Robertson (2009)

Note: s_u = undrained shear strength; σ_v' = effective vertical overburden stress = $\sigma_v - u_0$; σ_v = total vertical overburden stress = $\Sigma(\gamma_{mi} \bullet z_i)$; γ_{mi} = total unit weight of the i-th soil layer; z_i = thickness of the i-th soil layer; u_0 = hydrostatic pore pressure = $\gamma_w (z - z_w)$, where, z = depth below the ground surface; γ_w = unit weight of water = 9.81 kN/m^3 = 62.4 pcf; z_w = depth of the ground water table; DSS = direct simple shear mode of testing; *LOC* = lightly overconsolidated; *OC* = overconsolidated; *OCR* = overconsolidation ratio; ϕ' = friction angle of soil; Λ = plastic volumetric strain potential = $1 - C_s/C_c$; C_s = swelling index and C_c = virgin compression index of the soil material; σ_{vp}' = effective preconsolidation stress; *NC* = normally consolidated; $q_{t,net}$ = net cone resistance = $q_t - \sigma_v$; q_t = corrected cone resistance = $q_c + u_2$ (1 - a_n); a_n = cone net area ratio = A_n/A_c; A_n = cross-sectional area of the load cell behind the cone; A_c = projected cone cross-sectional area; u_2 = shoulder (behind the cone) pore pressure recorded during penetration of piezocone; q_c = measured cone resistance; N_{kt} = cone bearing factor; $s_{u(peak)}$ = peak undrained shear strength; Q_{tn} = normalized net corrected cone resistance = $(q_{t,net}/p_A)(p_A/\sigma_v')^n$; n = stress normalization exponent $=0.381 I_{c(R\&W98)} + 0.05\frac{\sigma_v'}{p_A} - 0.15$ where n $\leq$ 1.0; $I_{c(R\&W98)} = \sqrt{[3.47 - log Q_{tn}]^2 + [1.22 + Log F_R]^2}$; F_R = normalized friction ratio = $f_s/(q_t - \sigma_v)$; f_s = sleeve resistance; CPT = cone penetration test; CPTu = piezocone penetration test; B_q = normalized pore pressure parameter = $\Delta u_2/q_{t\text{-}net} = (u_2 - u_0)/(q_t$ -- $\sigma_v)$; q_E = effective cone resistance = $q_t - u_2$; N_{ke} = bearing factor; CK_0UC = Triaxial compression test; $N_{\Delta u}$ = pore pressure bearing factor; *FR* = friction ratio = f_s/qt; $s_{u(remolded)}$ = remolded undrained shear strength; p_A = atmospheric pressure = 1 bar = 100 kPa.

2.3.11 Effective Cohesion Intercept

For long-term stability analyses, the effective cohesion intercept (c') is conservatively taken to be zero ($c' = 0$). The intercept c' is actually a projection caused by the forced fitting of a straight line to a strength envelope that is actually curved. Several difficulties are associated with assessing a reliable value of c' to a particular soil, including its dependency on the magnitude of preconsolidation stress (σ_{vp}'), strain rate of loading, and age of the deposit. Mesri and Abdel-Ghaffar (1993) reviewed 60 slope failures in clays and backfigured strength parameters from stability analyses finding that:

$$0.003 < \frac{c'}{\sigma'_{vp}} < 0.11 \qquad \text{(Eq. 2.92)}$$

where σ_{vp}' = preconsolidation stress.

An indirect CPT-based approach of assessing the short-term loading conditions may be applied, and an apparent value of c' may be assessed from the stress history (Mayne, 2016):

$$c' \approx 0.03\,\sigma_{vp}' \qquad \text{(Eq. 2.93)}$$

2.3.12 Poisson's Ratio

As such, no direct correlation exists to estimate the value of Poisson's ratio from CPT data. However, its need cannot be overemphasized. The value of Poisson's ratio (ν) is used to represent elastic parameters of soil, important for the assessment of the common deformation problems in geotechnical engineering, where $\nu = -\varepsilon_h/\varepsilon_v$. Based on high-resolution strain measurements on soil samples (e.g., Burland, 1989; Lehane & Cosgrove, 2000), the value of drained Poisson's ratio (ν') ranges is generally lower than that inferred from earlier measurements that contained bedding and boundary errors. The newer and more reliable measurements indicate that $0.1 < \nu' < 0.2$ for all types of geomaterials (clays, silts, sands, rocks) at working load levels that correspond to relatively small-strains ($\gamma_s < 0.1\%$). At higher strains, ν' increases as failure states are approached. Thus, a characteristic $\nu' \approx 0.2$ can be adopted for drained loading conditions, while the value for undrained loading at constant volume is $\nu_u = 0.5$.

2.3.13 Soil Stiffness

The stiffness of soils can be represented by a number of different parameters, depending upon the theoretical framework adopted, drainage conditions, loading conditions (static, dynamic, cyclic), initial stress state, applied loading, and induced strain levels. Common frameworks include the following.

- One-dimensional consolidation theory (e.g., void ratio vs. logarithm of effective stress: e-log σ_v' curves).
- Elasticity theory (moduli).
- Subgrade reaction models (e.g., modulus of subgrade reaction).
- Spring models (e.g., spring constants).
- Empirical methods using various algorithms.

Consolidation theory can be combined with elasticity, such as in CSSM. Within the context of this manual, the focus is maintained on the soil stiffnesses represented by the elastic moduli. In particular, elastic

continuum theory allows for interrelationships between the equivalent elastic Young's modulus (E), shear modulus (G), and constrained modulus (D) in terms of the Poisson's ratio (ν), such that:

$$E = 2(1+\upsilon)G \qquad \text{(Eq. 2.94)}$$

$$D' = E'\frac{(1-\upsilon')}{[(1+\upsilon')(1-2\upsilon')]} = \frac{2G(1-\upsilon')}{(1-2\upsilon')} \qquad \text{(Eq. 2.95)}$$

where D' and E' represent drained values of moduli. The modulus E can have drained (E') as well as undrained values (E_u) value depending on the applicable condition. However, shear modulus (G) deforms primarily in shear and because it is usually assumed to be unaffected by whether the loading is drained of undrained, it may represent both the drainage conditions (Randolph & Wroth, 1978).

2.3.13.1 Constrained modulus, D'. The constrained modulus (D', also represented by the nomenclature M') takes on only a drained value as it is measured directly in a one-dimensional consolidation test (oedometer). At the drained value of $\nu' \approx 0.2$, the ratio $D'/E' = 1.1$ and, therefore, the constrained modulus and drained Young's modulus are often used somewhat interchangeably. In terms of the compressibility parameters from consolidation testing, D' can be expresses as:

$$\text{OC Soils}: \; D' = \frac{1+e_o}{C_s}\ln(10)\,\sigma_v' \qquad \text{(Eq. 2.96)}$$

$$\text{NC Soils}: \; D' = \frac{1+e_o}{C_c}\ln(10)\,\sigma_v' \qquad \text{(Eq. 2.97)}$$

where e_0 = in situ void ratio of soil, C_c = compression index; C_s = swelling index. The D' has been expressed in terms of a coefficient, α_D, and cone resistance (Lunne et al., 1997):

$$D' = \alpha_D q_c \qquad \text{(Eq. 2.98)}$$

Based on the work of Sanglerat (1972), Mitchell and Gardner (1975) presented an array of α_D values for different soil types and for different ranges of q_c (see Table 2.15). It may be noted that these values were assessed based on measured q_c, but not corrected q_t since the correction factor had not been introduced then.

For other quick evaluation of the constrained modulus (and drained Young's modulus) from CPT results, the common approach is expressed in the form:

$$D' = \alpha_D(q_t - \sigma_v) \qquad \text{(Eq. 2.99)}$$

where D' corresponds to the current effective stress state (i.e., σ_v') and α_D is an empirical scaling factor that has been shown to depend upon soil type, confining stress level, overconsolidation, soil plasticity and natural water content (e.g., Kulhawy & Mayne, 1990; Sanglerat, 1972). Meigh (1987) suggested a range of α_D = 2–8 for different soil types. Mayne (2007a) suggested a value of $\alpha_D \approx 5$ as an approximate starting place for a wide range of soil types, excepting soft plastic organic clays and cemented geomaterials.

Since most undisturbed natural soils are at least lightly-overconsolidated, if not moderately to heavily OC, then the use of a constrained modulus given by Eq. 2.99 would apply only during recompression loading up to the yield stress (σ_{vp}'). Thereafter, a modulus corresponding to *NC* conditions would need be applied.

Robertson (2009) suggested the following relationship for estimating D' and developed contours of constrained modulus number (K_D) on the normalized SBTn chart, Q_{tn}-F_R as shown in Figure 2.29.

$$D' = K_D\, p_A \left(\frac{\sigma_v'}{p_A}\right)^{a^*} \qquad \text{(Eq. 2.100)}$$

where a is a stress exponent. According to Janbu (1963), a = 1.0 for stresses above σ_{vp}' and zero below

TABLE 2.15
Coefficient α_D for estimation of constrained modulus D' (adapted from Sanglerat, 1972; after Mitchell & Gardner, 1975)

Soil Type	Applicable Range of q_c	Range of α_D
Clay of low plasticity (CL)	$q_c < 0.7$ MPa	$3.0 < \alpha_D < 8.0$
	$0.7 < q_c < 2.0$ MPa	$2.0 < \alpha_D < 5.0$
	$q_c > 2.0$ MPa	$1.0 < \alpha_D < 2.5$
Silts of low plasticity (ML)	$q_c > 2.0$ MPa	$3.0 < \alpha_D < 6.0$
	$q_c < 2.0$ MPa	$1.0 < \alpha_D < 3.0$
Highly plastic silts and clays (MH, CH)	$q_c < 2.0$ MPa	$2.0 < \alpha_D < 6.0$
Organic silts (OL)	$q_c < 1.2$ MPa	$2.0 < \alpha_D < 8.0$
Peat and organic clay (P_t, OH)	$q_c < 0.7$ MPa	
	$50 < w < 100$	$1.5 < \alpha_D < 4.0$
	$100 < w < 200$	$1.0 < \alpha_D < 1.5$
	$w < 200$	$0.4 < \alpha_D < 1.0$

Note: w = water content; q_c = measure cone resistance.

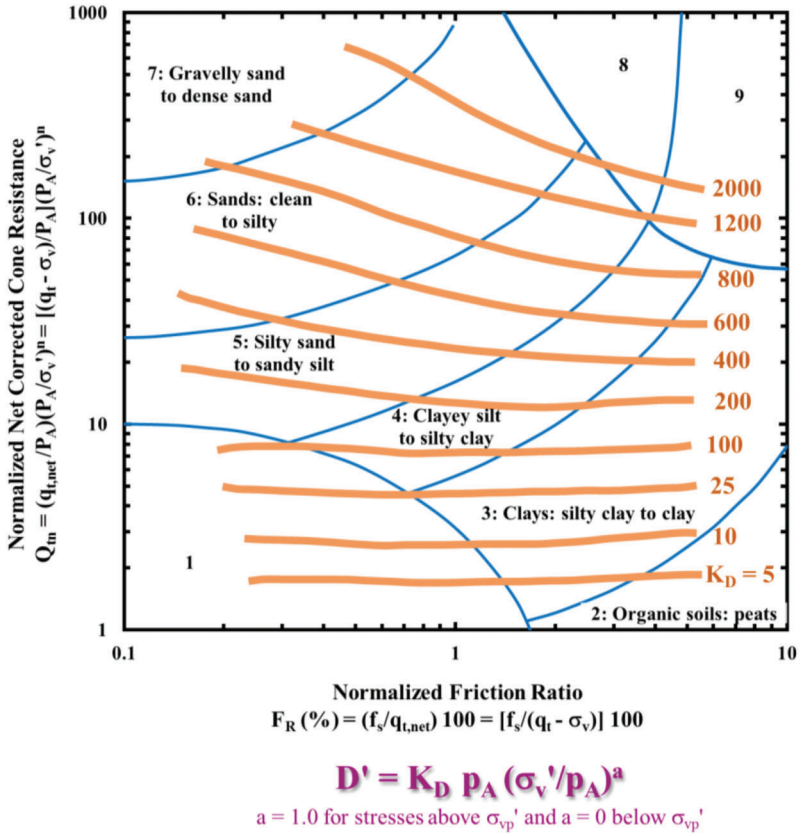

Figure 2.29 Contours of 1-D constrained modulus number, K_D, on normalized Q_{tn}-F_R chart (adapted from Robertson, 2009).

σ'_{vp} (i.e., D' is nearly constant below the σ'_{vp}, and hence $D' = K_D\, p_A$ below σ'_{vp}).

Based on the contours shown in Figure 2.29 and Eq. 2.99, Robertson (2009) suggested the following simplified correlation:

When $I_{c(R\&W98)} > 2.2$, use:

$$\alpha_D = Q_{tn} \text{ when } Q_{tn} \leq 14 \qquad \text{(Eq. 2.101)}$$

$$\alpha_D = 14 \text{ when } Q_{tn} > 14 \qquad \text{(Eq. 2.102)}$$

When $I_{c(R\&W98)} < 2.2$, use:

$$\alpha_D = 0.03\left[10^{\left(0.55 I_{c(R\&W98)} + 1.68\right)}\right] \qquad \text{(Eq. 2.103)}$$

2.3.13.2 Shear modulus, *G*. The slope of a shear stress-strain (τ - γ_s) curve is the shear modulus, G. The small-strain ($< 10^{-4}$%) shear modulus (termed G_0 or G_{max}) represents the fundamental stiffness that relates to the initial state of the soil. This stiffness applies to the initial range of loading on the stress-strain-strength curves for all types of loading, as well as undrained and drained conditions (Burland, 1989; Leroueil & Hight, 2003; Mayne, 2001). Elastic theory states that the small strain shear modulus, G_0 can be determined from:

$$G_0 = \rho_m V_s^{\,2} \qquad \text{(Eq. 2.104)}$$

where ρ_m = total soil mass density = γ_m/g_a; γ_m = unit weight of soil; V_s = shear wave velocity; and g_a = gravitational acceleration constant = 9.8 m/s^2.

Following the approach suggested by Tanaka and Tanaka (1998) for clays, Mayne (2007b) extended investigation on various soils ranging from sands to silts to clays, and presented a direct trend between small-strain stiffness and net cone resistance:

$$G_0 = 50\, p_A \left[\frac{(q_t - \sigma_v)}{p_A}\right]^{m^*} \qquad \text{(Eq. 2.105)}$$

where the exponent m^* = 0.6 for quartzite to silica sands, 0.8 for silts, and 1.0 for intact clays of low to medium sensitivity.

Burns and Mayne (2002b) offered an approach towards linking the D' with G_0 via empirical scaling factor $\alpha_{D'\text{-}G0}$:

$$D' = \alpha_{D'-G_0} G_0 \qquad \text{(Eq. 2.106)}$$

with assigned values of coefficient $\alpha_{D'\text{-}G0}$ ranging from 0.02 for organic plastic clays, 0.05–0.13 for intact clays, 0.2 for silts, 0.–0.8 for normally consolidated sands, and up to 2.0 for overconsolidated quartz sands.

Robertson (2009) suggested the following relationship for estimating G_0 and developed contours of

small-strain shear modulus number (K_G) on the normalized SBTn chart, Q_{tn}-F_R as shown in Figure 2.30.

$$G_0 = K_G\, p_A \left(\frac{\sigma_v'}{p_A}\right)^n \qquad \text{(Eq. 2.107)}$$

where n is a stress exponent with a value of about 0.5 for most coarse-grained soils. The relationship between G_0 and q_t can have a form similar to the one presented in Eq. 2.99:

$$G_0 = \alpha_G (q_t - \sigma_v) \qquad \text{(Eq. 2.108)}$$

where α_G = shear modulus factor. For an average unit weight γ_m = 18 kN/m^3, α_G is given by:

$$\alpha_G = 0.0188\left[10^{\left(0.55 I_{c(R\&W98)} + 1.68\right)}\right] \qquad \text{(Eq. 2.109)}$$

Figure 2.30 and Eq. 2.108 offer a simplified mean to estimate G_0 over a wide range of soils using CPT data. However, the contours in Figure 2.30 are less reliable in the region for fine-grained soils (i.e., when $I_{c(R\&W98)} > 2.6$) since F_R is strongly affected by soil sensitivity. The relationships are generally better in the coarse-grained region (i.e., when $I_{c(R\&W98)} < 2.6$) and are primarily for uncemented, predominantly silica-based soils of Holocene and Pleistocene age (Robertson, 2009).

Eslaamizaad and Robertson (1997) also showed that for young, uncemented sands, the ratio of G_0/q_t (i.e., α_G) varied with normalized cone resistance. The approximate range of values for sands suggested by Eslaamizaad and Robertson (1997) are shown in Table 2.16.

2.3.13.3 Drained Young's modulus, *E′*. In certain geotechnical problems, engineers prefer to use the Young's Modulus (E'). As given in Eqs. 2.94 and 2.95, the link between G and E' allows quick estimation of E'. Under drained conditions (essentially coarse-grained soils), where an average drained Poisson's ratio (ν') $\approx$ 0.2, $E' \approx$ 2.4 to 2.5 times of G.

Robertson (2009) noted that the stiffness of a soil for drained loading case can reduce from its in-situ state (G_0 or E_0) to nearly 30%–40% (i.e., G = 0.3–0.4 (G_0) or E = 0.3–0.4 (E_0)) for the common range (20%–30%) of mobilized strength of soil (or degree of loading) compared to its maximum (or ultimate) strength. This enabled development of a simplified relationship between E' and G_0 shown below for common design applications. This relationship was further exploited by Robertson (2009) to draw contours of Young's modulus number (K_E) on SBTn chart (see Figure 2.31), where:

$$E' \approx 0.8\, G_o \qquad \text{(Eq. 2.110)}$$

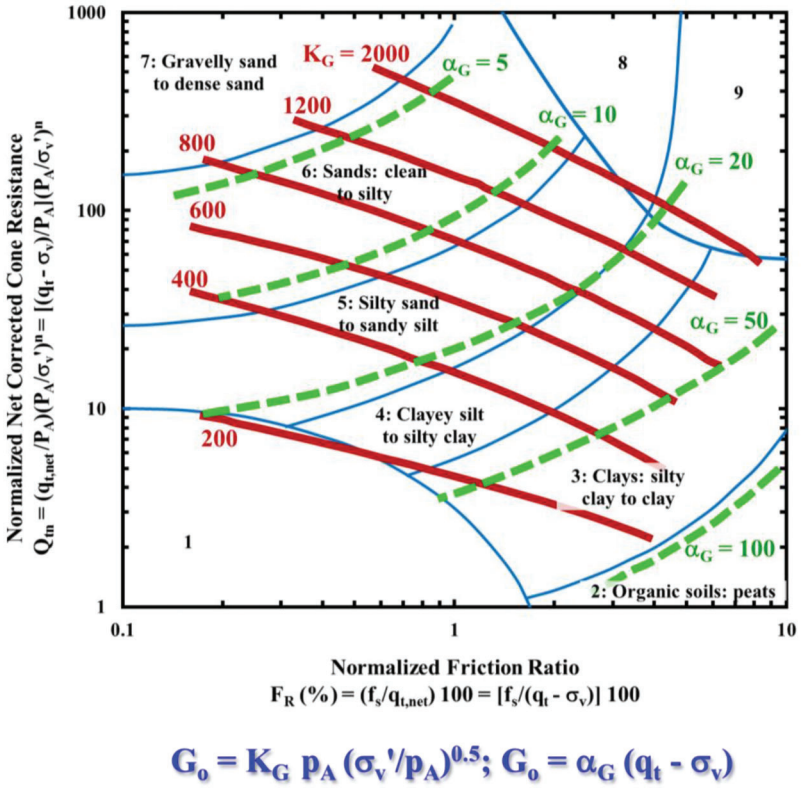

Figure 2.30 Contours of small-strain shear modulus number, K_G, and modulus factor α_G, on normalized SBTn Q_{tn}-F_R chart for uncemented Holocene- and Pleistocene-age soils (adapted from Robertson, 2009).

TABLE 2.16
Typical G_0/q_t values for normalized cone resistance Q_{tn} values of sands (after Eslaamizaad & Robertson, 1997)

Normalized Cone Resistance, Q_{tn}	α_G = Ratio G_0/q_t
500	2 to 4
100	5 to 10
20	15 to 20

Note: Q_{tn} = normalized net corrected cone resistance = $(q_{t,net}/p_A)(p_A/\sigma_v')^n$; $q_{t,net}$ = net cone resistance = $q_t - \sigma_v$; q_t = corrected cone resistance = $q_c + u_2\ (1 - a_n)$; a_n = cone net area ratio = A_n/A_c; A_n = cross-sectional area of the load cell behind the cone; A_c = projected cone cross-sectional area; q_c = measured cone resistance; σ_v = total vertical overburden stress = $\Sigma(\gamma_{mi} \bullet z_i)$; γ_{mi} = total unit weight of the i-th soil layer; z_i = thickness of the i-th soil layer; σ_v' = effective vertical overburden stress = $\sigma_v - u_0$; u_2 = shoulder (behind the cone) pore pressure recorded during penetration of piezocone; u_0 = hydrostatic pore pressure = $\gamma_w(z - z_w)$, where, z = depth below the ground surface, γ_w = unit weight of water = 9.81 kN/m^3 = 62.4 pcf; z_w = depth of the ground water table; n = stress normalization exponent = $0.381I_{c(R\&W98)} + 0.05\frac{\sigma_v'}{p_A} - 0.15$ where $n \leq 1.0$;

$I_{c(R\&W98)} = \sqrt{[3.47 - logQ_{tn}]^2 + [1.22 + LogF_R]^2}$;

p_A = atmospheric pressure = 1 bar = 100 kPa.

$$E' = K_E\, p_A \left(\frac{\sigma_v'}{p_A}\right)^n \qquad \text{(Eq. 2.111)}$$

where n is a stress exponent that has a value of about 0.5 for most coarse-grained soils. It can be seen in Figure 2.31 that the contours are limited to the soil regions defined by $I_{c(R\&W98)} < 2.6$ since E' is generally applicable to drained soils.

The other relationship between the soil modulus and cone resistance takes the following form:

$$E' \approx \alpha_E(q_t - \sigma_v) \qquad \text{(Eq. 2.112)}$$

where α_E = Young's modulus factor given by the following expression (also see Figure 2.31 for the contours of α_E; Robertson, 2009):

$$\alpha_E = 0.015\left[10^{(0.55I_{c(R\&W98)}+1.68)}\right] \qquad \text{(Eq. 2.113)}$$

It is important to note that values of the contours of α_E shown in Figure 2.31 represent the average degree of loading situations (i.e., about 0.25, or a factor of safety, FS around 4). Other set of contours can be drawn for higher degrees of loading, where α_E will decrease.

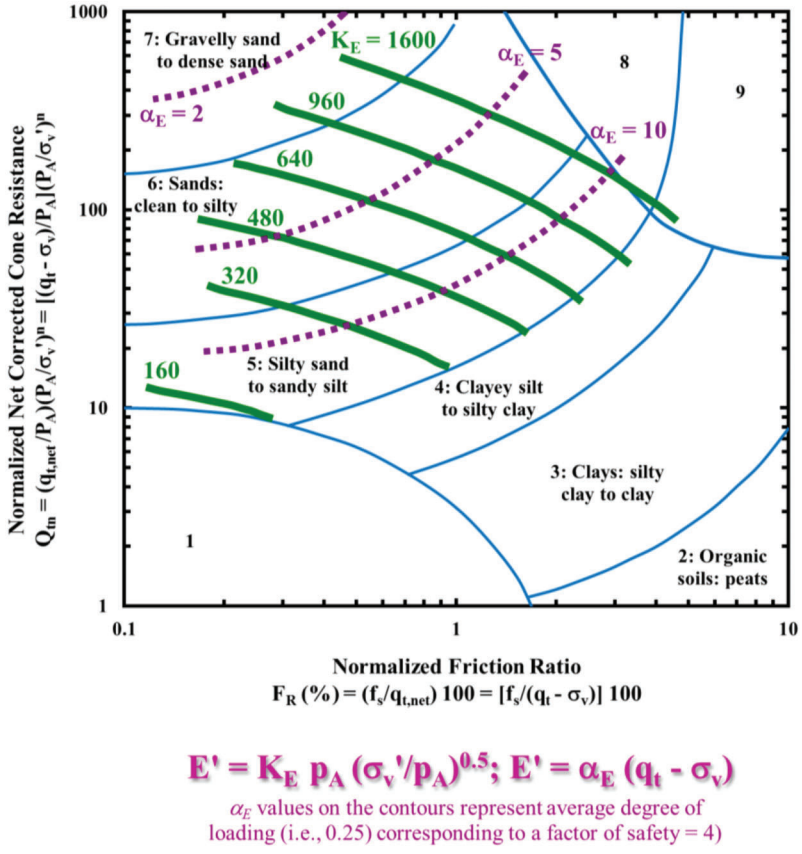

Figure 2.31 Contours of Young's modulus number (K_E) and modulus factor (α_E) on normalized SBTn chart for uncemented Holocene- and Pleistocene-age soils (adapted from Robertson, 2009).

2.3.13.4 Nonlinear moduli from small strain stiffness. The small-strain shear stiffness, G_0 explained in the previous section (or its corresponding E_0) represents stiffness in the very small-strain (non-destructive) range of loading, and this stiffness degrades (softens) with strain (or load) increments. In order to properly perform the complete load-deformation analysis, the softened values of G or E' must be applied in the analysis. Thus, for loading levels corresponding to higher strains, the use of modulus reduction factor ($MRF = G/G_0 = E/E_0$) must be implemented. While numerous modulus reduction algorithms are available, of particular significance and convenience is the one developed by Fahey and Carter (1993) involving a modified hyperbola, as given below:

$$MRF = \frac{G}{G_0} = \frac{E}{E_0} = 1 - f\left(\frac{\tau}{\tau_{max}}\right)^g = 1 - f\left(\frac{q}{q_{max}}\right)^g = 1 - f\left(\frac{1}{FS}\right)^g \quad \text{(Eq. 2.114)}$$

where q = applied stress, q_{max} = ultimate or failure stress, τ = applied shear stress, and τ_{max} = ultimate shear stress at failure, f and g are constants depending on soil type and stress history, FS = factor of safety. Accordingly, q/q_{max} and τ/τ_{max} represent the degree of loading, or mobilized stress level, or reciprocal of the current FS. Fahey and Carter (1993), and Mayne (2007a) suggested using $f = 1$, and $g \approx 0.3 \pm 0.1$ for "well-behaved" soils (uncemented, insensitive, not highly structured).

By comparing the above modified hyperbolic algorithm with the results from monotonic laboratory shear tests on assorted clays and sands under both drained and undrained loading, Mayne (2009) observed that this algorithm works well for intermediate range of mobilized strengths, corresponding to $4 < FS < 2$ (or $0.25 < \tau/\tau_{max} < 0.5$). However, for the range of small-strains to intermediate-strains, corresponding to $FS > 4$ (or $\tau/\tau_{max} < 0.25$), it gives moduli that are too low (see Figure 2.32a). Following improvement was thus proposed (also see Figure 2.32b):

$$MRF = \frac{G}{G_o} = \frac{E}{E_o} = 1 - \left(\frac{\tau}{\tau_{max}}\right)^{g\left[1.5 - \left(\frac{\tau}{\tau_{max}}\right)\right]} = 1 - \left(\frac{q}{q_{max}}\right)^{g\left[1.5 - \left(\frac{q}{q_{max}}\right)\right]} = 1 - \left(\frac{1}{FS}\right)^{g\left[1.5 - \left(\frac{1}{FS}\right)\right]} \quad \text{(Eq. 2.115)}$$

It should be noted that the curves shown in Figure 2.32 are representatives of soils loaded monotonically. It is reasonable to adopt an exponent of $g \approx 0.3$ for preliminary analysis. For structured geomaterials (e.g., cemented sands and calcareous clays), the value of g may be larger (≈0.5). Also indicated in Figure 2.32b are the general trends of stiffer response for increasing OCR, density and number of loading cycles for sands as noted by Robertson and Cabal (2014).

A concise summary of methods to estimate soil stiffness parameters form CPT/SCPT parameters is given in Table 2.17.

2.3.14 Coefficient of Consolidation from Piezocone Dissipation Tests

The flow and consolidation characteristics of soil are normally expressed in terms of the coefficient of consolidation, c, and hydraulic conductivity or permeability, k. Lunne et al. (1997) noted that these are some of the most difficult parameters to measure in geotechnical engineering, and that it is often considered that accuracy within one order of magnitude is acceptable.

Pore pressures generated during cone penetration in fine-grained soils are transient and they are caused due to the perturbation by insertion of the probe. Once the penetration process is halted, the excess pore pressures (Δu) decays with time and the readings from the pore pressure sensors will eventually reach equilibrium corresponding to the hydrostatic value (u_0). The rate of dissipation depends on the coefficient of consolidation (c_{vh}), which in turn, is governed by the compressibility and hydraulic conductivity/permeability (k_{vh}) of the soil. The subscript "vh" encompasses the coefficients in both vertical and horizontal directions depending on case in consideration (drainage and loading direction); clearly either c_v or c_h is determined at a time. In clean sands with high permeability, the Δu dissipate almost instantaneously. In soils of low permeability, such as clays and silts, however, the Δu will require a considerable time to trace back to u_0 conditions. Dissipation readings are normally plotted on log scales, therefore, in clays with low permeability, it becomes impractical to wait for full equilibrium that corresponds to $\Delta u = 0$ and $u_{measured} = u_0$, where $u_{measured}$ = measured pore pressure = Δu excess + u_0 hydrostatic. Sometimes a fixed period of dissipation is used for each layer, while in other cases, dissipation is continued to a predetermined percentage or degree of dissipation (U):

$$U = \left[\frac{(u_{measured-t} - u_o)}{(u_{measured-i} - u_o)}\right] 100\% = \left(\frac{\Delta u_{measured-t}}{\Delta u_{measured-i}}\right) 100\% \quad \text{(Eq. 2.116)}$$

where, $u_{measured\text{-}t}$ = pore pressure measured at time t, and $u_{measured\text{-}i}$ = pore pressure measured at start of dissipation test.

The coefficient of consolidation (c_{vh}) and hydraulic conductivity (k_{vh}) are linked through the following expression:

$$c_{vh} = \frac{(k_{vh} D')}{\gamma_w} \quad \text{(Eq. 2.117)}$$

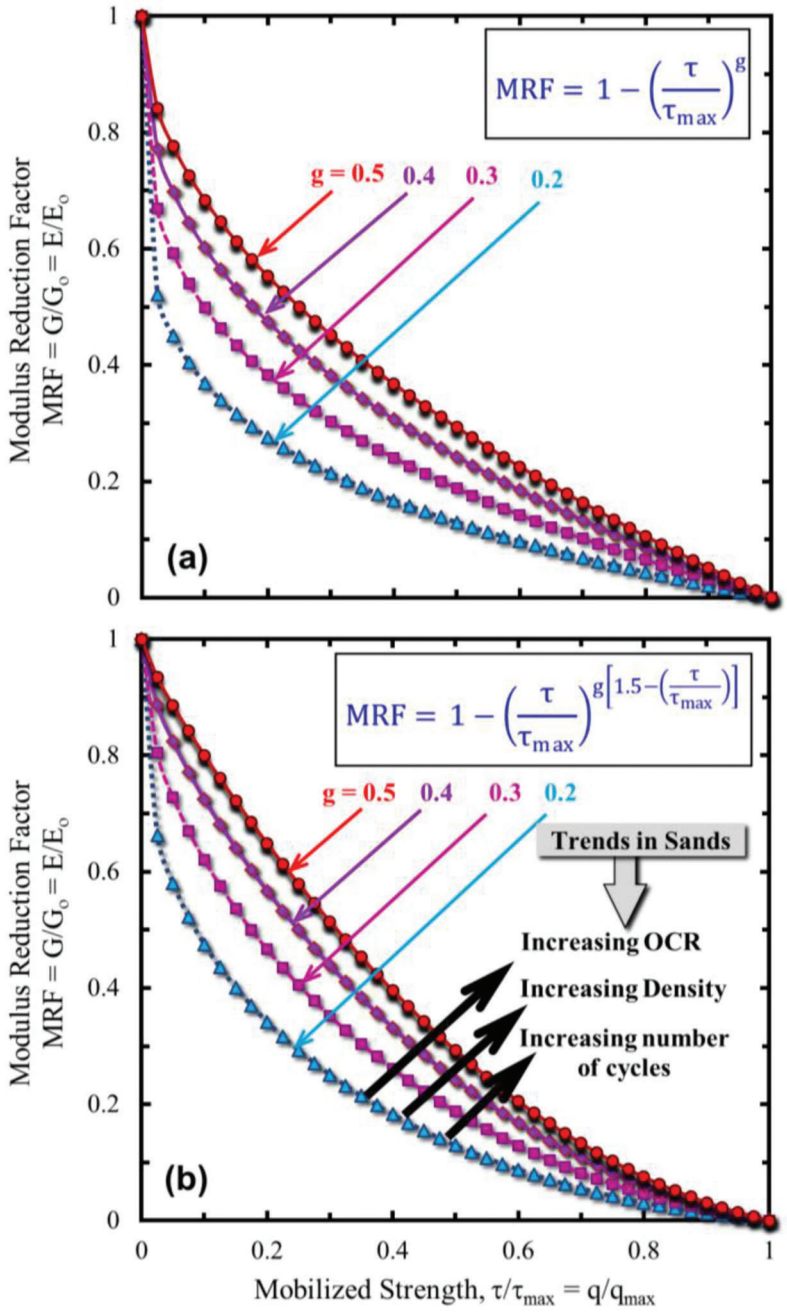

Figure 2.32 Modulus reduction curves: (a) using the original modified hyperbolic algorithm proposed by Fahey & Carter (1993), and (b) the Fahey and Carter (1993) algorithm improved by Mayne (2009) (adapted from Mayne, 2007a; Mayne, 2009).

where k_{vh} = coefficient of permeability (also called hydraulic conductivity) in vertical or horizontal direction (depending on the case in consideration), D' = constrained modulus, and γ_w = unit weight of water. Procedures regarding permeability (hydraulic conductivity) determination are discussed in Section 2.3.15.

For the evaluation of c_{vh} from piezocone-dissipation tests, multiple methods exist, such as interpretative approaches based on theory (cavity expansion (CE)), numerical simulations (finite elements (FE), strain path method (SPM)), and empiricism. Jamiolkowski et al. (1985) and Burns and Mayne (1998) discussed the available procedures. The traditional as well as some of the newer methods are reviewed herein.

2.3.14.1 Torstensson (1975, 1977) cavity expansion theory on elasto-plastic soil model and 1-D consolidation. Torstensson (1975; 1977) developed an interpretation model based on cavity expansion theories. Initial pore pressures were computed assuming an elasto-plastic soil model and spherical cavity expansion [Δu = (4/3) s_u $ln(I_R)$] or cylindrical cavity expansion theories [Δu = s_u $ln(I_R)$], where Δu = excess pore

TABLE 2.17
Summary of methods to estimate soil stiffness parameters form CPT/SCPT parameters

Soil Type and Applicability	Method/Relationship	Reference
Drained loading representing in terms of compressibility parameters; requires estimation of e_o, γ_m from CPT correlations, and knowledge of C_s and C_c	OC Soils: $D' = \frac{1+e_o}{C_s}\ln(10)\sigma_v'$ NC Soils: $D' = \frac{1+e_o}{C_c}\ln(10)\sigma_v'$	Lunne et al. (1997); Mayne (2009)
For intact clays (CL, ML, CH, MH), silts, and organic clays, silts and Peat (OL, OH, P_t)	$D' = \alpha_D q_c$ (see Table 2.15 for values of α_D for different soil types corresponding to q_c and w)	Lunne et al. (1997); Mitchell & Gardner (1975); Sanglerat (1972)
For quick and preliminary evaluation from CPT results (wide range of soil types, except soft plastic organic clays and cemented geomaterials)	$D' = \alpha_D q_{t,net} = \alpha_D(q_t - \sigma_v)$ Range of α_D = 2–8 for different soil types. The average value of 5 is an approximate starting place	Kulhawy & Mayne (1990); Mayne (2009); Meigh (1987); Sanglerat (1972)
For a wide range of NC to LOC natural soils	$D' = K_D p_A \left(\frac{\sigma_v'}{p_A}\right)^{a^*}$ a = 1.0 for stresses above σ'_{vp} and zero below σ'_{vp} (i.e., D' is nearly constant below the σ'_{vp}, and hence $D' = K_D\, p_A$ below σ'_{vp}) K_D estimate based on SBTn chart shown in Figure 2.29	Janbu (1963); Robertson (2009)
For quick and preliminary evaluation from CPT results (wide range of NC to LOC natural soils, except soft plastic organic clays and cemented geomaterials)	$D' = \alpha_D(q_t - \sigma_v)$ When $I_{c(R\&W98)} > 2.2$, use: $\alpha_D = Q_{tn}$ when $Q_{tn} < 14$ $\alpha_D = 14$ when $Q_{tn} > 14$ When $I_{c(R\&W98)} < 2.2$, use: $\alpha_D = 0.03\left[10^{(0.55I_{c(R\&W98)}+1.68)}\right]$	Robertson (2009)
Based on elastic theory; requires the use of SCPT	$G_0 = \rho_t V_s^2$	Burland (1989); Leroueil & Hight (2003); Mayne (2001)
For wide variety of soils (sands to silts to clays)	$G_0 = 50 p_A \left[\frac{(q_t-\sigma_v)}{p_A}\right]^{m^*}$ m^* = 0.6 for quartzite to silica sands, 0.8 for silts, and 1.0 for intact clays of low to medium sensitivity	Tanaka & Tanaka (1998); Mayne (2007b)
For wide variety of soils (organic plastic clays, intact and fissured clays, silts, normally consolidated and overconsolidated sands)	$D' = \alpha_{D'\text{-}G_0} G_0$ $\alpha_{D'\text{-}Go}$ ranging from 0.02 for organic plastic clays, 0.05–0.13 for intact clays, 0.2 for silts, 0.6–0.8 for normally consolidated sands, and up to 2.0 for overconsolidated quartz sands	Burns & Mayne (2002b); Mayne (2009)
For a wide range of NC to LOC natural soils	$G_0 = K_G p_A \left(\frac{\sigma_v'}{p_A}\right)^n$ n = 0.5 for stresses for most coarse-grained soils; K_G estimate based on SBTn chart shown in Figure 2.30	Robertson (2009)
For quick and preliminary evaluation from CPT results; contours of a_D are less reliable in the region for fine-grained soils [$I_{c(R\&W98)} > 2.6$], but generally better in the coarse-grained region [$I_{c(R\&W98)} < 2.6$] and are primarily for uncemented, predominantly silica-based soils of Holocene and Pleistocene age	$G_0 = \alpha_G(q_t - \sigma_v)$ For an average unit weight γ_m = 18 kN/m^3: $\alpha_G = 0.0188\left[10^{(0.55I_{c(R\&W98)}+1.68)}\right]$ Also see Figure 2.30 for the contours of α_G.	Janbu (1963); Robertson (2009)
For young, uncemented sands	$\alpha_G = \frac{G_0}{q_t} = f(Q_{tn})$ See Table 2.16 for values of α_G	Eslaamizaad & Robertson (1997)
For drained conditions (essentially coarsegrained soils)	$E' = 2.5G$ (using drained Poisson's ratio $\approx$ 0.2) $E' \approx 0.8G_0$ (for common value of q/q_{max} of 25% or a FS = 4)	Robertson (2009)
For quick and preliminary evaluation from CPT results; contours of K_E are limited to the region for coarse-grained soils [$I_{c(R\&W98)} <$ 2.6] and applicable to uncemented Holocene- and Pleistocene-age soils	$E' = K_E p_A \left(\frac{\sigma_v'}{p_A}\right)^n$ n = 0.5 for stresses for most coarse-grained soils; K_E estimate based on SBTn chart shown in Figure 2.31	Janbu (1963); Robertson (2009)
For quick and preliminary evaluation from CPT results; limited to the SBTn region for coarse-grained soils [$I_{c(R\&W98)} < 2.6$] and applicable to uncemented Holocene- and Pleistocene-age soils	$E' = \alpha_E(q_t - \sigma_v)$ $\alpha_E = 0.015\left[10^{(0.55I_{c(R\&W98)}+1.68)}\right]$ Also see Figure 2.31 for the contours of α_E (the values on the contours represent the average degree of loading (for common value of q/q_{max} of 25% or a FS = 4); other set of contours can be drawn for higher degrees of loading	Robertson (2009)
For "well-behaved" soils (uncemented, insensitive, not highly-structured), and some structured soils (e.g., cemented sands and calcareous clays)	$MRF = \frac{G}{G_0} = \frac{E}{E_0} = 1 - f\left(\frac{\tau}{\tau_{max}}\right)^g = 1 - f\left(\frac{q}{q_{max}}\right)^g = 1 - f\left(\frac{1}{FS}\right)^g$ f = 1.0; $g \approx 0.3 \pm 0.1$ for well-behaved soils (uncemented, insensitive, not highly structured); $\approx$ 0.5 for structured geomaterials (e.g., cemented sands and calcareous clays); also see Figure 2.32a	Fahey & Carter (1993)

Continued

TABLE 2.17
(Continued)

Soil Type and Applicability	Method/Relationship	Reference
For "well-behaved" soils (uncemented, insensitive, not highly-structured) , and some structured soils (e.g., cemented sands and calcareous clays)	$MRF = \frac{G}{G_0} = \frac{E}{E_0} = 1 - \left(\frac{\tau}{\tau_{max}}\right)^{g\left[1.5-\left(\frac{\tau}{\tau_{max}}\right)\right]}$ $= 1 - \left(\frac{q}{q_{max}}\right)^{g\left[1.5-\left(\frac{q}{q_{max}}\right)\right]} = 1 - \left(\frac{1}{FS}\right)^{g\left[1.5-\left(\frac{1}{FS}\right)\right]}$ $g \approx 0.3 \pm 0.1$ for well-behaved soils uncemented, insensitive, not highly structured); ≈ 0.5 for structured geomaterials (e.g., cemented sands and calcareous clays); also see Figure 2.32b	Fahey & Carter (1993); Mayne (2009)

Note: *OC* = overconsolidated; *OCR* = overconsolidation ratio; *NC* = normally consolidated; *LOC* = lightly overconsolidation; D' = constrained modulus of soil; e_0 = in situ void ratio of soil; C_s = swelling index and C_c = virgin compression index of the soil material; σ'_v = effective vertical overburden stress = $\sigma_v - u_0$; σ_v = total vertical overburden stress = $\Sigma(\gamma_{mi} \bullet z_i)$; γ_{mi} = total unit weight of the i-th soil layer; z_i = thickness of the i-th soil layer; u_0 = hydrostatic pore pressure = $\gamma_w (z - z_w)$, where, z = depth below the ground surface, γ_w = unit weight of water = 9.81 kN/m^3 = 62.4 pcf; z_w = depth of the ground water table; α_D = empirical scaling factor that depends on soil type, confining stress level, *OCR*, soil plasticity and natural water content (w); q_c = measured cone resistance; $q_{t,net}$ = net cone resistance = $q_t - \sigma_v$; F_R = normalized friction ratio = $f_s/(q_t - \sigma_v)$; q_t = corrected cone resistance = $q_c + u_2 (1 - a_n)$; a_n = cone net area ratio = A_n/A_c; A_n = cross-sectional area of the load cell behind the cone; A_c = projected cone cross-sectional area; u_2 = shoulder (behind the cone) pore pressure recorded during penetration of piezocone; K_D = constrained modulus number; p_A = atmospheric pressure = 1 bar = 100 kPa; a^* = stress exponent that depends on the σ'_{vp}; σ'_{vp} = effective preconsolidation stress; CPT = cone penetration test; SCPT = seismic cone penetration test; $I_{c(R\&W98)} = \sqrt{[3.47 - logQ_{tn}]^2 + [1.22 + LogF_R]^2}$; Q_{tn} = normalized net corrected cone resistance = $(q_{t,net}/p_A)(p_A/\sigma'_v)^n$; f_s = sleeve resistance; n = stress normalization exponent = $0.381 I_{c(R\&W98)} + 0.05 \frac{\sigma_v'}{p_A} - 0.15$ where n ≤ 1.0; G_0 = small-strain shear modulus; ρ_m = total soil mass density = γ_m/g; V_s = shear wave velocity; g_a = gravitational acceleration constant = 9.8 m/s^2; m^* = stress exponent; $\alpha_{D'\text{-}G0}$ = empirical scaling factor for converting G_0 to D'; K_G = small-strain shear modulus number; α_G = shear modulus factor; E' = drained Young's modulus; q/q_{max} = mobilized strength of soil; *FS* = factor of safety; K_E = Young's modulus number; q = applied stress; q_{max} = ultimate or failure stress; α_E = Young's modulus factor; τ = applied shear stress, and τ_{max} = ultimate shear stress at failure; f and g are constants depending on soil type and stress history.

pressure recorded during penetration of piezocone, I_R = rigidity index = G/s_u, G = shear modulus, s_u = undrained shear strength. Furthermore, linear one-dimensional consolidation was used to compute the dissipation of pore pressure. It was suggested that the coefficient of consolidation should be interpreted at 50% dissipation from the formula:

$$c = \frac{T_{50}}{t_{50}} r_o^2 \qquad \text{(Eq. 2.118)}$$

where the time factor T_{50} is found from the theoretical solutions, t_{50} is measured time for 50% dissipation and r_o = penetrometer radius (cylindrical model) or equivalent penetrometer radius for spherical model.

The selection of the appropriate model depends on the location of the porous filter element. The spherical solution may be most suitable for the filter elements located on the cone tip or the mid-face of the cone (i.e., u_1 location). For filter located on the cylindrical shaft (e.g., u_2), the cylindrical solution is the most applicable.

2.3.14.2 Jones and Van Zyl (1981) empirical correlation. The empirical method of Jones and Van Zyl (1981) was developed for type 2 piezocone dissipation data and uses the time measured to reach 50% completion of the full Δu decay, designated t_{50} (Robertson et al., 1992b). That is, t_{50} is the measured time required to go from the maximum penetration value of u_2 to the half-way point decaying back towards the equilibrium value u_0. The pore pressures data are recorded with respect to time axis. Typical dissipation curve for a soft clay is plotted on a logarithmic time scale (Figure 2.33a). The results are replotted in normalized form in Figure 2.33b.

Note that in routine production testing, it is usually not convenient to continue the test beyond t_{50}. In the example shown here, a full completion to 100% consolidation was achieved at around 850 minutes.

Once the t_{50} is found, the coefficient of consolidation by the method of Jones and Van Zyl (1981) can be simply calculated from:

$$c_h\,(cm^2/min) = \frac{[d(cm)]^2}{[13.4\, t_{50}(min)]} \qquad \text{(Eq. 2.119)}$$

where d = penetrometer diameter (= 3.57 cm for the standard 10-cm^2 cone size and 4.37 cm for 15 cm^2 cone).

2.3.14.3 Baligh and Levadoux (1980; 1986) strain path method for nonlinear total stress soil model. Levadoux and Baligh (1986), and Baligh and Levadoux (1980; 1986) performed a comprehensive study on pore pressure dissipation. They used the strain path method (Baligh, 1985) to predict the initial pore pressure distribution for normally consolidated Boston Blue Clay with rigidity index (I_R) = 500. Important conclusions from their study include the following.

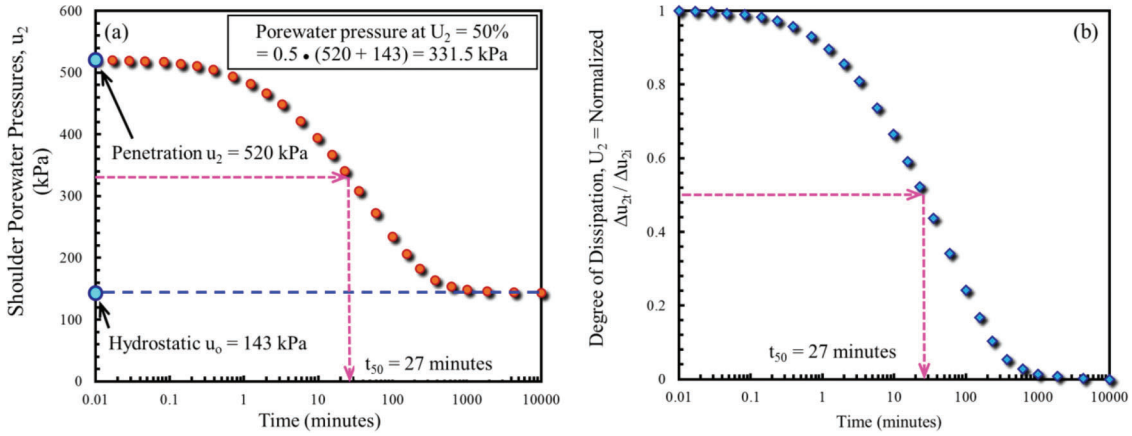

Figure 2.33 Illustrative monotonic dissipation test results from Bothkenner, UK: (a) direct measurement of shoulder pore pressures versus time; (b) normalized results of dissipation test (adapted from Lunne et al., 1997).

- Consolidation takes place predominantly in the recompression mode for dissipation less than 50%.
- Initial distribution of excess pore pressures around the probe has a significant influence on the dissipation process.
- Dissipation is predominantly in the horizontal direction.

2.3.14.4 Houlsby and Teh (1988) strain path method. For the SPM solution by Houlsby and Teh (1988), theoretical time factors (T^*) for different degrees of monotonic pore pressure dissipation are given at several key points on a penetrometer (e.g., apex, mid-face, shoulder, upper shaft above sleeve). Using the aforementioned measured reference value for 50% decay, the value of c is calculated from:

$$c_h = \frac{\left[T^*_{50}(a_c)^2\sqrt{I_R}\right]}{t_{50}} \qquad \text{(Eq. 2.120)}$$

where the time factors for 50% consolidation are T^*_{50} = 0.118 and 0.245, respectively, for type 1 (midface, u_1) and type 2 filter elements (shoulder position, u_2), a_c = probe radius = 1.78 cm for a 10 cm^2 cone and 2.20 for a 15 cm^2 size, and $I_R = G/s_u$ = undrained rigidity index, where G = shear modulus and s_u = undrained shear strength.

If the rigidity index is unknown, a common default value is taken as I_R = 100. However, this is done at the risk of errors and uncertainty. If desired, other degrees of consolidation can be handled by this method (e.g., 30%, 80%, etc.) as detailed by Houlsby and Teh (1988) (see Table 2.18).

2.3.14.5 Robertson et al. (1992b) empirical approach. Robertson et al. (1992b) reviewed dissipation data from piezocone tests to predict the coefficient of consolidation using Houlsby and Teh (1988) solutions with reference the values from laboratory tests and field observations. The simplified relationship thus developed for the coefficient of consolidation in horizontal direction (c_h) as a function of the time for 50% dissipation (t_{50}, in minutes) for a 10 cm^2 piezocone can be approximated in the following expression:

$$c_h(m^2/s) = \left(1.67 \times 10^{-6}\right) 10^{[1 - \log(t_{50})]} \qquad \text{(Eq. 2.121)}$$

For a 15 cm^2 cone, the values of c_h are increased by a factor 1.5. They also developed contours of the c_h versus t_{50} relationship for high stiffness to strength ratio (I_R = 500) and for low stiffness to strength ratio (I_R = 50) for piezocones with porous filter element placed on the cone face (u_1: dashed lines, and u_2: solid lines), as shown in Figure 2.34.

2.3.14.6 Teh (1987) analytical approach. Teh (1987) also proposed the interpretation of the consolidation data on a root time scale, as the initial section of the plot approximates closely to a straight line. If the pore pressure dissipation is plotted on a square-root time scale, the gradient of this linear section is m (see insert graph in Figure 2.34). Then c_h can be evaluated from the following equation:

$$c_h = \left(\frac{m}{M^*}\right)^2 \sqrt{I_R} r^2 \qquad \text{(Eq. 2.122)}$$

where M^* = gradient corresponding to the theoretical curve for a given probe geometry and porous element location, m = measured gradient of the initial linear dissipation $\left[\sqrt{(time)}\ units\right]$. Values for M^* are given in Table 2.19 The square-root time method is useful for short dissipation tests and/or where initial excess pore pressure (u_i) is uncertain.

Table 2.20 presents a summary of the methods and correlations for estimating the coefficient of consolidation from piezocone tests.

2.3.14.7 Effect of soil anisotropy on coefficient of consolidation. Due to soil anisotropy, the coefficient of consolidation (c) is also directional. The relevant design values depend on drainage and loading direction

TABLE 2.18
Modified time factors T^* from consolidation analysis (from Houlsby & Teh, 1988)

	Location	
Degree of Consolidation	**Cone (u_1)**	**Cylindrical Expansion Above Cone Base (u_2)**
20%	0.014	0.038
30%	0.032	0.078
40%	0.063	0.142
50%	0.118	0.245
60%	0.226	0.439
70%	0.463	0.804
80%	1.04	1.60

Note: u_1 = apex or mid-face pore pressure recorded during penetration of piezocone; u_2 = shoulder (behind the cone) pore pressure recorded during penetration of piezocone.

(typically represented as c_h in the horizontal direction and c_v in the vertical direction). An approximate estimate of the c_h and c_v can be obtained using the ratios of permeability in the horizontal and vertical direction given in the Table 2.21 using the following simplified relationship:

$$c_v = c_h\left(\frac{k_v}{k_h}\right) \qquad \text{(Eq. 2.123)}$$

For most natural soft marine clays, the horizontal permeability is only around 10% to 20% higher than the vertical value (Leroueil & Hight, 2003; Mesri, 1994). Generally, the ratio of k_h/k_v averages about 1.1 for intact clays of marine and water-borne origins. For varved clays and highly stratified deposits, the ratio of horizontal to vertical permeabilities may range from 1.5 to 5. Very rarely, k_h/k_v approaches 10 in the case of highly stratified deposits and formations. Adapting the approach by Leroueil and Jamiolkowski (1991), a guideline to geologic situations governing permeability anisotropy is given in Table 2.21.

2.3.15 Coefficient of Permeability

During the preliminary site characterization, it is helpful to estimate soil permeability from the simple, and relatively inexpensive tests, such as the CPT. The methods proposed to estimate the coefficient of permeability or the hydraulic conductivity (k) of soils using CPT results can be broadly coupled within two approaches: (1) based on the estimate of the soil type using the SBT charts, and (2) estimation from the rate of dissipation recording during CPTu dissipation test.

2.3.15.1 Permeability estimates based on soil type. Lunne et al. (1997) provided the following estimates of k from CPT soil behavior chart by Robertson et al. (1986) (see Figure A.16 and Table 2.22).

Robertson (2010a) provided estimates for k based on the CPT SBTn chart by Robertson and Wride (1998) and updated by Robertson (2009) with the modified definition of $I_{c(R\&W98)}$ based on Q_{tn}. These estimates

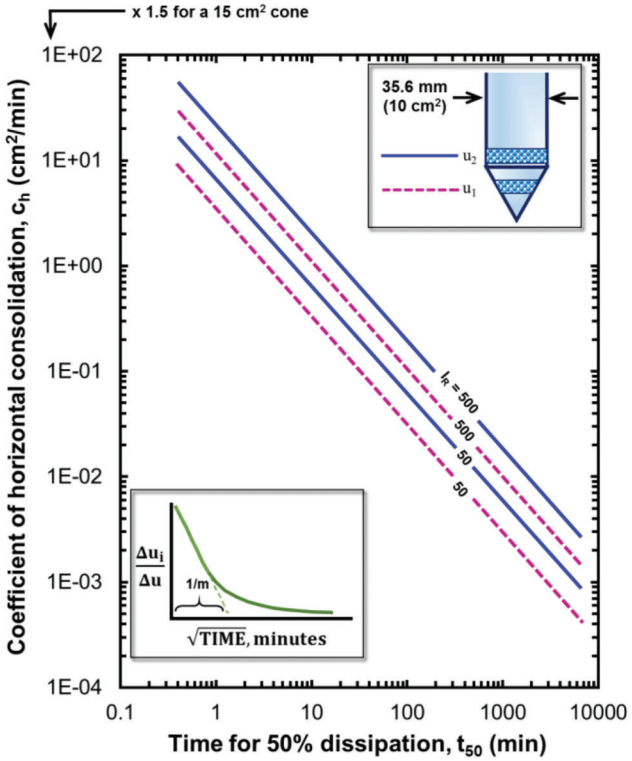

Figure 2.34 Chart for finding the horizontal coefficient of consolidation (c_h) in terms of the time (t_{50}) for 50% consolidation (adapted from Robertson et al., 1992b).

are provided in Table 2.23. Figure 2.35 shows the range of k values from Table 2.23 as a function of $I_{c(R\&W98)}$ and the average bilinear trend defined by Robertson (2010a) is given by the following relationships:

When $1.0 < I_{c(R\&W98)} \leq 3.27$

$$k_v(m/s) = 10^{[0.952 - 3.04 I_{c(R\&W98)}]} \qquad \text{(Eq. 2.124)}$$

When $3.27 < I_{c(R\&W98)} < 4.0$

$$k_v(m/s) = 10^{[-4.52 - 1.37 I_{c(R\&W98)}]} \qquad \text{(Eq. 2.125)}$$

TABLE 2.19
Gradient of dissipation curve (M), root time plot (from Teh, 1987)

	Location of Porous Filter Element on the Cone	
	Cone (u_1)	Cylindrical Expansion Above Cone Base (u_2)
Gradient (M^*)	1.63	1.15

Note: M^* = gradient corresponding to the theoretical curve for a given probe geometry and porous filter element location; u_1 = apex or mid-face pore pressure recorded during penetration of piezocone; u_2 = shoulder (behind the cone) pore pressure recorded during penetration of piezocone.

TABLE 2.20
Summary of the methods and correlation for estimating the coefficient of consolidation (c_h) from piezocone tests

Model Type and Application	Method/Relationship	Reference
Empirical Correlation	$c_h(cm^2/min) = \frac{[d(cm)]^2}{[13.4t_{50}(min)]}$	Jones & Van Zyl (1981)
Strain Path Method	$c_h = \frac{[T^*_{50}(a_c)^2\sqrt{I_R}]}{t_{50}}$ If the rigidity index is unknown, a common default value is taken as $I_R = 100$ at the risk of uncertainty. Other degrees of consolidation can be handled by this method (e.g., 30%, 80%, etc.) (see Table 2.18)	Houlsby & Teh (1988)
Empirical Approach	$c_h(m^2/s) = (1.67 \times 10^{-6})10^{[1-\log(t_{50})]}$ (for a 10 cm^2 piezocone) For a 15 cm^2 cone, the values of c_h are increased by a factor 1.5 Alternatively, use Figure 2.34 to estimate c_h from t_{50} for a range of I_R between 50 and 500 for either u_1 or u_2 types of piezocone tests	Robertson et al. (1992b)
Based on analytical approach; for interpretation of the consolidation data on a root time scale; the method is useful for short dissipation tests and/or where initial excess pore pressure (u_i) is uncertain	$c_h = \left(\frac{m}{M}\right)^2\sqrt{I_R}r^2$ If the pore pressure dissipation is plotted on a square-root time scale, the gradient of this linear section is m (see insert graph in Figure 2.34; initial section of the plot approximates closely to a straight line); values for M are given in Table 2.19	Teh (1987)

Note: c_{vh} = coefficient of consolidation in vertical or horizontal direction (depending on the case in consideration); d = penetrometer diameter (= 3.57 cm for the standard 10 cm^2 cone, and 4.37 cm for 15 cm^2 cone; t_{50} = measured time for 50% dissipation of excess pore pressure in a dissipation test from CPTu; T^*_{50} = time factors for 50% consolidation = 0.118 and 0.245 respectively for type 1 (midface, u_1) and type 2 filter elements (shoulder position, u_2), a_c = penetrometer probe radius (= 1.78 cm for a 10 cm^2 cone and 2.20 for a 15 cm^2 size); $I_R = G/s_u$ = undrained rigidity index; G = shear modulus; s_u = undrained shear strength; m = measured gradient of the initial linear dissipation $[\sqrt{(time)}units]$; M = gradient corresponding to the theoretical curve for a given probe geometry and porous element location.

Robertson and Cabal (2014) noted that these estimates are approximate at best but can provide a guide to variations of possible permeability.

2.3.15.2 Permeability estimates based on dissipation test from CPTu. The evaluation of k can be made by reference to its relationship with the coefficient of consolidation (c_{vh}) and constrained modulus (D'):

$$k_{vh} = \frac{c_{vh}\gamma_w}{D'} \qquad \text{(Eq. 2.126)}$$

where D' may be estimated from the correlations presented in Section 2.3.13 above.

Schmertmann (1978a), Parez and Fauriel (1988), and Robertson et al. (1992b) presented summaries of available data of the measured time for 50% dissipation (t_{50}) from 35.6 mm (10 cm^2) piezocone dissipation tests and their corresponding laboratory determined hydraulic conductivity (k_h) values. Accordingly, they proposed simplified approximate relationships based on their respective findings. An approximate expression for the overall mean trend is presented for Parez and Fauriel (1988) empirical relationship shown by the shaded regions for different soil types in Figure 2.36.

$$k_h(m/s) \approx \left[\frac{1}{2.244 \times 10^5\, t_{50}\,(min)}\right]^{1.32} \qquad \text{(Eq. 2.127)}$$

Figure 2.36 also presents the original data from Robertson et al. (1992b), as well as the newer contours of k_h versus t_{50} developed by Robertson (2010a) for various values of Q_{tn} and σ'_v. Robertson (2010a) indicated the general influence of soil compressibility [expressed in terms of constrained modulus (D')] on the k_h versus t_{50} relationship. It may be observed from a comparison between Parez and Fauriel (1988) and Robertson (2010a) plots in Figure 2.36 that the Robertson contours represent soft to stiff, fine-grained soils, with $t_{50} > 30$ seconds (i.e., the undrained response).

Robertson (2010a) also noted that it is better to first estimate the coefficient of consolidation (c_h) from the

TABLE 2.21
Permeability anisotropy in natural soils (after Leroueil & Jamiolkowski, 1991)

Nature of the Formation	k_h/k_v
Homogeneous clays of marine, alluvial, deltaic, and lacustrine origin	1 to 1.5
Sedimentary clays with discontinuous lenses and layers, well-developed macrofabric	2 to 3
Varved clays and silts with continuous permeable layers	1.5 to 5
Highly stratified soils with interbedded layers of clay, silt, sand, and/or gravel	2 to 10

Note: k_h = horizontal hydraulic conductivity; k_v = vertical hydraulic conductivity.

TABLE 2.22
Estimated soil permeability (k_v) based on the CPT SBT chart by Robertson et al., 1986 (after Lunne et al., 1997)

SBTn Zone	Soil Behavior Type (SBT)	Range of k (m/s)
1	Sensitive fine-grained	3×10^{-9} to 3×10^{-8}
2	Organic soils	1×10^{-8} to 1×10^{-6}
3	Clay	1×10^{-10} to 1×10^{-9}
4	Silty clay to clay	1×10^{-9} to 1×10^{-8}
5	Clayey silt to silty clay	1×10^{-8} to 1×10^{-7}
6	Sandy silt to clayey silt	1×10^{-7} to 1×10^{-6}
7	Silty sand to sandy silt	1×10^{-5} to 1×10^{-6}
8	Sand to silty sand	1×10^{-5} to 1×10^{-4}
9	Sand	1×10^{-4} to 1×10^{-3}
10	Gravelly sand to sand	1×10^{-3} to 1
11	Very stiff fine-grained soil (cemented and/or *OC*)	1×10^{-9} to 1×10^{-7}
12	Very stiff sand to clayey sand (cemented and/or *OC*)	1×10^{-8} to 1×10^{-6}

Note: k_v = coefficient of permeability in vertical direction (hydraulic conductivity).

piezocone dissipation test; then combine it with an estimate of the soil compressibility, expressed in terms of constrained modulus (D') (see Section 2.3.13) to be used in Eq. 2.126. He emphasized that this approach provides an improved estimate of k_h.

In addition, c_h versus t_{50} correlation by Robertson (2010a) given in Eq. 2.121 can also be extended to present a simplified approximation for a k_h determination from a dissipation test conducted on a 10 cm^2 cone via:

$$k_h(m/s) = \left(1.67\times10^{-6}\right)10^{[1-\log(t_{50})]}\frac{\gamma_w}{\left(Q_{t1}{}^2\sigma_v'\right)} \quad \text{(Eq. 2.128)}$$

where k_h = horizontal coefficient of permeability; t_{50} = time corresponding to 50% of consolidation; γ_w = unit weight of water; $Q_{t1} = (q_t - \sigma_v')/\sigma_v$; q_t = corrected cone resistance; σ_v = total vertical stress; and σ_v' = effective vertical stress.

Ansari et al. (2014) also developed an algorithm to estimate k_h based on dissipation test from piezocone tests. The method summarized below is applicable to both monotonic and dilative dissipation data, but only for soils with $OCR \leq 1.2$.

- Calculate 50% dissipation time, t_{50}, for the measured dissipation data once the excess pore pressure is normalized by U in the form of:

$$U = \left[\frac{(u_{measured-t} - u_o)}{(u_{measured-i} - u_o)}\right]100\% \quad \text{(Eq. 2.129)}$$

where, $u_{measured\text{-}t}$ = pore pressure measured at time t, and $u_{measured\text{-}i}$ = pore pressure measured at start of dissipation test, u_0 = initial (hydrostatic) pore pressure.

- Calculate t^*_{50} by modifying t_{50} for the effect of penetration depth, in-situ stresses, rigidity index, and cone radius through the following equation

$$t^*_{50} = t_{50}\left[\frac{\sigma_v'(kPa)}{27kPa}\right]^{0.97}\left(\frac{1+2K_o}{1.6}\right)^{-0.75}\left(\frac{I_R}{108}\right)^{0.48}\left[\frac{1.784(cm)}{a_c(cm)}\right]^2 \quad \text{(Eq. 2.130)}$$

where σ_v', K_0, and I_R are in-situ vertical effective stress, at-rest earth pressure coefficient, and rigidity index of the tested soil at the u_2 porous element position, respectively; and a_c is the radius of the piezocone.

- Finally, obtain an estimate of the horizontal permeability through the following correlation:

$$k_h(m/s) = \frac{6\times10^{-6}}{t^*{}_{50}(s)} \quad \text{(Eq. 2.131)}$$

Ansari et al. (2014) noted that this methodology is an initial attempt to develop a robust method for estimating soil permeability via piezocone dissipation tests. Since the methodology is verified against a series of experimental data, the method is expected to be generally applicable to all normally- to slightly-overconsolidated clays. However, the effect of anisotropy

TABLE 2.23
Estimated soil permeability (k_v) based on Robertson and Wride (1998) CPT SBTn classification (after Robertson, 2010a)

SBTn Zone	Soil Behavior Type (SBTn)	SBTn $I_{c(R\&W98)}$	Range of k
1	Sensitive fine-grained	*NA*	3×10^{-10} to 3×10^{-8}
2	Organic soils–clay	$I_{c(R\&W98)} > 3.6$	1×10^{-10} to 1×10^{-8}
3	Clay	$2.95 < I_{c(R\&W98)} < 3.60$	1×10^{-10} to 1×10^{-9}
4	Silt mixture	$2.60 < I_{c(R\&W98)} < 2.95$	1×10^{-10} to 1×10^{-7}
5	Sand mixture	$2.05 < I_{c(R\&W98)} < 2.60$	1×10^{-7} to 1×10^{-5}
6	Sand	$1.31 < I_{c(R\&W98)} < 2.05$	1×10^{-5} to 1×10^{-3}
7	Dense sand to gravelly sand	$I_{c(R\&W98)} < 1.31$	1×10^{-3} to 1
8	Very dense/stiff (cemented and/or *OC*)	*NA*	1×10^{-8} to 1×10^{-3}
9	Very stiff fine-grained (cemented and/or *OC*)	*NA*	1×10^{-9} to 1×10^{-7}

Note: k_v = coefficient of vertical permeability; *OC* = overconsolidated; Q_{tn} = normalized net corrected cone resistance = $(q_{t,net}/p_A)(p_A/\sigma'_v)^n$; $q_{t,net}$ = net cone resistance = $q_t - \sigma_v$; q_t = corrected cone resistance = $q_c + u_2\ (1 - a_n)$; q_c = measured cone resistance; u_2 = shoulder (behind the cone) pore pressure recorded during penetration of piezocone; a_n = cone net area ratio = A_n/A_c; A_n = cross-sectional area of the load cell behind the cone; A_c = projected cone cross-sectional area; σ_v = total vertical overburden stress = $\Sigma(\gamma_{mi} \bullet z_i)$; γ_{mi} = total unit weight of the i-th soil layer; z_i = thickness of the i-th soil layer; σ'_v = effective vertical overburden stress = $\sigma_v - u_0$; u_0 = hydrostatic pore pressure = $\gamma_w(z - z_w)$, where, z = depth below the ground surface, γ_w = unit weight of water = 9.81 kN/m^3 = 62.4 pcf; z_w = depth of the ground water table; p_A = atmospheric pressure = 1 bar = 100 kPa; n = stress normalization exponent = $0.381 I_{c(R\&W98)} + 0.05\frac{\sigma_v'}{p_A} - 0.15$ where $n \leq 1.0$;
$I_{c(R\&W98)} = \sqrt{[3.47 - logQ_{tn}]^2 + [1.22 + LogF_R]^2}$.

remains to be studied, and due care must be exercised when directional anisotropy is evident from geologic information of the site.

A summary of different correlations and methods for permeability assessment is presented in Table 2.24.

2.4 Closing Comments

Soils are naturally occurring complex materials with diverse mineralogical compositions and geologic origins that have experienced the evolving environmental and climatic conditions during their formation. Their response to the type of loading introduced by insertion of a penetrometer is influenced by their stress history, dimensional anisotropy, drainage characteristics, presence of structures due to ageing and cementation, fissuring etc. All correlations thus formulated between the penetrometer data and the soil behavior type response, as well as with various soil properties and parameters are influenced by the site-specific conditions. Correlations do offer convenience in the first order approximation of the soil type and those properties/parameters. They are often helpful in confirming or verifying results from more specific laboratory classification, strength, and compressibility tests also. However, in application of these relationships' attention must be paid to the source data, and the prevalent conditions at the site in question. Engineering judgement of the parameters interpreted and estimated from these correlations must be exercised by experienced design engineers.

The idea of redundancy via production of several separate CPT-based profiles of these parameters and properties in the soil formation from more than just one correlation/expression is actually quite useful. If the profiles show agreement, then this helps to validate a "well-behaved" soil, and a higher degree of reliance might be afforded in the value used in design. However, if the profiles disagree, the results may serve as a warning to implement a higher level of scrutiny by the engineer. For instance, the porous filter element may become desaturated after passing through a dilatant layer. Alternatively, the soil formation itself may have unusual aspects and therefore not behave as "clay" or "sand" or "silt," e.g., one soil type may have a rather substantial fraction of other types, or unusual mineralogy, or an abnormal structure and fabric that would place it within the domain of "nontextbook geomaterials." In these situations, a closer examination of the laboratory and/or field data may be warranted, providing justification for additional tests and investigation.

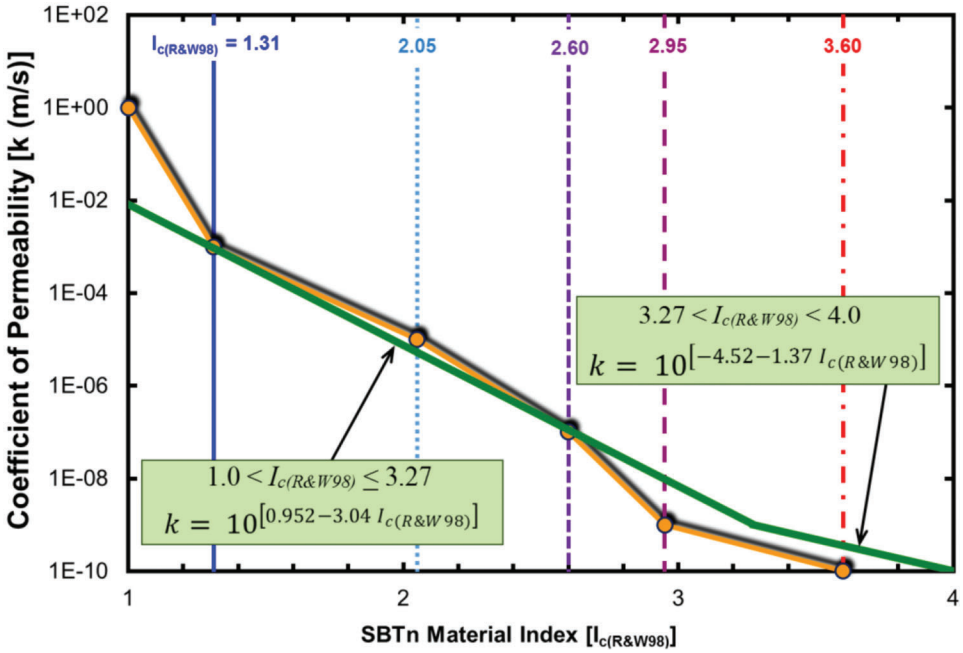

Figure 2.35 Suggested variations of soil permeability (k_v) as a function of SBTn $I_{c(R\&W98)}$ (adapted from Robertson, 2010a)

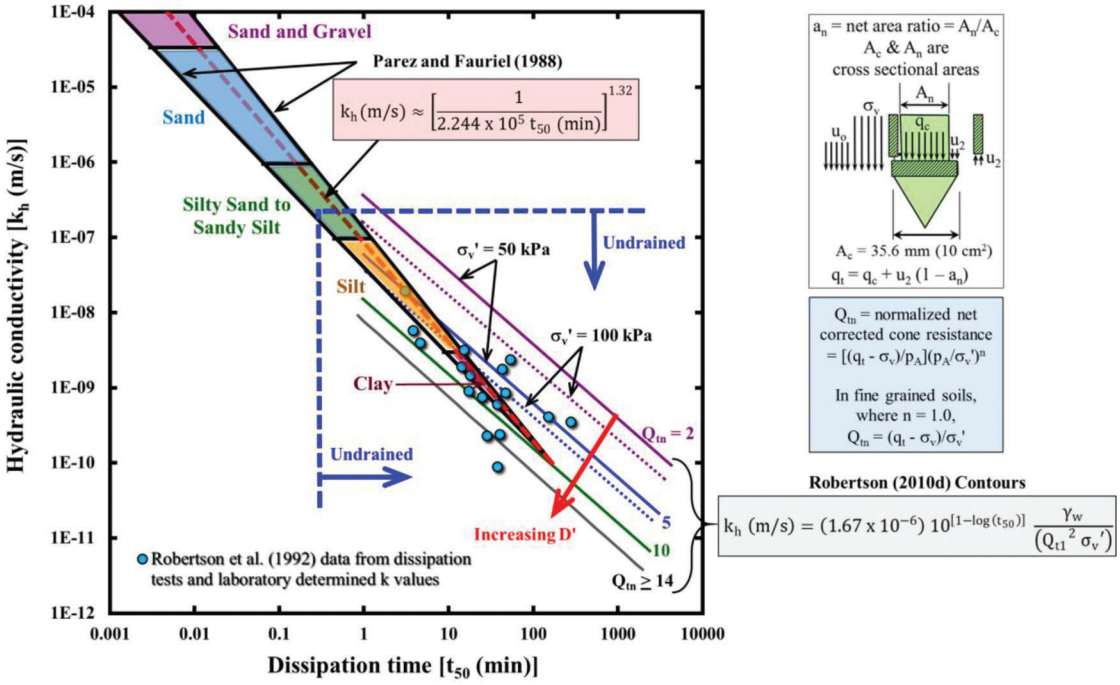

Figure 2.36 Relationship between CPTu t_{50}, based on u_2 pore pressure sensor location and 10 cm^2 cone, and soil permeability (k_h) (adapted from Mayne, 2007a and Robertson & Cabal, 2014).

TABLE 2.24
Summary of the methods and correlation for estimating the hydraulic conductivity (k_{vh}) from CPT/CPTu

Basis for the Method/Correlation	Method/Relationship	Reference
Based on SBT classification	Select from the range of k_v values based on Robertson et al. (1986) SBT classification system (use Table 2.22)	Lunne et al. (1997)
Based on SBT classification	Select from the range of k_v based on the CPT SBTn classification by Robertson (2009) (use Table 2.23) Alternatively use by the following relationships: When $1.0 < I_c(R\&W98) < 3.27$ $k_v(m/s) = 10^{[0.952 - 3.04 I_{c(R\&W98)}]}$ When $3.27 < I_{c(R\&W98)} < 4.0$	Robertson (2010a)
Based on Dissipation Test from CPTu	$k_h(m/s) \approx \left[\frac{1}{2.244 \times 10^5 t_{50}(min)}\right]^{1.32}$ (for a 10 cm^2 piezocone) This correlation is based on the mean trend of the shaded zones shown in Figure 2.36	Parez & Fauriel (1988)
Based on Dissipation Test from CPTu	Use t_{50} value determined from dissipation test together with the closest applicable contours of Q_{tn} and σ_v' in Figure 2.36 to estimate k_h values (contours represent soft to stiff, fine-grained soils, with $t_{50} > 30$ seconds (i.e., the undrained response) Alternatively use the following approximate relationship: $k_h(m/s) = (1.67 \times 10^{-6}) 10^{[1 - \log(t_{50})]} \frac{\gamma_w}{(Q_{tn}{}^2 \sigma_v')}$ Applies to u_2 pore pressure sensor location and 10 cm^2 piezocone	Robertson (2010a)
Based on Dissipation Test from CPTu and empirical approach	$k_h = \frac{c_h \gamma_w}{D'}$ Coefficient of consolidation (c_h) and the constrained modulus (D') are estimated using the methods summarized in Table 2.20 and Table 2.17, respectively	Robertson (2010a)
Based on Dissipation Test from CPTu; applicable to both monotonic and dilative dissipation data, but only for soils with $OCR \leq 1.2$	Calculate t_{50} corresponding from the measured dissipation Calculate t^*_{50} by modifying t_{50} for the effect of penetration depth, in-situ stresses, rigidity index, and cone radius through the following equation: $t^*_{50} = t_{50} \left[\frac{\sigma_v'(kPa)}{27kPa}\right]^{0.97} \left(\frac{1+2K_o}{1.6}\right)^{-0.75} \left(\frac{I_R}{108}\right)^{0.48} \left[\frac{1.784(cm)}{a_c(cm)}\right]^2$ Obtain an estimate of c_h from the following correlation: $k_h(m/s) = \frac{6 \times 10^{-6}}{t^*{}_{50}(s)}$ Use Tables 2.5, 2.11, and 2.12 for gm estimates needed for σ_v calculations, I_R estimates, and K_0 estimates, respectively.	Ansari et al. (2014)

Note: k_{vh} = coefficient of permeability (hydraulic conductivity) in vertical or horizontal direction (depending on the case in consideration); $I_{c(R\&W98)} = \sqrt{[3.47 - log Q_{tn}]^2 + [1.22 + Log F_R]^2}$; Q_{tn} = normalized net corrected cone resistance = $(q_{t,net}/p_A)(p_A/\sigma_v')^n$; $q_{t,net}$ = net cone resistance = $q_t - \sigma_v$; p_A = atmospheric pressure = 1 bar = 100 kPa; q_t = corrected cone resistance = $q_c + u_2 (1 - a_n)$; q_c = measured cone resistance; a_n = cone net area ratio = A_n/A_c; A_n = cross-sectional area of the load cell behind the cone; A_c = projected cone cross-sectional area; a_c = radius of the piezocone; u_2 = shoulder (behind the cone) pore pressure recorded during penetration of piezocone; F_R = normalized friction ratio = $f_s/(q_t - \sigma_v)$; f_s = sleeve resistance; k_h = coefficient of permeability (hydraulic conductivity) in horizontal direction; c_h = coefficient of horizontal consolidation; D' = constrained modulus; γ_w = unit weight of water; t_{50} = time (in minutes) corresponding to 50% of consolidation; σ_v' = effective vertical overburden stress = $\sigma_v - u_0$; σ_v = total vertical overburden stress = $\Sigma(\gamma_{mi} \bullet z_i)$; γ_{mi} = total unit weight of the i-th soil layer; z_i = thickness of the i-th soil layer; u_0 = hydrostatic pore pressure = $\gamma_w (z - z_w)$; z = depth below the ground surface; z_w = depth of the ground water table; K_0 = lateral stress coefficient = σ_h'/σ_v'; $I_R = G/s_u$ = undrained rigidity index; G = shear modulus; s_u = undrained shear strength.

REFERENCES

Agaiby, S. S., & Mayne, P. W. (2018). Evaluating undrained rigidity index of clays from piezocone data. In M. A. Hicks, F. Pisanò, & J. Peuchen (Eds.), *Proceedings of the 4th International Symposium on Cone Penetration Testing* (pp. 65–72). CRC Press.

Al-Awkati, Z. A. (1975). *On problems of soil bearing capacity at depth* [Doctoral dissertation, Duke University].

Al-Hussaini, M. M., & Townsend, F. C. (1975). Stress deformation of sand under K_0 conditions. *Proceedings of the 5th Pan-American Conference on Soil Mechanics and Foundation Engineering*, *1*, 129–136.

Almeida, M. S. S., & Parry, R. H. G. (1985). Small cone penetrometer tests and piezocone tests in laboratory consolidated clays. *Geotechnical Testing Journal*, *8*(1), 14–24.

Andresen, A., Berre, T., Kleven, A., & Lunne, T. (1979). Procedures used to obtain soil parameters for foundation engineering in the North Sea. *Marine Geotechnology*, *3*(3), 201–266.

Andrus, R. D., Mohanan, N. P., Piratheepan, P., Ellis, B. S., & Holzer, T. L. (2007). Predicting shear-wave velocity from cone penetration resistance (Paper No. 1454). In K. D. Pitilakis (Ed.), *Proceedings of the 4th International Conference on Earthquake Geotechnical Engineering*. Springer.

Ansari, Y., Merifield, R. S., & Sheng, D. (2014). A piezocone dissipation test interpretation method for hydraulic conductivity of soft clays. *Soils and Foundations*, *54*(6), 1104–1116.

A.P. van den Berg. (n.d.). *Brochures* [Webpage]. Retrieved December 2017, from https://www.apvandenberg.com/en/brochures-supplier-cpt-equipment

Baldi, G., Bellotti, R., Ghionna, V., Jamiolkowski, M., & Pasqualini, E. (1981). Cone resistance of a dry medium sand. *Proceedings of 10th International Conference on Soil Mechanics and Foundation Engineering*, *2*, 427–432. A. A. Balkema.

Baldi, G., Bellotti, R., Ghionna, V., Jamiolkowski, M., & Pasqualimi, E. (1985). Penetration resistance and liquefaction of sands. *Proceedings of 11th International Conference on Soil Mechanics and Foundation Engineering*. A. A. Balkema.

Baldi, G., Bellotti, R., Ghionna, V., Jamiolkowski, M., & Pasqualini, E. (1986, November). Interpretation of CPTs and CPTUs–2nd part: Drained penetration of sands. *Proceedings of the 4th International Geotechnical Seminar Field Instrumentation and In-Situ Measurements* (pp. 143–156).

Baldi, G., Bellotti, R., Ghionna, V., Jamiolkowski, M., & Lo Presti, D. C. F. (1989). Modulus of sands from CPTs and DMTs. *Proceedings of the 12th International Conference of Soil Mechanics and Foundation Engineering*, *1*, 165–170.

Baldi, G., Bruzzi, D., Superbo, S., Battaglio, M., & Jamiolkowski, M. (1988). Seismic cone in Po River Sand. *Proceedings of the 1st International Symposium on Penetration Testing*, *2*, 643–650.

Baligh, M. M. (1985, September). Strain path method. *Journal of the Geotechnical Engineering Division*, *111*(9), 1108–1136. American Society of Civil Engineers.

Baligh, M. M. (1986). Undrained deep penetration, II: Pore pressures. *Géotechnique*, *36*(4), 487–501.

Baligh, M. M., & Levadoux, J.-N. (1980). *Pore pressure dissipation after cone penetration*. (Report R 80-11) MIT.

Baligh, M. M., & Levadoux, J.-N. (1986). Consolidation after undrained piezocone penetration. II: Interpretation. *Journal of Geotechnical Engineering*, *112*(7), 727–745.

Baligh, M. M., Azzouz, A. S., Wissa, A. Z. E., Matyin, R. T., & Morrison, M. J. (1981). The piezocone penetrometer. In G. M. Norris & R. D. Holtz (Eds.), *Cone Penetration Testing and Experience* (pp. 247–263). American Society of Civil Engineers.

Baligh, M. M., Ladd, C. C., & Vivatrat, V. (1980). Cone penetration in soil profiling. *Journal of the Geotechnical Engineering Division*, *106*(4), 447–461.

Barentsen, P. (1936). Short description of a field testing method with cone-shaped sounding apparatus. *1st International Conference on Soil Mechanics and Foundation Engineering*, *1*(B/3), 7–10.

Been, K. I., Crooks, J. H. A., & Jefferies, M. G. (1988). Interpretation of material state from the CPTu in sands and clays. *Penetration Testing in the UK: Proceedings of the Geotechnology Conference* (pp. 215–218). Thomas Telford Publishing.

Begemann, H. K. S. (1953). Improved method of determining resistance to adhesion by sounding through a loose sleeve placed behind the cone. *Proceedings of the 3rd International Conference on Soil Mechanics and Foundation Engineering*, *1*, 213–217.

Begemann, H. K. S. (1965). The friction jacket cone as an aid in determining the soil profile. *Proceedings of the 6th International Conference on Soil Mechanics and Foundation Engineering*, *2*, 17–20.

Bemben, S. M., & Myers, H. J. (1974). The influence of rate of penetration on static cone resistance in Connecticut river valley carved clay. *Proceedings of the European Symposium on Penetration Testing*, *2*(2), 33–34.

Bolton, M. D. (1986, March). The strength and dilatancy of sands. *Géotechnique*, *36*(1), 65–78.

Briaud, J.-L., & Miran, J. (1992). *The cone penetrometer test* (Report No. FHWA-SA-91-043). Federal Highway Administration.

Broms, B. B., & Flodin, N. (1990). History of soil penetration testing. *Proceeding of the 1st International Symposium on Penetration Testing*, *1*, 157–220. A. A. Balkema.

Brooker, E. W., & Ireland, H. O. (1965). Earth pressure at rest related to stress history. *Canadian Geotechnical Journal*, *2*(1), 1–15.

Bugno, W. T., & McNeilan, T. W. (1985). Cone penetration test results in offshore California silts. In R. Chaney & K. Demars (Eds.), *Strength Testing of Marine Sediments: Laboratory and In-Situ Measurements* (ASTM Special Technical Publication, STP 883), pp. 55–71.

Burland, J. B. (1989). Ninth Laurits Bjerrum Memorial Lecture: "Small is beautiful"—the stiffness of soils at small strains. *Canadian Geotechnical Journal*, *26*(4), 499–516.

Burns, S. E., & Mayne, P. W. (1996). Small and high-strain measurements of in situ soil properties using the seismic cone penetrometer. *Transportation Research Record of the Transportation Research Board*, *1548*(1), 81–88.

Burns, S. E., & Mayne, P. W. (1998). *Penetrometers for soil permeability and chemical detection* (Report No. GIT-CEEGEO-98-1). Georgia Institute of Technology.

Burns, S. E., & Mayne, P. W. (2002a). Analytical cavity expansion-critical state model for piezocone dissipation in fine-grained soils. *Soils and Foundations*, *42*(2), 131–137. https://doi.org/10.3208/sandf.42.2_131

Burns, S. E., & Mayne, P. W. (2002b). Interpretation of seismic piezocone results for the estimation of hydraulic conductivity in clays. *ASTM Geotechnical Testing Journal*, *25*(3), 333–340.

Campanella, R. G., & Robertson, P. K. (1981). Applied cone research. *Proceedings of the Cone penetration testing*

and experience (pp. 343–362). American Society of Civil Engineers.

Campanella, R. G., Robertson, P. K., & Gillespie, D. (1986). Seismic cone penetration test. In S. P. Clemence (Ed.), *Use of In-Situ Tests in Geotechnical Engineering*, Geotechnical Special Publication 6, 116–130. American Society of Civil Engineers.

Campanella, R. G., Gillespie, D., & Robertson, P. K. (1982). Pore pressure during cone penetration testing. In A. Verruijt, F. L. Beringen, & E. H. De Leeuw (Eds.), *Proceedings of the 2nd European Symposium on Penetration Testing*, ESOPT-II, 507–512. A. A. Balkema.

Chen, B. S.-Y., & Mayne, P. W. (1994, August). *Profiling the overconsolidation ratio of clays by piezocone tests* (Report No. GIT-CEEGEO-94-1) [PDF file]. Georgia Tech Research Corporation. http://geosystems.ce.gatech.edu/Faculty/Mayne/papers/OCR-CPTu by Chen & Mayne 1994.pdf

Chen, B. S.-Y., & Mayne, P. W. (1996). Statistical relationships between piezocone measurements and stress history of clays. *Canadian Geotechnical Journal*, *33*(3), 488–498.

Chung, S. F., Randolph, M. F., & Schneider, J. A. (2006). Effect of penetration rate on penetrometer resistance in clay. *Journal of Geotechnical and GeoEnvironmental Engineering*, *132*(9), 1188–1196.

Collin, A. (1956). *Recherches experimentales sur les glissements spontanes des terrains argileux* (W. R. Schriever, Trans.). University of Toronto Press. (Original work published 1846).

ConeTec Inc. (n.d.). [Homepage of website]. Retrieved December 2017, from https://www.conetec.com/

Cubrinovski, M., & Ishihara, K. (2002, December). Maximum and minimum void ratio characteristics of sands. *Soils and Foundations*, *42*(6), 65–78.

Danziger, F. A. B., & Lunne, T. (2012, December). Rate effect on cone penetration test in sand. *Geotechnical Engineering Journal of the SEAGS & AGSSEA*, *43*(4), 72–81.

Dayal, U., & Allen, J. H. (1975). The effect of penetration rate on the strength of remolded clay and sand samples. *Canadian Geotechnical Journal*, *12*(3), 336–348.

De Beer, E. E. (1963, March). The scale effect in the transposition of the results of deep-sounding tests on the ultimate bearing capacity of piles and caisson foundations. *Géotechnique*, *13*(1), 39–75.

de Lima, D. C., & Tumay, M. T. (1991). Scale effects in cone penetration test. *Proceedings Geotechnical Engineering Congress*, *1*, 38–51.

de Ruiter, J. (1971). Electric penetrometer for site investigations. *Journal of the Soil Mechanics and Foundations Division*, *97*(2), 457–472.

de Ruiter, J. (1981). Current penetrometer practice: Cone penetration testing and experience. *Proceedings of the ASCE National Convention: Cone Penetration Testing and Experience* (pp. 1–48).

DeJong, J. T., Jaeger, R. A., Boulanger, R. W., Randolph, M. F., & Wahl, D. A. J. (2013). Variable penetration rate cone testing for characterization of intermediate soils. *Geotechnical and Geophysical Site Characterization 4*, *1*, 25–42. CRC Press.

DeJong, J. T., Yafrate, N. J., DeGroot, D. J., Lo, H. E., & Randolph, M. F. (2010). Recommended practice for full-flow penetrometer testing and analysis. *Geotechnical Testing Journal*, *33*(2), 137–149.

Douglas, B. J., & Olsen, R. S. (1981). Soil classification using electric cone penetrometer. *Proceedings of the Conference on Cone Penetration Testing and Experience* (pp. 209–227). American Society of Civil Engineers.

Eslaamizaad, S., & Robertson, P. K. (1996). Seismic cone penetration test to identify cemented sands. In J. I. Clark (Ed.), *Proceedings of the 49th Canadian Geotechnical Conference* (pp. 352–360).

Eslaamizaad, S., & Robertson, P. K. (1997). Evaluation of settlement of footings on sand from seismic in-situ tests. *Proceedings of the 50th Canadian Geotechnical Conference*, *2*, 755–764.

Eslami, A., & Fellenius, B. H. (1997, December). Pile capacity by direct CPT and CPTu methods applied to 102 case histories. *Canadian Geotechnical Journal*, *34*(6), 886–904. https://doi.org/10.1139/t97-056

Fahey, M., & Carter, J. P. (1993). A finite element study of the pressuremeter in sand using a nonlinear elastic plastic model. *Canadian Geotechnical Journal*, *30*(2), 348–362.

Fear, C. E., & Robertson, P. K. (1995). Estimating the undrained strength of sand: a theoretical framework. *Canadian Geotechnical Journal*, *32*, 859–870.

Fellenius, B. H., & Eslami, A. (2000, November 27–30). *Soil profile interpreted from CPTu data* [Conference session]. "Year 2000 Geotechnics" Geotechnical Engineering Conference. Asian Institute of Technology.

Finnie, I. M. S., & Randolph, M. F. (1994). Punch-through and liquefaction induced failure of shallow foundations on calcareous sediments. *Proceedings of the 7th International Conference on Behavior of Offshore Structures*, *1*, 217–230. Pergamon.

Ganju, E., Prezzi, M., & Salgado, R. (2017, October). Algorithm for generation of stratigraphic profiles using cone penetration test data. *Computers and Geotechnics*, *90*(2017), 73–84. https://doi.org/10.1016/j.compgeo.2017.04.010

Geomil Equipment B.V. (n.d.). [Homepage of website]. Retrieved December 2017, from https://www.geomil.com/

Geosoft Sp. z o.o. (n.d.). [Homepage of website]. Retrieved December 2017, from https://www.geosoft.com.pl/

Gillespie, D. G. (1990). *Evaluating shear wave velocity and pore pressure data from the cone penetration test* [Doctoral dissertation, University of British Columbia]. http://hdl.handle.net/2429/30573

Gorman, C. T., Drnevich, V. P., & Hopkins, T. C. (1975). Measurement of in-situ shear strength. *Proceedings of the ASCE Raleigh Conference: In-Situ Measurement of Soil Properties*, *2*, 139–140. American Society of Civil Engineers.

Hamouche, K. K., Leroueil, S., Roy, M., & Lutenegger, A. J. (1995, August). In-situ evaluation of K_0 in Eastern Canada clays. *Canadian Geotechnical Journal*, *32*(4), 677–688. https://doi.org/10.1139/t95-067

Hegazy, Y. A., & Mayne, P. W. (1995). Statistical correlations between Vs and cone penetration data for different soil types. *Proceedings of the International Symposium on Cone Penetration Testing*, *2*, 173–178.

Hegazy, Y. A., & Mayne, P. W. (2006, May). A global statistical correlation between shear wave velocity and cone penetration data. *Proceedings of the GeoShanghai International Conference, Site and Geomaterial Characterization* (pp. 243–248). American Society of Civil Engineers.

Houlsby, G. T. (1988). Session leader's introduction to papers 14–19. *Proceedings of the Geotechnology Conference on Penetration Testing in the U.K.* (pp. 141–146). Thomas Telford Limited.

Houlsby, G. T., & Hitchman, R. (1988, March). Calibration chamber tests of a cone penetrometer in sand. *Géotechnique*, *38*(1), 39–44.

Houlsby, G. T., & Teh, C. I. (1988). Analysis of the piezocone in clay. *Proceedings of the International Symposium on Penetration Testing*, *1*, 777–783, A. A. Balkema.

House, A. R., Oliveira, J. R. M. S., & Randolph, M. F. (2001). Evaluating the coefficient of consolidation using penetration tests. *International Journal of Physical Modelling in Geotechnics*, *1*(3), 17–25.

Huntsman, S. R., Mitchell, J. K., Klejbuk, L. W., Jr., & Shinde, S. B. (1986). Lateral stress measurements during cone penetration. *Proceedings of In Situ '86, Use of In Situ Tests in Geotechnical Engineering*, ASCE Geotechnical Special Publication 6, 617–634.

IRTP. (1999). International reference tests procedure for cone penetration test (CPT). In F. B. J. Barends, J. Lindenberg, & H. J. Luger (Eds.), *12th European Conference on Soil Mechanics and Geotechnical Engineering Proceedings* (pp. 2195–2222). A. A. Balkema.

Jaeger, R. A., DeJong, J. T., Boulanger, R. W., Low, H. E., & Randolph, M. F. (2010, May). Variable penetration rate CPT in an intermediate soil [PDF file]. *Proceedings of the 2nd International Symposium on Cone Penetration Testing*. https://www.geoengineer.org/storage/publication/18393/publication_file/2632/50Jaevpr.pdf

Jaky, J. (1944). The coefficient of earth pressure at rest. *Journal of the Society of Hungarian Architects and Engineers*, *7*, 355–358.

Jamiolkowski, M., & Pepe, M. C. (2001, October). Vertical yield stress of Pisa clay from piezocone tests. *Journal of Geotechnical and Geoenvironmental Engineering*, *127*(10), 893–897.

Jamiolkowski, M., Ladd, C. C., Germaine, J. T., & Lancellotta, R. (1985). New developments in field and laboratory testing of soils. *Proceedings of the 11th International Conference Soil Mechanics and Foundation Engineering*, *1*, 57–154.

Jamiolkowski, M., LoPresti, D. C. F., & Manaserro, M. (2001). Evaluation of relative density and shear strength of sands from CPT and DMT. *Soil Behavior and Soft Ground Construction*, ASCE Geotechnical Special Publication No. 119, 201–238.

Janbu, N. (1963). Soil compressibility as determined by oedometer and triaxial tests. *Proceedings of the 2nd European Conference on Soil Mechanics and Foundation Engineering*, *1*, 19–25.

Jefferies, M. G., & Been, K. (2006). *Soil liquefaction*: *A critical state approach*. Taylor and Francis.

Jefferies, M. G., & Davies, M. P. (1991, February). Soil classification by the cone penetration test. Discussion. *Canadian Geotechnical Journal*, *28*(1), 173–176. http://dx.doi.org/10.1139/t91-023

Jefferies, M. G., & Davies, M. P. (1993). Use of CPTU to estimate equivalent SPT N60. *Geotechnical Testing Journal*, *16*(4), 458–468. http://dx.doi.org/10.1520/GTJ10286J

Jefferies, M. G., Jønsson, L., & Been, K. (1987, December). Experience with measurement of horizontal geostatic stress in sand during cone penetration test profiling. *Géotechnique*, *37*(4), 483–498. https://doi.org/10.1680/geot.1987.37.4.483

Jones, G. A., & Rust, E. (1982, May 24–27). Piezometer penetration testing, CPTU. *Proceedings of the 2nd European Symposium on Penetration Testing, 2*, 607–614.

Jones, G. A., & Van Zyl, D. J. A. (1981). The piezometer probe: a useful investigation tool. *Proceedings of the 10th International Conference on Soil Mechanics and Foundation Engineering*, *2*, 489–495. A. A. Balkema.

Jones, G. A., Van Zyl, D. J. A., & Rust, E. (1981). Mine tailings characterization by piezometer cone. *Proceedings of Symposium on Cone Penetration Testing and Experience* (pp. 303–324). American Society of Civil Engineers.

Juran, I., & Tumay, M. T. (1989). Soil stratification using the dual pore-pressure piezocone test. *Transportation Research Record*, *1235*(1), 68–78.

Karlsrud, K., Lunne, T., & Brattlien, K. (1996). Improved CPTU interpretations based on block samples. *Nordic Geotechnical Conference Proceedings*, *1*, 195–201.

Karray, M., & Hussien, M. N. (2018). Why is there a discrepancy in shear wave velocity–cone tip resistance (Vs–qc) correlations' trends with respect to grain size? *Canadian Geotechnical Journal*, *55*(7), 1041–1047. https://doi.org/10.1139/cgj-2017-0316

Karray, M., Lefebvre, G., Ethier, Y., & Bigras, A. (2011, April). Influence of particle size on the correlation between shear wave velocity and cone tip resistance. *Canadian Geotechnical Journal*, *48*(4), 599–615. https://doi.org/10.1139/t10-092

Keaveny, J. M., & Mitchell, J. K. (1986). Strength of fine-grained soils using the piezocone. *Use of In-Situ Tests in Geotechnical Engineering*, Geotechnical Special Publication, 668–699.

Kim, K., Prezzi, M., Salgado, R., & Lee, W. (2008). Effect of penetration rate on cone penetration resistance in saturated clayey soils. *Journal of Geotechnical and Geoenvironmental Engineering*, *134*(8), 1142–1153.

Konrad, J.-M., & Law, K. T. (1987). Undrained shear strength from piezocone tests. *Canadian Geotechnical Journal*, *24*(3), 392–405.

Krage, C. P., Broussard, N. S., & DeJong, J. T. (2014, May). Estimating rigidity index (IR) based on CPT measurements. *Proceedings of the 3rd International Symposium on Cone Penetration Testing* (pp. 727–735).

Kulhawy, F. H., & Mayne, P. W. (1990, August). *Manual on estimating soil properties for foundation design*. (Report No. EL-6800) Electric Power Research Institute.

Ladd, C. C. (1991, April). Stability evaluation during staged construction. *Journal of Geotechnical Engineering*, *117*(4), 540–615.

Ladd, C. C., & DeGroot, D. J. (2003). Recommended practice for soft ground site characterization. *Soil and Rock: Proceedings of the 12th Pan American Conference*, *1*, 3–57. Verlag Glückauf Publishing.

Ladd, C. C., Germaine, J. T., Baligh, M. M., & Lacasse, S. M. (1980, November). *Evaluation of self-boring pressuremeter tests in Boston Blue clay* (Report FHWARD-80/052) Massachusetts Institute of Technology.

Larsson, R., & Åhnberg, H. (2005). On the evaluation of undrained shear strength and preconsolidation pressure from common field tests in clay. *Canadian Geotechnical Journal*, *42*(4), 1221–1231.

Larsson, R., & Mulabdic, M. (1991). *Piezocone tests in clay*. Statens Geotekniska Institute Report No. 42). Statens Geotekniska Institut.

Le Doan, V. (2019). *A unified approach for the assessment of the axial capacity of bored piles* [Doctoral dissertation, The University of Western Australia]. https://doi.org/10.26182/5ef54a65b5e0a

Lehane, B., & Cosgrove, E. (2000). Applying triaxial compression stiffness data to settlement prediction of shallow foundations. *Geotechnical Engineering*, *142*, 191–200.

Lehane, B. M., O'Loughlin, C. D., Gaudin, C., & Randolph, M. F. (2009, February). Rate effects on penetrometer resistance in kaolin. *Géotechnique*, *59*(1), 41–52. https://doi.org/10.1680/geot.2007.00072

Leroueil, S., & Hight, D. (2003). Behavior and properties of natural soils and soft rocks. *Characterization and Engineering Properties of Natural Soils*, *1*, 229–254. Swets and Zeitlinger.

Leroueil, S., & Jamiolkowski, M. (1991). Exploration of soft soil and determination of design parameters. *Proceedings of GeoCoast'91, Yokohama*, *2*, 969–998.

Levadoux, J.-N., & Baligh, M. M. (1986, July). Consolidation after undrained peizocone penetration. I: Prediction. *Journal of Geotechnical Engineering*, *112*(7), 707–726.

L'Heureux, J. S., & Long, M. (2017, June). Relationship between shear-wave velocity and geotechnical parameters for Norwegian clays. *Journal of Geotechnical and Geoenvironmental Engineering*, *143*(6), 1–20. https://doi.org/10.1061/(asce)gt.1943-5606.0001645

Locat, J., Tanaka, H., Tan, T. S., Dasari, G. R., & Lee, H. (2003). Natural soils: geotechnical behavior and geological knowledge. In T. S. Tan, K. K. Phoon, D. W. Hight, & S. Lerouleil (Eds.), *Characterisation and Engineering Properties of Natural Soils*, *1*, 3–28. Swets and Zeitlinger.

Lunne, T. (1976). *Results of some penetration tests with different cones in overconsolidated clays* (Internal Report 52155-4) Norwegian Geotechnical Institute.

Lunne, T., & Christoffersen, H. P. (1983, May). Interpretation of cone penetrometer data for offshore sands. *Proceedings of the 15th Offshore Technical Conference* (pp. 181–192).

Lunne, T., Eidsmoen, T., Gillespie, D., & Howland, J. D. (1986). Laboratory and field evaluation of cone penetrometers. *Proceedings of the ASCE Specialty Conference*. In Situ '86: Use of In Situ Tests in Geotechnical Engineering (pp. 714–729). American Society of Civil Engineers.

Lunne, T., & Powell, J. J. M. (1992). Recent developments in in situ testing in offshore soil investigation. In D. A. Ardus, D. Clare, A. Hill, R. Hobbs, R. J. Jardine, & J. M. Squire (Eds.), *Offshore Site Investigations and Foundation Behavior*. Advances in Underwater Technology, Ocean Science and Offshore Engineering, *28*, 147–180. Springer, Dordrecht.

Lunne, T., Powell, J. J. M., & Robertson, P. K. (1996). *Use of piezocone tests in non-textbook materials. Advances in Site Investigation Practice* (pp. 438–451). Thomas Telford Ltd, London.

Lunne, T., Robertson, P. K., & Powell, J. J. M. (1997). *Cone Penetration Testing in Geotechnical Practice*. Blackie Academic.

Masood, T., & Mitchell, J. K. (1993, October). Estimation of in situ lateral stresses in soils by cone penetration tests. *Journal of Geotechnical Engineering*, *119*(10), 1624–1639.

Mayne, P. W. (1991, June). Determination of OCR in clays by piezocone tests using cavity expansion and critical state concepts. *Soils and Foundations*, *31*(2), 65–76.

Mayne, P. W. (2001). Invited Keynote: Stress-strain-strength-flow parameters from enhanced in-situ tests. *Proceedings of the International Conference on In-Situ Measurement of Soil Properties and Case Histories* (pp. 27–47).

Mayne, P. W. (2005). Integrated ground behavior: in-situ and lab tests. In H, Di Benedetto, T. Doanh, H. Geoffroy, & C. Sauzéat (Eds.), *Deformation Characteristics of Geomaterials*, *2*, 55–177. Taylor & Francis Group.

Mayne, P. W. (2006a). In-situ test calibrations for evaluating soil parameters. *Characterization & Engineering Properties of Natural Soils*, *3*, 1602–1652. Taylor & Francis Group.

Mayne, P. W. (2006b). The second James K. Mitchell Lecture: Undisturbed sand strength from seismic cone tests. *Geomechanics and Geoengineering: An International Journal*, *1*(4), 239–257.

Mayne, P. W. (2007a). *Cone penetration testing–A synthesis of highway practice* (NCHRP Synthesis 368). Transportation Research Board.

Mayne, P. W. (2007b). In-situ test calibrations for evaluating soil parameters. *Characteristics and Engineering Properties of Natural Soils*, *3*, 1602–1652. Taylor and Francis Group.

Mayne, P. W. (2008, September 15–18.). Piezocone profiling of clays for maritime site investigations. *Proceedings of the 11th Baltic Sea Geotechnical Conference: Geotechnics in Maritime Engineering* (pp. 333–350). Polish Committee on Geotechnics.

Mayne, P. W. (2009). *Geoengineering design using the cone penetration test: geotechnical applications guide for the cpt and its derivatives. (CPTu, SCPT, SCPTu)* [Unpublished manuscript]. ConeTec Investigations Inc.

Mayne, P. W. (2013). *Evaluating yield stress of soils from laboratory consolidation and in-situ cone penetration tests*. Sound Geotechnical Research to Practice, (Holtz Volume, Geotechnical Special Publication 230) pp. 406–420. American Society of Civil Engineers.

Mayne, P. W. (2014). KN2: Interpretation of geotechnical parameters from seismic piezocone tests. In P. K. Robertson & K. I. Cabal (Eds.), *Proceedings of the 3rd International Symposium on Cone Penetration Testing* (pp. 47–73).

Mayne, P. W. (2016). Evaluating effective stress parameters and undrained shear strength of soft-firm clays from CPT and DMT. *Australian Geomechanics Journal*, *51*(4), 27–55.

Mayne, P. W. (2017). Stress history of soils from cone penetration tests. *Soils and Rocks*, *40*(3), 203–216.

Mayne, P. W., & Agaiby, S. S. (2019). Profiling yield stresses and identification of soft organic clays using piezocone tests. *Proceedings of the 16th Pan American Conference on Soil Mechanics and Geotechnical Engineering* (pp. 220–227). Geotech Society.

Mayne, P. W., & Brown, D. A. (2003). Site characterization of Piedmont residuum of North America. *Characterization and Engineering Properties of Natural Soils*, *2*, 1323–1339. Swets & Zeitlinger.

Mayne, P. W., Coop, M. R., Springman, S., Huang, A-B., & Zornberg, J. (2009). State-of-the-art paper (SOA-1): Geomaterial behavior and testing. *Proceedings of the 17th International Conference Soil Mechanics and Geotechnical Engineering*, *4*, 2777–2872. Millpress/IOS Press.

Mayne, P. W., & Kulhawy, F. H. (1982, June). K_0-OCR relationship in soil. *Journal of Geotechnical Engineering*, *108*(6), 851–872.

Mayne, P. W., Kulhawy, F. H., & Kay, J. N. (1990). Observations on the development of porewater pore water stresses during piezocone penetration in clays. *Canadian Geotechnical Journal*, *27*(4), 418–428.

Mayne, P. W., & Peuchen, J. (2012, September). Unit weight trends with cone resistance in soft to firm clays. In R. Q. Coutinho & P. W. Mayne (Eds.), *Geotechnical and Geophysical Site Characterization 4*, *1*, 903–910. CRC Press.

Mayne, P. W., & Peuchen, J. (2018). Evaluation of CPTU Nkt cone factor for undrained strength of clays. *Proceedings of the 4th International Symposium on Cone Penetration Testing* (pp. 423–430). CRC Press/Balkema.

Mayne, P. W., Peuchen, J., & Bouwmeester, D. (2010, May). Soil unit weight estimation from CPTs. *Proceedings of the 2nd International Symposium on Cone Penetration Testing*. https://www.geoengineer.org/storage/publication/18348/publication_file/2587/5MaySuw.pdf

Mayne, P. W., & Rix, J. G. (1995, June). Correlations between shear wave velocity and cone tip resistance in natural clays. *Soils and Foundations*, *35*(2), 107–110.

Mayne, P. W., Robertson, P. K., & Lunne, T. (1998). Clay stress history evaluated from SCPTu. *Geotechnical Site Characterization*, *2*, 1113–1118. A. A. Balkema.

Meigh, A. C. (1987). *Cone penetration testing: methods and interpretation*. Butterworths.

Mesri, G. (1975, April). New design procedure for stability of soft clays. *Journal of the Geotechnical Engineering Division*, *101*(GT4), 409–412.

Mesri, G., & Abdel-Ghaffar, M. E. M. (1993, August). Cohesion intercept in effective stress stability analysis. *Journal of Geotechnical Engineering*, *119*(8), 1229–1249.

Mesri, G., Dominic O., Kwan Lo, D. O., & Feng, T.-W. (1994). Settlement of embankments on soft clay. In A. T. Yeung & G. Y. Felio (Eds.), *Vertical and Horizontal Deformations of Foundations and Embankments*, *1*, 8–56.

Mitchell, J. K. (1988). New developments in penetration tests and equipment. *1st International Symposium on Penetration Testing*, *1*, 245–261.

Mitchell, J. K., & Gardner, W. S. (1975). In situ measurement of volume change characteristics. *Proceedings of the ASCE Specialty Conference on In-Situ Measurements of Soil Properties*, *2*, 279–345.

Muhs, H. (1978). 50 years of deep soundings with static penetrometers. Berlin Universität, Deutsche Forschungsgesellschaft fur Boden-Mechanik (Degebo). *Mitteilungen*, *34*, 45–50.

Mulabdić, M., Eskilson, S., & Larsson, R. (1990). *Calibration of piezocones for investigations in soft soils and demands for accuracy of the equipments* (SGI Varia No. 270). Swedish Geotechnical Institute.

Muromachi, T. (1981). Cone penetration testing in Japan. *Proceedings of the Symposium on Cone Penetration Testing and Experience* (pp. 49–75). American Society for Civil Engineering.

Niazi, F. S. (2014). *Static axial pile foundation response using seismic piezocone data* [Doctoral dissertation, Georgia Institute of Technology].

Niazi, F. S., Mayne, P. W., & Woeller, D. J. (2010a). Drilled shaft O-Cell response at Golden Ears Bridge from seismic cone tests. In M. H. Hussein, J. B. Anderson, & W. M. Camp III (Eds.), *The Art of Foundation Engineering Practice*, Geotechnical Special Publication No. 198, 452–469.

Niazi, F. S., Mayne, P. W., & Woeller, D. J. (2010b). Review of CPT-based methods for response evaluation of driven piles in dense sands. In S. Kibria, H. M. Qureshi, & A. M. Rana (Eds.), *Proceedings of the International Conference on Geotechnical Engineering* (pp. 259–266).

Olsen, R. S. (1984, July). Liquefaction analysis using the cone penetration test (CPT). *Proceedings of the 8th World Conference on Earthquake Engineering*, vol. 3. Prentice Hall.

Olsen, R. S. (1994, August). *Normalization and prediction of geotechnical properties using the cone penetrometer test (CPT)* [Doctoral dissertation, University of California].

Olsen, R. S., & Farr, J. V. (1986). Site characterization using the cone penetrometer test. In S. P. Clemence (Ed.), *In-situ'86: Use of In-Situ Tests in Geotechnical Engineering*, Geotechnical Special Publication 6, 864–868.

Olsen, R. S., & Malone, P. G. (1988). Soil classification and site characterization using the cone penetrometer test. In J. de Ruiter (Ed.), *Proceedings of the 1st International Symposium on Cone Penetration Testing*, *2*, 887–893. A. A. Balkema.

Olsen, R. S., & Mitchell, J. K. (1995). CPT stress normalization and prediction of soil classification. *Proceedings of International Symposium on Cone Penetration Testing*, (SGF Report 3:95), *2*, 257–262.

Parez, L., & Faureil, R. (1988). Le piézocône a méliorations apportées à la reconnaissance de sols. *Revue Française de Géotech*, *44*, 13–27.

Peuchen, J., Vanden Berghe, J. F., & Coulais, C. (2010, May). Estimation of u1/u2 conversion factor for piezocone. *2nd International Symposium on Cone Penetration Testing*, Huntington Beach, CA.

Plewes, H. D., Davies, M. P., & Jefferies, M. G. (1992). CPT based screening procedure for evaluating liquefaction susceptibility. *Proceedings of the 45th Canadian Geotechnical Conference*, *4*, 41–49. BiTech Publishers.

Powell, J. J. M., & Quarterman, R. S. T. (1988). The interpretation of cone penetration tests in clays with particular reference to rate effects. *Proceedings of the International Symposium on Penetration Testing*, *2*, 903–910. A. A. Balkema.

Powell, J. J. M., Quarterman, R. S. T., & Lunne, T. (1989). Interpretation and use of the piezocone test in UK clays. *Penetration Testing in the UK: Proceedings of the Geotechnology Conference* (pp. 151–156). Thomas Telford.

Power, P., & Geise, J. (1995). Seascout mini CPT system. *International Symposium on Cone Penetration Testing* (SGF Report 3.95), *2*, 79–84.

Ramsey, N. (2002, November). A calibrated model for the interpretation of cone penetration tests (CPTs) in North Sea quaternary soils (Paper No. SUT-OSIG-02-341). *Proceedings of the Offshore Site Investigation and Geotechnics: Diversity and Stability* (pp. 341–356). Society for Underwater Technology.

Randolph, M. F. (2004). Characterisation of soft sediments for offshore applications. In A. V. Da Fonseca & P. W. Mayne (Eds.), *Proceedings of the 2nd International Conference on Geotechnical and Geophysical Site Characterization 4*, *1*, 209–232. Millpress.

Randolph, M. F., & Wroth, C. P. (1978). Analysis of deformation of vertically loaded piles. *Journal of Geotechnical and Geoenvironmental Engineering Division*, *104* (GT12), 1465–1488.

Rix, G. J., & Stokoe, K. H. I. I. (1991). Correlation of initial tangent modulus and cone penetration resistance. In A. B. Huang (Ed.) *Proceedings of the 1st International Symposium on Calibration Chamber Testing* (pp. 351–362).

Robertson, P. K. (1990). Soil classification using the cone penetration test. *Canadian Geotechnical Journal*, *27*(1), 151–158. http://dx.doi.org/10.1139/t90-014

Robertson, P. K. (1991, February). Soil classification using the cone penetration test: Reply. *Canadian Geotechnical Journal*, *28*(1), 176–178. https://doi.org/10.1139/t91-024

Robertson, P. K. (2009, November). Interpretation of cone penetration tests—a unified approach. *Canadian Geotechnical Journal*, *46*(11), 1337–1355. https://doi.org/10.1139/T09-065.

Robertson, P. K. (2010a). Estimating in-situ soil permeability from CPT and CPTu. *The 2nd International Symposium on Cone Penetration Testing*, Huntington Beach, CA.

Robertson, P. K. (2010b). Estimating in-situ state parameter and friction angle in sandy soils from the CPT. *The 2nd International Symposium on Cone Penetration Testing*, Huntington Beach, CA.

Robertson, P. K. (2010c). Evaluation of flow liquefaction and liquefied strength using the cone penetration test. *Journal of Geotechnical and Geoenvironmental Engineering*, *136*(6), 842–853. https://doi.org/10.1061/(ASCE)GT.1943-5606.0000286

Robertson, P. K. (2010d). Soil behaviour type from the CPT: an update. *The 2nd International Symposium on Cone Penetration Testing*, Huntington Beach, CA.

Robertson, P. K. (2016). CPT-based soil behaviour type (SBT) classification system—an update. *Canadian Geotechnical Journal*, *53*(12), 1910–1927, https://doi.org/10.1139/cgj-2016-0044

Robertson, P. K., & Campanella, R. G. (1983). Interpretation of cone penetration tests. Part I: sands. *Canadian Geotechnical Journal*, *20*(4), 718–733.

Robertson, P. K., & Campanella, R. G. (1984). *Guidelines for use and interpretation of the electronic cone penetration test*. Hogentogler & Company, Inc.

Robertson, P. K., & Campanella, R. G. (1985, March). Liquefaction potential of sands using the CPT. *Journal of Geotechnical Engineering*, *111*(3), 384–403.

Robertson, P. K., & Cabal, K. L. (2012). *Guide to cone penetration testing for geotechnical engineering* (5th ed.). Gregg Drilling and Testing.

Robertson, P. K., & Cabal, K. L. (2014, December). *Guide to cone penetration testing for geotechnical engineering* (6th ed.). Gregg Drilling and Testing.

Robertson, P. K., Campanella, R. G., Gillespie, D., & Grieg, J. (1986, June). Use of piezometer cone data. In S. Clemence (Ed.), *Proceedings of American Society of Civil Engineers*, Geotechnical Special Publication No. 6, 1263–1280.

Robertson, P. K., Campanella, R. G., & Wightman, A. (1983). SPT-CPT correlations. *Journal of Geotechnical Engineering*, *109*(11), 1449–1459.

Robertson, P. K., & Fear, C. E. (1995). Application of CPT to evaluate liquefaction potential (SGF Report 3:95). *Proceedings of the International Symposium on Cone Penetration Testing*, *3*, 57–79. Swedish Geotechnical Society.

Robertson, P. K., Sully, J. P., Woeller, D. J., Lunne, T., Powell, J. J. M., & Gillespie, D. G. (1992b). Estimating coefficient of consolidation from piezocone tests. *Canadian Geotechnical Journal*, *29*(4), 539–550.

Robertson, P. K., Woeller, D. J., & Finn, W. D. L. (1992a). Seismic cone penetration test CPT for evaluating liquefaction potential under cyclic loading. *Canadian Geotechnical Journal*, *29*, 686–695.

Robertson, P. K., & Wride, C. E. (1998, January). Evaluating cyclic liquefaction potential using the cone penetration test. *Canadian Geotechnical Journal*, *35*(3), 442–459.

Rocha Filho, P. (1982). Influence of excess pore pressure on cone measurements. *Proceedings of the 2nd European Symposium of Penetration Testing*, *2*, 805–811. A. A. Balkema.

Roy, M., Tremblay, M., Tavenas, F., & La Rochelle, P. (1982, May). Development of pore pressures in quasi-static penetration tests in sensitive clay. *Canadian Geotechnical Journal*, *19*(2), 180–183. https://doi.org/10.1139/t82-015

Salgado, R. (2008). *The Engineering of Foundations*. McGraw-Hill.

Salgado, R., Bandini, P., & Karim, A. (2000, May). Shear strength and stiffness of silty sand. *Journal of Geotechnical and Geoenvironmental Engineering, 126*(5), 451–462.

Salgado, R., Mitchell, J.K., & Jamiolkowski, M. (1997, April). Cavity expansion and penetration resistance in sands. *Journal of Geotechnical and Geoenvironmental Engineering*, *123*(4), 344–354.

Salgado, R., Mitchell, J. K., & Jamiolkowski, M. (1998, September). Calibration chamber size effects on penetration resistance in sands. *Journal of Geotechnical and Geoenvironmental Engineering*, *124*(9), 878–888.

Salgado, R., & Prezzi, M. (2007, July). Computation of cavity expansion pressure and penetration resistance in sands. *International Journal of Geomechanics*, *7*(4), 251–65.

Salgado, R., Prezzi, M., & Ganju, E. (2015). *Assessment of site variability from analysis of cone penetration test data* (Joint Transportation Research Program Publication No. FHWA/IN/JTRP-2015/04). West Lafayette, IN: Purdue University. http://dx.doi.org/10.5703/1288284315523

Sandven, R. (1990). *Strength and deformation properties of fine grained soils obtained from piezocone tests* [Doctoral dissertation, Norwegian Institute of Technology].

Sandven, R., Senneset, K., & Janbu, N. (1988, March). Interpretation of piezocone tests in cohesive soils. In J. de Ruiter (Ed.), *Proceedings of the First International Symposium on Penetration Testing*, *2*, 939–953.

Sanglerat, G. (1972). *The Penetrometer and Soil Exploration*. Elsevier Publishing Company.

Sanglerat, G., Nhim, T. V., Sejourne, M., & Andina, R. (1974). Direct soil classification by static penetrometer with special friction sleeve. *Proceedings of the First European Symposium on Penetration Testing*, *2.2*, 337–344.

Schmertmann, J. H. (1966, November). Penetrometers–A choice for soil exploration. *The Florida Architect, 16*(11), 4–6.

Schmertmann, J. H. (1967, June). Static cone penetrometers for soil exploration. *The Magazine of Construction: Civil Engineering*, *37*(6), 71–73.

Schmertmann, J. H. (1969, October). *Dutch friction-cone penetrometer exploration of research area at field 5, Eglin Air Force Base, Florida* (Contract Report No. S-69-4). U.S. Army Engineer Waterways Experiment Station.

Schmertmann, J. H. (1974). Penetration pore pressure effects on quasi-static cone bearing, qc. *Proceedings of the European Symposium on Penetration Testing*, *2.2*, 345–351.

Schmertmann, J. H. (1975). Measurement of in-situ shear strength. *Proceedings of the ASCE Specialty Conference on In-situ Measurement of Soil Properties*, *2*, 57–13.

Schmertmann, J. H. (1978a). *Guidelines for cone penetration test: Performance and design* (Report No. FHWA-TS-78-209). Federal Highway Adminstration.

Schmertmann, J. H. (1978b). *Study of feasibility of using Wissa-type piezometer probe to identify liquefaction potential of saturated fine sands* (Technical Report, S-78-2). Waterways Experiment Station.

Schmertmann, J. H. (1991). The mechanical ageing of soils. *Journal of Geotechnical Engineering*, *117*(9), 1288–1330.

Schmidt, B. (1983). Discussion of "K_0-OCR relationships in soils" by Paul W. Mayne and Fred H. Kulhawy (June, 1982). *Journal of Geotechnical Engineering*, *109*(6).

Schnaid, F. (2009). *In-situ testing in geomechanics: The main tests*. Taylor & Francis Group.

Schneider, J. A., Hotstream, J. N., Mayne, P. W., & Randolph, M. F. (2012). Comparing CPTU Q-F and Q-$\Delta u2/\sigma v0'$ soil classification charts. *Géotechnique Letters*, *2*(4), 209–215. https://doi.org/10.1680/geolett.12.00044

Schneider, J. A., Lehane, B. M., & Schnaid, F. (2007, June). Velocity effects on Piezocone tests in normally and overconsolidated clays. *International Journal of Physical Modelling in Geotechnics, 7*(2), 23–34.

Schneider, J. A., & Mayne, P. W. (1999, October). *Soil liquefaction response in mid-America evaluated by seismic*

piezocone tests (Mid-America Earthquake Center Report No. MAE-GT-3A). Georgia Institute of Technology.

Schneider, J. A., & Moss, R. E. S. (2011). Linking cyclic stress and cyclic strain based methods for assessment of cyclic liquefaction triggering in sands. *Géotechnique Letters*, *1*(1), 31–36. http://dx.doi.org/10.1680/geolett.11.00021

Schneider, J. A., Randolph, M. F., Mayne, P. W., & Ramsey, N. R. (2008). Analysis of factors influencing soil classification using normalized piezocone tip resistance and pore pressure parameters. *Journal of Geotechnical and Geoenvironmental Engineering*, *134*(11), 1569–1586. https://doi.org/10.1061/(ASCE)1090-0241(2008)134:11(1569)

Searle, I. W. (1979). The interpretation of Begemann friction jacket cone results to give soil types and design parameters. *Proceedings of 7th European Conference on Soil Mechanics and Foundation Engineering*, *2*, 265–270.

Senneset, K., & Janbu, N. (1985). Shear strength parameters obtained from static cone penetration tests (Special Technical Publication, STP 883). In R. Chaney & K. Demars (Eds.), *Proceedings of the Symposium on strength testing of marine sediments; laboratory and in situ measurements* (pp. 41–54).

Senneset, K., Janbu, N., & Svanø, G. (1982, May). Strength and deformation parameters from cone penetration tests. In A. Verruijt, F. L. Beringen, & E. H. de Leeuw (Eds.), *Proceedings of the 2nd European Symposium on Penetration Testing*, *2*, 863–70. A. A. Balkema.

Senneset, K., Sandven, R., & Janbu, N. (1989). *Evaluation of soil parameters from piezocone test*. Transportation Research Record, No. 1235, 24–37.

Senneset, K., Sandven, R., Lunne, T., By, T., & Amundsen, T. (1988). Piezocone tests in silty soils. *In Proceedings of the international symposium on penetration testing*, *2*, 955–974, A. A. Balkema.

Subcommittee D18.02. (2012). ASTM D5778: *Standard test method for electronic friction cone and piezocone penetration testing of soils*. ASTM International.

Subcommittee D18.02. (2016). *ASTM D3441: Standard test method for mechanical cone penetration testing of soils*. ASTM International.

Sully, J. P., & Campanella, R. G. (1991, July). Effect of lateral stress on CPT penetration pore pressure. *Journal of Geotechnical Engineering, 117*(2), 1082–1088.

Sully, J. P., & Campanella, R. G. (1994, January). Evaluation of field CPTu dissipation data in overconsolidated fine-grained soils. *Proceedings of the 13th International Conference on Soil Mechanics and Foundation Engineering*, *1*, 201–204.

Sully, J. P., Campanella, R. G., & Robertson, P. K. (1988). Overconsolidation ratio of clays from penetration pore water pressures. *Journal of Geotechnical Engineering, 114*(2), 209–215. American Society of Civil Engineers.

Sully, J. P., Robertson, P. K., Campanella, R. G., & Woeller, D. J. (1999). An approach to evaluation of field CPTU dissipation data in overconsolidated fine-grained soils. *Canadian Geotechnical Journal*, *36*(2), 369–381.

Tanaka, H., & Tanaka, M. (1998). Characterization of sandy soils using CPT and DMT. *Soils and Foundations*, *38*(3), 55–65.

Tani, K., & Craig, W. H. (1995). Development of centrifuge cone penetration test to evaluate the undrained shear strength profile of a model clay bed. *Soils and Foundations*, *35*(2), 37–47.

Tavenas, F., & Leroueil, S. (1987). State-of-the-art on laboratory and in-situ stress-strain-time behaviour of soft clays. *Proceedings of the International Symposium on Geotechnical Engineering of Soft Soils* (pp. 1–146).

Te Kamp, W. G. B. (1982). The influence of the rate of penetration on the cone resistance qc in sand. *Proceedings of the 2nd European Symposium on Penetration Testing*, *2*, 627–633.

Teh, C.-I. (1987). *An analytical study of the cone penetration test* [Doctoral dissertation, Oxford University].

Tokimatsu, K., Suzuki, Y., Taya, Y., & Kubota, Y. (1995). Correlation of CPT data with static and dynamic properties of in-situ frozen samples. *Proceedings of the 1st International Symposium on Cone Penetration Testing* (SGF Report 3:95), *2*, 323–328. Swedish Geotechnical Society.

Torstensson, B. A. (1975). Pore pressure sounding instrument. *Proceedings of the Specialty Conference on In-situ Measurement of Soil Properties*, *2*, 48–54, American Society of Engineers.

Torstensson, B. A. (1977). *The pore pressure probe. Norsk jord- og fjellteknisk forbund*. Fjellsprengningsteknikk - bergmekanikk - geoteknikk, Oslo, Foredrag, 34.1–34.15, Trondheim, Norway, Tapir.

Treadwell, D. D. (1976). *The influence of gravity, prestress, compressibility and layering on soil resistance to static penetration* [Doctoral dissertation, University of California].

Tumay, M. T. (1985, July). *Field calibration of electric cone penetrometers in soft soils* (Publication No. FHWA/LA/LSU-GE-85/02). Federal Highway Administration.

Tumay, M. T., Bogges, R. L., & Acar, Y. (1981). *Subsurface investigation with piezo-cone-penetrometer* [Conference session]. Cone Penetration Testing and Experience. ASCE National Convention, St. Louis, MI. American Society of Engineers.

Uzielli, M., Mayne, P. W., & Cassidy, M. J. (2013). Probabilistic assignment of design strength for sands from in-situ testing data. In P. Arnold, G. A. Fenton, M. A. Hicks, T. Schweckendiek, & B. Simpson (Eds.), *Modern Geotechnical Design Codes of Practice: Implementation, Application and Development*, *1*, 214–227. IOS-Millpress.

Van de Graaf, H. C., & Jekel, J. W. A. (1982). *New guidelines for the use of inclinometer with the CPT. European Symposium on Penetration Testing* (ESOPT), *2*, 581–584.

Van de Graaf, H. C., & Vermeiden, J. (1988). Half a century of static cone penetration techniques. *LGM Mededelingen*, Part XXXII, 95.

Vermeulen, N., & Rust, E. (1995). CPTu profiling: a numerical method. *Proceedings of the 1st International Symposium on Cone Penetration Testing* (pp. 343–350). Swedish Geotechnical Institute.

Vertek. (n.d.). [Homepage of website]. Retrieved December 2017, from https://www.vertekcpt.com/

Villet, W. C. B., & Mitchell, J. K. (1981). Cone resistance, relative density and friction angle. *Cone Penetration Testing and Experience* (pp. 178–207).

Vos, J. D. (1982). The practical use of CPT in soil profiling. *2nd European Symposium on Penetration Testing*, *2*, 933–939.

Whittle, A. J. (1993, June). Evaluation of a constitutive model for overconsolidated clay. *Géotechnique, 43*(2), 289–313.

Whittle, A. J., & Aubeny, C. P. (1991). Pore pressure fields around piezocone penetrometers installed in clay. *Proceedings of the 7th International Conference on Computer*

Methods and Advances in Geomechanics, *1*, 285–90. A. A. Balkema.
Wissa, A. E. Z., Martin, R. T., & Garlanger, J. E. (1975). The piezometer probe. *Proceedings of the ASCE Specialty Conference on In Situ Measurement of Soil Properties*, *1*, 536–545.
Wroth, C. P. (1984). Interpretation of in-situ soil test. *Géotechnique*, *34*(4), 449–489.
Wroth, C. P., & Houlsby, G. (1985). Soil mechanics: property characterization and analysis procedures. *11th International Conference on Soil Mechanics and Foundation Engineering*, *124*(2), 1–54.
Yu, H. S. & Houlsby, G. T. (1991). Finite cavity expansion in dilatant soils: loading analysis. *Géotechnique*, *41*(2), 173–183.
Yu, H. S., & Mitchell, J. K. (1998). Analysis of cone resistance: Review of methods. *Journal of Geotechnical and Geoenvironmental Engineering*, *124*(2), 140–149.
Zhang, Z., & Tumay, M. T. (1999). Statistical to fuzzy approach toward CPT soil classification. *Journal of Geotechnical and Geoenvironmental Engineering*, *125*(3), 179–186.

APPENDICES

Appendix A to Chapter 2: Estimation of Soil Variables from CPT Results

Appendix B to Chapter 2: Instructions for the Use of Spreadsheet for Estimation of Soil Variables from CPT Results

APPENDIX A TO CHAPTER 2: ESTIMATION OF SOIL VARIABLES FROM CPT RESULTS

A.1 CPT-Based Soil Behavior Type Classification Systems

This appendix provides a concise review of the chronological development of the soil behavior type (SBT) classification systems advanced during the past 55 years of CPT history. This is a unique document that provides information regarding each SBT classification system, originating from the Begemann soil profiling chart in year 1965 to the Doan SBT classification index assessment method proposed in 2019. A total of 31 methods have been presented along with their respective charts, tables, and significant information regarding their formulation, source data, whether each method has developed on the earlier one(s), and the uniqueness of each method from the previous forms. Since, SBT classification system has been one of the most researched areas in the realm of CPT interpretations, and since many of the correlations are founded on these classification systems, a full review of this appendix is highly recommended for use of this manual in applications.

A.1.1 Begemann (1965) Chart

The earliest known soil profiling chart was developed by Begemann (1965) using data from mechanical cone penetrometers having friction sleeve. Based on 250 soundings (and their corresponding bore-logs) scattered across the Netherlands, the data of measured cone resistance (q_c) were plotted against sleeve resistance (f_s) on a arithmetic scale. Then using information from the corresponding borings, lines were drawn showing the percentages of particles smaller than 16μ. The chart is shown in Figure A.1. As indicated, the graph holds good for undisturbed natural deposits situated below the ground water table. The soil names indicated on the chart are based on the terminology used by the Delft Soil Mechanics Laboratory. In essence, Begemann (1965) indirectly introduced the concept of friction ratio (*FR*) and that the soil type is a function of *FR* which is essentially inverse of slopes of the lines. Thus, Fellenius and Eslami (2000) noted the range of applicable ratios for the soil types of this chart in tabulated form as shown in Figure A.1. Douglas and Olsen (1981) presented the findings of Begemann (1965) in a different format (q_c vs. *FR*) as shown in Figure A.2.

A.1.2 Schmertmann (1969) SBT Interpretations from Friction Ratio

Using Begemann type Dutch friction cone penetrometer for explorations in North-Central Florida, Schmertmann (1969) developed simple interpretations of soil type from friction ratio (*FR*). Here, the *FR* was directly used as a single parameter in a soil classification scheme. Data from a total of 20 sounding with average penetration depth of 21.5 m were employed. The *FR*-based soil interpretations are noted in Table A.1 below.

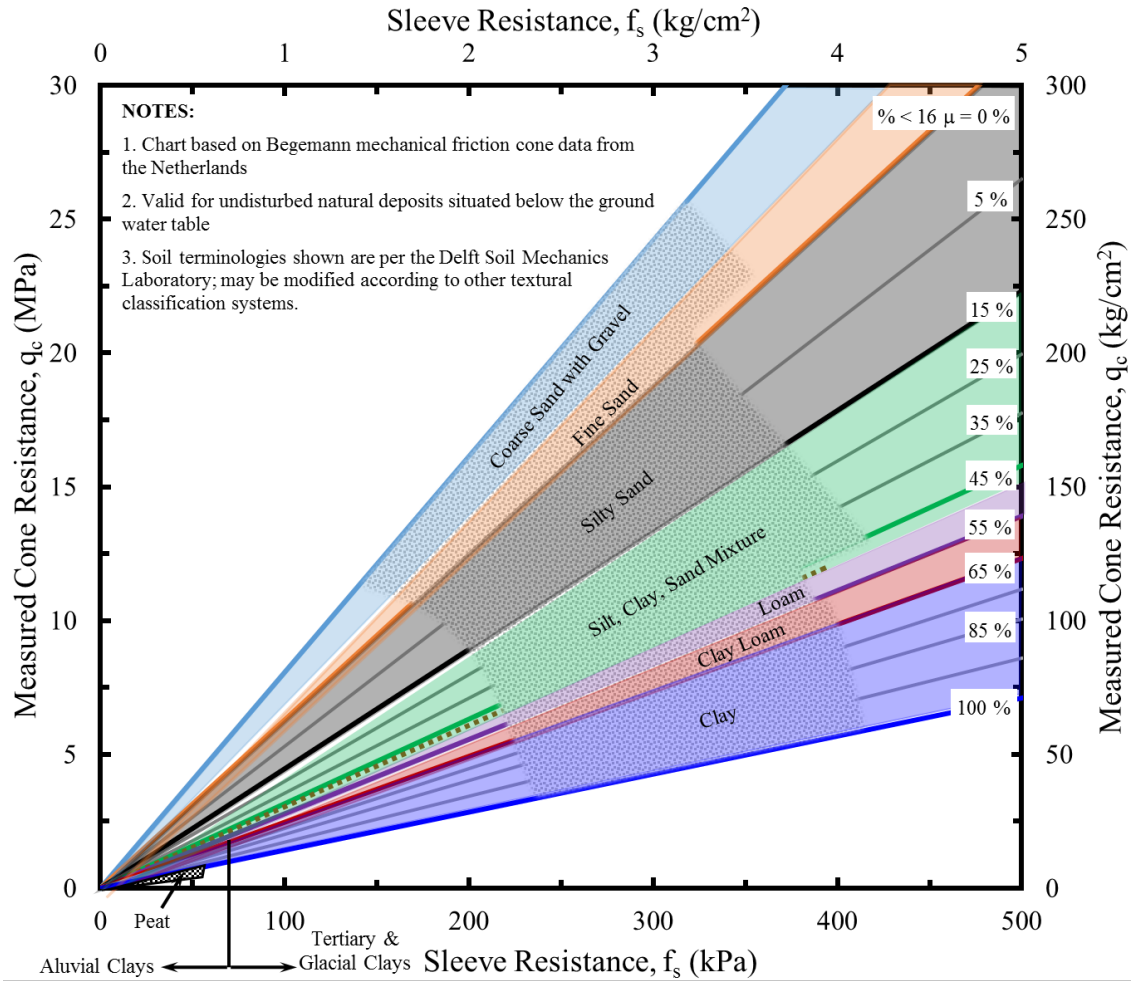

Begemann Soil Classification in terms of Friction Ratio (after Fellenius and Eslami, 2000)

Soil type	Range of Friction Ratio, FR (%) = (f_s/q_c) 100
Coarse sand with gravel through fine sand	1.2 to 1.6
Silty sand	1.6 – 2.2
Silt, sand, clay mixture	2.2 – 3.2
Clay loam and loam	3.2 – 4.1
Clay	4.1 – 7.0
Peat	> 7.0

Figure A.1 The Begemann SBT profiling chart (adapted from Begemann, 1965).

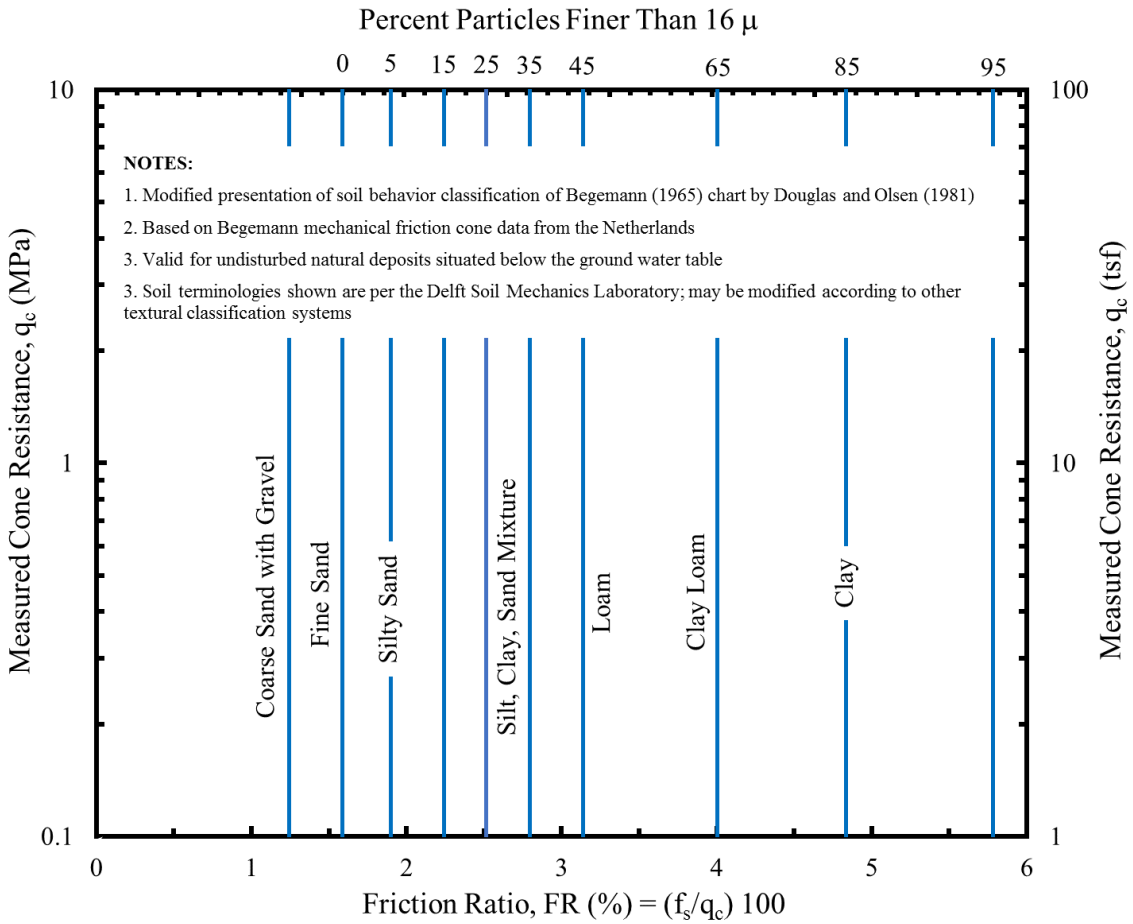

Figure A.2 Modified presentation of Begemann (1965) SBT classification (adapted from Douglas & Olsen, 1981).

Table A.1 Friction ratio values for soil identification in North-Central Florida (after Schmertmann, 1969)

Soil Type	Friction Ratio, *FR* (%) = (f_s/q_c) 100
Very shelly deposits, lime rock (soft, shelly, partially indurated limestone)	0 – ½
Clean sand, no plastic fines (independent of relative density)	½ – 2
Silty sand	1 ¾ –2 ½
Clayey sand, silts, marls, moderately sensitive clays	2 1/3 – 3 ½
Sandy clay	3 – 4 ½
Relatively insensitive clay	Over 5

Note: Data based on Begemann mechanical friction cone penetrometer.

A.1.3 Sanglerat et al. (1974) Chart

The next acknowledged work in this regard is the one by Sanglerat et al. (1974), who formulated a graph with cone resistance plotted as ordinate on logarithmic scale and friction ratio as abscissa on arithmetic scale (see Figure A.3). As previously established that *FR* depends on the soil type, q_c also appears to be a function of the soil type. The data used in developing this graph was obtained from 80 mm diameter Andina mechanical friction penetrometer employed for research. The smaller graph placed within the main chart in Figure A.3 is an alternative scheme presented by Sanglerat et al. (1974) based on the percentage of fines (< 80 μ), and it gives soil classification similar to the one presented by Begemann (1965). Fellenius and Eslami (2000) noted following observations regarding this chart:

- Indeed, the manner in which the penetrometer parameters are plotted is quite misleading: it gives the impression that friction ratio (*FR*) is independent while the measured cone resistance (q_c) is dependent. In this way, the q_c is plotted against its own inverse ($FR = f_s/q_c \cdot 100$), and therefore, the *FR* is, indeed, not independent. Plotting one as a function of the other, thus, distorts the true information.
- Since the chart was developed from a non-standard size of research penetrometer, it's accuracy in routine application is uncertain.

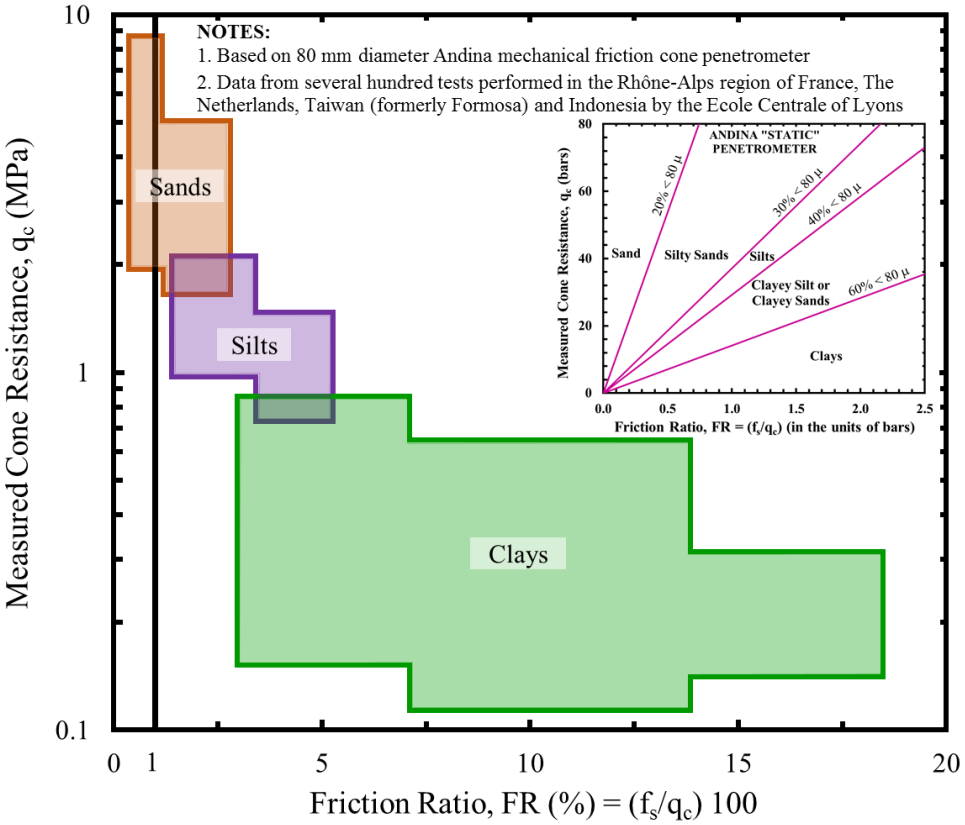

Figure A.3 Soil classification chart based on 80-mm Andina mechanical friction cone penetrometer (adapted from Sanglerat et al., 1974).

A.1.4 Schmertmann (1978a) Chart

In 1978, Schmertmann, based on his earlier findings from 1969, presented a more formalized form of SBT classification chart shown in Figure A.4. As evident, the formulation of this graph is same as that of Sanglerat et al. (1974): q_c as ordinate (logarithmic scale) vs. *FR* as abscissa (arithmetic scale). However, additional soil zones were demarcated to indicate sand density, stiffness of clays, mixed soil types and organic clays. Indeed, this chart by Schmertmann was first published in Sanglerat (1972). It may also be noticed from Figure A.4 that some of the zones have incomplete boundary. Schmertmann noted the following soil behavioral observations for cautious use of this graph:

- Correlations shown are based on local geology in North-Central Florida and are likely to differ in different geologic areas. It may, however, be noted that Sanglerat (1972), with his dataset from several hundred tests performed in a discrete geologic setting of the Rhône-Alps region of France, confirmed agreement of Schmertmann's findings.
- Evidence indicates that the measured sleeve friction (f_s), and therefore, the calculated friction ratio (*FR*) are more than the true values because of the bottom bevel of the friction sleeve. True values are $^1/_2 - ^1/_3$ the measured values in sands, while the difference is negligible in clays.
- Soils with high ductility (i.e., strength to modulus ratio) exhibit high *FR* (e.g., clays, Piedmont micaceous silts), while those with low ductility yield low *FR* (e.g., sands).
- Very high *FR* values can develop in loose, silty sands below the ground water table possibly due to liquefaction during the q_c measurement, followed by rapid dissipation of pore pressure and substantially increased shear strength during the f_s measurement.
- The *FR* values decrease in accuracy in soils with low q_c, such as in quick clays.

In order to mitigate the observation regarding distortion of true information caused by plotting of dependent variable (q_c) against its inverse (f_s/q_c), Fellenius and Eslami (2000) replotted the zones and boundaries of the original Schmertmann (1978a) chart: q_c (logarithmic scale) vs. f_s (logarithmic scale) (see Figure A.5). The format shown in Figure A.5 has the advantage that the parameters on ordinate and abscissa axes are independent, but the disadvantage that the data becomes more compressed. Furthermore, the boundaries do not appear very logical and easy to apply in this undistorted style of presentation.

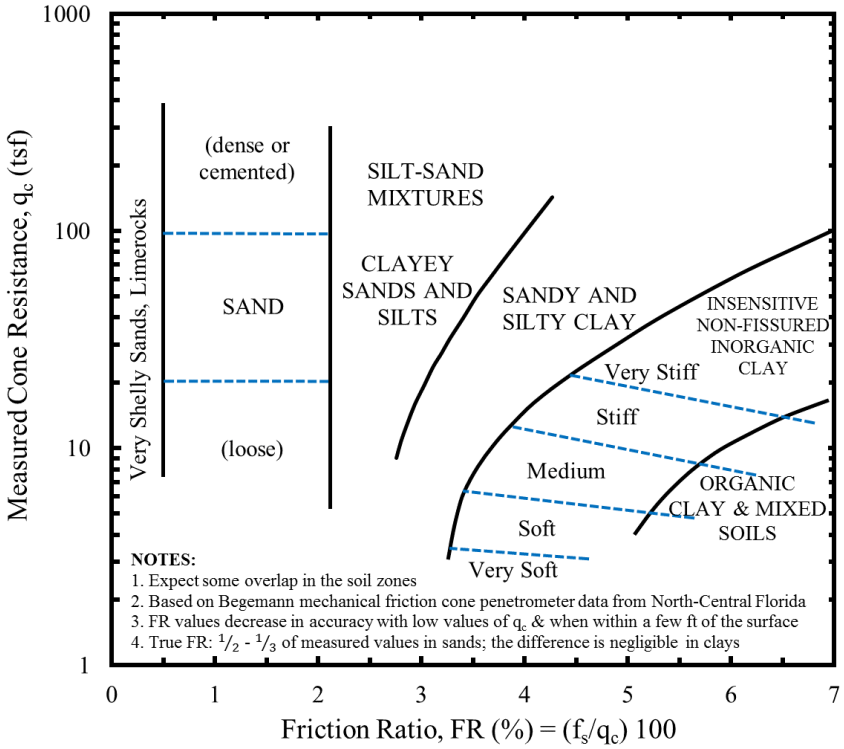

Figure A.4 SBT profiling chart by Schmertmann (1978a).

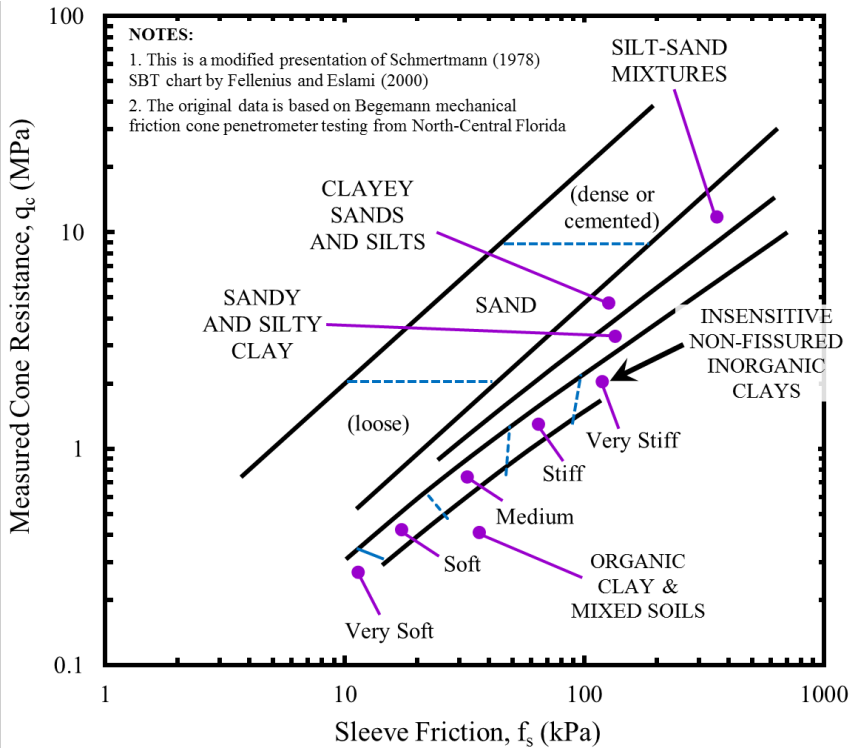

Figure A.5 Modified presentation of Schmertmann (1978a) SBT classification (adapted from Fellenius & Eslami, 2000).

A.1.5 Searle (1979) Chart

The classification chart presented by Searle (1979) represents the cone resistance (q_c), expressed in the units of MPa versus *FR* (%) (see Figure A.6). Like the Schmertmann method, this chart provides additional indications, such as the density as well as stiffness of fine soils. In addition, it also provides equations for the assessment of friction angle (ϕ'), relative density (D_R) and undrained cohesion (c_u), which are discussed in later relevant subsections.

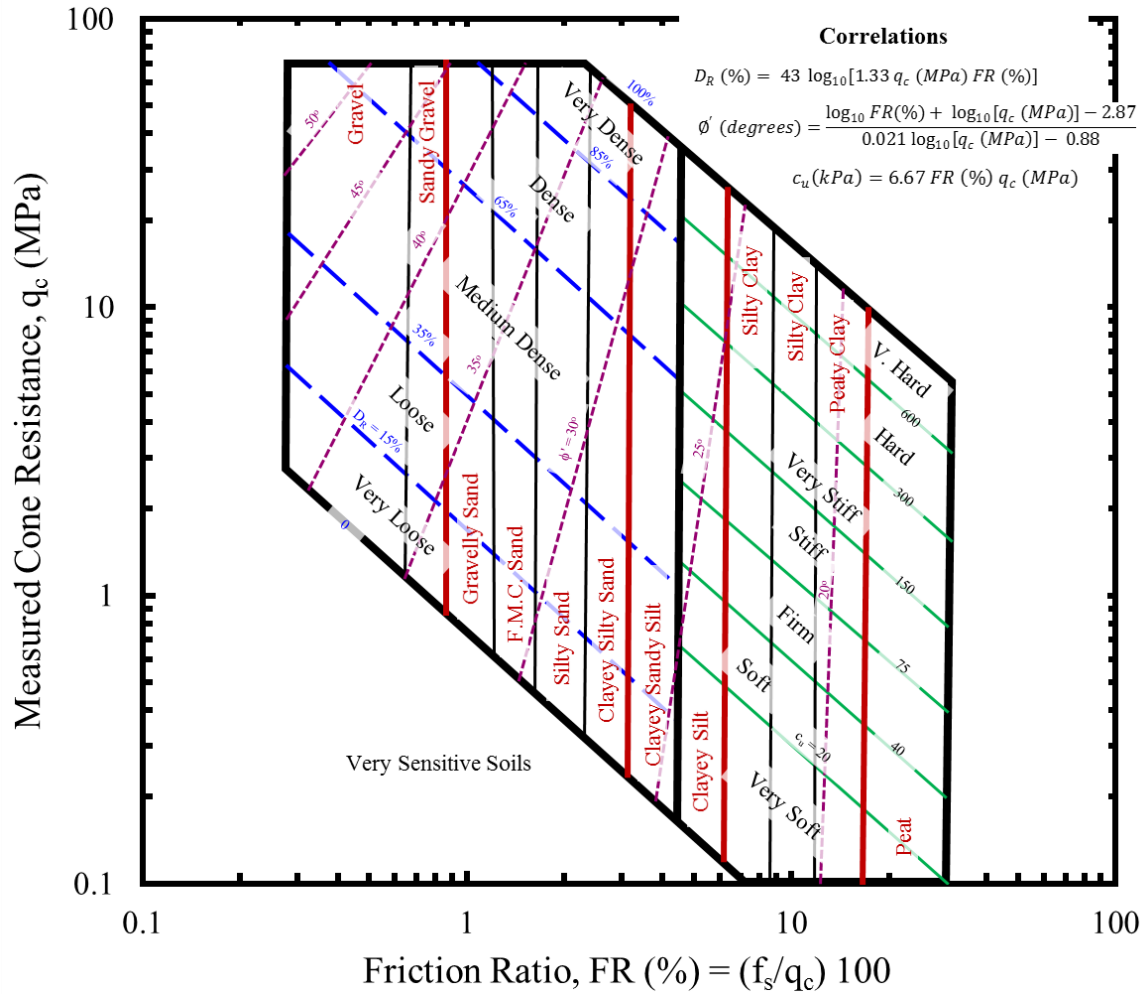

Figure A.6 Searle (1979) SBT classification chart.

A.1.6 Douglas and Olsen (1981) Findings

Douglas and Olsen (1981) developed the first soil behavior type guidelines based on electric CPT (60° apex angle, 10 cm^2 base area, 150 cm^2 friction sleeve area). They indicated two common features of deficiency within the earlier SBT charts: (1) ambiguity of prediction in mixed soils, and (2) difficulty in relating the information to other laboratory indices such as textural classification, plasticity, soil sensitivity, geostatic lateral earth pressure etc. They highlighted the use of different penetrometer types as a cause of discrepancies between the earlier charts. They also indicated that the greatest

uncertainty in the degree of drainage during soundings in mixed soils was the cause of difficulty in assessing the mechanical behavior of such soils.

The CPT data used by Douglas and Olsen (1981) included several sites in California, Oklahoma, Utah, Arizona, and Nevada. Through comparison of CPT data with laboratory tests (e.g., USCS grain size classification, Atterberg limits etc.) on adjacent samples taken from their nearest standard penetration tests, they published the chart shown in Figure A.7, which relates classification per the USCS, indicate trends of liquidity index, earth pressure coefficient, sensitivity and stability of soils. The format of their graph is same as that of Sanglerat et al. (1974) and Schmertmann (1978a): q_c as ordinate (logarithmic scale) versus FR as abscissa (arithmetic scale). This chart envelops three zones of different SBT using upward curving lines: cohesionless coarse-grained soils, ductile fine-grained soils, and mixed soils. The chart also presents zones demarcated by four lines with equal f_s.

Douglas and Olsen (1981) recommended standardization of equipment and procedure and consideration of the effect of penetration mechanics in layered media. To help improved differentiation of material types due to differences in pore pressure generation and dissipation characteristics, and to resolve the question of drained versus undrained response, they recommended inclusion of pore pressure information into standard sounding logs.

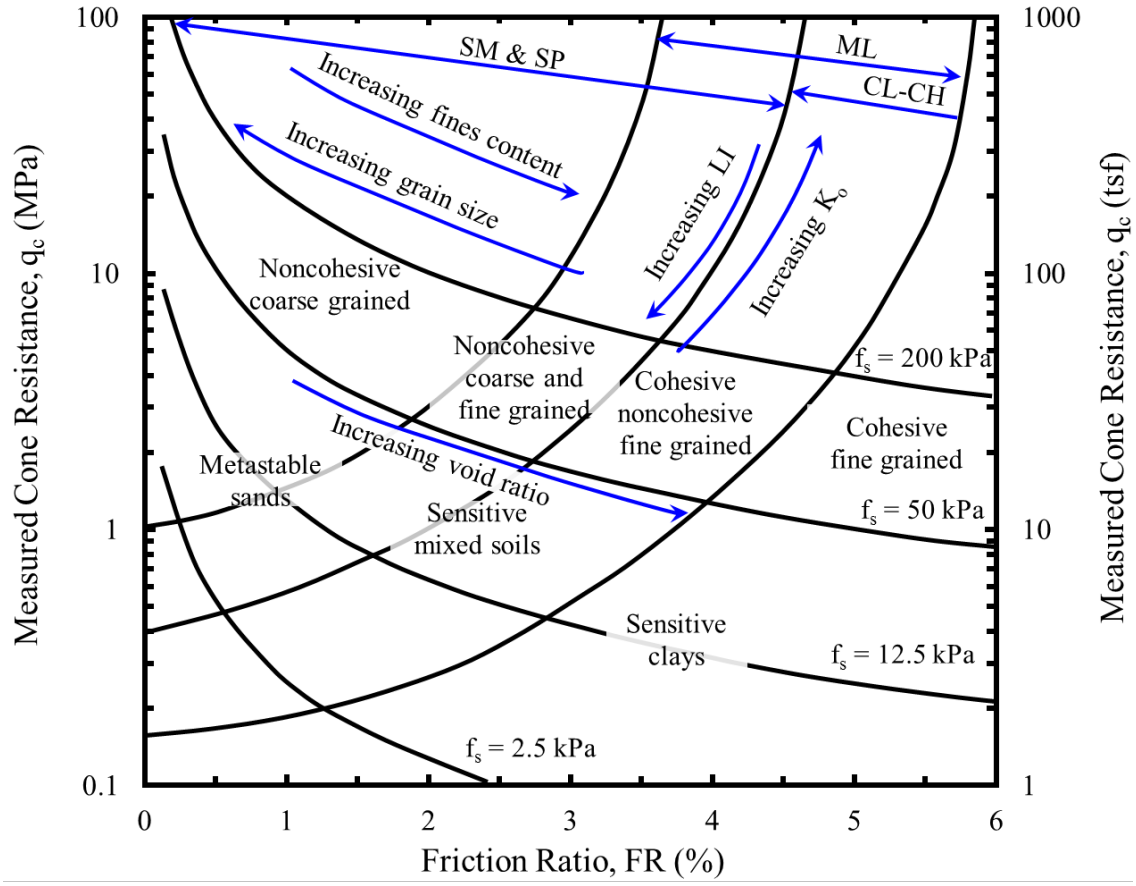

NOTES:
1. Based on 10 cm² electric friction CPT
2. Data from California, Oklahoma, Utah, Arizona, and Nevada in the USA

Figure A.7 SBT chart adapted from Douglas and Olsen (1981).

A.1.7 Jones et al. (1981) and Jones and Rust (1982) Chart from CPTu

Although not widely known, Jones et al. (1981) are the pioneers in developing the SBT chart based on piezocone test (CPTu) data as well as presenting their findings in the form of normalized parameters shown in Figure A.8. By this time, it was well established that there is a general tendency of increase in q_c, f_s, and u in deeper soil layers owing to increasing confinement and overburden stress (σ_v). Accordingly, different stress normalization schemes were already being proposed. Jones et al. (1981) adopted the following formats for stress normalization and their chart: $\Delta u_2/\sigma_v$ as ordinate (arithmetic scale) versus $q_{c\text{-}net}/\sigma_v$ as abscissa (arithmetic scale). Here, Δu_2 = excess pore pressure measured at the shoulder behind the cone = $u_2 - u_0$; σ_v = total overburden stress, and $q_{c\text{-}net}$ = net measured cone resistance = $q_c - \sigma_v$. Accordingly, they urged the use of excess pore pressure over the measured values.

The motivations behind their work include: (1) development of reliable cone penetration probes with the registration of pore pressure as well as cone resistance, (2) establishment of consensus that sleeve friction (f_s) measurements are less accurate and reliable than cone resistance, and (3) experience that it is possible to record pore pressures behind the tip that are less than the static equilibrium pressure (u_0) in overconsolidated and dilative soils. They presented findings from piezocone tests conducted for the characterization of gold and platinum mine tailing materials as well as natural normally consolidated materials (varying from soft, highly plastic clays to dense medium grained sands). The two curved lines in Figure A.8 present the margins within which the entire data lies, whereas the dashed lines represent the soil type envelopes.

In their later published work by Jones and Rust (1982), they claimed that normalization does not offer significant advantage over non-normalized CPT parameters, and thus presented a revised chart shown in Figure A.9, formatted as: excess shoulder pore pressure (Δu_2) as ordinate (arithmetic scale) versus net measured cone resistance ($q_{c\text{-}net} = q_c - \sigma_v$) as abscissa (arithmetic scale). In this revised chart they also demarcated zones presenting qualitative description of densities of coarse-grained soils and the consistency of fine-grained soils. Fellenius and Eslami (2000) pointed out that zones indicating soft and very soft clays together with negative pore pressures (dilatancy response) do not represent their true behavior, and accordingly, it could be a result of an attempt to bring symmetry in the chart. Vermeulen and Rust (1995) present a large number of data plotted using the chart (with slight modification of the plotting axes) (see Figure A.10).

Jones and Rust (1982) indicated that if normalized pore pressure parameter ratio is used instead of non-normalized (Δu) close to or above the water table, it becomes very large for small overburden pressure and log plots would be necessary to accommodate such values. They also indicated that log-log representation would be an improvement in demarcating the overall material boundaries.

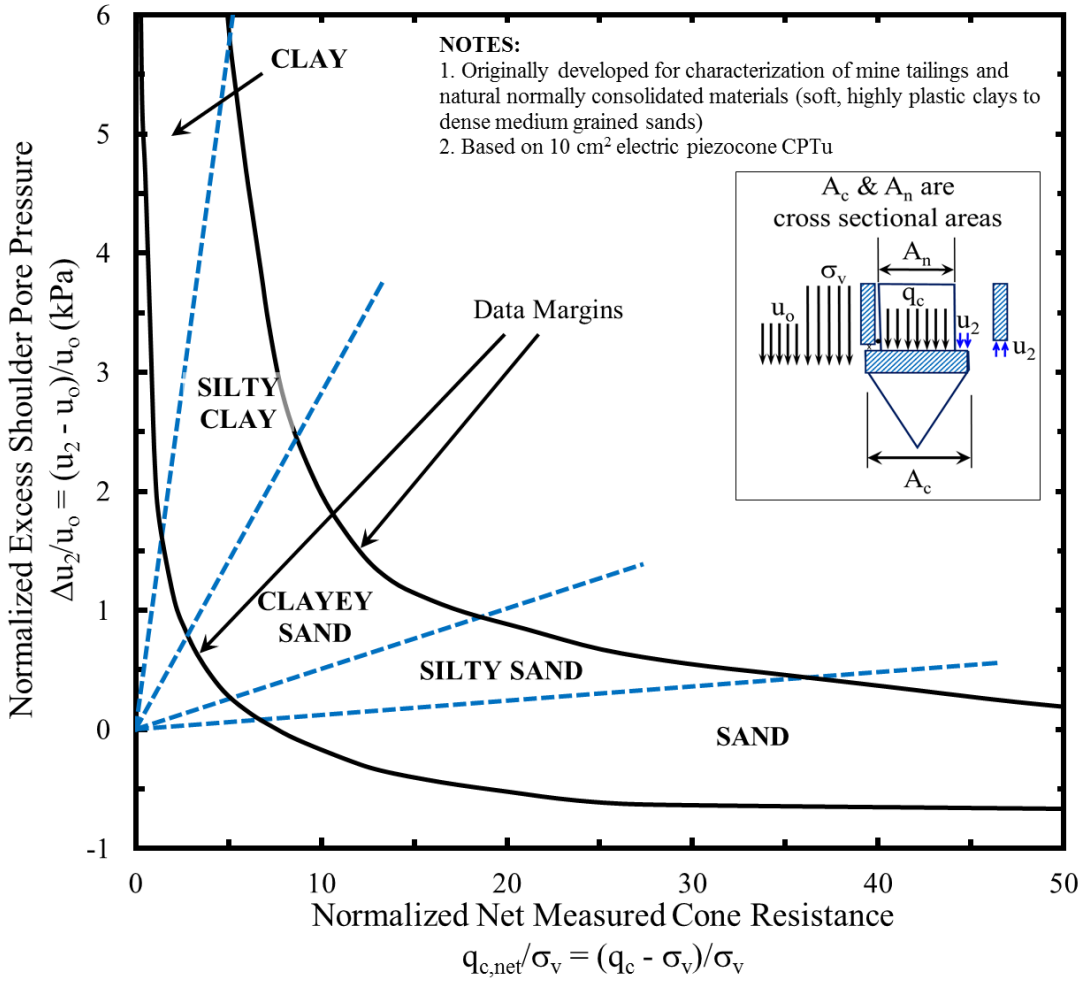

NOTES:
1. Originally developed for characterization of mine tailings and natural normally consolidated materials (soft, highly plastic clays to dense medium grained sands)
2. Based on 10 cm² electric piezocone CPTu

Figure A.8 Piezocone-based SBT chart (adapted from Jones et al., 1981).

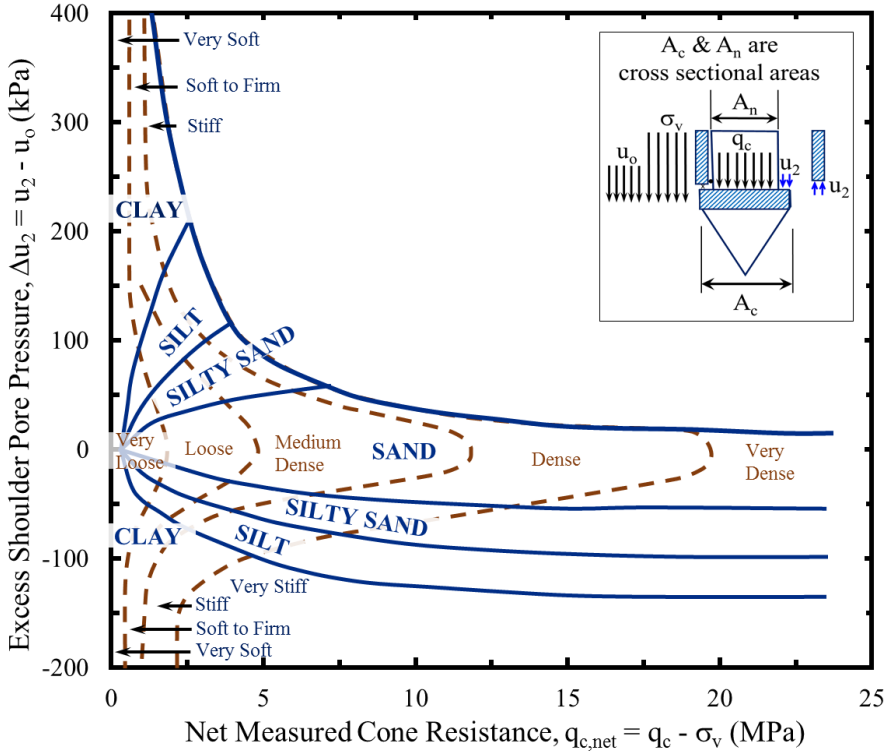

Figure A.9 Piezocone-based SBT chart by Jones and Rust (1982).

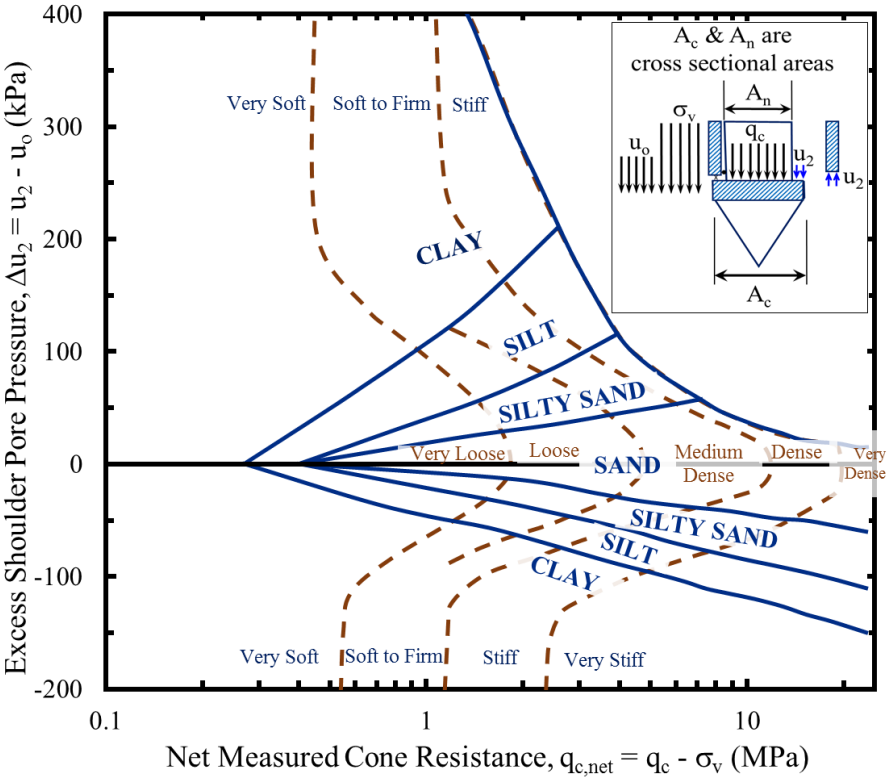

Figure A.10 Modified presentation of Jones and Rust (1982) piezocone-based SBT chart by Vermeulen and Rust (1995).

A.1.8 Vos (1982) SBT Interpretations from Friction Ratio

Vos (1982) suggested using the electric cone penetrometer for soils in the Netherlands to identify SBT from the friction ratio as shown in Table A.2 below. The percent values are similar but not consistent with those recommended by Begemann (1965) and Schmertmann (1969).

Table A.2 Friction ratio values for identification of Dutch soils (Vos, 1982)

Soil Type	Friction Ratio, FR (%) = (f_s/q_c) 100
Coarse sand and gravel	< 0.5
Fine sand	≈ 1
Silt	1.5 – 3.0
Clay	2.2 – 5.0
Peat	> 5.0

Note: Data based on electric friction cone penetrometer. Applicable to soils under the ground water table. For layers above the ground water table a higher FR is found due to desiccation.

A.1.9 Olsen (1984) Normalized SBT Chart

Olsen (1984) presented SBT classification chart also based on normalized CPT parameters. Their chart, shown in Figure A.11, was presented in reference to the analysis of liquefaction potential using the CPT. For cone resistance (q_c), Olsen (1984) used the stress normalization scheme based on effective vertical overburden stress (σ_v') that employs C_p factor originally developed based on large scale laboratory chamber tests using fine sands (Schmertmann, 1978a). The exponent technique shown in Figure A.11 and equation A.1 was developed based on various soil types ranging from fine to coarse sand, and mixed soils (e.g., Al-Awkati, 1975; Baldi et al., 1981; 1985; Villet & Mitchell, 1981). Equation A.2 shows the simpler normalization technique adopted for f_s for direct comparison to an assumed undrained strength to vertical effective stress ratio (s_u/σ_v').

$$q_{cn} = q_c\, C_p = q_c \left[\frac{1}{(\sigma_v')^n}\right] \tag{A.1}$$

$$f_{s1} = \frac{f_s}{\sigma_v'} \tag{A.2}$$

where q_{cn} = exponent based normalized cone resistance, q_c = measured cone resistance, C_p = empirical factor for converting the q_c to an equivalent value q_{cn}, σ_v' = effective overburden stress, n = cone exponential value that relates to soil behavior as related to the confining stress, f_{s1} = normalized sleeve friction (the subscript "1" represents a stress normalization exponent of 1.0), and f_s = measured sleeve friction.

The two normalization parameters, q_{cn} and f_{s1} provide assessments of soil consistency and soil sensitivity, respectively. The soil characterization lines (i.e., soil-type boundaries) for this chart originated from Douglas and Olsen (1981) and were refined based on normalized CPT data. Calculating the q_{cn} requires the exponential n value, which is estimated by associating it with the soil characterization lines shown in Figure A.11 and requires an iterative solution starting with lowest n value and repeating

calculations until the assumed n value and calculated q_{cn} matches the n and q_{cn} on a constant f_{s1} line.

A narrow band of normally consolidated non-sensitive packed soil of uniform grain size is based on CPT from sites with known stress/strength conditions. Overconsolidation causes an increase in q_{cn} and f_{s1} at a slope away from a point on this band, whereas, increasing sensitivity falls to the left of this band at a shallow slope as shown.

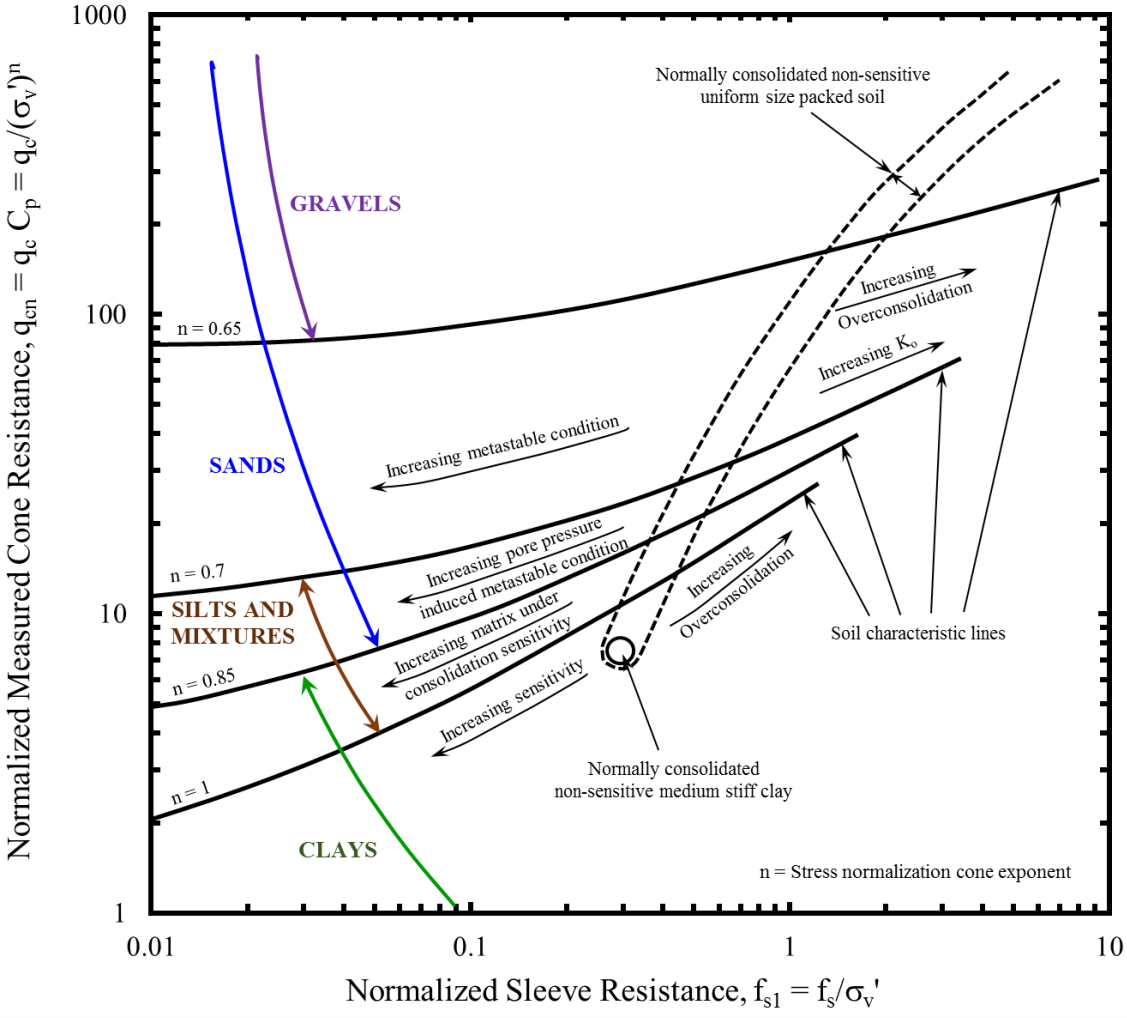

NOTES:
1. Originally developed for liquefaction potential assessment
2. Based on electric friction CPT
3. C_p factor and exponent n values determined based on large scale laboratory chamber tests on fine to coarse sands, and mixed soils
4. n requires an iterative solution starting with lowest n value and repeating calculations until the assumed n value and calculated q_{cn} matches the n and q_{cn} on a constant f_{s1} line

Figure A.11. Normalized SBT chart (adapted from Olsen, 1984; Olsen & Farr, 1986).

A.1.10 Senneset and Janbu (1985); Senneset et al. (1989) SBT Classification for Marine Soils

Senneset and Janbu (1985) presented their tentative SBT classification scheme in tabulated as well as graphical forms from piezocone data in marine sediments and founded it on theoretical solutions. Their classification shown in Table A.3 is based on normalized (dimensionless) shear strength parameters of cone resistance number (N_m) and the pore pressure parameter ratio (B_q) defined as follows:

$$N_m = \frac{q_{t,net}}{(\sigma_v' + a)} = \frac{(q_t - \sigma_v)}{(\sigma_v' + a)} \tag{A.3}$$

$$B_q = \frac{\Delta u_2}{q_{t,net}} = \frac{(u_2 - u_o)}{(q_t - \sigma_v)} \tag{A.4}$$

where, q_t = corrected total cone resistance (as defined in Chapter 1), $q_{t,net}$ = net corrected total cone resistance, a = in-situ attraction, σ_v = total overburden stress = $\gamma_m z$, γ_m = total unit weight of soil, z = depth, σ_v' = effective overburden stress = $\sigma_v - u_0$, Δu_2 = excess pore pressure measured at the shoulder position behind the cone tip, u_0 = equilibrium static pore pressure, u_2 = pore pressure measured at the shoulder position behind the cone tip (also see Figure A.12 for further description of the terms). Accordingly, additional information on the unit weight and the ground water table are required. The attraction a value may be determined from the theoretical principle illustrated in Figure A.12 by plotting $q_{t,net}$ versus σ_v' and seeking the negative intercept on σ_v' axis or chosen on the basis of information on soil type and conditions. Accordingly, they were the first to present a SBT classification based on the piezocone with cone resistance corrected for pore pressure at the shoulder.

The graphical presentation of the SBT classification by Senneset and Janbu (1985) is shown in Figure A.13(a). They are among the pioneers in the use of corrected total cone resistance (q_t) which is plotted as ordinate (arithmetic scale) against pore pressure parameter ratio (B_q) as abscissa (arithmetic scale). As evident, the chart is limited to q_t < 16 MPa. Senneset et al. (1989) presented a modified version of this chart with additional discretization of SBT (see Figure A.13(b)). They also accounted for the dilative response of hard stiff overconsolidated soil and dense cemented sands where negative pore pressures can develop during penetration of piezocone probe. Besides the soil types, this chart also identifies limits of density and consistency: dense, stiff, soft etc. Fellenius and Eslami (2000) indicated that these limits were lower than those applied in North American practice.

Table A.3 Soil type indicated by N_m and B_q
(after Senneset & Janbu, 1985; Senneset et al., 1989)

	Shear Strength Parameters		
Possible Type of Soil	a	N_m	B_q
Soft clay, mud	5–10	1–3	0.8–1.0
Medium clay	10–20	3–5	0.6–0.8
Stiff clay, silty	20–50	5–8	0.3–0.6
Silt, soft	0–5	–	–
Silt, medium	5–15	–	–
Silt, stiff	15–30	5–30	0–0.4
Sand, loose	0	–	–
Sand, medium	10–20	–	–
Sand, dense	20–50	30–100	<0.1
Hard, stiff soil; overconsolidated; cemented	>50	100	≈0

Note: a = in-situ attraction; $N_m = q_{t,net}/(\sigma_v' + a) = (q_t - \sigma_v)/(\sigma_v' + a)$; $B_q = \Delta u_2/q_{t\text{-}net} = (u_2 - u_0)/(q_t - \sigma_v)$; σ_v = total vertical overburden stress; σ_v' = effective vertical overburden stress; u_2 = shoulder pore pressure; u_0 = hydrostatic pore pressure; q_t = corrected total cone resistance = $q_c + u_2 (1 - a_n)$; a_n = net area ratio = A_n/A_c (see Figure A.12); q_c = measured cone resistance.

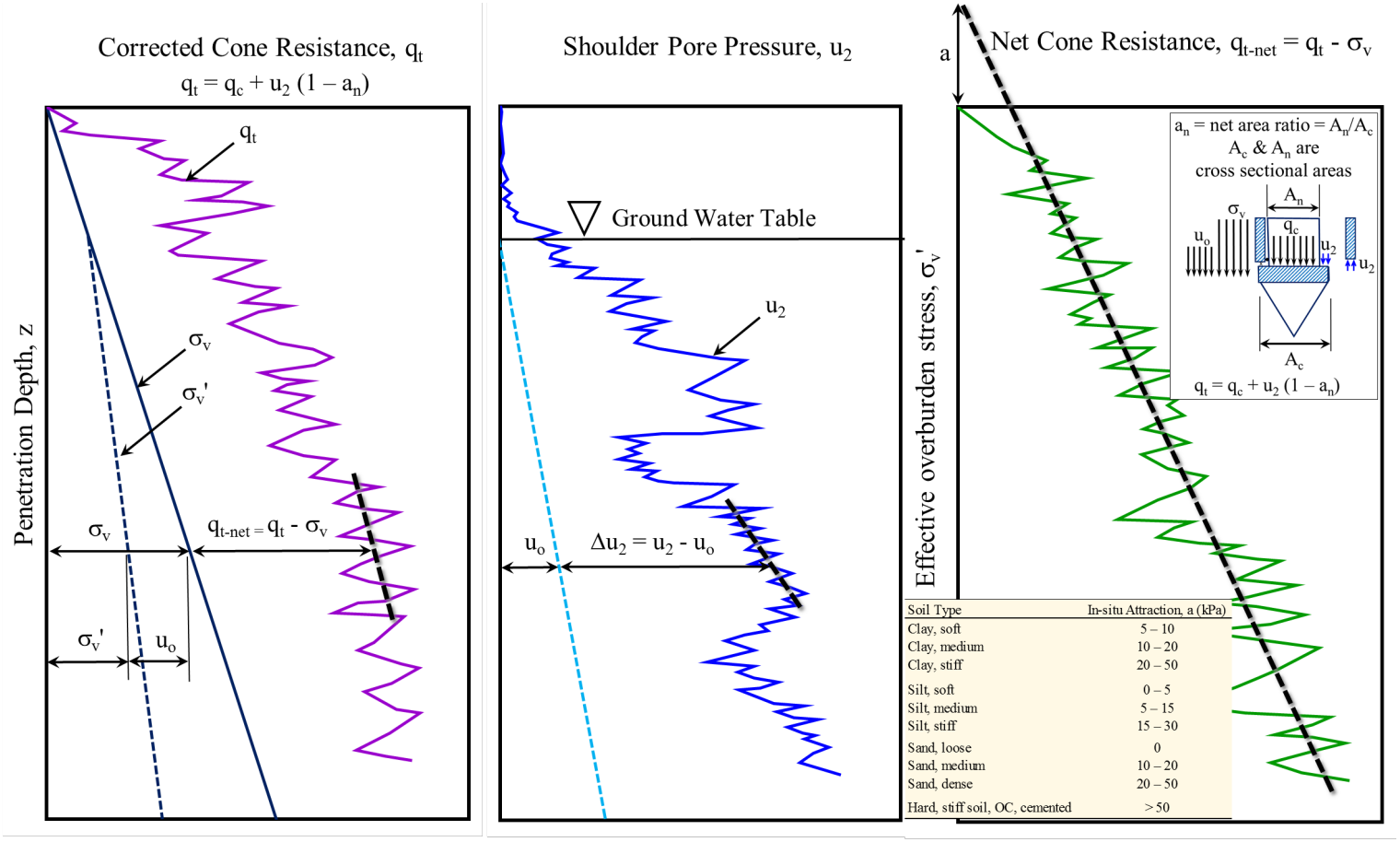

Soil Type	In-situ Attraction, a (kPa)
Clay, soft	5 – 10
Clay, medium	10 – 20
Clay, stiff	20 – 50
Silt, soft	0 – 5
Silt, medium	5 – 15
Silt, stiff	15 – 30
Sand, loose	0
Sand, medium	10 – 20
Sand, dense	20 – 50
Hard, stiff soil, OC, cemented	> 50

NOTES:
q_c = uncorrected measured cone resistance; q_t = corrected total cone resistance; q_{t-net} = net corrected total cone resistance; u_2 = shoulder pore pressure measured behind the cone; u_o = equilibrium static pore pressure; Δu_2 = excess pore pressure measured behind the cone; σ_v = total overburden stress = $\gamma_t z$; γ_t = total unit weight of soil; z = depth; σ_v' = effective overburden stress = $\sigma_v - u_o$; a = in-situ attraction.

Figure A.12 Key sketches showing CPT measurements and notations
(adapted from Senneset & Janbu, 1985).

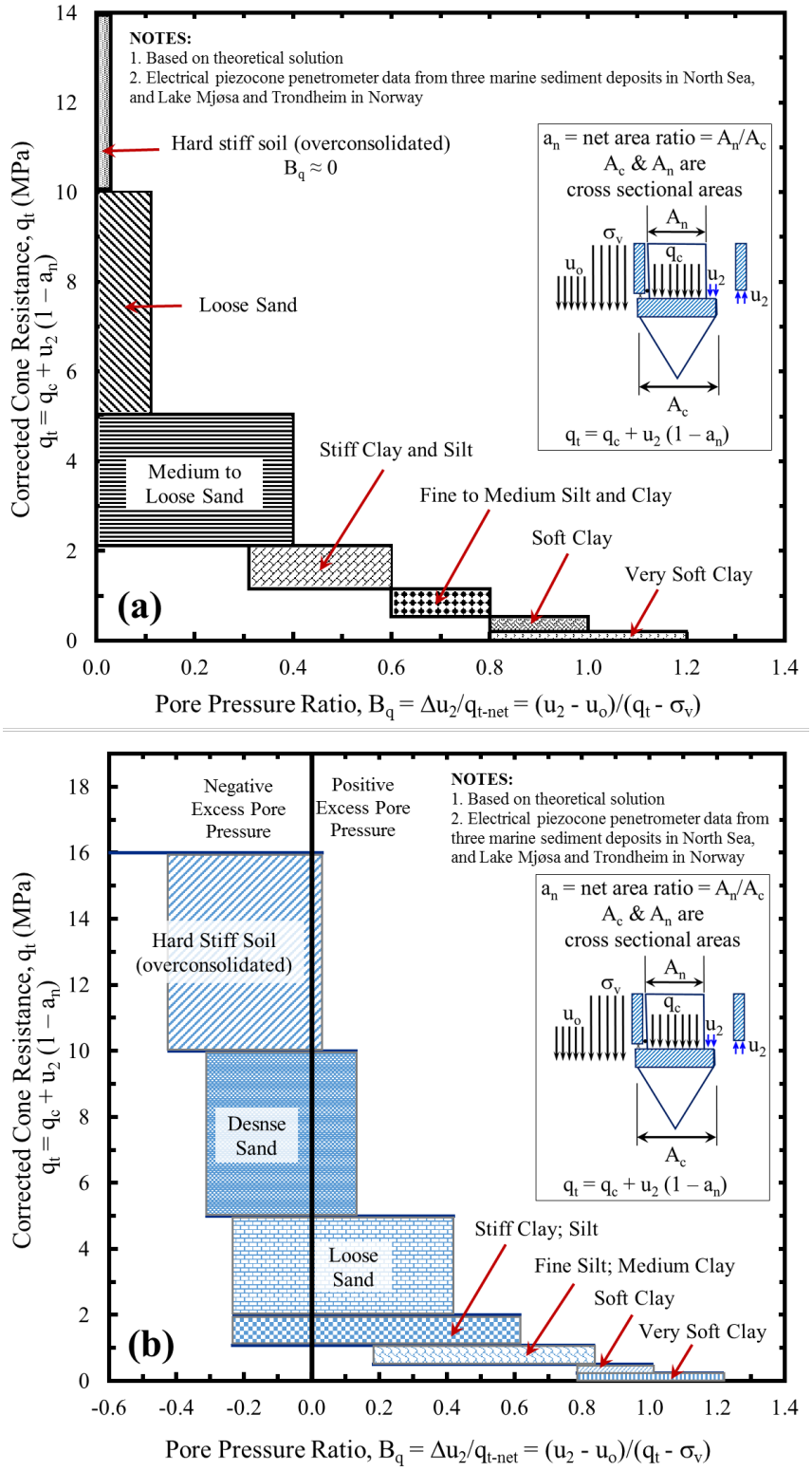

Figure A.13 (a) Preliminary SBT chart based on corrected total cone resistance and pore pressure parameter (adapted from Senneset & Janbu, 1985); (b) modified SBT chart (adapted from Senneset et al., 1989).

A.1.11 Tumay (1985) SBT Chart

Figure A.14 shows the SBT chart proposed by Tumay (1985). It can be seen that they used the same format as Douglas and Olsen (1981) and Schmertmann (1978a). This chart is based on data of approximately 5,000 m soundings from twelve sites in Louisiana, and the earlier data from Douglas and Olsen (1981) and Schmertmann (1978a). A wide variety of electric penetrometers were employed at these sites including different apex angles, cross-sectional areas, and cone types. The type of cones includes friction cones ($q_c + f_s$) with different friction sleeve areas, first- and second-generation piezocones ($q_c + u$) with piezometric element placed on collar (u_2) and cone tip (u_1), respectively, and newer piezocone with friction sleeve ($q_c + fs + u_1$). This chart depicts four distinct regions similar to those identified by Douglas and Olsen (1981). Additionally, each region is further divided into sub-regions sorted out using the Schmertmann (1978a) classification chart and adjusted to reflect experience in Louisiana geology. This chart also identifies limits of density and consistency.

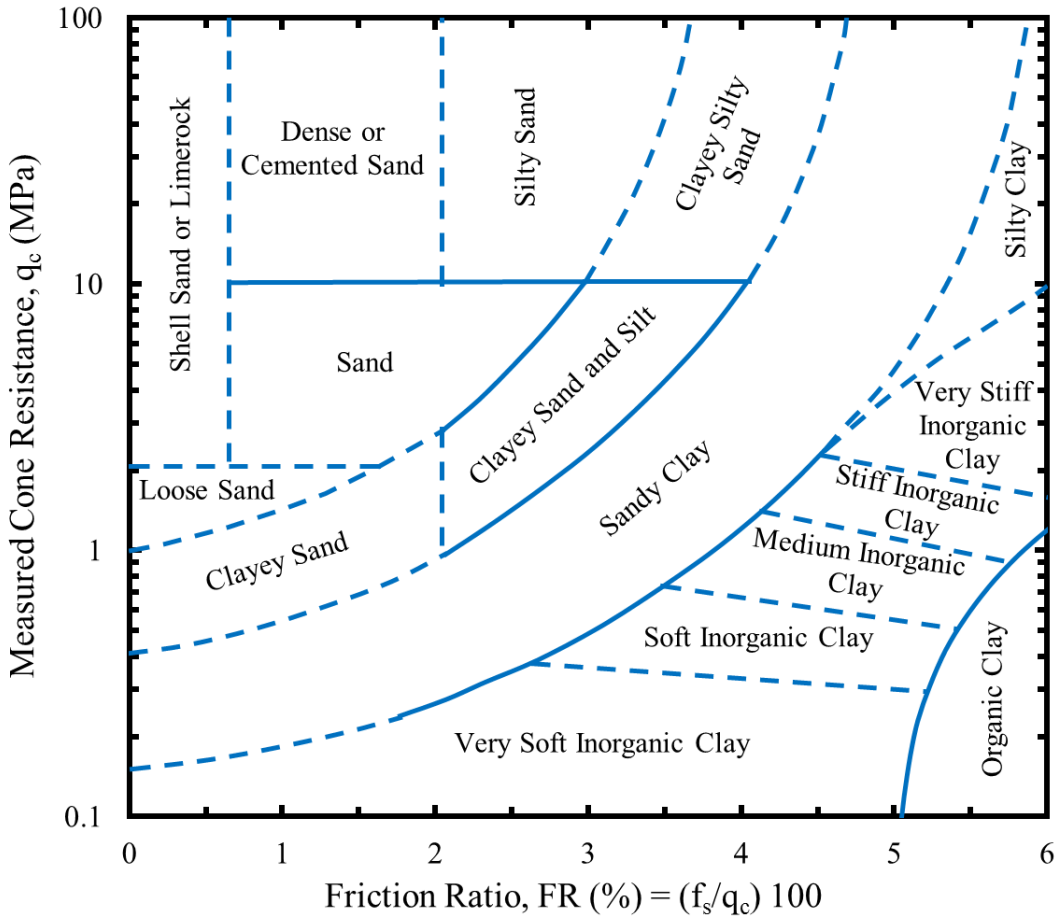

NOTES:
1. Based on wide variety of electric cone penetrometers including different apex angles, cross-sectional areas, and cone types ($q_c + f_s$, $q_c + u_1$, $q_c + u_2$, $q_c + f_s + u_1$)
2. Data of approximately 5000 m soundings from twelve sites in Louisiana, USA. Additional data from the earlier studies by Douglas and Olsen (1981) and Schmertmann (1978) includingn sites in California, Oklahoma, Utah, Arizona, and Nevada in the USA

Figure A.14 Tumay (1985) SBT classification chart.

A.1.12 Douglas and Olsen (1981) SBT Chart Update by Olsen and Farr (1986)

Olsen and Farr (1986) presented a modified version of the Douglas and Olsen (1981) SBT chart, plotted on cone resistant (q_c) on logarithmic scale versus friction ratio on arithmetic scale. The new SBT chart can be seen in Figure A.15. The main changes introduced include: (1) demarcation of the newer boundaries between actual soil types (gravel, sand, silt, clay, peat, and mixtures) instead of the original cohesive versus non-cohesive and coarse-grained versus fine-grained classification, (2) removal of the USCS classification from the chart, (3) inclusion of the information relating to the state of consolidation and sensitivity for the relevant soil zones.

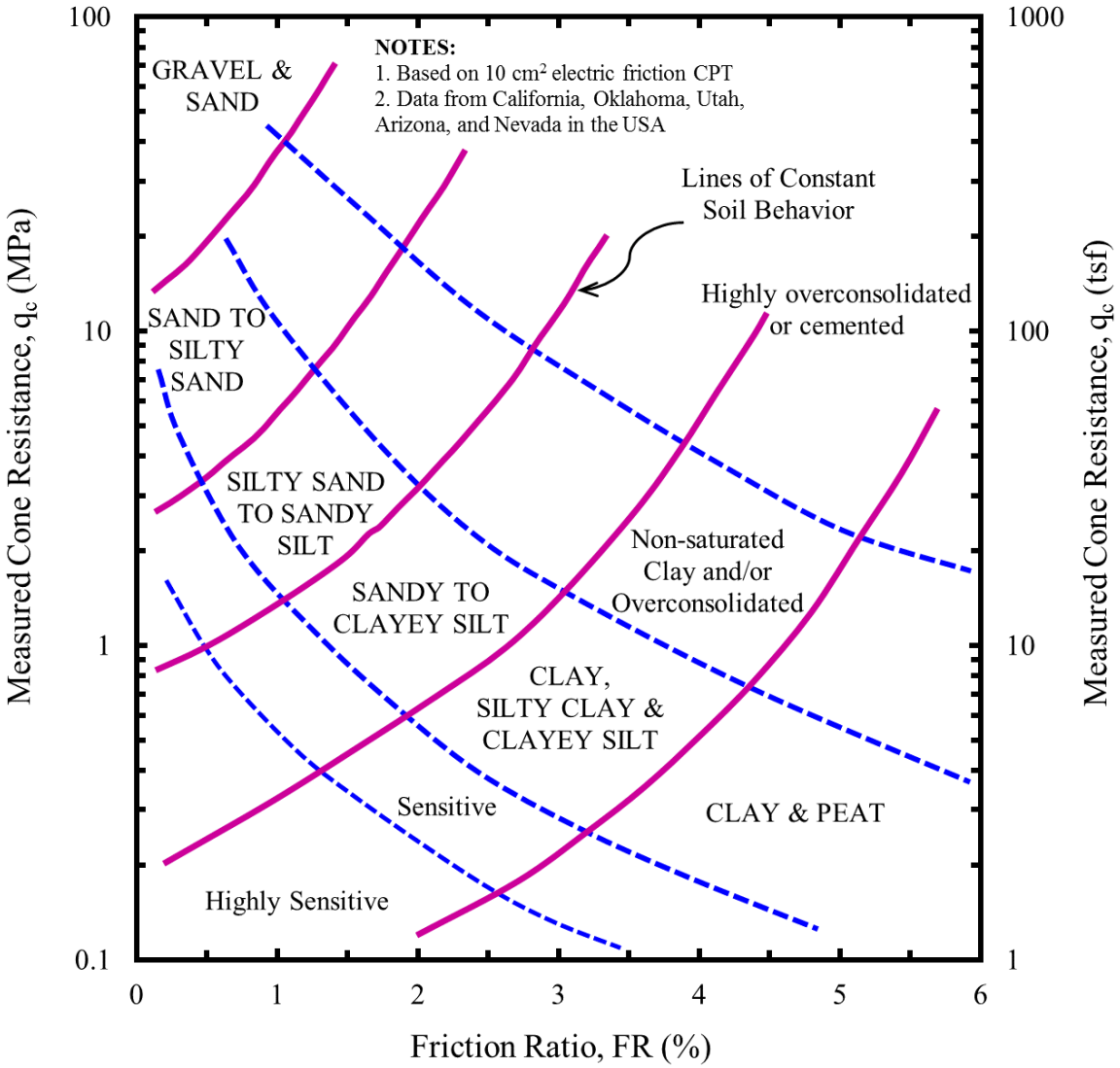

Figure A.15. SBT chart adapted from Olsen and Farr (1986)

A.1.13 Robertson et al. (1986) SBT Schemes

Figure A.16 (a) and (b) show the two SBT charts proposed by Robertson et al. (1986) with 12 soil behavior types each (indicated by zone numbers from 1 to 12). These charts are based on variety of electric friction piezocone penetrometers developed by Fugro, Hogentogler, Geotech, and the University of British Columbia (UBC) with pore pressure measurements at different locations (u_1; u_2; $u_1 + u_2$; $u_1 + u_2 + u_3$). The soundings data consist of sites mainly near Vancouver, British Columbia, Canada and few others throughout the world.

As evident from Figure A.16, Robertson et al. (1986) used all three pieces of data (q_t, u_2, and f_s) to define SBT, and classified these charts as their first attempted. They recommended use of both the charts to validate SBT classification. In case of discrepancy, they also recommended final determination of SBT via dissipation tests. Interestingly, these charts show few unique features, such as, increasing relative density

(D_R), stress history (OCR), void ratio (e), and sensitivity (S_t), delineation of intermediate soil zones (mixed soils), and extreme soil responses (very stiff clays, heavily overconsolidated and cemented sands and clayey sands, sensitive clays). The B_q chart also indicates zones where u_2 pore pressures becomes negative during CPTu soundings (e.g., very stiff overconsolidated fissured clays and very dense cemented sands).

Since these charts were developed from CPTu soundings shallower than 30 m, Robertson et al. (1986) indicated possibility of error in SBT classification in deeper soil layers. They referred to the earlier work by Robertson and Campanella (1985), Olsen (1984), and Baldi et al. (1985) to account for such tendencies via stress normalization using effective overburden stress (σ_v'). Accordingly, they pointed to the benefits of adopting a formal normalization scheme for all three parameters, and until then, recommended interim caution as indicated in the appended notes of Figure A.16.

Fellenius and Eslami pointed out that the formulation of this q_t versus B_q chart is also flawed since B_q is an inverse function of q_t (in conflict with the general principles of data presentation).

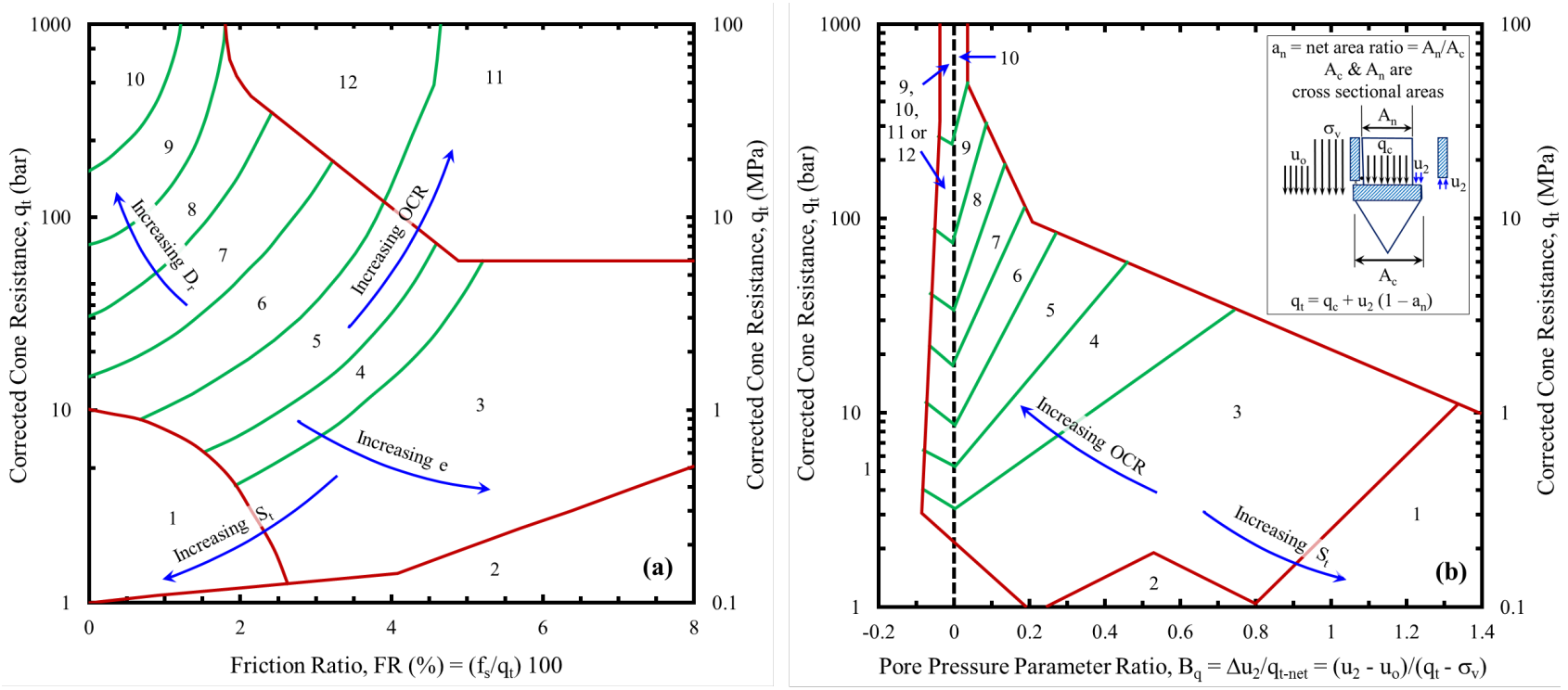

Soil Behavior Type Zones

1: Sensitive fine grained	4: Silty clay to clay	7: Silty sand to sandy silt	10: Gravelly sand to sand
2: Organic material	5: Clayey silt to silty clay	8: Sand to silty sand	11: Very stiff fine grained*
3: Clay	6: Sandy silt to clayey silt	9: Sand	12: Sand to clayey sand*

*Overconsolidated of cemented

NOTES:

1. Based on wide variety of electric friction piezocone penetrometers including Fugro, Hogentogler, Geotech and the University of British Columbia (UBC) developed, and pore pressure measurements at different locations (u_1; u_2; $u_1 + u_2$; $u_1 + u_2 + u_3$)
2. Data of soundings from sites mainly near Vancouver, British Columbia, Canada and few others throughout the world
3. Charts best applicable for depth (z) shallower than 30 m; for z > 30 m, use normalize cone resistance q_{t1}: $q_t/(\sigma_v')^{0.7}$

Figure A.16 SBT classification chart based on q_t, f_s, and u_2 (adapted from Robertson et al., 1986).

A.1.14 Olsen and Malone (1988) SBT Scheme

Olsen and Malone (1988) also presented a CPT SBT chart using stress normalized parameters of q_{cn} and FR_n, both plotted on logarithmic scales (see Figure A.17). Their cone resistance normalization is similar to the one used in Olsen (1984) chart, except that their soil characteristic lines (or contours) were drawn slightly displaced along with different cone stress exponent n values to distinguish soil types. They assigned CPT soil characterization number (SCN) to each contour. They also presented improved assessment of overconsolidation ratio, soil sensitivity ratio and relationship of SBT classification with the traditional textural based USCS.

Olsen and Malone (1988) also conjectured out that in-situ vertical and horizontal effective stresses affect the q_c and f_s measurements differently in that FR is only useable for normally consolidated, relatively non-sensitive soils near a σ_v' of 1 tsf. Therefore, they recommended a modified normalized friction ratio, $FR_n = (f_{s1}/q_{cn})100 = \{(f_s/\sigma_v')/[q_c/(\sigma_v')^n]\}100 = \{f_s/[q_c\ (\sigma_v')^{(1-n)}]\}100$. Like in Olsen (1984), determination of q_{cn}, FR_n and SBT with this chart is an iterative process. The lowest starting cone exponent n value recommended by Olsen and Malone (1988) for this iterative process is 0.6. Typically, less than 5 iterations converge the assumed and calculated values to within 0.02.

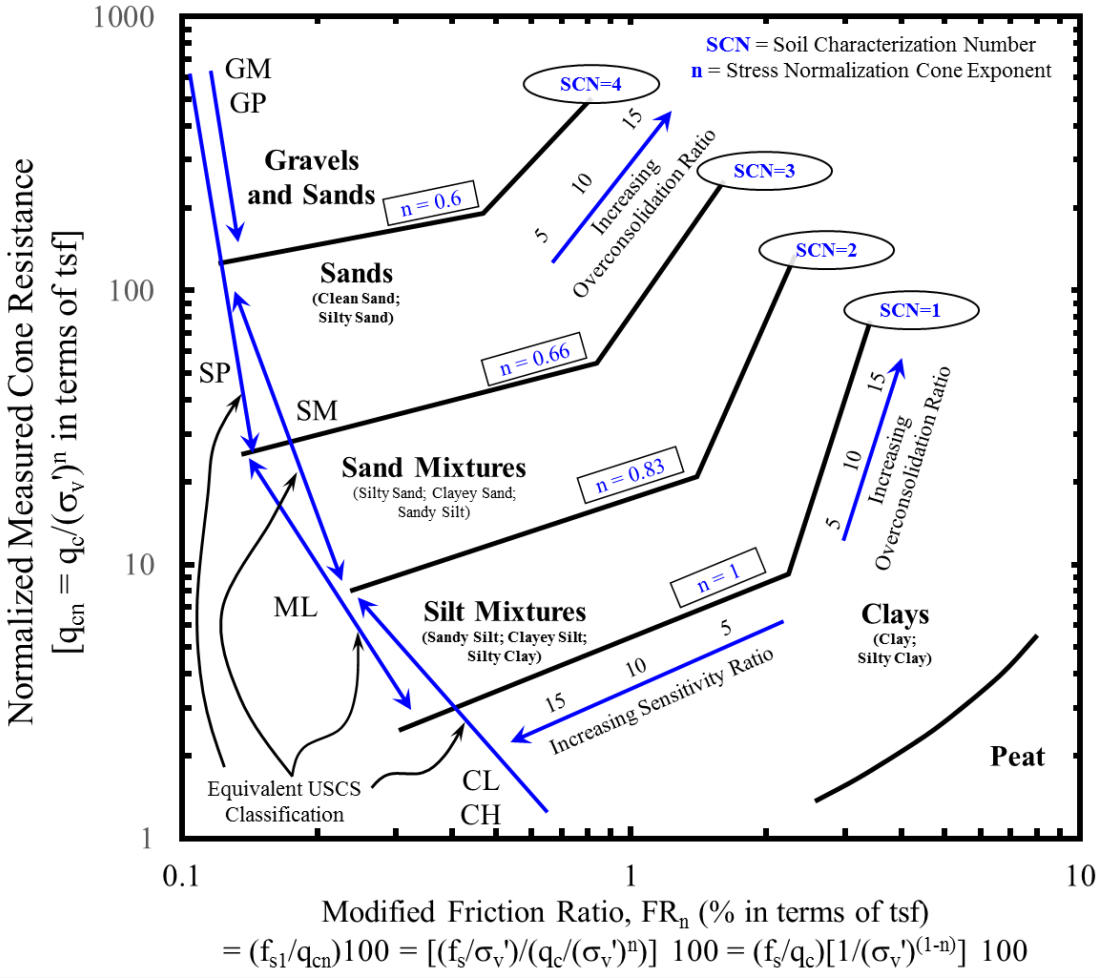

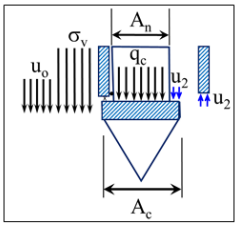

NOTES:

1. Based on electric friction CPT data from Douglas and Olsen (1981), Olsen (1984), Schmertmann (1978)
2. Exponent n values determined based on large scale laboratory chamber tests on fine to coarse sands, and mixed soils
3. n requires an iterative solution starting with lowest n value of 0.6, and repeating the calculations until the assumed n value and calculated q_{cn} matches the n and q_{cn} on a constant FR_n line.

Figure A.17 SBT chart based on dimensionless parameters (after Olsen & Malone, 1988).

A.1.15 Robertson (1990), Jefferies and Davies (1991) and Robertson (1991) Normalized SBT Charts

For improvement of his earlier SBT charts (e.g., Robertson et al., 1986; Robertson, 1990) presented the newer SBT classification scheme based on normalized piezocone parameters on log-log scales shown in Figure A.18. He adopted the normalization suggested by Wroth (1984) and Houlsby (1988) as below:

$$Q_t = \frac{q_{t,net}}{\sigma_{v'}} = \frac{(q_t - \sigma_v)}{\sigma_{v'}} \quad \text{(A.5)}$$

$$F_R = \frac{f_s}{q_{t,net}} = \frac{f_s}{(q_t - \sigma_v)} \quad \text{(A.6)}$$

$$B_q = \frac{\Delta u_2}{q_{t,net}} = \frac{(u_2 - u_o)}{(q_t - \sigma_v)} \quad \text{(A.7)}$$

where, $q_{t,net}$ = net corrected total cone resistance, q_t = corrected total cone resistance (also defined in Chapter 1), σ_v = total overburden stress = $\gamma_m z$, γ_m = total unit weight of soil, z = depth, σ_v' = effective overburden stress = $\sigma_v - u_0$, u_0 = equilibrium static pore pressure, f_s = sleeve resistance, Δu_2 = excess pore pressure measured at the shoulder position behind the cone tip, u_2 = pore pressure measured at the shoulder position behind the cone tip.

Besides normalization, the SBT zones and their boundaries were slightly adjusted. Like Olsen and Malone (1988) and Senneset at el. (1989) SBT classification schemes, Robertson (1990) charts require additional information of the soil unit weight (γ_m) and the ground water elevation. Robertson (2010a) mentioned that there is typically little difference between the SBT resulting from Robertson et al. (1986) non-normalized charts and Robertson (1990) normalized charts if the in situ vertical effective stress (σ_v') is between 50 kPa and 150 kPa. Also included in this three-dimensional classification system is a zone that represents approximately normally consolidated soil behavior. A guide is also provided to indicate the variation of normalized CPT and CPTu data for changes in: (1) overconsolidation ratio (*OCR*), age, and sensitivity (S_t) for fine-grained soils, where cone penetration is essentially undrained, and (2) OCR, age, cementation, and friction angle (ϕ') for cohesionless soils, where cone penetration is generally drained. Like for the earlier three-dimensional classification scheme (e.g., Robertson et al., 1986; Robertson, 1990) recommended the use of both charts, together with close observation of the excess pore pressure dissipation trends during a pause in penetration as an aid in classification.

Fellenius and Eslami (2000) pointed out that at very shallow depths, the proposed normalization tends to classify a soil coarser than is necessarily the case. They also indicated that normalization becomes cumbersome for stratified soils with alternating layers of stark contrast in densities (low to high).

Jefferies and Davies (1991) noted that the proposed Q_t-F_R chart correctly identifies offshore soils; however, the Q_t-B_q chart is a poor fit to such data. They presented examples from two offshore sites in Canadian Beaufort Shelf which exhibit behavior of stiffer silty clay sediments characterized by dilatant response (generating high negative excess pore pressures). To accommodate the behavior of such soils, Jefferies and Davies (1991) followed the recommendation of Houlsby (1988) and Been et al. (1988) and proposed a modified classification chart that incorporates the pore pressure parameter directly into a grouped parameter [$Q_t (1 - B_q)$], as shown in Figure A.19. The intended effect of incorporating pore pressure data from the CPTu was to expand the interpretation range in finer soil while leaving the interpretation in sand unchanged.

Robertson (1991) pointed out that the accuracy of the Q_t $(1 - B_q)$ versus F_R chart could be a problem in soft sensitive clays where B_q can be greater than 1.0. He also presented improvement to his Q_t versus B_q chart as shown in Figure A.20.

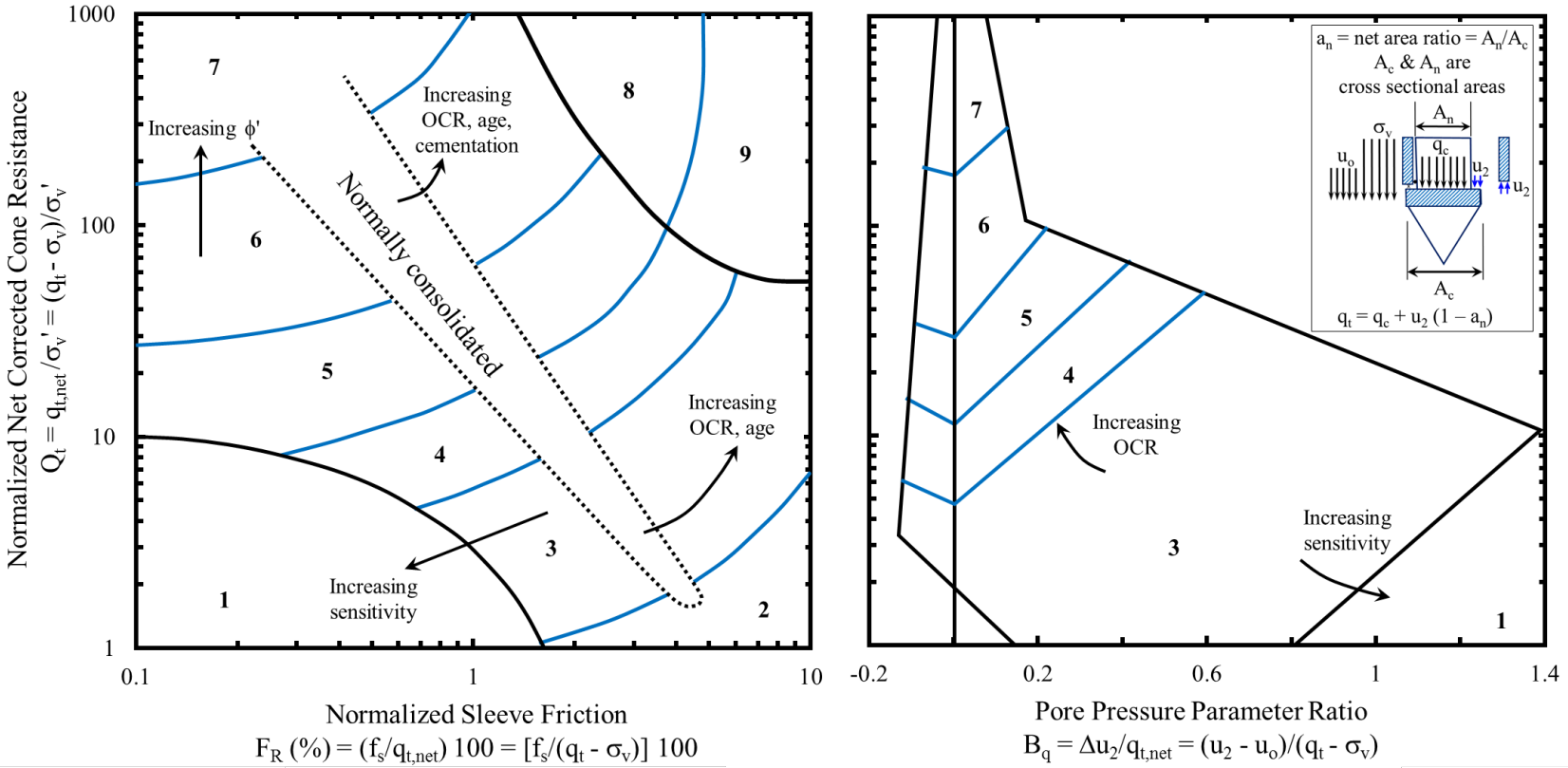

Soil Behavior Type Zones

1: Sensitive fine grained	4: Silt mixtures: clayey silt to sitly clay	7: Gravelly sand to sand
2: Organic material	5: Sand mixtures: silty sand to sandy silt	8: Very stiff sand to clayey sand*
3: Clays: clay to silty clay	6: Sands: clean sand to silty sand	9: Vey stiff fine grained*

*Overconsolidated of cemented

NOTES:

1. Based on wide variety of electric friction piezocone penetrometers including Fugro, Hogentogler, Geotech and the University of British Columbia (UBC) developed, and pore pressure measurements at different locations (u_1; u_2; $u_1 + u_2$; $u_1 + u_2 + u_3$)
2. Data of CPTu soundings across the world (mostly from onshore sites < 30 m deep)

Figure A.18 SBT classification chart based on normalized CPTu parameters (adapted from Robertson, 1990).

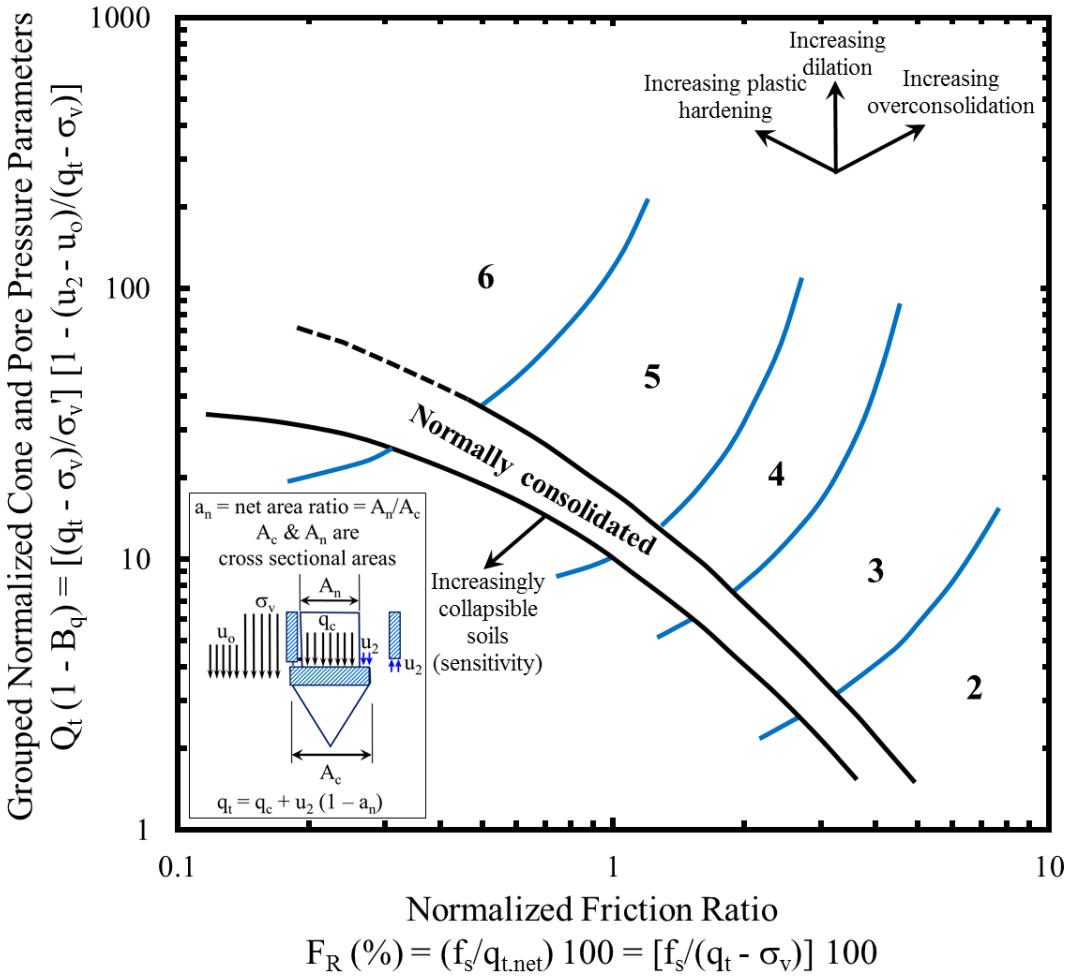

Soil Behavior Type Zones

2: Organic material
3: Clays: clay to silty clay
4: Silt mixtures: clayey silt to sitly clay
5: Sand mixtures: silty sand to sandy silt
6: Sands: clean sand to silty sand

NOTES:

1. This is an enhancement of Robertson (1990) SBT classification chart to accomodate soils that exhibit highly dilatant response of high negative excess pore pressures to CPTu penetration
2. New data includes offsore sites in Canadian Beaufort Shelf consisting of very stiffer silty clay sediments

Figure A.19 SBT classification chart based on normalized CPTu parameters (adapted from Jefferies & Davies, 1991).

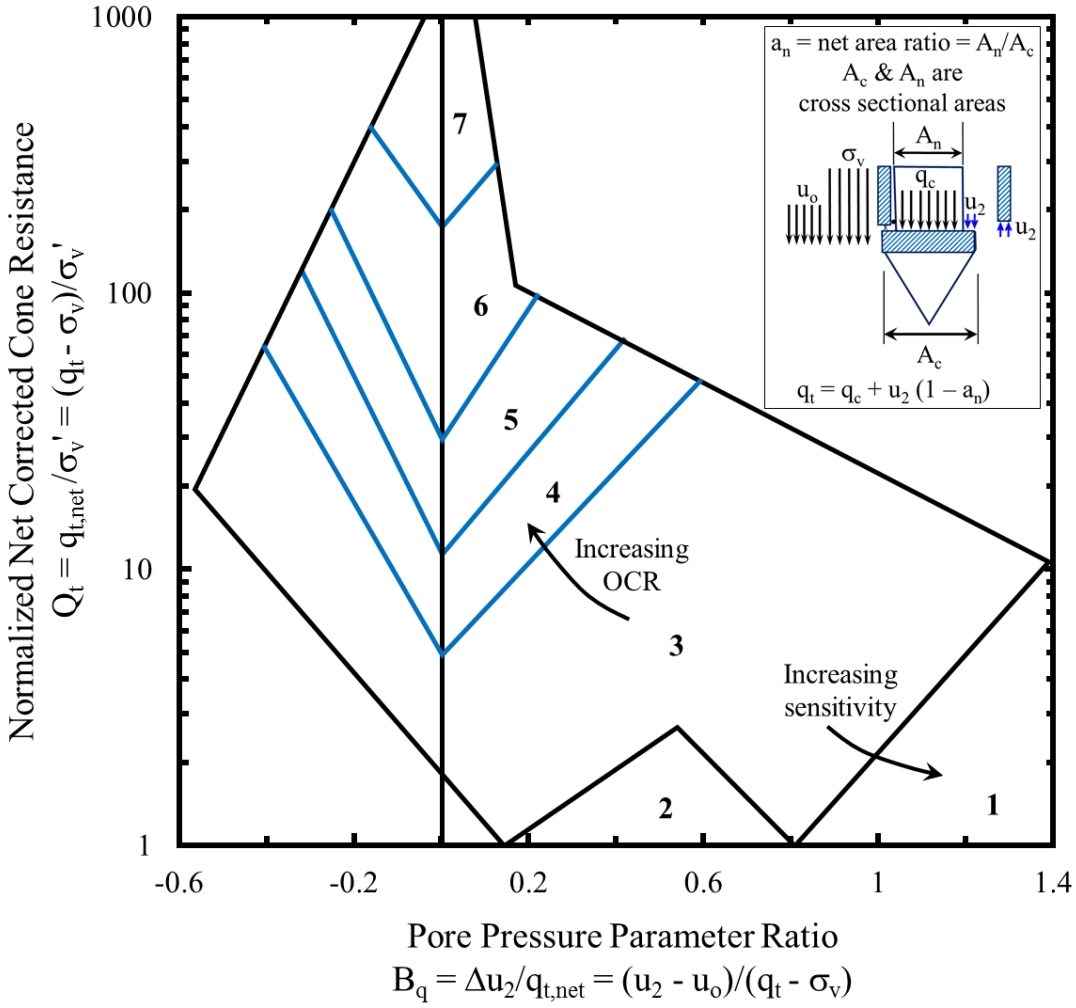

Soil Behavior Type Zones

1: Sensitive fine grained	5: Sand mixtures: silty sand to sandy silt
2: Organic material	6: Sands: clean sand to silty sand
3: Clays: clay to silty clay	7: Gravelly sand to sand
4: Silt mixtures: clayey silt to sitly clay	

NOTES:

1. Based on wide variety of electric friction piezocone penetrometers including Fugro, Hogentogler, Geotech and the University of British Columbia (UBC) developed, and pore pressure measurements at different locations (u_1; u_2; $u_1 + u_2$; $u_1 + u_2 + u_3$)
2. Data of CPTu soundings across the world (onshore and offshore sites)

Figure A.20 SBT classification chart based on normalized CPTu parameters (adapted from Robertson, 1991).

A.1.16 Larsson and Mulabdic (1991) Chart

Based on their own tests in Swedish clays as well as Norway and the UK, Larsson and Mulabdic (1991) proposed a chart shown in Figure A.21. Although this chart was basically developed for obtaining a rough estimate of soil density for clays, it also presents SBT boundaries based on net corrected total cone resistance ($q_{t,net}$) versus pore pressure parameter ratio (B_q). Since soil unit weight is needed to compute both $q_{t,net}$ as well as B_q, it requires an iterative process to converge the solution.

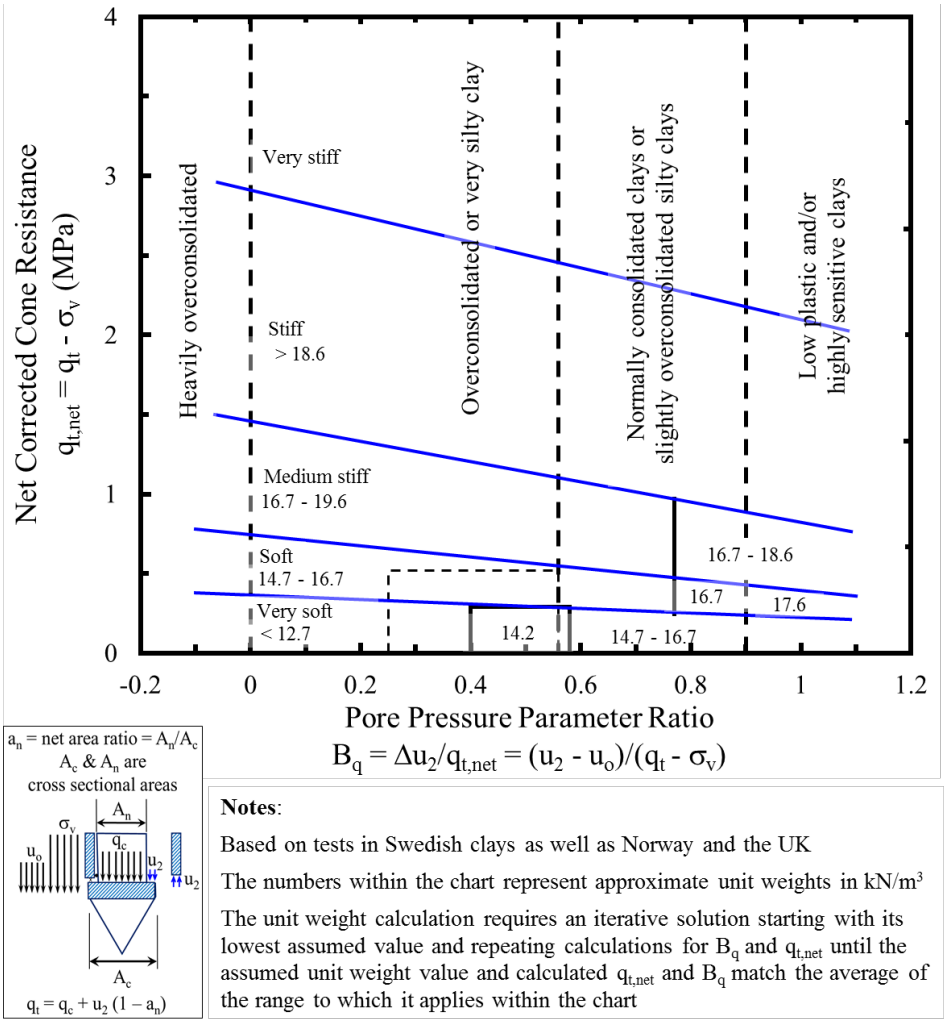

Figure A.21 SBT chart (adapted from Larsson & Mulabdic, 1991).

A.1.17 Jefferies and Davies (1993) SBT Classification Index [$I_{c(J\&D93)}$]

In reference to the envelopes of the soil types within different SBT charts, Jefferies and Davies (1993) noted that soil has no cognizance of the classification boundaries, and therefore, a continuum approach of fitting an equation to the trend is desirable. They further noted that the boundaries between soil behavior type zones, such as Jefferies and Davies (1991) can be approximated as concentric circles, if the vertical and horizontal scales are distorted by using differing length scales. Within this approximation, soil type

can be indicated by circle radius, and the radius may be used as a soil behavior type index. Accordingly, they proposed the following equation, thus, pioneering the soil behavior type classification index [$I_{c(J\&D93)}$] from the normalized piezocone parameters Q_t, F_R and B_q:

$$I_{c(J\&D93)} = \sqrt{\{3 - log[Q_t(1 - B_q)]\}^2 + [1.5 + 1.3(LogF_R)]^2} \quad \text{(A.8)}$$

where, Q_t, F_R and B_q are the same as defined earlier, and the subscript *J&D93* indicates classification index by Jefferies and Davies (1993). The logarithms used are base 10. Within this classification of piezocone data, soil SBTs are attributed from $I_{c(J\&D93)}$ as summarized in Table A.4 and Figure A.22. The boundaries shown nearly match with those shown by Jefferies and Davies (1991) in Figure A.19.

Table A.4 Soil Behavior Type from Classification Index $I_{c(J\&D93)}$ (after Jefferies & Davies, 1993).

Possible Type of Soil	Zone	CPTu Index, $I_{c(J\&D93)}$
Gravelly sands	7	$I_{c(J\&D93)} < 1.25$
Sands: clean sand to silty sand	6	$1.25 < I_{c(J\&D93)} < 1.90$
Sand mixtures: silty sand to sandy silt	5	$1.90 < I_{c(J\&D93)} < 2.54$
Silt mixtures: clayey silt to silty clay	4	$2.54 < I_{c(J\&D93)} < 2.82$
Clays	3	$2.82 < I_{c(J\&D93)} < 3.22$
Organic soils	2	$I_{c(J\&D93)} > 3.22$

Note: $I_{c(J\&D93)} = \sqrt{\{3 - log[Q_t(1 - B_q)]\}^2 + [1.5 + 1.3(LogF_R)]^2}$; $Q_t = (q_t - \sigma_v)/\sigma_v'$; $F_R = f_s/q_{t\text{-}net} = f_s/(q_t - \sigma_v)$; $B_q = \Delta u_2/q_{t\text{-}net} = (u_2 - u_0)/(q_t - \sigma_v)$; $q_t = q_c + u_2\,(1 - a_n)$; σ_v = total vertical overburden stress; σ_v' = effective vertical overburden stress = $\sigma_v - u_0$; u_2 = total shoulder pore pressure measured during piezocone penetration; u_0 = hydrostatic pore pressure, Δu_2 = excess shoulder pore pressure = $u_2 - u_0$.

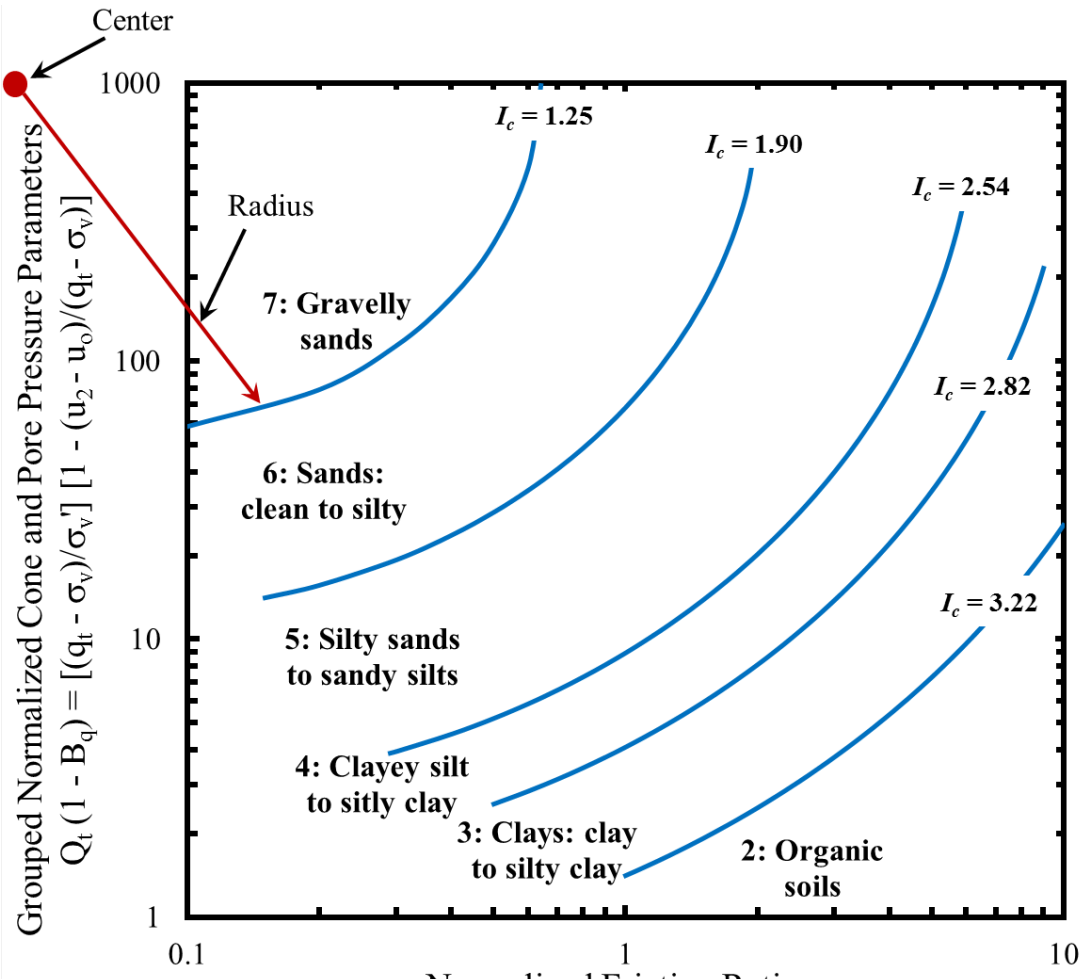

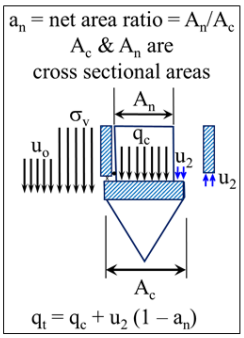

Possible Type of Soil	Zone	CPTu Index, $I_{c(J\&D93)}$
Gravelly sands	7	$I_{c(J\&D93)} < 1.25$
Sands: clean sand to silty sand	6	$1.25 < I_{c(J\&D93)} < 1.90$
Sand mixtures: silty sand to sandy silt	5	$1.90 < I_{c(J\&D93)} < 2.54$
Silt mixtures: clayey silt to silty clay	4	$2.54 < I_{c(J\&D93)} < 2.82$
Clays	3	$2.82 < I_{c(J\&D93)} < 3.22$
Organic soils	2	$I_{c(J\&D93)} > 3.22$

NOTES:

$$I_{c(J\&D93)} = \sqrt{\{3 - \log[Q_t(1 - B_q)]\}^2 + [1.5 + 1.3(\log F_R)]^2}$$

σ_v = total vertical overburden stress; σ_v' = effective vertical overburden stress = $\sigma_v - u_o$; u_2 = total shoulder pore pressure measured during piezocone penetration; u_o = hydrostatic pore pressure, Δu_2 = excess shoulder pore pressure = $u_2 - u_o$.

Figure A.22 SBT classification chart based on normalized CPTu parameters and classification index $I_{cJ\&D93}$ (adapted from Jefferies & Davies, 1993).

A.1.18 Olsen and Mitchell (1995) SBT Chart

Based on a modified cone resistance normalization technique, Olsen and Mitchell (1995) presented an updated SBT classification chart, shown in Figure A.23. They attributed three reasons for this improvement over the Olsen and Malone (1988) version of the SBT chart: (1) an improved stress normalization scheme to account for exponential increase in the cone resistance, q_c, with increasing vertical effective stress, σ_v', (2) much larger CPT and boring database, and (3) improved understanding of how to predict strength (e.g., Olsen, 1994). This newer chart was the result of employing the Stress Focus concept deduced from the results of high-pressure laboratory chamber CPT tests, and extensive field CPT in uniform soil layers. According to Olsen and Mitchell (1995), the Stress Focus is an in-situ point at a vertical effective stress in the range of approximately 10 to 30 MPa (100 to 300 atmosphere) where sand densities and strength have values independent of the initial relative density at lower stress states. They used a variant of normalized net measured cone resistance, Q_c in developing this chart:

$$Q_c = \frac{q_{c,net}}{(\sigma_v')^c} = \frac{(q_t - \sigma_v)}{(\sigma_v')^c} \quad \text{(A.9)}$$

where, $q_{c,net}$ = net measured cone resistance, c = variable stress exponent based on the "Stress Focus" concept.

CPT predicted strength contours on the CPT soil characterization chart allowed improved positioning of the soil classification contours. The variable stress exponent (c) is considered a strength index. Each CPT SBT classification zone has a range of normalized strengths. Strength contours, therefore, a seen approximately perpendicular to the soil classification contours in Figure A.23. The CPT Soil Classification Number (SCN) scaling on this newer chart was also changed.

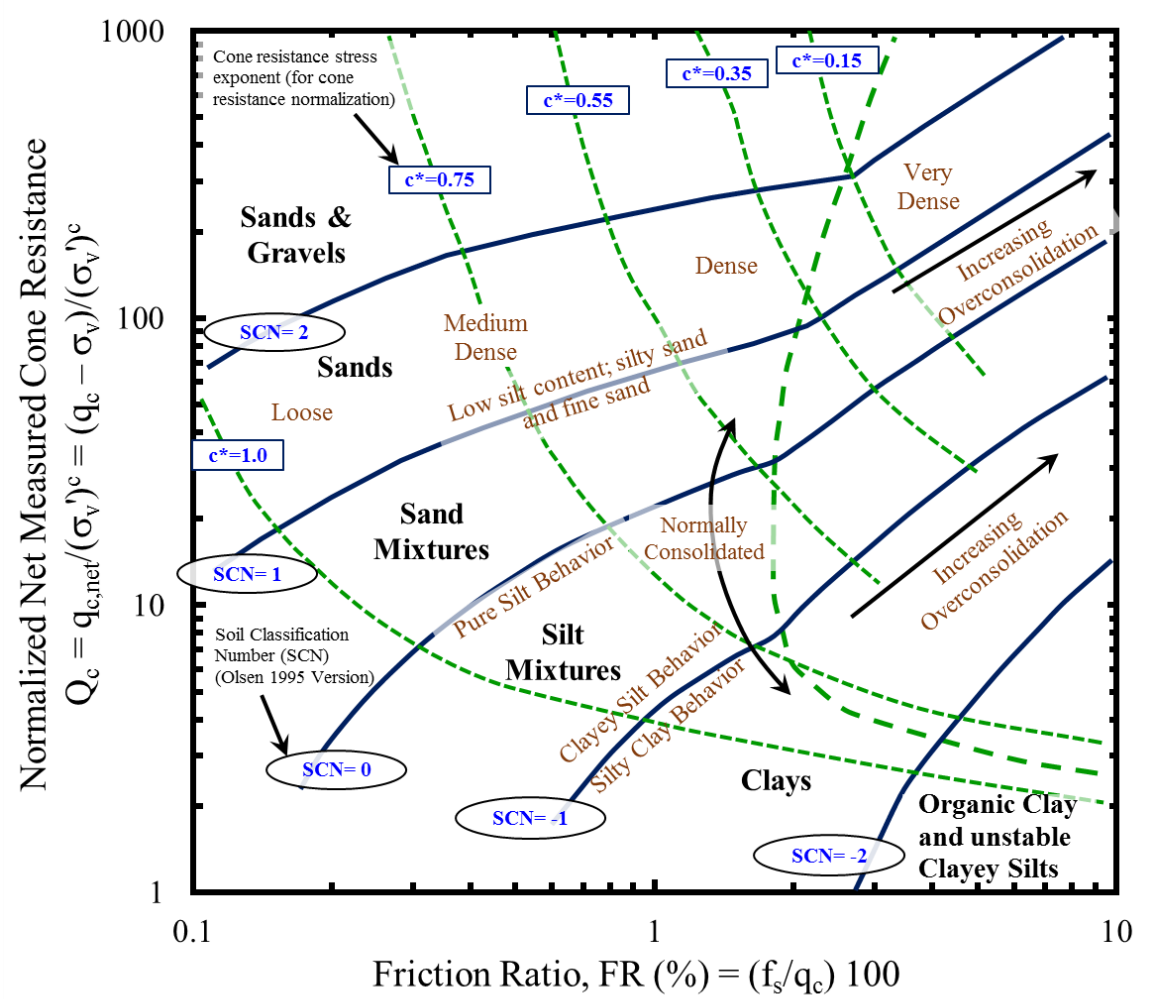

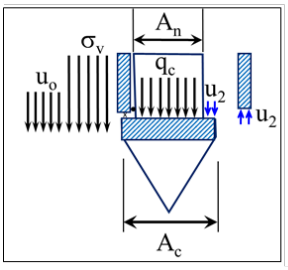

Notes:

Use the best possible cone resistance normalization technique; the variable stress exponent technique (Olsen, 1994), (Olsen & Mitchell, 1995) provides good results for shallow (e.g., 1 meter) to deep foundations (> 60 meters)

The variable cone resistance stress exponent, c*, requires an iterative solution starting with lowest c value and repeating calculations until the assumed c value and calculated Q_c match the c and Q_c on a constant FR line

Figure A.23 SBT chart (adapted from Olsen & Mitchell, 1995).

A.1.19 Robertson and Fear (1995) SBT Chart

The post-deposition processes that can possibly generate microstructure within the soil deposits are likely to influence any SBT classification system (Robertson, 2016). Following the realization of this factor, Robertson and Fear (1995) and Eslaamizaad and Robertson (1996) suggested that the seismic CPT can be used to identify soils with microstructure. In Chapter 1, it was explained that the small-strain shear modulus (G_0) can be estimated by utilizing the shear wave velocity (V_s) data from seismic CPT:

$$G_o = \rho_m V_s^2 \qquad \text{(A.10)}$$

where ρ_m = total mass density = γ_m/g_a, γ_m = total unit weight, and g_a = gravitational acceleration.

Robertson and Fear (1995) and Eslaamizaad and Robertson (1996) noted that there was a link between the ratio G_0/q_t and the normalized net corrected cone resistance (Q_t), since both aging and bonding tend to increase the small-strain stiffness (G_0) significantly more than they increase the large-strain strength of a soil (reflected in both q_t and Q_t), all other factors (in situ stress state, etc.) being constant. The ratio G_0/q_t is essentially a small-strain rigidity index (I_G), since it defines stiffness to strength ratio, where G_0 is the small-strain stiffness and q_t is a measure of soil strength.

Robertson and Fear (1995) presented a chart based on Q_t versus I_G plotted on log-log scale format (see Figure A.24). This chart can be used to identify unusual soils such as highly compressible sands, cemented and aged soils and clays with either a high or low void ratio.

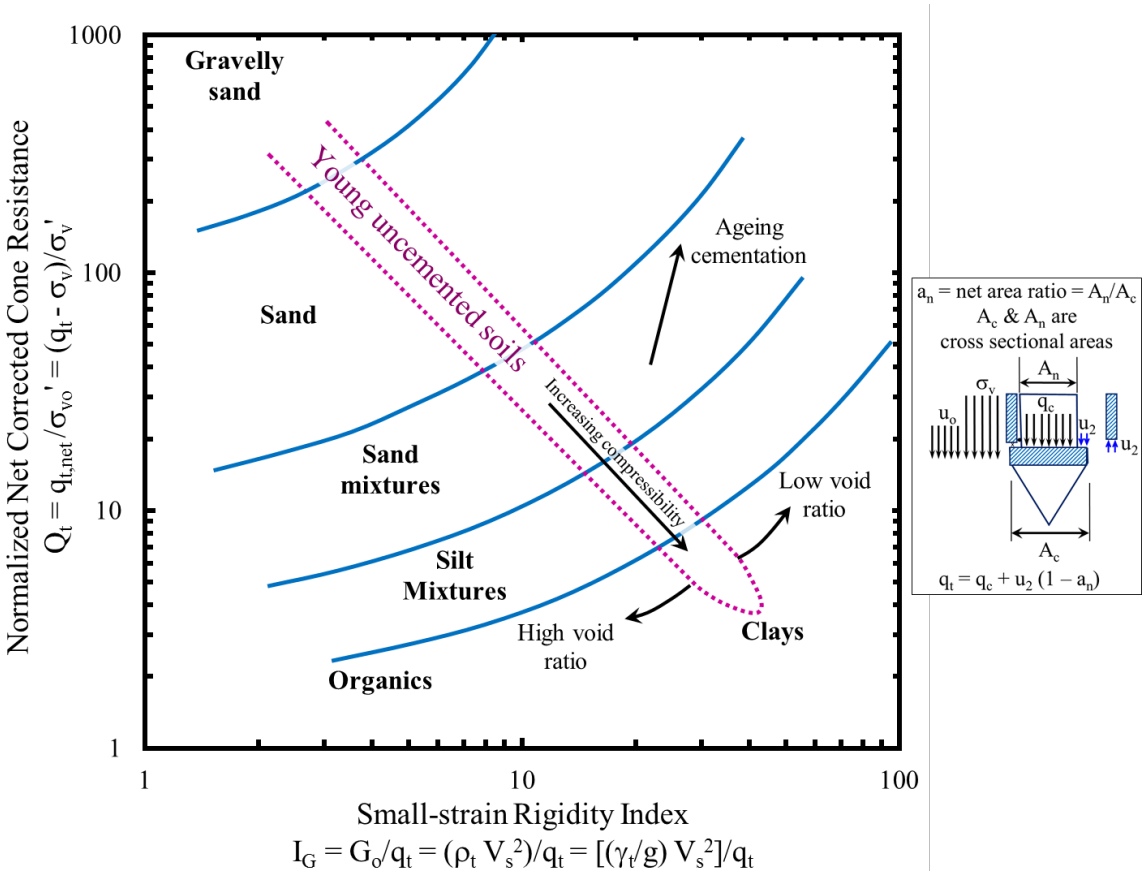

Figure A.24 SBT classification chart based on normalized corrected total cone resistance and small-strain rigidity index (adapted from Robertson & Fear, 1995).

A.1.20 Eslami and Fellenius (1997) SBT Chart

Eslami and Fellenius (1997) presented extensive database of CPT and CPTu together with the information regarding soil profiling and routine laboratory testing on samples retrieved from their respective nearby borings. The primary purpose of their

study was to investigate the use of CPTu in pile design. Besides their primary research, they also utilized this database in developing a new scheme of SBT classification in the form of "effective" cone resistance ($q_E = q_t - u_2$) versus sleeve friction (f_s) both plotted on logarithmic scales (see Figure A.25). As such, their plot follows the original formulation of Begemann (1965), except for the variation of subtracting the shoulder pore pressure (u_2) from the corrected total cone resistance (q_t), instead of plotting the measured cone resistance (q_c) along the ordinate. They explained their purpose for the use of these parameter as follows:

- The charts based on q_c versus FR (or their respective normalized variants) are mathematically incorrect for statistical analyses, since qc vs. FR and Normalized Cone Resistance vs. Normalized Friction Ratio in the pair sets use cone resistance. In other words, plotting of the cone resistance (or its normalized dimensionless parameter) along the ordinate axis versus friction ratio ($FR = f_s/q_c$) [or its normalized variant, $F_R = f_s/(q_c - \sigma_v)$] along the abscissa axis is misleading. It gives the impression that friction ratio is independent while the cone resistance is dependent; this is far from reality. In this way, the cone resistance is plotted against its own inverse, and therefore, the friction ratio is, indeed, not independent. Plotting one as a function of the other distorts the true information.
- Subtracting the pore pressure, indeed, does not make the value an "effective" stress, but rather allows convenient delineation of SBT zones.

As shown in Figure A.25, the SBT chart by Eslami and Fellenius (1997) presents envelopes enclosing five main soil types. Their database does not include cases with cemented soils or very stiff clay, and for this reason, no envelopes for such soil types are presented.

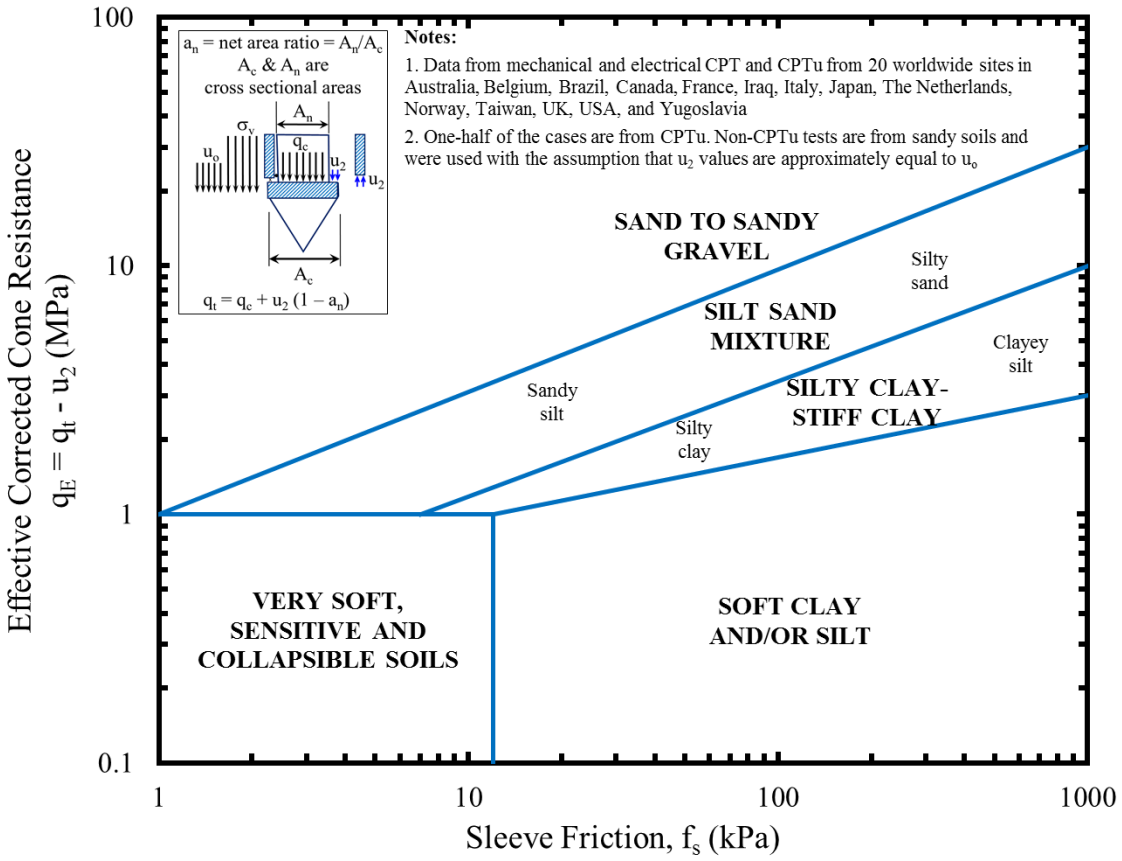

Figure A.25 SBT chart by Eslami and Fellenius (1997).

A.1.12 Robertson and Wride (1998) SBT Classification Index [$I_{c(R\&W98)}$]

Following the methodology of Jefferies and Davies (1993) regarding the SBT classification index [$I_{c(J\&D93)}$], Robertson and Wride (1998) also developed a classification index [$I_{c(R\&W98)}$] by adopting a continuum approach of fitting an equation to the trend of their Q_t-F_R chart:

$$I_{c(R\&W98)} = \sqrt{[3.47 - logQ_{tn}]^2 + [1.22 + LogF_R]^2} \qquad (A.11)$$

where, Q_{tn} is the normalized net corrected cone resistance = $(q_{t,net}/p_A)(p_A/\sigma_v')^n = [(q_t - \sigma_v)/p_A](p_A/\sigma_v')^n\, Q_t$; F_R is the same as defined earlier; the subscript *R&W98* indicates classification index by Robertson and Wride (1998); p_A is a reference stress in the same units as q_t and σ_v'. The logarithms used are base 10.

Within this classification of CPT data, soil SBTs are attributed from $I_{c(R\&W98)}$ as summarized in Table A.5 and Figure A.26. This soil behaviour type index does not apply to zones 1, 8, or 9. It may also be noted that a stress normalization exponent n for the net corrected total cone resistance uses. The Robertson (1990) procedure was to use n = 1.0 for all soil types. Robertson and Wride (1998) recommended an iterative procedure as follows. First use n = 1.0 to calculate Q_{tn}, and an initial value of $I_{c(R\&W98)}$ for CPT data. If $I_{c(R\&W98)} > 2.6$ (clay type soils), the data should be plotted directly on this chart. However,

if $I_{c(R\&W98)} \leq 2.6$ (sandy soils), the exponent to calculate Q_{tn} should be changed to $n = 0.5$ and $I_{c(R\&W98)}$ should be recalculated. If the recalculated $I_{c(R\&W98)}$ remains less than 2.6, the data should be plotted on the Robertson chart. If, however, $I_{c(R\&W98)}$ iterates above and below a value of 2.6, depending which value of n is used, a value of $n = 0.75$ should be selected and plot the calculated data on the Robertson chart. As indicated earlier, if the in-situ effective overburden stresses (σ_v') are in the order of 50–150 kPa, the choice of normalization has little effect on the calculated normalized net penetration resistance.

Table A.5 Soil Behavior Type from Classification Index $I_{c(R\&W98)}$
(after Robertson & Wride, 1998)

Possible Type of Soil	Zone	CPTu Index, $I_{c(R\&W98)}$
Gravelly sand to dense sand	7	$I_{c(R\&W98)} < 1.31$
Sands: clean sand to silty sand	6	$1.31 < I_{c(R\&W98)} < 2.05$
Sand mixtures: silty sand to sandy silt	5	$2.05 < I_{c(R\&W98)} < 2.60$
Silt mixtures: clayey silt to silty clay	4	$2.60 < I_{c(R\&W98)} < 2.95$
Clays: silty clay to clay	3	$2.95 < I_{c(R\&W98)} < 3.60$
Organic soils: peats	2	$I_{c(R\&W98)} > 3.60$

Note: $I_{c(R\&W98)} = \sqrt{[3.47 - logQ_{tn}]^2 + [1.22 + LogF_R]^2}$; $Q_{tn} = [(q_t - \sigma_v)/p_A]/(p_A/\sigma_v')^n$; $F_R = f_s/q_{t\text{-}net} = f_s/(q_t - \sigma_v)$; $q_t = q_c + u_2 (1 - a_n)$; σ_v = total vertical overburden stress; σ_v' = effective vertical overburden stress = $\sigma_v - u_0$; u_2 = total shoulder pore pressure measured during piezocone penetration; u_0 = hydrostatic pore pressure, Δu_2 = excess shoulder pore pressure = $u_2 - u_0$; n = stress normalization exponent.

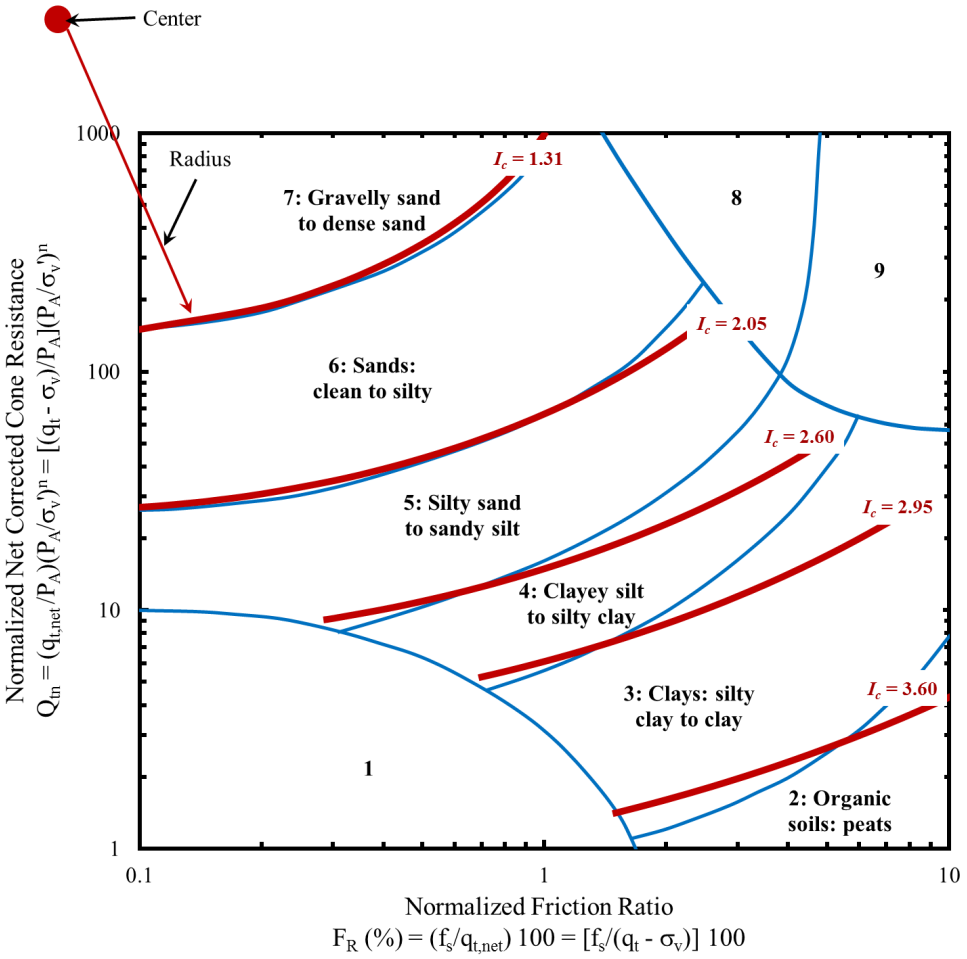

Possible Type of Soil	Zone	CPTu Index, $I_{c(R\&W98)}$
Gravelly sand to dense sand	7	$I_{c(R\&W98)} < 1.31$
Sands: clean sand to silty sand	6	$1.31 < I_{c(R\&W98)} < 2.05$
Sand mixtures: silty sand to sandy silt	5	$2.05 < I_{c(R\&W98)} < 2.60$
Silt mixtures: clayey silt to silty clay	4	$2.60 < I_{c(R\&W98)} < 2.95$
Clays: silty clay to clay	3	$2.95 < I_{c(R\&W98)} < 3.60$
Organic soils: peats	2	$I_{c(R\&W98)} > 3.60$

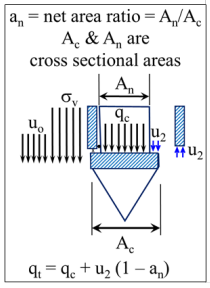

NOTES:

$q_t = q_c + u_2 (1 - a_n)$; σ_v = total vertical overburden stress; σ_v' = effective vertical overburden stress = $\sigma_v - u_o$; u_2 = total shoulder pore pressure measured during piezocone penetration; u_o = hydrostatic pore pressure, Δu_2 = excess shoulder pore pressure = $u_2 - u_o$; n = stress exponent

$I_{cR\&W98}$ does not apply to zones 1, 8, or 9.

Follow this iterative procedure: First use n = 1.0 to calculate Q_{tn}; if calculated $I_{cR\&W98} > 2.6$ (clay type soils), the data should be plotted directly on this chart. However, if $I_{cR\&W98} \leq 2.6$ (sandy soils), the n should be changed to 0.5 and $I_{cR\&W98}$ recalculated. If the recalculated $I_{cR\&W98}$ remains less than 2.6, the data should be plotted on the chart. If, however, $I_{cR\&W98}$ iterates above and below a value of 2.6, depending which value of n is used, a value of n = 0.75 should be selected and plot the calculated data on the chart. If the σ_v' is 50–150 kPa, the choice of normalization has little effect on the calculated Q_{tn}.

Figure A.26 SBT classification chart based on normalized CPTu parameters and classification index $I_{c(R\&W98)}$ (adapted from Robertson & Wride, 1998).

A.1.22 Zhang and Tumay (1999) Probabilistic Approach

In a unique approach to indirect soil classification by CPT, Zhang and Tumay (1999) proposed a probabilistic method (fuzzy logic) of assessing percentages of clay, silt, and sand. Accordingly, the method uses the cone tip resistance (q_t) and sleeve friction (f_s) to evaluate probability of soil type. The method is fully automated by computer software and available as a free download from the LTRC website. Mayne (2007a) showed good agreement of the results from this method with the true soil profile. This method is beyond the scope of further discussion herein.

A.1.23 Ramsey (2002) SBT Charts

Figure A.27 shows the SBT charts proposed by Ramsey (2002). The charts were developed using Fugro's database of CPTu results with adjacent laboratory test results in the Quaternary soils of North, Norwegian and Irish Seas. This model consists of nine SBT zones, somewhat similar to those of Robertson (1990; 1991). However, key developments include: (1) all zones are presented on both graphs, (2) the range of Q_t in each zone of the two graphs is same, i.e., better consistency, and (3) more specific categorization guidelines, listed as follows.

- **Zone 1**: *Extra Sensitive Clay*, i.e., soils with sensitivity, S_t [= $s_{u(peak)}/s_{u(residual)}$] > 8, where s_u = undrained shear strength, and subscripts *peak* and *residual* represent undisturbed and remolded, respectively.
- **Zone 2**: *Organic Soil and Peat*, i.e., soils with an organic content > 5% by weight
- **Zone 3**: *Clay Soil with* $s_u/\sigma_v' \leq 1$ (approximately corresponding to NC to slightly OC clay)
- **Zone 4**: *Clay Soil with* $s_u/\sigma_v' > 1$ (approximately corresponding to significantly OC clay)
- **Zone 5**: *Clayey Sand* (fines content ≤ 35%; clay content ≥ 15%–20%)
- **Zone 6**: *Sandy Very Clayey Silt* (fines content > 35%–65%; clay content ≥ 15%–20%)
- **Zone 7**: *Sandy Silt* (fines content > 35%–65%; clay content < 5%)
- **Zone 8**: *Silty Sand* (fines content > 12%–35%; clay content < 5%)
- **Zone 9**: *Clean to Slightly Silty Sand/Gravel* (fines content ≤ 12%; clay content < 5%)

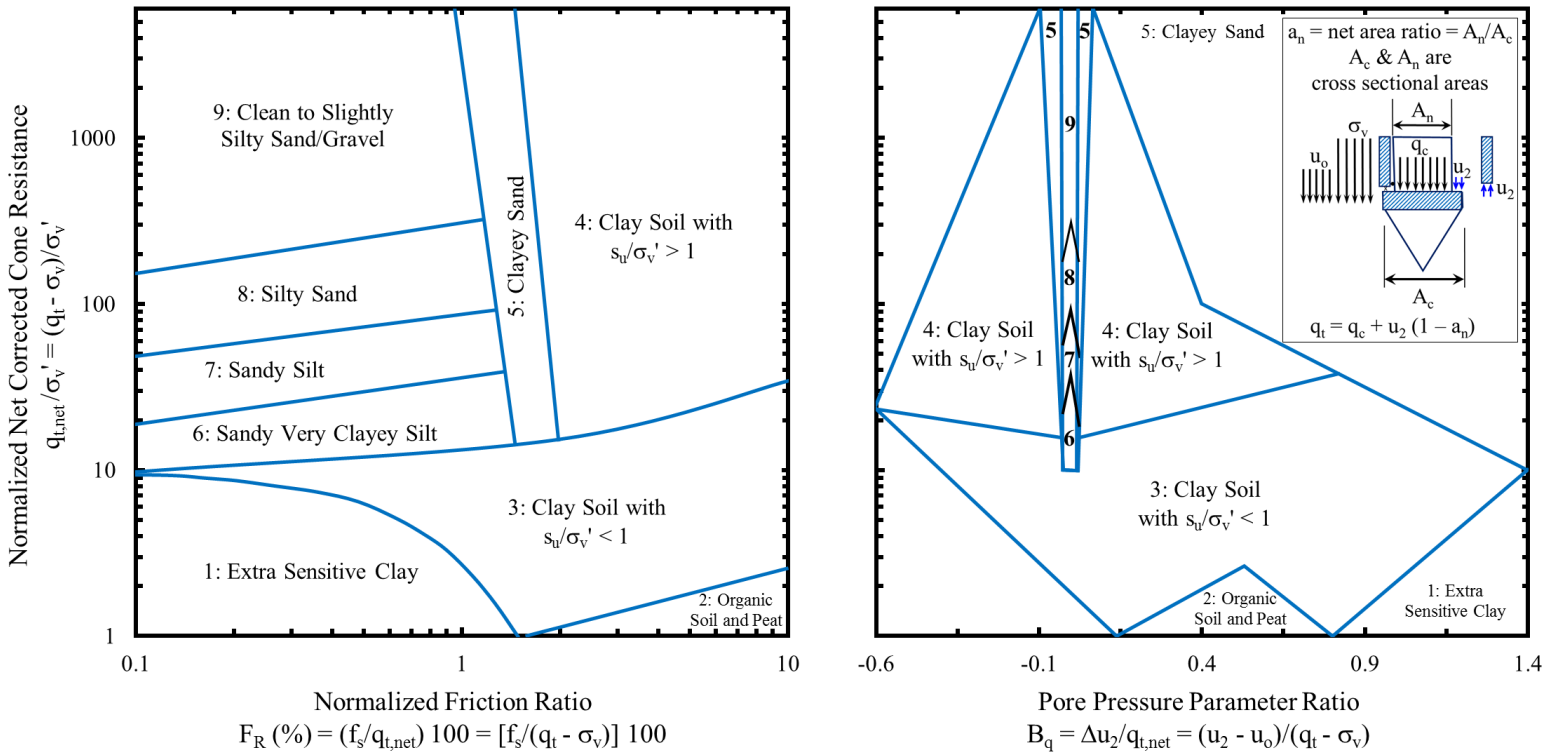

Soil Behavior Type Zones

Zone 1: Extra Sensitive Clay, i.e., soils with sensitivity, S_t [= $s_{u(peak)}/s_{u(residual)}$] > 8, where s_u = undrained shear strength, and subscripts 'peak' and 'residual' represent undisturbed and remolded, respectively

Zone 2: Organic Soil and Peat, i.e., soils with an organic content > 5% by weight

Zone 3: Clay Soil with $s_u/\sigma_v' \leq 1$ (approximately corresponding to NC to slightly OC clay)

Zone 4: Clay Soil with $s_u/\sigma_v' > 1$ (approximately corresponding to significantly OC clay)

Zone 5: Clayey Sand (fines content ≤ 35%; clay content ≥ 15-20%)

Zone 6: Sandy Very Clayey Silt (fines content > 35-65%; clay content ≥ 15-20%)

Zone 7: Sandy Silt (fines content > 35-65%; clay content < 5%)

Zone 8: Silty Sand (fines content > 12-35%; clay content < 5%)

Zone 9: Clean to Slightly Silty Sand/Gravel (fines content ≤ 12%; clay content < 5%)

NOTES:

Based on Fugro's database of 10 cm^2 and 15 cm^2 CPTu results in the Quaternary soils of North, Norwegian and Irish Seas

Figure A.27 SBT interpretation graph (adapted from Ramsey, 2002).

A.1.24 Jefferies and Been (2006) Updated SBT Classification Index [$I_{c(J\&B06)}$]

In reference to Jefferies and Davies (1991) SBT chart, Robertson (1991) had pointed out that the accuracy of the $Q_t(1 - B_q)$ versus F_R chart could be a problem in soft sensitive clays where B_q can be greater than 1.0. Jefferies and Been (2006) suggested that it is better to use $Q_t(1 - B_q) + 1$, as originally identified by Houlsby (1988). They indicated that the "+1" term proves useful when dealing with loose silts. They also modified their SBT index, as:

$$I_{c(J\&B06)} = \sqrt{\left\{3 - log\left[Q_t\left(1 - B_q\right) + 1\right]\right\}^2 + [1.5 + 1.3(LogF_R)]^2} \qquad \text{(A.12)}$$

where, Q_t, F_R and B_q are the same normalized parameters as defined earlier (Jefferies & Davies, 1991; 1993), and the subscript *J&B06* indicates classification index by Jefferies and Been (2006). Here, the stress normalization exponent, $n = 1.0$ was suggested for all cases. Within this classification of piezocone data, soil SBT boundaries are slightly modified as summarized in Table A.6 and Figure A.28. Jefferies and Been (2006) also noted that:

$$Q_t\left(1 - B_q\right) + 1 = \frac{q_E}{\sigma_{v'}} = \frac{(q_t - u_2)}{\sigma_{v'}} \qquad \text{(A.13)}$$

where, q_E is the effecive cone resistance (this parameter was used by Eslami and Fellenius (1997) in their SBT chart). Robertson (2009) further suggested that the concept of incorporating pore pressure into the normalized cone resistance may be attractive, but it lacks accuracy in soft fine-grained soils where q_E (= $q_t - u_2$) is very small and lacks accuracy and reliability in most soft soils.

Table A.6 Soil behavior type from classification index $I_{c(J\&B06)}$
(after Jefferies & Been, 2006)

Possible Type of Soil	Zone	CPTu Index, $I_{c(J\&B06)}$
Gravelly sands	7	$I_{c(J\&B06)} < 1.25$
Sands: clean sand to silty sand	6	$1.25 < I_{c(J\&B06)} < 1.80$
Sand mixtures: silty sand to sandy silt	5	$1.80 < I_{c(J\&B06)} < 2.40$
Silt mixtures: clayey silt to silty clay	4	$2.40 < I_{c(J\&B06)} < 2.76$
Clays	3	$2.76 < I_{c(J\&B06)} < 3.22$
Organic soils	2	$I_{c(J\&B06)} > 3.22$

Note: $I_{c(J\&B06)} = \sqrt{\left\{3 - log\left[Q_t\left(1 - B_q\right) + 1\right]\right\}^2 + [1.5 + 1.3(LogF_R)]^2}$; $Q_t = (q_t - \sigma_v)/\sigma_v'$; $F_R = f_s/q_{t\text{-}net} = f_s/(q_t - \sigma_v)$; $B_q = \Delta u_2/q_{t\text{-}net} = (u_2 - u_0)/(q_t - \sigma_v)$; $q_t = q_c + u_2\,(1 - a_n)$; σ_v = total vertical overburden stress; σ_v' = effective vertical overburden stress = $\sigma_v - u_0$; u_2 = total shoulder pore pressure measured during piezocone penetration; u_0 = hydrostatic pore pressure, Δu_2 = excess shoulder pore pressure = $u_2 - u_0$.

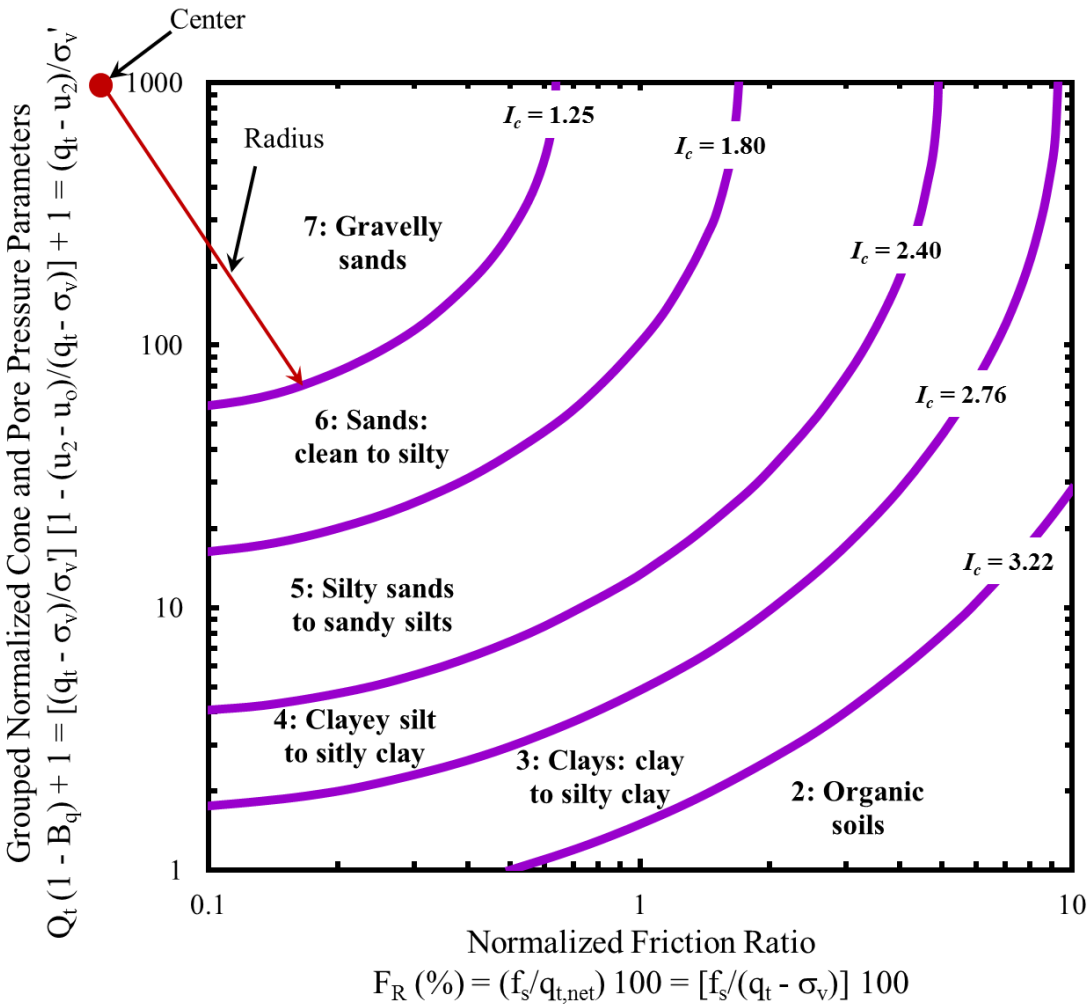

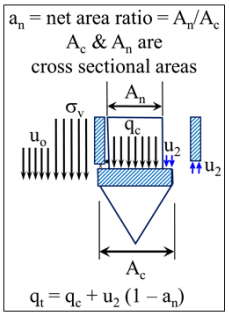

Possible Type of Soil	Zone	CPTu Index, $I_{c(J\&B06)}$
Gravelly sands	7	$I_{c(J\&B06)} < 1.25$
Sands: clean sand to silty sand	6	$1.25 < I_{c(J\&B06)} < 1.80$
Sand mixtures: silty sand to sandy silt	5	$1.80 < I_{c(J\&B06)} < 2.40$
Silt mixtures: clayey silt to silty clay	4	$2.40 < I_{c(J\&B06)} < 2.76$
Clays	3	$2.76 < I_{c(J\&B06)} < 3.22$
Organic soils	2	$I_{c(J\&B06)} > 3.22$

NOTES:

$$I_{c(J\&B06)} = \sqrt{\{3 - \log[Q_t(1 - B_q) + 1]\}^2 + [1.5 + 1.3(\text{Log}F_R)]^2}$$

σ_v = total vertical overburden stress; σ_v' = effective vertical overburden stress = $\sigma_v - u_o$; u_2 = total shoulder pore pressure measured during piezocone penetration; u_o = hydrostatic pore pressure, Δu_2 = excess shoulder pore pressure = $u_2 - u_o$.

Figure A.28 SBT classification chart based on normalized CPTu parameters and classification index $I_{c(J\&B06)}$ (adapted from Jefferies & Been, 2006).

A.1.25 Schneider et al. (2008) SBT Charts with Modified Normalization Scheme

Using parametric studies on piezocone data (q_t and u_2) from clay sites, relatively thick deposits of sands, silts, and varietal clays from around the globe, Schneider et al. (2008) provided a different framework for evaluation of soil type. Three SBT charts developed by them are shown in Figure A.29. In addition to the typical framework of pore pressure parameter ratio [i.e., $B_q = \Delta u_2/(q_t - u_2)$], they also investigated a different normalization scheme, i.e., $\Delta u_2/\sigma_v'$. Schneider et al. (2008) noted that theoretically the soil behavior is controlled by the degree of pore pressure dissipation during loading, stress level at failure, and initial overconsolidation ratio. Accordingly, these new charts were primarily developed to aid in separating drained, undrained, or partially drained penetration, as well as to extract the influence of overconsolidation ratio from that of partial consolidation on the normalized piezocone parameters.

The resulting recommended classification charts are significantly different from earlier charts and imply that assessment of data in Q_t versus $\Delta u_2/\sigma_v'$ space is superior to Q_t versus B_q space when evaluating piezocone data for a range of soil types. The soil types have been classified in five categories: silts and low rigidity index I_R clays ($I_r = G/s_u$, where G = shear modulus and s_u = undrained shear strength), clays, sensitive clays, essentially drained sands, and transitional soils. For onshore sites above the water table with lack of pore pressure readings, Schneider et al. (2008) recommended additional use of soil classification based on Q_t versus F_R (%). Furthermore, they also promoted use of piezocone dissipation tests, or variable rate piezocone tests to aid in the analysis of separating partial consolidation and OCR.

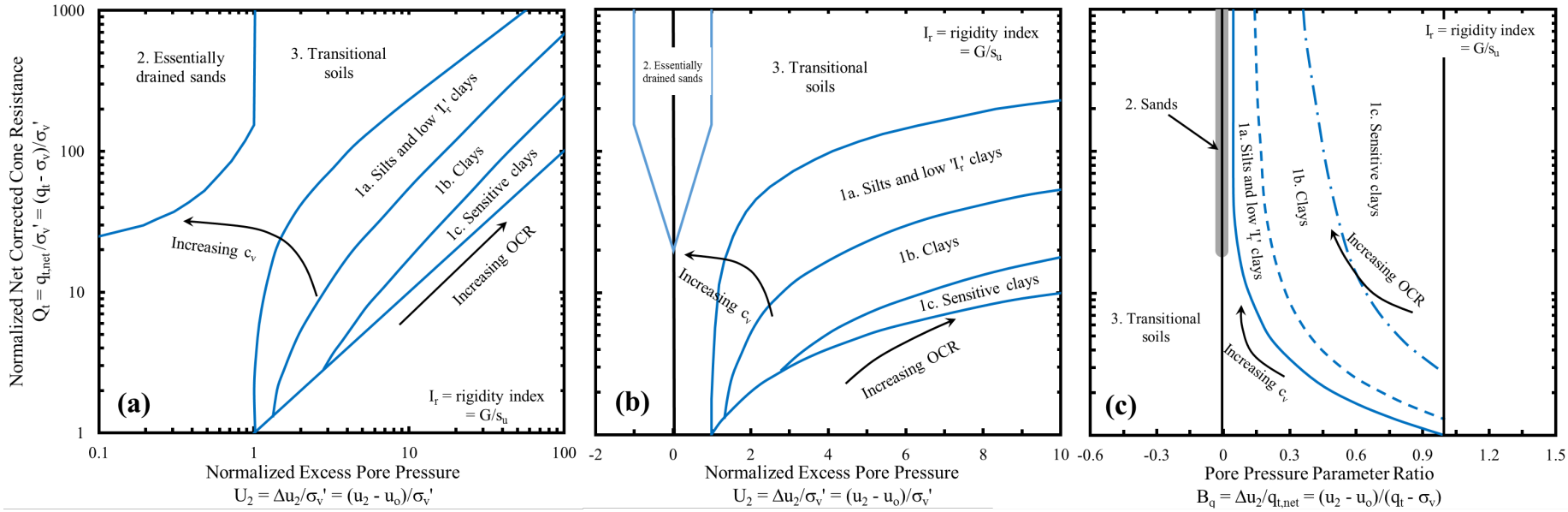

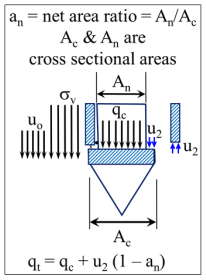

Descriptions and Notes:

Based on 10 cm^2 and 15 cm^2 electric CPTu with pore pressure measurements mainly at shoulder location (u_2)

Database of clay, sand, silt, and varietal clay sites from Australia, Bangladesh, Canada, Sweden, and The Netherlands, North Sea, Norway, UK, USA

Q_t vs. B_q space tends to provide detail for separating clay behavior, whereas Q_t vs. U_2 space is more useful for identifying sands, silts and clays, or soil type.

Zone 1a: Low I_r clays and silts; penetration may occur under conditions of partial consolidation or in soils with high unloading stiffness/large negative local shear induced pore pressures.

Zone 1b: Undrained penetration in clays

Zone 1c: Clays with a higher than average sensitivity.

Zone 2: Essentially drained penetration in sands, gravels, and silty sands. Penetration in very loose or compressible sands at great depths may result in Q_t below 20 during drained penetration.

Zone 3: Transitional Soils. A wide variety of soils fall within this range, and soil classification should be augmented using CPT friction ratio F_R (%), dissipation tests, variable rate penetration testing, and/or sampling. It is important to recognize that typical correlations based on drained or undrained penetration likely have lower levels of reliability if applied to soils in Zone 3.

Figure A.29 SBT charts based on q_t and u_2 data (adapted from Schnieder et al., 2008).

A.1.26 Robertson (2009) Modification of Normalized Cone Resistance (Q_{tn})

Robertson (2009) presented an extensive review of the overburden stress exponent (n) used in normalization of the cone resistance {i.e., for $Q_{tn} = [(q_t - \sigma_v)/p_A](p_A/\sigma_v')^n$}. Accordingly, he recommended the following expression for evaluating the variation of the stress exponent with both SBT $I_{c(R\&W98)}$ and effective overburden stress (σ_v'):

$$n = 0.381\, I_{c(R\&W98)} + 0.05\, \frac{\sigma_v'}{p_A} - 0.15 \qquad \text{(A.14)}$$

where $n \leq 1.0$. The proposed updated contours of n (for ($\sigma_v'/p_A = 1.0$) are shown in Figure A.30, where p_A = reference stress of atmospheric pressure of 0.1 MPa (or its equivalent in other units). Figure A.30 shows that for most fine-grained soils, the stress exponent will be 1.0. The stress exponent will range from 0.5 to 0.9 for most coarse-grained soils when in situ vertical stresses are not high. The region where $n = 1.0$ moves up the chart with increasing confining stress. When the in situ vertical effective stress is greater than 1 MPa, the stress exponent will be essentially 1.0 for most soils.

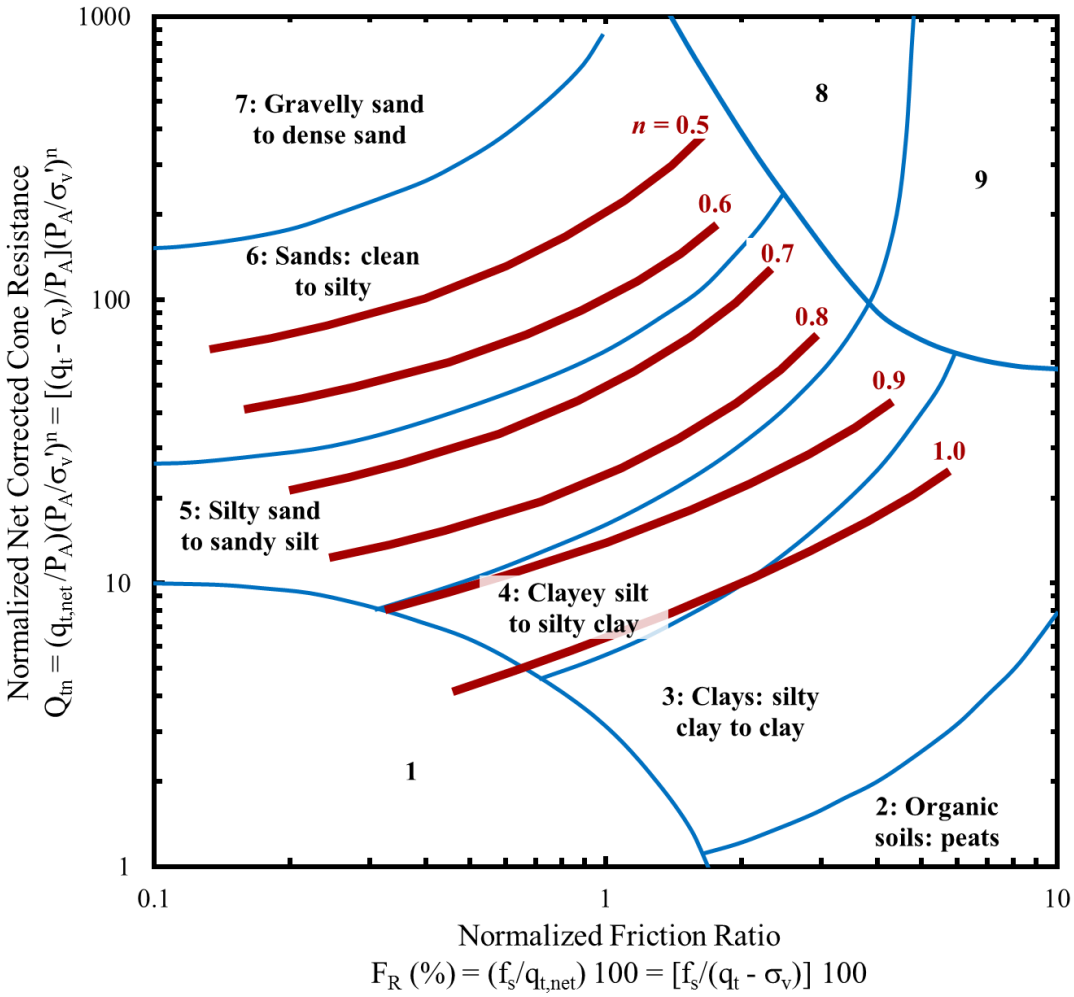

a_n = net area ratio = A_n/A_c
A_c & A_n are cross sectional areas

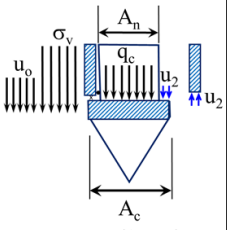

$q_t = q_c + u_2 (1 - a_n)$

Possible Type of Soil	Zone	CPTu Index, $I_{c(R\&W98)}$
Gravelly sand to dense sand	7	$I_{c(R\&W98)} < 1.31$
Sands: clean sand to silty sand	6	$1.31 < I_{c(R\&W98)} < 2.05$
Sand mixtures: silty sand to sandy silt	5	$2.05 < I_{c(R\&W98)} < 2.60$
Silt mixtures: clayey silt to silty clay	4	$2.60 < I_{c(R\&W98)} < 2.95$
Clays: silty clay to clay	3	$2.95 < I_{c(R\&W98)} < 3.60$
Organic soils: peats	2	$I_{c(R\&W98)} > 3.60$

NOTES:

$$I_{c(R\&W98)} = \sqrt{[3.47 - \log Q_{tn}]^2 + [1.22 + \log F_R]^2}$$

$$n = 0.381\,[I_{c(R\&W98)}] + 0.05\,(\sigma_v'/P_A) - 0.15 \leq 1.0$$

$q_t = q_c + u_2 (1 - a_n)$; σ_v = total vertical overburden stress; σ_v' = effective vertical overburden stress = $\sigma_v - u_o$; u_2 = total shoulder pore pressure measured during piezocone penetration; u_o = hydrostatic pore pressure, Δu_2 = excess shoulder pore pressure = $u_2 - u_o$; n = stress exponent

$I_{cR\&W98}$ does not apply to zones 1, 8, or 9

Figure A.30 Contours of stress exponent (n) for (σ_v'/p_A = 1.0) on Robertson and Wride (1998) SBT chart (adapted from Robertson, 2009).

A.1.27 Schneider et al. (2012) Q_t-F_R and Updated Q_t-$\Delta u_2/\sigma_v'$ SBT Charts

Schneider et al. (2012) extended the previous semi-empirical framework of Q_t versus $\Delta u_2/\sigma_v'$ space for SBT classification (e.g., Schneider et al., 2008) to include Q_t versus F_R chart. This complementary chart also offered slight modifications to the assignment of soil types in few zones of Q_t versus $\Delta u_2/\sigma_v'$ chart. The complementary charts are shown in Figure A.31 with more hyperbolic shaped soil-type boundaries in the new Q_t-F_R space.

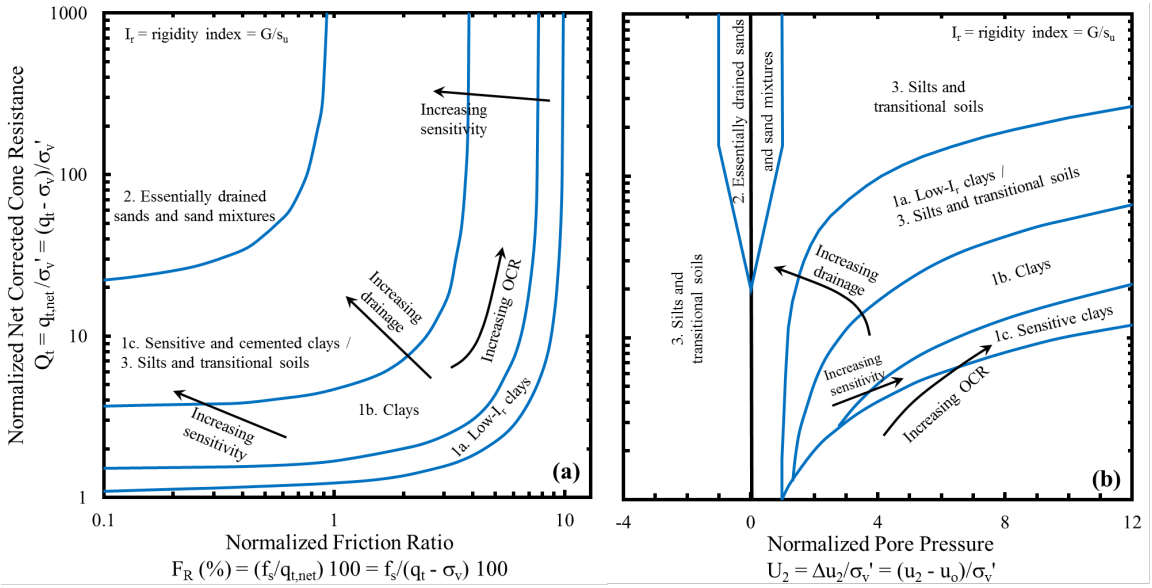

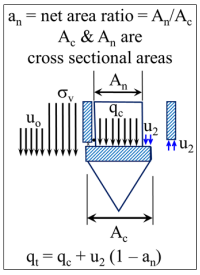

Descriptions and Notes:

Based on 10 cm^2 and 15 cm^2 electric CPTu with pore pressure measurements mainly at shoulder location (u_2)

Database of clay, sand, silt, and varietal clay sites from Australia, Bangladesh, Canada, Sweden, and The Netherlands, North Sea, Norway, UK, USA

Q_t vs. B_q space tends to provide detail for separating clay behavior, whereas Q_t vs. U_2 space is more useful for identifying sands, silts and clays, or soil type.

Zone 1a: Low-I_r clays; penetration may occur under conditions of partial consolidation or in soils with high unloading stiffness/large negative local shear induced pore pressures.

Zone 1b: Undrained penetration in clays

Zone 1c: Clays with a higher than average sensitivity.

Zone 2: Essentially drained penetration in sands, gravels, and silty sands. Penetration in very loose or compressible sands at great depths may result in Q_t below 20 during drained penetration.

Zone 3: Silts and transitional Soils. A wide variety of soils fall within this range, and soil classification should be augmented using CPT friction ratio F_R (%), dissipation tests, variable rate penetration testing, and/or sampling. It is important to recognize that typical correlations based on drained or undrained penetration likely have lower levels of reliability if applied to soils in Zone 3.

Figure A.31 Complementary SBT charts (adapted from Schneider et al., 2012).

A.1.28 Modified Tumay (1985) and Robertson (1990) SBT Charts by Salgado et al. (2015)

In order to develop algorithms for generating stratigraphic profile from the CPT data, Salgado et al. (2015) modified the Tumay (1985) and the Robertson (1990) charts. These modifications were needed for a clearer distinction between soil intrinsic variables (related closely to composition) and soil state variables. While the soil generation

algorithms were briefly discussed in Section 3.2, their further details may be seen in Salgado et al. (2015) and Ganju et al. (2017). However, the modified charts are presented here in Figures A.32 and A.32. The modifications made in the q_c versus FR (%) Tumay (1985) chart includes the following.

- The envelopes of the original chart representing “loose sand,” “sand,” “shell sand or limerock,” “dense or cemented sand” and “silty sand” were combined into a single envelop referred to as "clean sand or silty sand." Further classification within this region of the chart is done on the basis of relative density (D_R) estimated from the expression by Salgado and Prezzi (2007), shown in Figure A.32.
- The “silty clay” zone in the original chart was removed.
- The “sandy clay” region in the original chart was renamed “sandy clay or silty clay.”
- The “organic clay” region in the original chart was removed. All the “inorganic clays” of different stiffnesses in the original chart were renamed as their respective “clays.”
- The “clayey sands” region in the original chart was renamed as “clayey silt” in the modified chart. This was done to be consistent with the expected progressive increase in cone resistance with increasing sand content from “clayey silt” to “clayey sand or silt” and then to “clayey silty sand.”
- A new region of “sensitive clay” was added to indicate clays with FR (%) < 1. As shown in Figure A.33, the modifications made in the normalized Q_t versus F_R (%) Robertson (1990) chart include the following.
    - The “organic soils—peats” region (zone 2) was renamed “organic clay” in the modified chart.
    - The “very stiff sand to clayey sand” region (zone 8) in the original chart was merged into two regions: “sand mixtures: silty sand to sandy silt” (zone 5 of the original chart) and “clean sand to silty sand” (zone 6 of the original chart) of the modified chart. The rationale behind this modification is that the “very stiff sand to clayey sand” region (zone 8) in the original chart indicates similar soil behavior type to those suggested by the “sand mixtures: silty sand to sandy silt” (zone 5) and “clean sand to silty sand” (zone 6) regions (i.e., zone 8 in the original chart also indicates mixed soil types).
    - The “clean sand to silty sand” region (zone 6) was further classified into five different subtypes depending on the relative density estimated from the expression by Salgado and Prezzi (2007), also shown in Figure A.33.
    - The “very stiff, fine-grained” region (zone 9) in the original chart was merged into the “clay to silty clay” (zone 3 of the original chart) and “clayey silt to silty clay” (zone 4 of the original chart) of the modified chart. The rationale behind this modification is that the “very stiff, fine-grained” (zone 9) region in the original chart indicates similar soil behavior type to those suggested by “clay to silty clay” (zone 3) and “clayey silt to silty clay” (zone 4) regions.

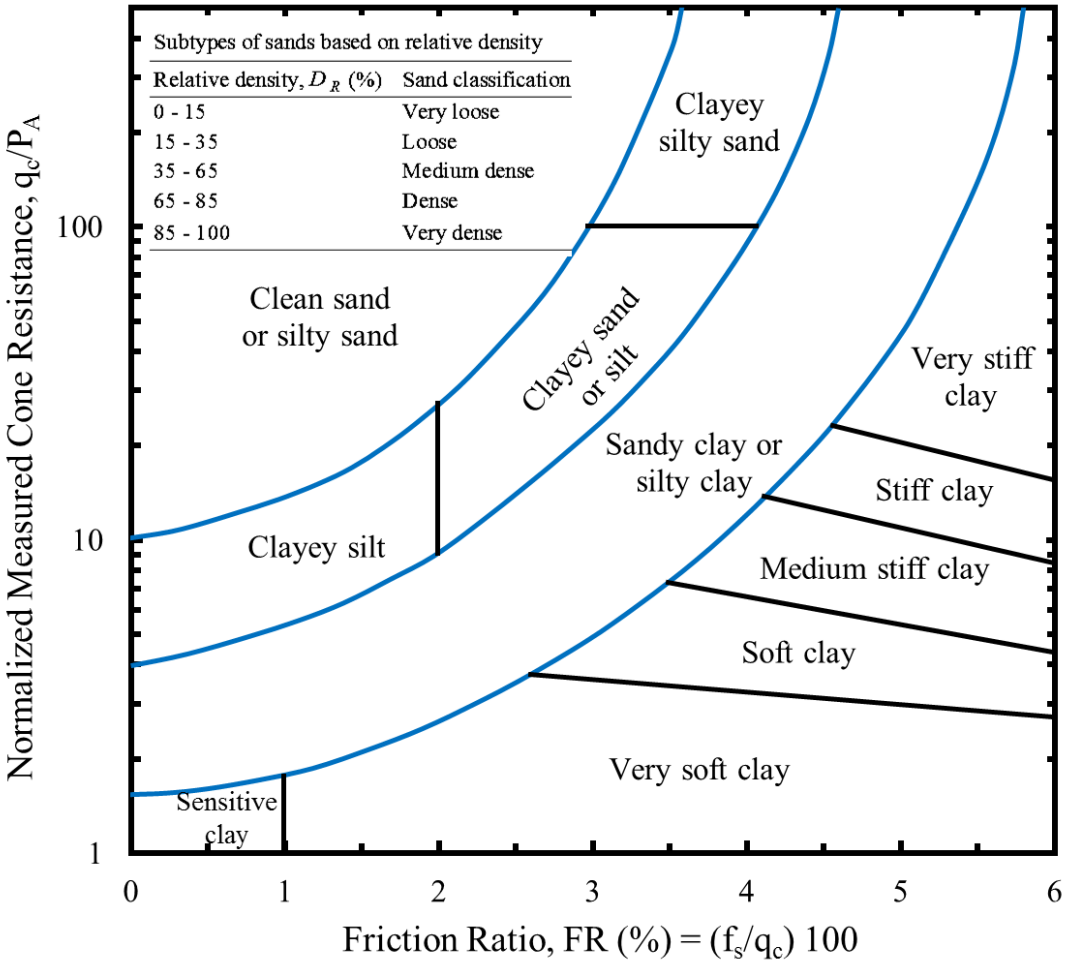

$$D_R = \frac{\ln\left(\frac{q_c}{p_A}\right) - 0.4947 - 0.841 - 0.1041\phi_c \times \ln\left(\frac{\sigma'_h}{p_A}\right)}{0.0264 - 0.0002\phi_c - 0.0047 \times \ln\left(\frac{\sigma'_h}{p_A}\right)} \leq 100\%$$

D_R = relative density
q_c = cone resistance
ϕ_c = critical-state friction angle
σ'_h = horizontal effective stress = $K_o\ \sigma'_v$
K_o = coefficient of lateral earth pressure at-rest
σ'_v = vertical effective stress
p_A = reference stress

Salgado and Monica (2007)

Figure A.32 Modified Tumay (1985) SBT chart (after Salgado et al., 2015).

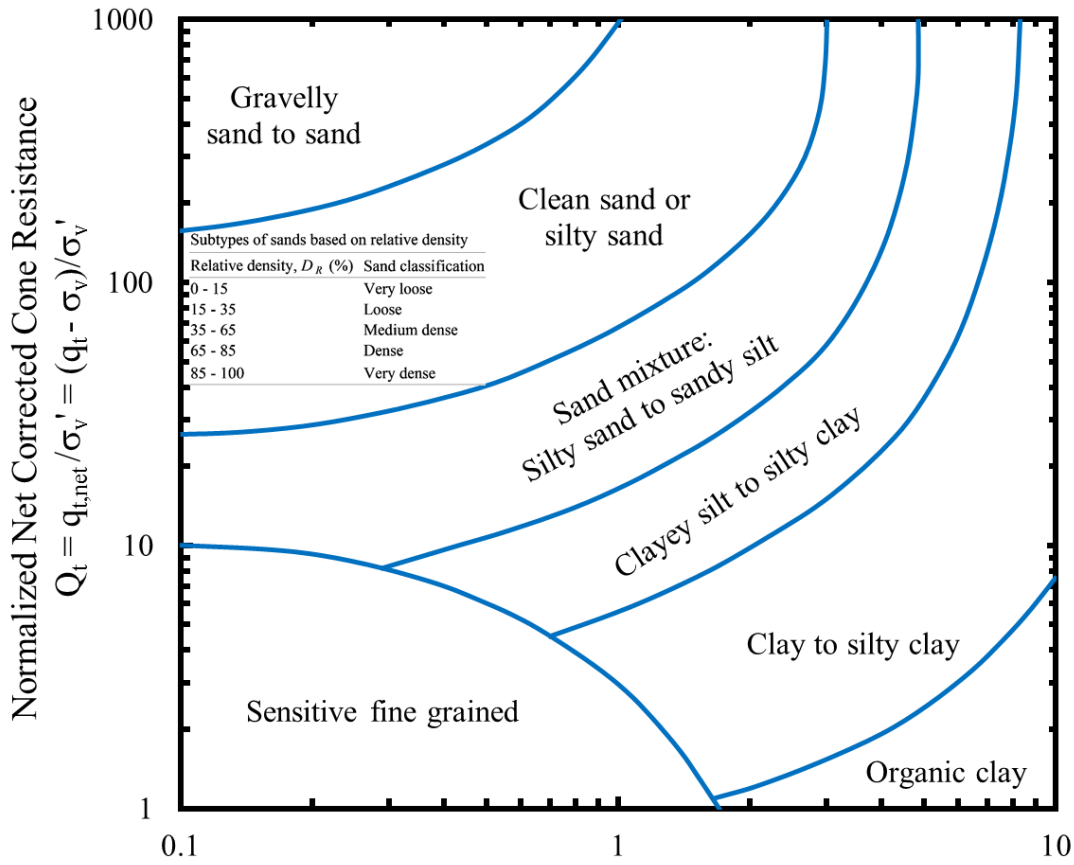

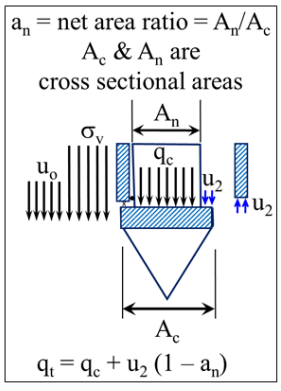

$$D_R = \frac{\ln\left(\frac{q_c}{p_A}\right) - 0.4947 - 0.841 - 0.1041\phi_c \times \ln\left(\frac{\sigma'_h}{p_A}\right)}{0.0264 - 0.0002\phi_c - 0.0047 \times \ln\left(\frac{\sigma'_h}{p_A}\right)} \leq 100\%$$

D_R = relative density
q_c = cone resistance
ϕ_c = critical-state friction angle
σ'_h = horizontal effective stress = $K_o\ \sigma'_v$
K_o = coefficient of lateral earth pressure at-rest
σ'_v = vertical effective stress
p_A = reference stress

Salgado and Monica (2007)

Figure A.33 Modified Robertson (1990) SBT chart (after Salgado et al., 2015).

A.1.29 Robertson (2016) Alternative SBT Definitions

Robertson (2016) noted that the soil descriptions used by most CPT-based SBT classifications is that from the textural-based systems, such as sand and clay, leading to

certain confusions. He further detailed that most of the early concepts of soil mechanics (from where these soil descriptions were developed) were based on tests performed on isotropically consolidated reconstituted samples, representative of saturated "ideal soils," whereas, the natural in-situ behavior of soils could be different from those of ideal soils due to the influence of macrostructure at the deposit scale (e.g., layering and fissures), or microstructure at the particle scale (e.g., bonding or cementation). Hence, identification of any significant structures within the soils was considered important towards understanding their in-situ behavior and the effectiveness of any derived classification system. Accordingly, extending the prior work by Schneider and Moss (2011), Robertson (2016) proposed a new chart: normalized net corrected cone resistance (Q_{tn}) versus small-strain net rigidity index ($I^*_G = G_0/q_{t,net}$), shown in Figure A.34, and a modified normalized small-strain net rigidity index $\{K^*_G = [G_0/(q_t - \sigma_v)](Q_{tn})^{0.75}\}$ to identify coarse and fine-grained soils with microstructure. Thus, very young uncemented soils tend to have K^*_G values closer to 100, whereas soils with some microstructure (e.g., older deposits) tend to have K^*_G values closer to 330. Soils with $K^*_G < 330$ tend to have little or no Microstructure where existing empirical CPT-based soil classification or correlations tend to provide good estimates of soil behavior. However, the soils with $K^*_G > 330$ represent significant microstructure, where traditional CPT-based classification and correlations should be used with care and significant insight. The suggested relationship shown in Figure A.34 is based on G_{0VH} (and V_{sVH}) that is measured primarily using the SCPT, where the subscript "VH" represents vertically propagating wave with particles motion in the horizontal direction.

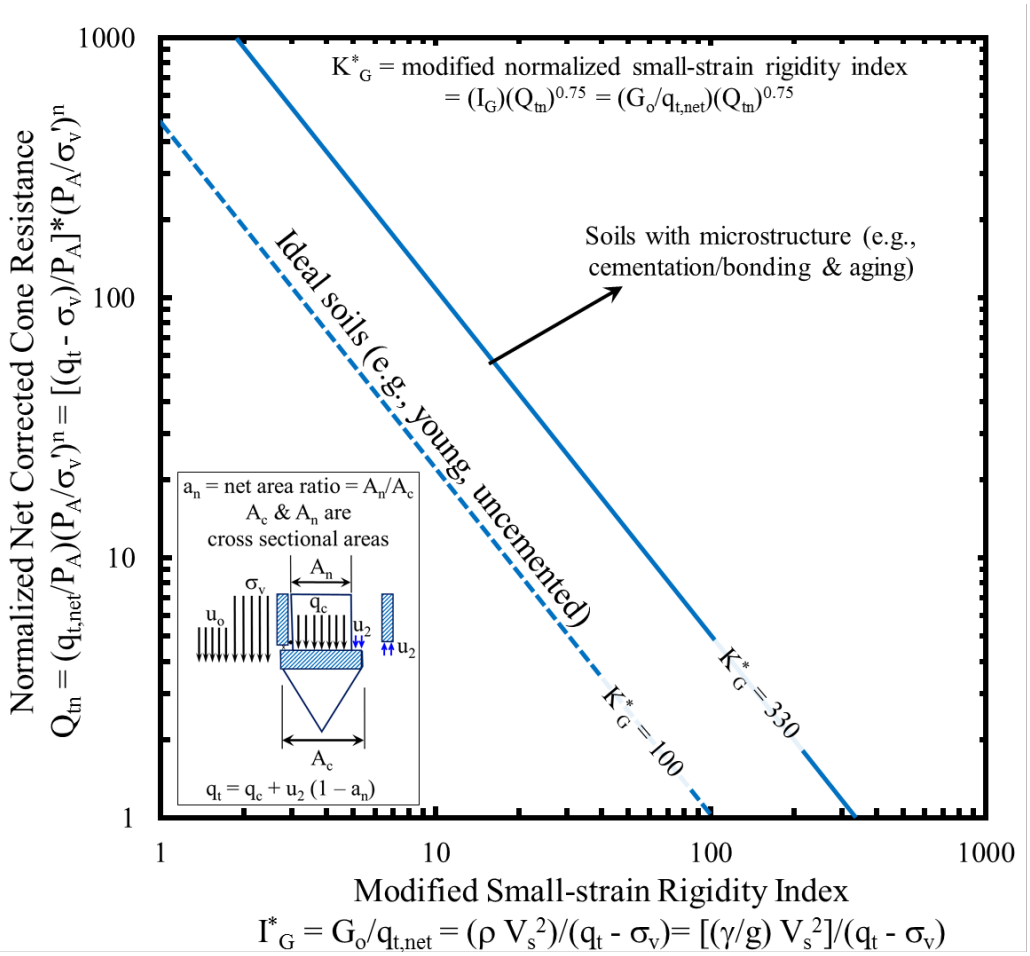

NOTES:

$$n = 0.381\,[I_{c(R\&W98)}] + 0.05\,(\sigma_v'/P_A) - 0.15 \leq 1.0$$

$$I_{c(R\&W98)} = \sqrt{[3.47 - \log Q_{tn}]^2 + [1.22 + \log F_R]^2}$$

1. G_o = small-strain shear stiffness; V_s = shear wave velocity; I_G = small-strain rigidity index; q_t = corrected cone resistance; σ_v = total vertical overburden stress; σ_v' = effective vertical overburden stress = $\sigma_v - u_o$; u_2 = total shoulder pore pressure measured during piezocone penetration; u_o = hydrostatic pore pressure, Δu_2 = excess shoulder pore pressure = $u_2 - u_o$; n = stress exponent.

2. The suggested relationship is based on G_{oVH} (and V_{sVH}) that is measured primarily using the SCPT. The subscript 'VH' represent vertically propagating wave with particle motion in the horizontal direction.

3. Very young uncemented soils tend to have K^*_G values closer to 100, whereas soils with some microstructure (e.g., older deposits) tend to have K^*_G values closer to 330. Soils with $K^*_G < 330$ tend to have little or no microstructure where existing empirical CPT-based soil classification tend to provide good estimates of soil behavior. However, the soils with $K^*_G > 330$ represent significant microstructure, where traditional CPT-based classification should be used with care and significant insight.

Figure A.34 Proposed Q_{tn}–I^*_G chart to identify soils with microstructure (after Robertson, 2016).

In addition to the above contribution, Robertson (2016) developed new boundaries on Q_{tn} versus F_R (%) space for separating soils that are either contractive or dilative at large shear strains. This is shown in Figure A.35(a) by the solid thick blue line (marked CD = 70), and also represented by the following expression:

$$CD = 70 = (Q_{tn} - 11)[1 + 0.06\, F_R\ (\%)]^{17} \quad \text{(A.15)}$$

where *CD* signifies the contractive-dilative boundary, and Q_{tn} and F_R are the same as defined in Robertson and Wride (1998) and Robertson (2009). Robertson (2016) further detailed that this chart, which also displays the SBT soil grouping boundaries based on physical characteristic descriptions (e.g., sand and clay) suggested by Robertson (1990; 2009), applies primarily to soils with little or no microstructure (i.e., ideal soils).

The dotted thick green line in Figure A.35(a) (marked *CD* = 60), and also represented by the following expression, shows approximate lower most limit for ideal soils that are predominantly dilative at large strains:

$$CD_{(lower\ bound)} = 60 = (Q_{tn} - 9.5)[1 + 0.06\, F_R\ (\%)]^{17} \quad \text{(A.16)}$$

Following the suggestion by Schneider et al. (2012) for improved zonation of Q_{tn} versus F_R (%) SBT space, Robertson (2016) superimposed the plots of additional boundaries based on a more hyperbolic shape. These boundaries are shown in solid thick red lines in Figure A.35(a), and also defined via a modified SBT classification index, $I_{B(R16)}$:

$$I_{B(R16)} = \frac{100\ (Q_{tn}+10)}{[70+Q_{tn}\ F_R\ (\%)]} \quad \text{(A.17)}$$

In Figure A.35(a), the thick solid red line designated as $I_{B(R16)} = 32$ is the lower boundary for most sand-like ideal soils, while that represented by $I_{B(R16)} = 22$ is the upper boundary for most clay-like ideal soils. The intermediate region represented by $22 < I_{B(R16)} < 32$ is defined as "transitional soils" (e.g., low plasticity fine-grained soils, such as silts). This classification is also summarized in Table A.7. Some transitional soils respond in a partially drained manner during CPT and are also referred to as "intermediate soils."

According to Robertson (2009; 2016), the soils with $F_R < 2\%$ typically have a sensitivity (S_t) > 3–4. Accordingly, within the region of clay-like contractive soils, this boundary was marked in Figure A.35 (as shown by the dashed thick black line) to distinguish between clay-like–contractive (*CC*) ideal soils [moderate to low sensitivity ($S_t < 3$)] and clay-like–contractive (*CCS*) ideal soils (higher sensitivity, $S_t > 3$).

The calculation involved in Q_{tn} requires an iterative procedure to determine the stress exponent (n) using $I_{c(R\&W98)}$ (e.g., Robertson, 2009). Since, the proposed modified SBT chart in Q_{tn} and F_R (%) space contains a modified index [$I_{B(R16)}$] instead to $I_{c(R\&W98)}$ to define the main boundaries between sand-like and clay-like behavior, Robertson (2016) recommended to continue using $I_{c(R\&W98)}$ and n detailed in the iterative procedure by Robertson (2009) to determine Q_{tn}, since $I_{c(R\&W98)}$ captures the variation in the soil behavior to estimate n.

Table A.7 Soil Behavior Type from Classification Index $I_{B(R16)}$ (after Robertson, 2016)

Possible Type of Soil	CPTu Index, $I_{B(R16)}$
Sand-like ideal soils	$I_{B(R16)} > 32$
Transitional ideal soils	$22 < I_{B(R16)} < 32$
Clay-like ideal soils	$I_{B(R16)} < 22$

Note: $I_{B(R16)} = 100(Q_{tn} + 10)[70 + Q_{tn} F_R(\%)]$; $Q_{tn} = [(q_t - \sigma_v)/p_A](p_A/\sigma_v')^n$; p_A = atmospheric reference stress = 100 kPa; n for Q_{tn} should be determined using iterative procedure with $I_{c(R\&W98)}$; $F_R = f_s/q_{t\text{-}net} = f_s/(q_t - \sigma_v)$; $q_t = q_c + u_2 (1 - a_n)$; σ_v = total vertical overburden stress; σ_v' = effective vertical overburden stress = $\sigma_v - u_0$; u_2 = total shoulder pore pressure measured during piezocone penetration; u_0 = hydrostatic pore pressure, Δu_2 = excess shoulder pore pressure = $u_2 - u_0$; $I_{c(R\&W98)} = \sqrt{[3.47 - logQ_{tn}]^2 + [1.22 + LogF_R]^2}$.

Furthermore, to address the earlier observation by Fellenius and Eslami (2000) regarding mathematical inaccuracy of the charts based on cone resistance versus friction ratio, Robertson (2016) also presented the newly proposed SBT classification in a modified format using normalized sleeve friction. As shown in Figure A.35(b), the revised format provides independence to the normalized parameters, however, the data becomes more compressed. The dashed lines displaying the SBT boundaries based on physical characteristic descriptions by Robertson (1990; 2009) indicate the same general trend as in Q_{tn}–F_R format. Robertson (2016) demonstrated preference of Q_{tn}–F_R format (Figure A.35a) over Q_{tn}–f_{s1} (Figure A.35b).

Robertson (2016) also applied the newly proposed SBT terms to the Schneider et al. (2008; 2012) chart in Q_{tn} versus U_2 space, as shown in Figure A.36 (note that the normalized net cone resistance Q_t has been replaced to Q_{tn}). Robertson (2016) proposed using B_q as a soil classification index for this chart; accordingly, the B_q curves that coincide with the new SBT boundaries are also shown in Figure A.36. The summary of range of different parameters defining the boundaries of the new SBT zones is given in Table A.8. This chart also serves as an aid in identifying soils with microstructure.

Table A.8 New SBT based on modified Schneider et al. (2008; 2012) Q_{tn}-U_2 chart (adapted from Robertson, 2016)

Possible Type of Soil	Range of Normalized Parameters
Contractive ideal soil	$U_2 > 0$
Dilative ideal soil	$U_2 < 0$
Clay-like dilative ideal soil, CD	$U_2 < 0$; $Q_{tn} > 12$
Clay-like contractive ideal soil, CC	$U_2 > 0$; $Q_{tn} > 12$, or $0.2 < B_q < 0.6$
Clay-like contractive-sensitive ideal soil, CCS	$0.6 < B_q < 1.0$ & $Q_{tn} > 4$
Soils with significant microstructure	*Region defined by* $U_2 > 0$ with $Q_{tn} = 20$ and $U_2 > 10$ with $Q_{tn} = 10$
Contractive soil with significant microstructure	$U_2 > 4$; $Q_{tn} > 12$

Note: $U_2 = \Delta u_2/\sigma_v'$; Δu_2 = excess shoulder pore pressure = $u_2 - u_0$; u_2 = total shoulder pore pressure measured during piezocone penetration; u_0 = hydrostatic pore pressure; σ_v' = effective vertical overburden stress = $\sigma_v - u_0$; σ_v = total vertical overburden stress; $Q_{tn} = [(q_t - \sigma_v)/p_A](p_A/\sigma_v')^n$; p_A = atmospheric reference stress = 100 kPa; n for Q_{tn} should be determined using iterative procedure with $I_{c(R\&W98)}$; $B_q = \Delta u_2/q_{t,net}$; $q_{t,net}$ = net corrected cone resistance = $q_t - \sigma_v$; $q_t = q_c + u_2 (1 - a_n)$; $I_{c(R\&W98)} = \sqrt{[3.47 - logQ_{tn}]^2 + [1.22 + LogF_R]^2}$.

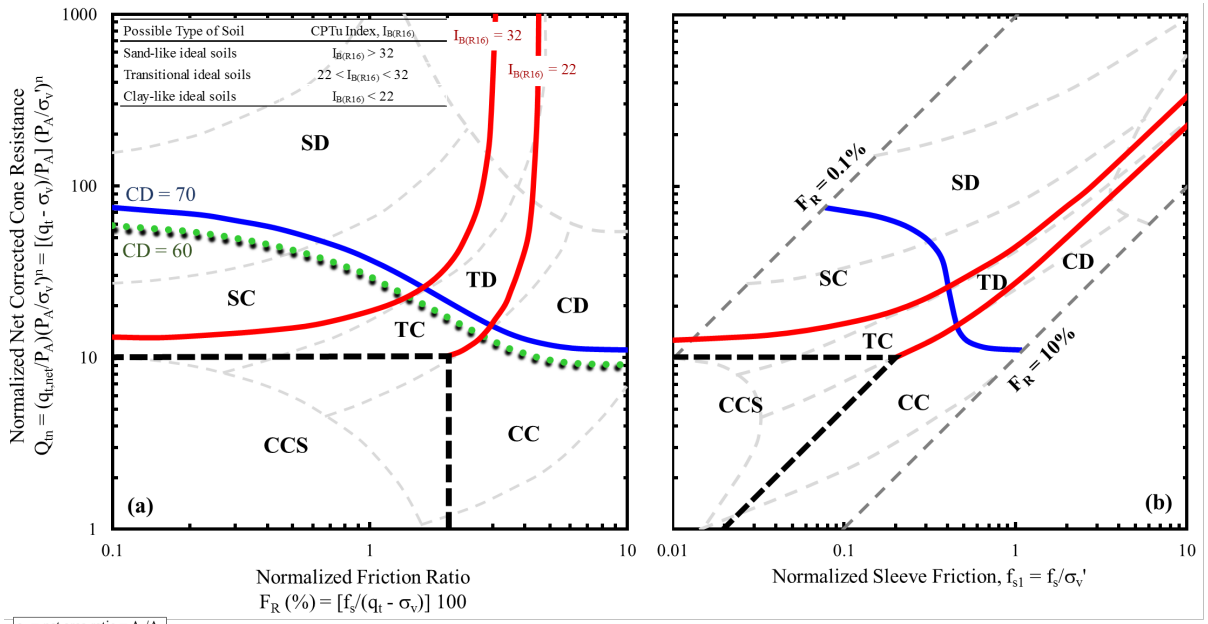

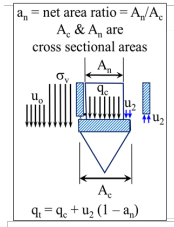

$$CD = 70 = (Q_{tn} - 11)[1 + 0.06\ F_R\ (\%)]^{17}$$

$$CD_{(lower\ bound)} = 60 = (Q_{tn} - 9.5)[1 + 0.06\ F_R\ (\%)]^{17}$$

$$I_{B(R16)} = 100(Q_{tn} + 10)[70 + Q_{tn}\ F_R\ (\%)]$$

$$Q_{tn} = [(q_t - \sigma_v)/P_A](P_A/\sigma_v')^n$$

$$n = 0.381\ [I_{c(R\&W98)}] + 0.05\ (\sigma_v'/P_A) - 0.15 \leq 1.0$$

$$I_{c(R\&W98)} = \sqrt{[3.47 - \log Q_{tn}]^2 + [1.22 + \log F_R]^2}$$

$$F_R\ (\%) = [(f_s/(q_t - \sigma_v)] \ 100$$

Soil Behavior Type Zones

CCS: Clay-like, contrative-sensitive	CC: Clay-like, contractive
CD: Clay-like, dilative	TC: Transitional, contractive
TD: Transitional, dilative	SC: Sand-like, contractive
SD: Sand-like, dilative	

NOTES:

1. σ_v = total vertical overburden stress; σ_v' = effective vertical overburden stress = $\sigma_v - u_o$; u_2 = total shoulder pore pressure measured during piezocone penetration; u_o = hydrostatic pore pressure, Δu_2 = excess shoulder pore pressure = $u_2 - u_o$; n = stress exponent.
2. Stress exponent n for Q_{tn} should be determined using iterative procedure with $I_{c(R\&W98)}$.
3. Q_{tn} vs. F_R chart applies primarily to soils with little or no microstructure (i.e., ideal soils).
4. Structured soils should be distinguished from ideal soils using Robertson (2016) Q_{tn} vs. I^*_G chart.
5. CD = 70 line represents slightly conservative boundary between dilative and contractive ideal soils at large shear strains; CD = 60 is the approximate lower most limit for ideal soils that are predominantly dilative at large strains.
6. $I_{B(R16)} = 32$ is the lower boundary for most sand-like ideal soils, while that represented by $I_{B(R16)} = 22$ is the upper boundary for most clay-like ideal soils; $22 < I_{B(R16)} < 32$ is for transitional soils.

Figure A.35 *Q_{tn}–F_R* and *Q_{tn}–f_{s1}* charts with modified SBT boundaries (adapted from Robertson, 2016).

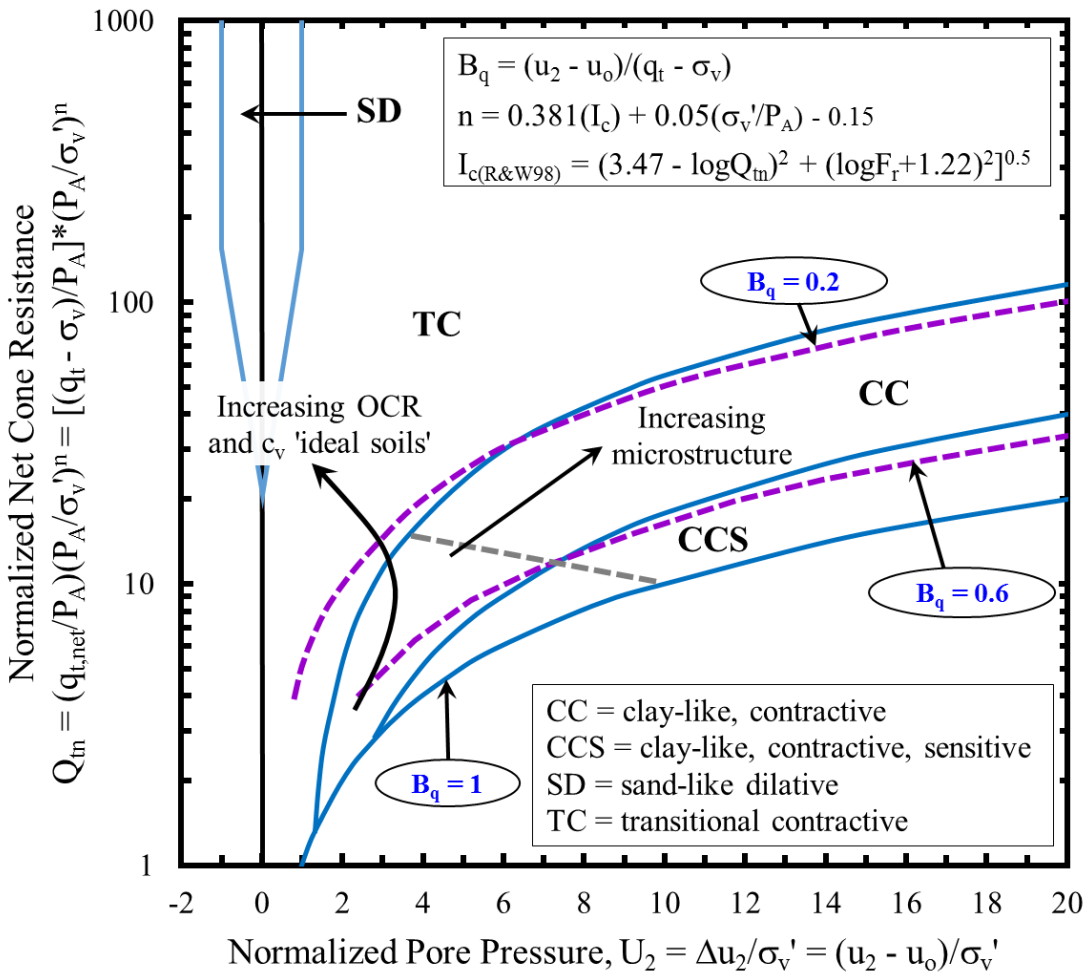

Possible Type of Soil	Range of normalized parameters
Contractive ideal soil	$U_2 > 0$
Dilative ideal soil	$U_2 < 0$
Clay-like dilative ideal soil, CD	$U_2 < 0$; $Q_{tn} > 12$
Clay-like contractive ideal soil, CC	$U_2 > 0$; $Q_{tn} > 12$, or $0.2 < B_q < 0.6$
Clay-like contractive-sensitive ideal soil, CCS	$0.6 < B_q < 1.0$ & $Q_{tn} > 4$
Soils with significant microstructure	Region defined by $U_2 > 0$ with $Q_{tn} = 20$ and $U_2 > 10$ with $Q_{tn} = 10$
Contractive soil with significant microstructure	$U_2 > 4$; $Q_{tn} > 12$

Figure A.36 Q_{tn}–U_2 Schneider (2008; 2012) chart with modified SBT boundaries (adapted from Robertson, 2016).

A.1.30 Salgado et al. (2015) and Ganju et al. (2017) Algorithms for Stratigraphic Profiles

Besides proposing the modified Tumay and the modified Robertson SBT charts, Salgado et al. (2015) and Ganju et al. (2017) also developed novel algorithms for generating stratigraphic soil profile using data from a CPT sounding and a SBT chart. These algorithms allow improved representation of thin layers present within a stratigraphic profile to account for the fact that the conventional CPT sensors cannot accurately sense layers with thickness below a certain limit and a representative cone resistance cannot be obtained if the layer is too thin. The algorithms also prevent the creation of a soil profile with adjacent layers of essentially the same soil by consolidating layers appropriately. The process is iterative, yet it allows improved soil profiling. The discussion herein is limited on the approach since the formal methodology is presented quite comprehensively by Salgado et al. (2015) in the FHWA/IN/JTRP Report # SPR-3408.

A.1.31 Le Doan (2019) SBT Index Assessment Method

Le Doan (2019) showed that $I_{c(R\&W98)}$ in normally consolidated reconstituted or recent deposits can be determined approximately from the following relationship with the normalized CPT end resistance, Q_{tn}, without knowledge of the friction ratio:

$$I_{c(R\&W98)} = 4.2\ {Q_{tn}}^{0.2}\ for\ OCR = 1 \tag{A.18}$$

APPENDIX B TO CHAPTER 2: INSTRUCTIONS FOR THE USE OF SPREADSHEET FOR ESTIMATION OF SOIL VARIABLES FROM CPT RESULTS

B.1 Important Features of the Spreadsheet and Preliminary Verification Step in the Use of the Spreadsheet Template

The spreadsheet has been developed to handle data from a variety of cone penetration testing methods, including the following:

- Seismic Piezocone Penetration Test (SCPTu): q_t, f_s, u_2 or u_1, and V_s
- Seismic Cone Penetration Test (SCPT): q_t, f_s, and V_s
- Piezocone Penetration Test (CPTu): q_t, f_s, and u_2 or u_1
- Cone Penetration Test (CPT): q_t, f_s

These data can be used for convenient interpretation of soil variables from a variety and sets of correlations. The spreadsheet has the capability of converting the measured cone resistance (q_c) to corrected total cone resistance (q_t), provided the net area ratio (a_n) of the cone is known and the shoulder pore pressure (u_2) measurements are recorded. If a type 1 piezocone penetrometer is used for apex or face pore pressures, i.e., u_1 measurements (with filter element placed along the cone tip), the spreadsheet instinctively calculates approximate values of the shoulder pore pressures from a corresponding type 2 piezocone penetrometer, i.e., u_2 readings (which are often needed in many important variables). These conversions are performed using the relationships detailed in Section 2.3.5. With the information of the ground water table (GWT) entered, the spreadsheet calculates the hydrostatic pore pressures. In the case of non-availability of shear wave velocity (V_s) data, which are the basis for estimating soil stiffness parameters often needed in the settlement analysis, the spreadsheet generates their estimates based on the correlations presented in Section 4.3.4.

There are numerous correlations for the estimation of soil parameters that require input of other soil variables in addition to the CPT/CPTu/SCPTu readings. In such cases, a prudent approach is to provide measured values of those soil variables (obtained from laboratory testing of soil samples) as the input. However, in the absence of measured values, the CPT-based estimates of those input variables may be used for the first order approximation of the intended soil parameter. The spreadsheet has been so designed that it picks values from the column titled “measured” (if available) over the CPT-based estimated values as the input variables. However, if no values are entered in the columns titled “measured,” the spreadsheet picks the average of estimated values. To understand what is implied from the term “average”: when multiple correlations provide estimates for the same quantity (or variable), a column averaging those values has been added for each parameter. Figure B.1 shows example of the columns organized in the spreadsheet for estimation of 4 different properties and variables. The first column (highlighted in purple box in Figure B.1) in each case allows entry of the “measured” or laboratory determined values of the quantity at their applicable depths.

The column titled “average” (highlighted in orange box) provides the average of the values calculated from multiple correlations applicable to the soil type. A column titled “selected” (highlighted in blue box) picks value between the column “measured” if available and “average” of the estimated if measure values are not available.

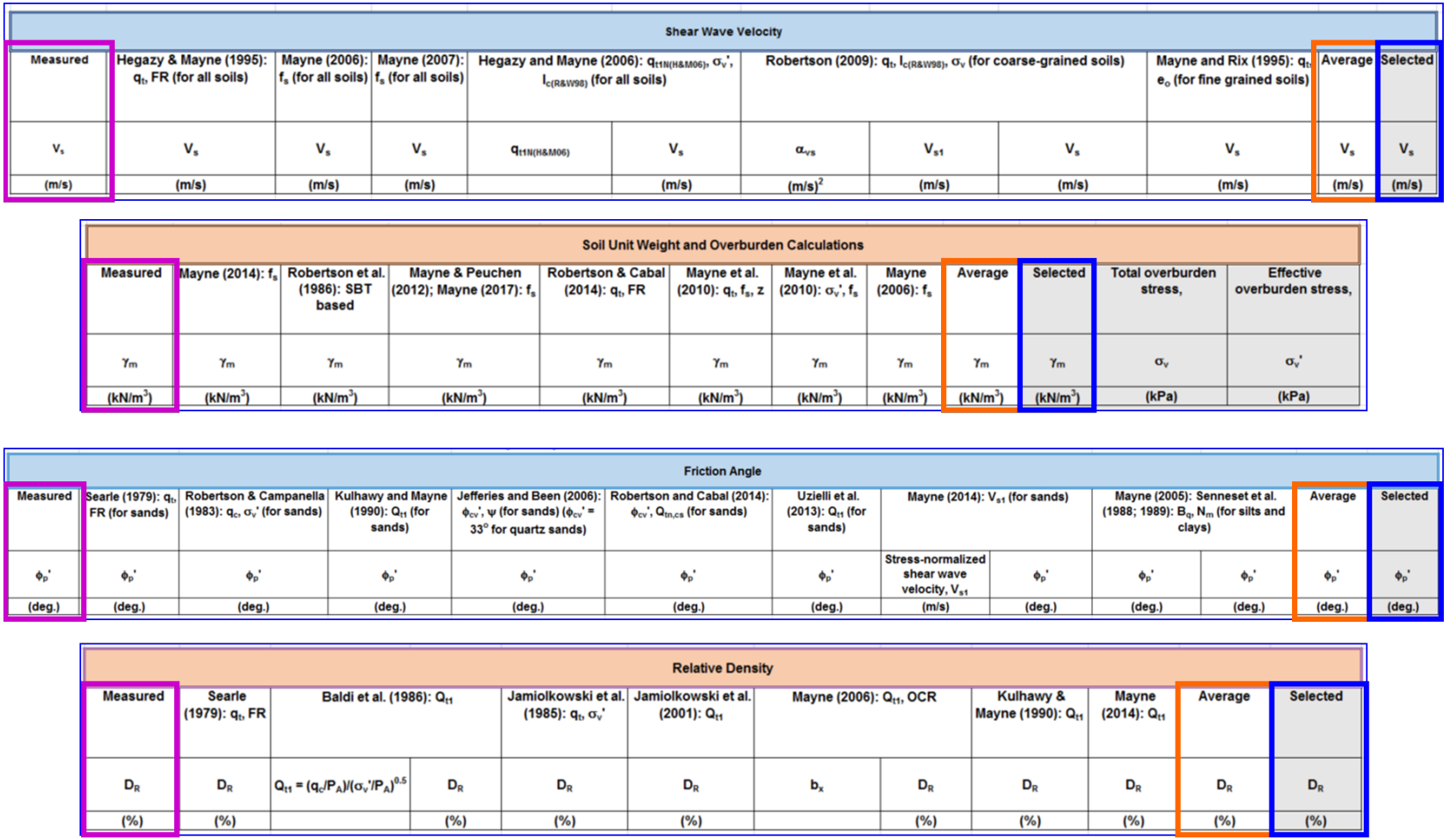

Figure B.1 Sample of the set of columns in the spreadsheet template.

Certain CPT-based correlations were developed solely from the cohesive soils data, while few others were based on cohesionless soils. The spreadsheet has been so formulated that it identifies the soil type based on the soil behavior type (SBT) classification systems, and accordingly picks the applicable correlation to estimate the intended soil variable. Similarly, there are variables that are properties purely of cohesionless soils (e.g., relative density, D_R), while other are fundamentally relevant to cohesive soils (e.g., undrained shear strength, s_u and soil sensitivity, S_t). In the manner mentioned above, the applicable parameters are estimated based on the SBT classification and are not calculated for the soil types to which those do not apply.

In addition to the complete set of calculations for estimation of different soil variables, the spreadsheet also plots the complete profiles of CPT/CPTu/SCPT/SCPTu readings, and each variable versus depth in both Imperial as well as Metric units.

In developing this spreadsheet, the logic functions [e.g., nested IF(), IFNA(), IF(AND()), IF(OR())] were frequently used. In some cases, circular references had to be given to the output and input parameters for correct implementation of the correlation of the variable/parameter. It is, therefore, important that the "enable iterative calculation" in the formula option of Excel file settings is checked. Figure B.2 explains how this must be verified and confirmed before using the template for each new set of CPT data interpretations.

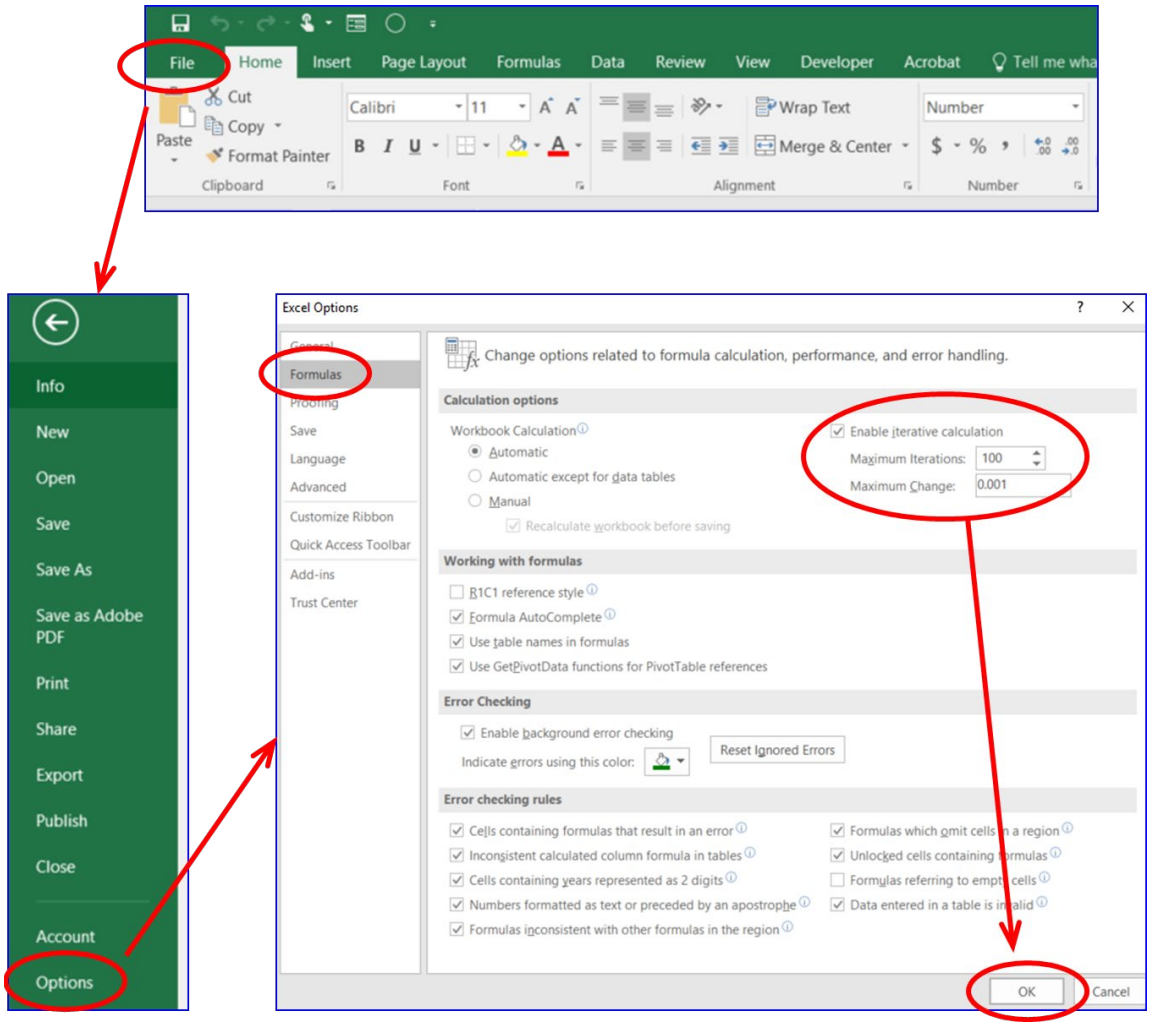

Figure B.2 Step for verification that iterative calculations are enabled in the template.

B.2 Spreadsheet Format

The Microsoft Excel file titled "Template_Soil_Parameters_Ch_2_Vol._1" contains five sheets, namely (also see Figure B.3):

- Data Input
- Postprocessing (Metric)
- Plots & Graphs (Metric)
- Postprocessing (Imperial)
- Plots & Graphs (Imperial)
- Supplementary data

The sheet titled "Data Input," also displayed in Figure B.3, is where the data must be entered in either metric or imperial units in a certain format via method explained in Section B.3 below. The next sheet "Postprocessing (Metric)" is where the calculations of the values of each variable are formulaically and methodically calculated by simply reproducing the formulas row down to the last row of the CPT data entry (see Figure B.4 for a screen capture of the sheet). The sheet "Postprocessing (Imperial)" provides the same set of information as "Postprocessing (Metric), except that the values are all calculated and displayed in Imperial units (see Figure B.5 for a screen capture). The corresponding sets of graphs and plots of CPT readings as well as all interpreted variables/parameters versus depth in Metric and Imperial units are synchronously plotted on the sheets titled "Plots & Graphs (Metric)" and "Plots & Graphs (Imperial)," respectively (see Figure B.6 through Figure B.13 for the sample screen captures). The last sheet "Supplementary data" has the data necessary for design graphs and charts in other sheets.

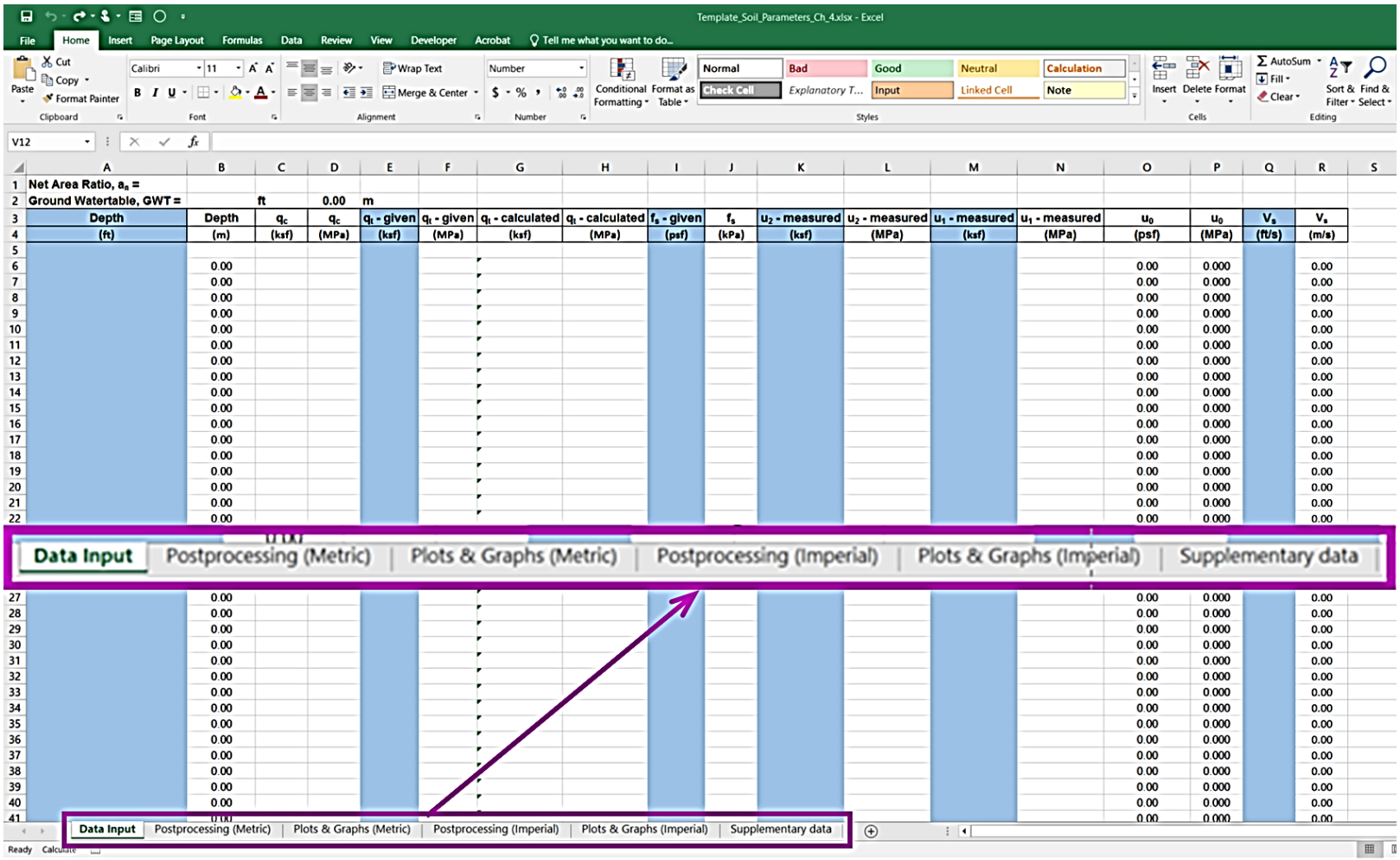

Figure B.3 A screen capture of the spreadsheet template showing its five different sheets (the displayed image is the data input sheet, showing all the entry columns).

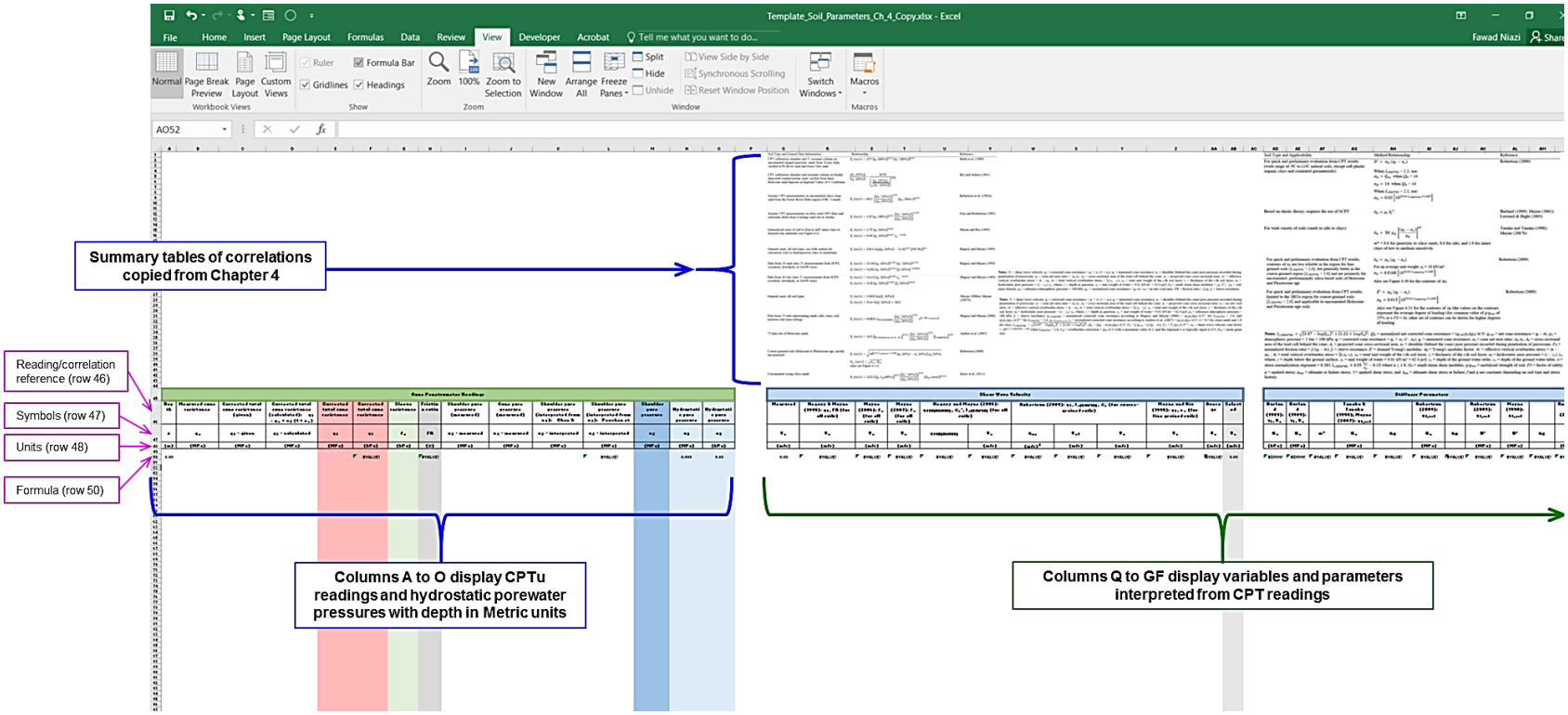

Figure B.4 A screen capture of the “Postprocessing (Metric)” sheet showing samples of its different parts.

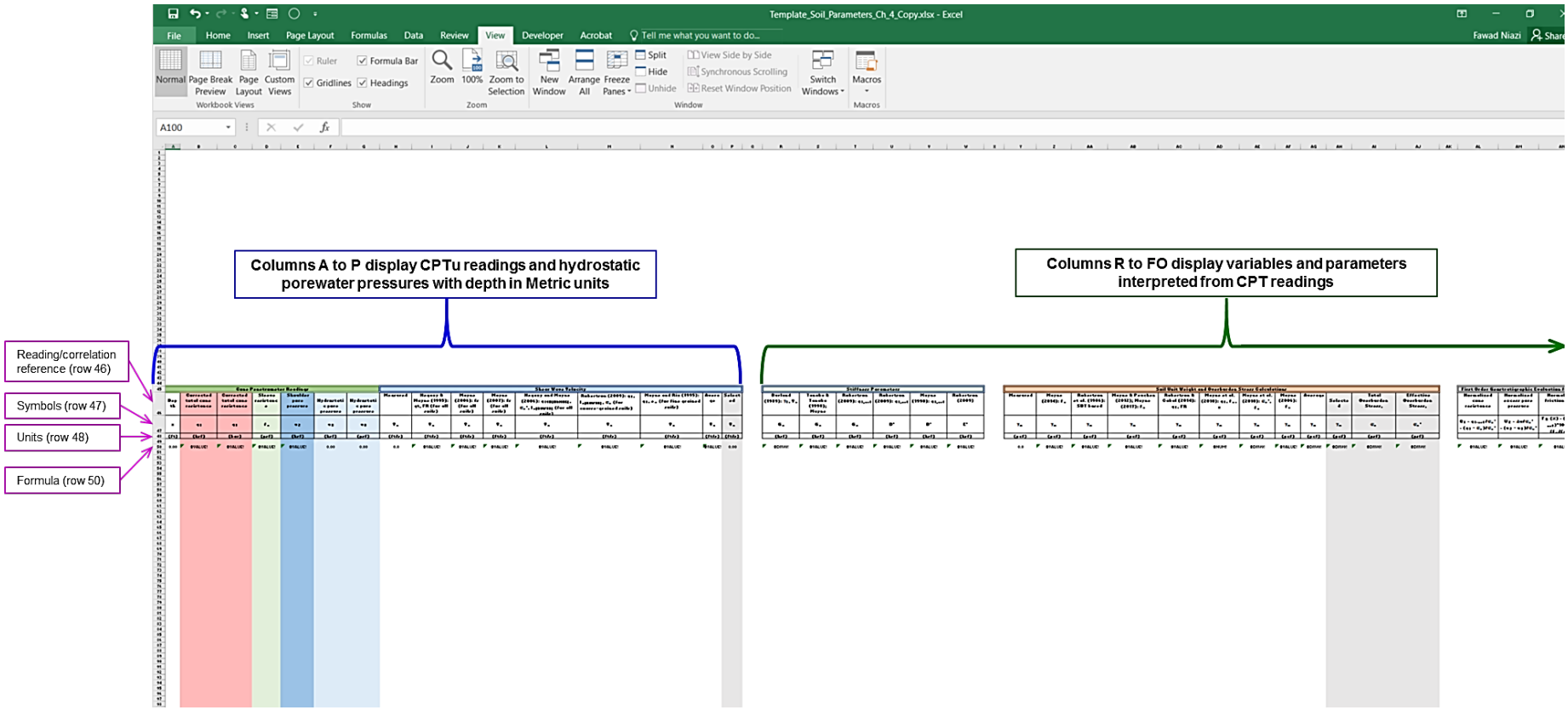

Figure B.5 A screen capture of the “Postprocessing (Imperial)” sheet showing samples of its different parts.

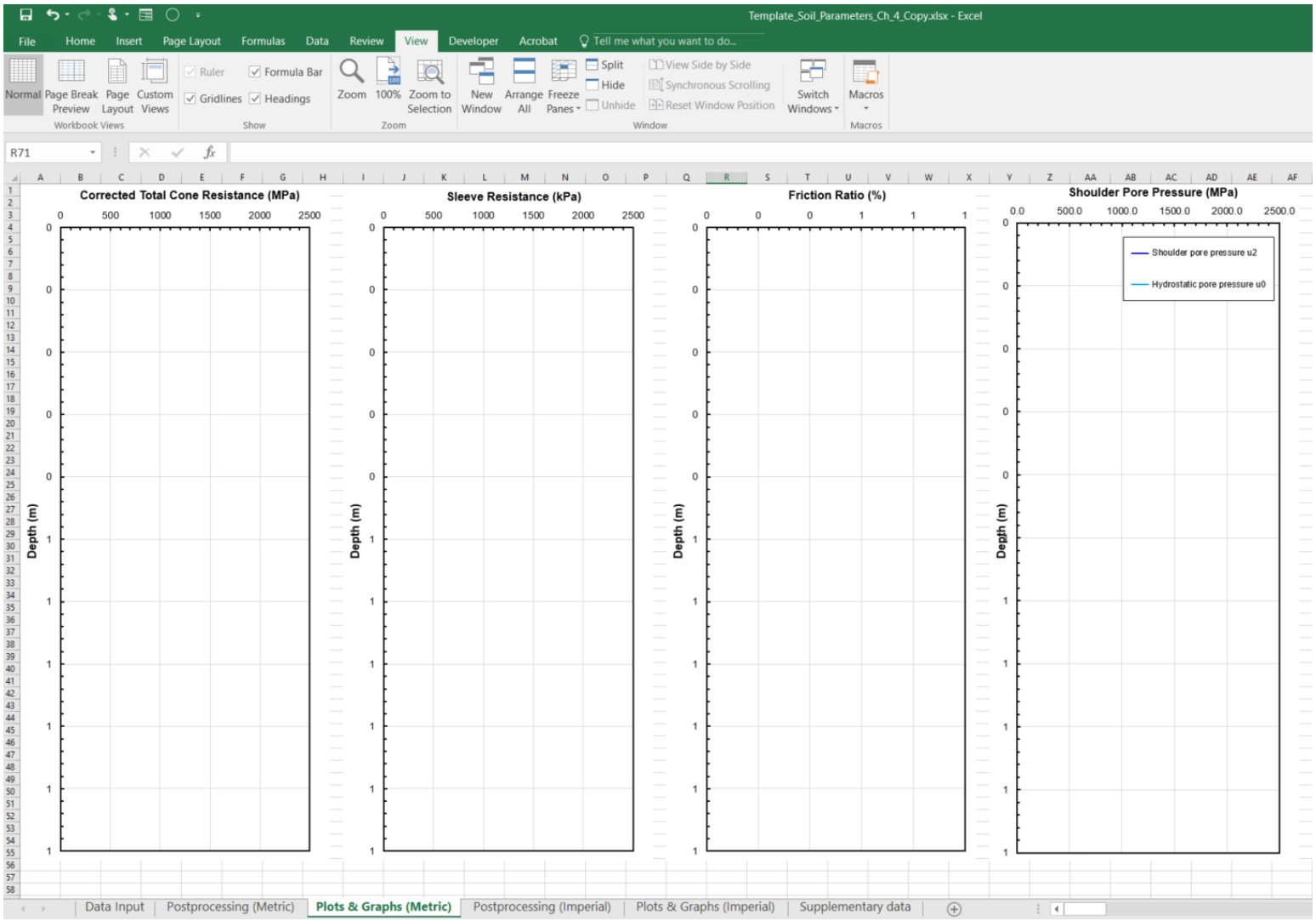

Figure B.6 A screen capture of the “Plots & Graphs (Metric)” sheet showing profiles of CPT data.

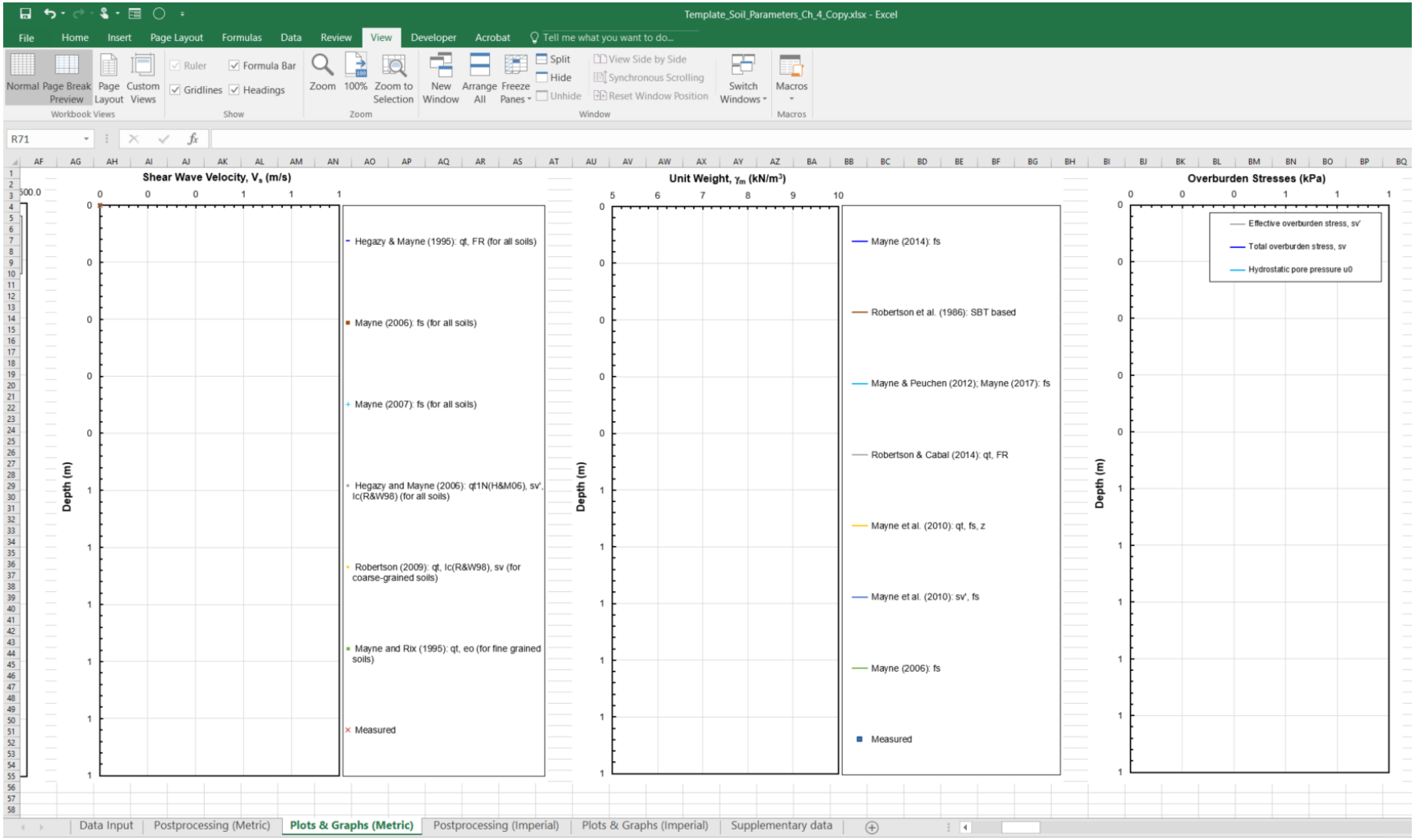

Figure B.7 A screen capture of the "Plots & Graphs (Metric)" sheet showing profiles of interpreted soil variables.

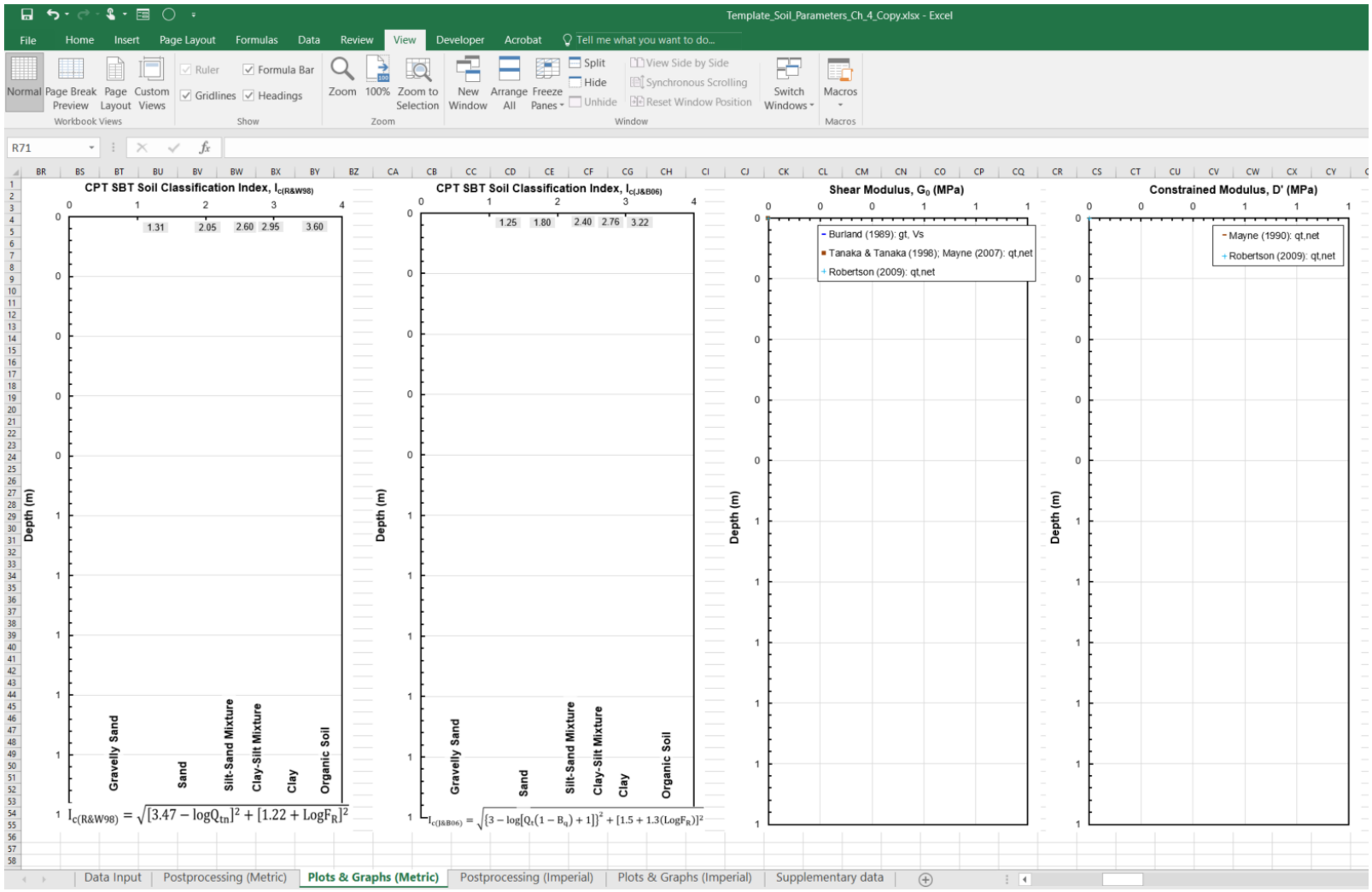

Figure B.8 A screen capture of the "Plots & Graphs (Metric)" sheet showing profiles of SBT classification and interpreted soil variables.

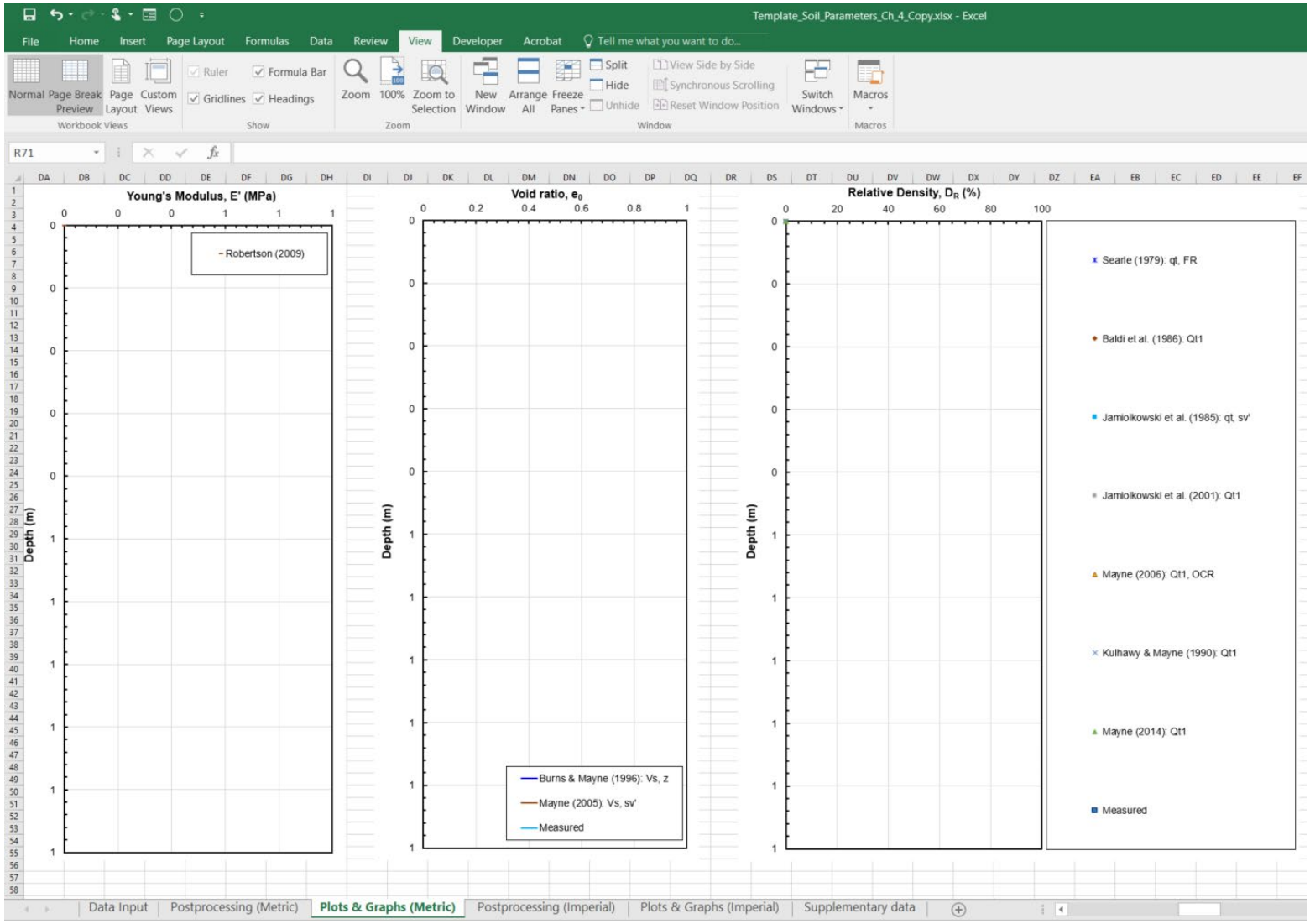

Figure B.9 A screen capture of the "Plots & Graphs (Metric)" sheet showing profiles of interpreted soil variables.

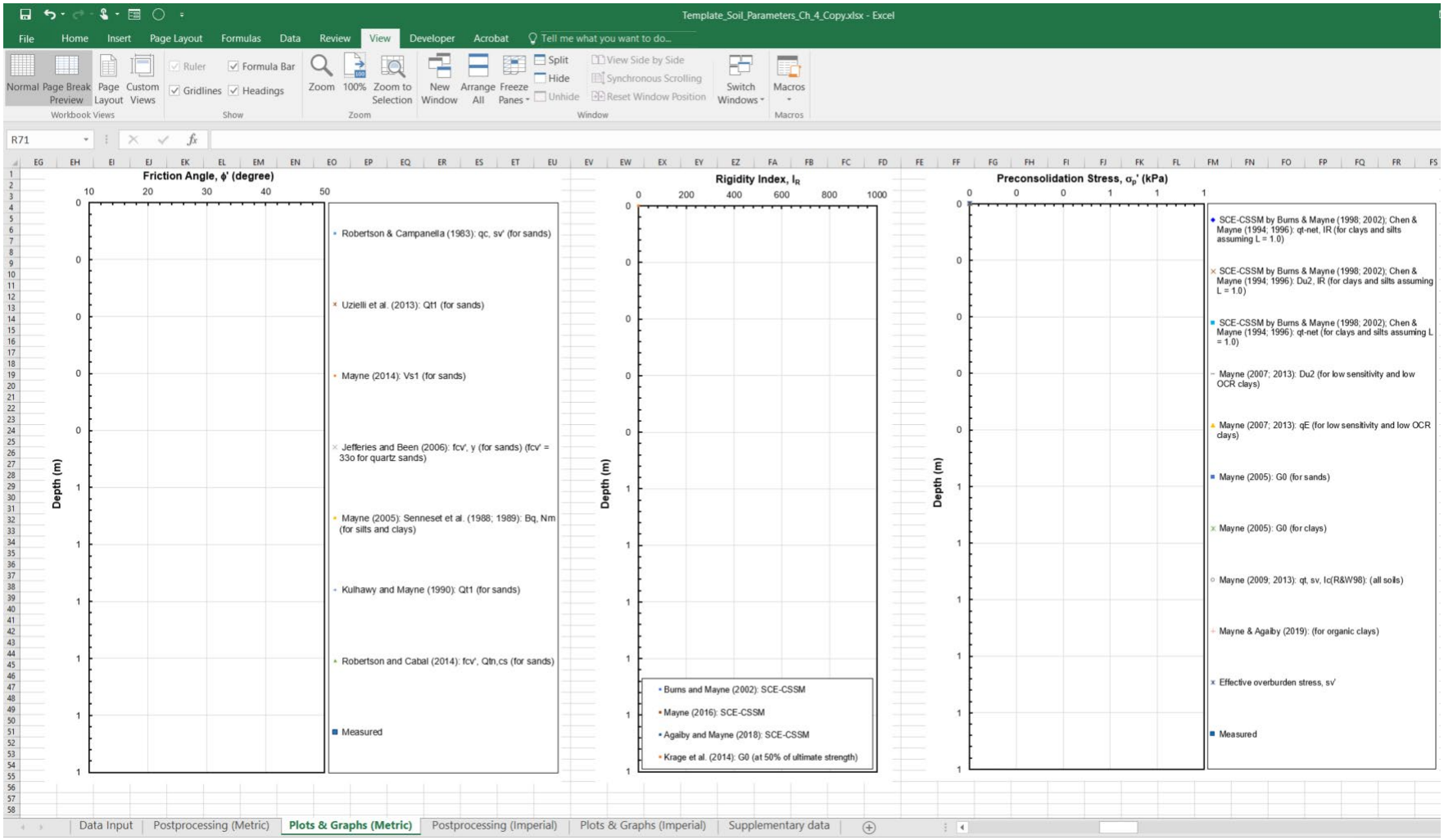

Figure B.9 A screen capture of the "Plots & Graphs (Metric)" sheet showing profiles of interpreted soil variables (continued).

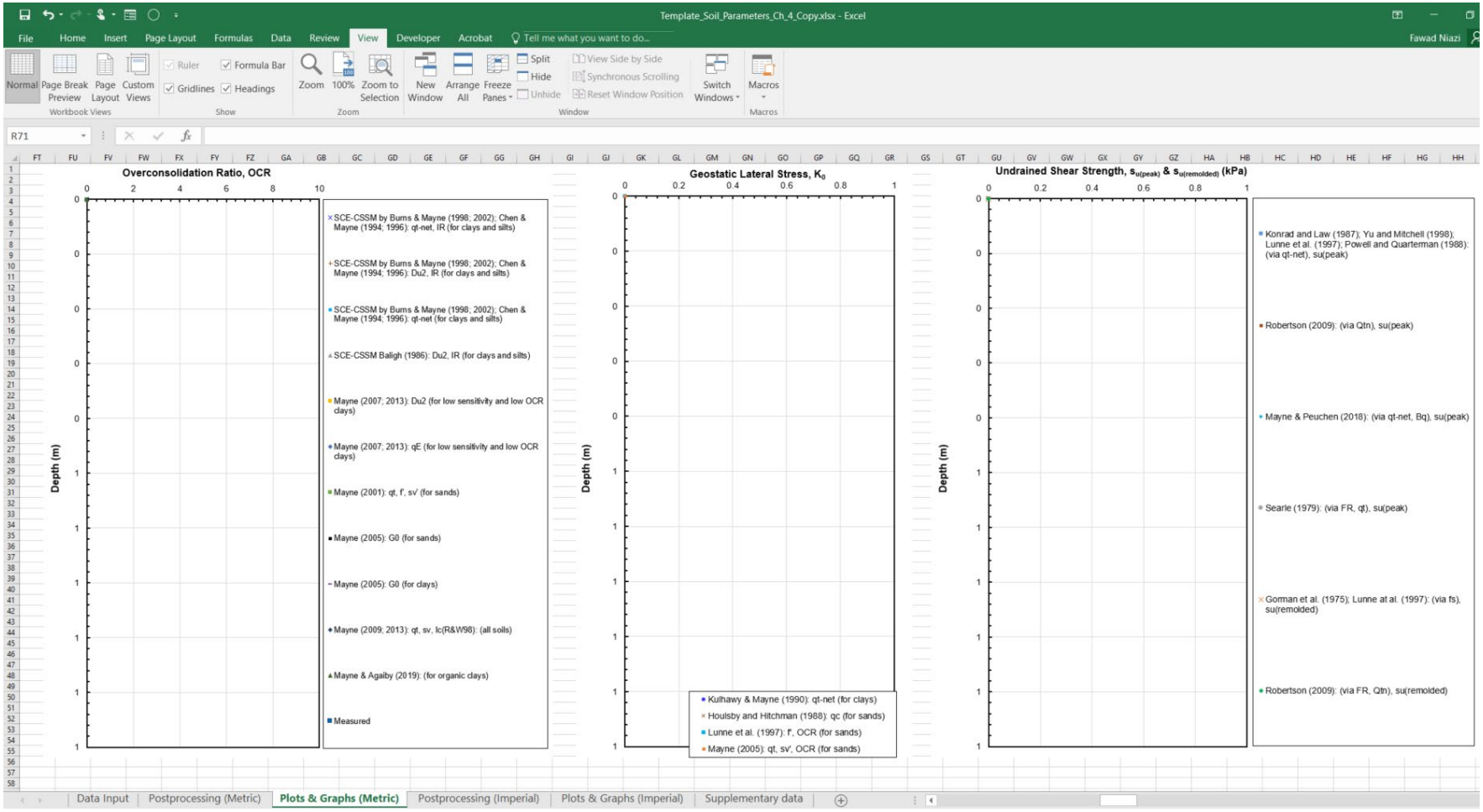

Figure B.9 A screen capture of the "Plots & Graphs (Metric)" sheet showing profiles of interpreted soil variables (continued).

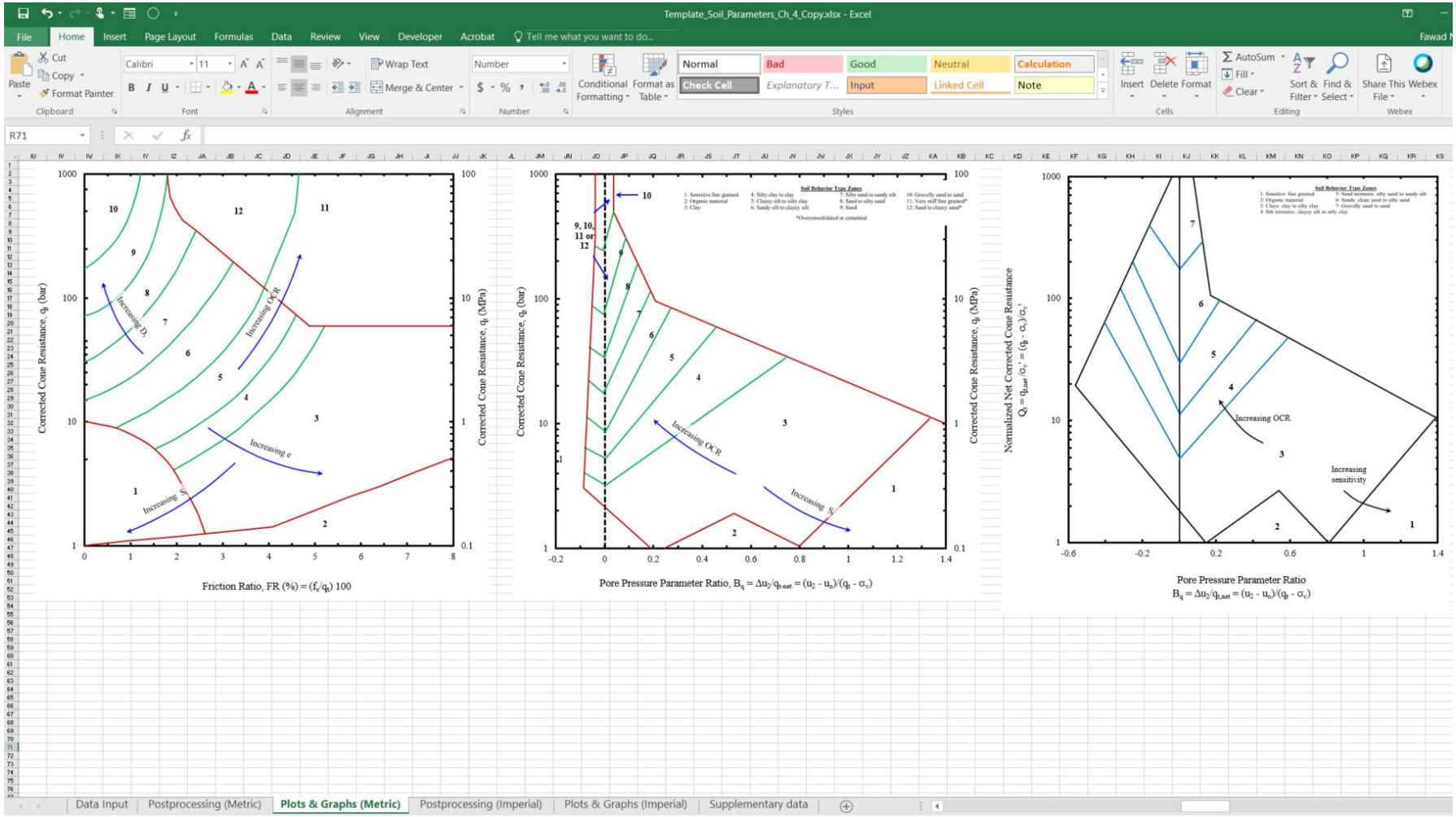

Figure B.10 A screen capture of the "Plots & Graphs (Metric)" sheet showing CPT-based SBT classification.

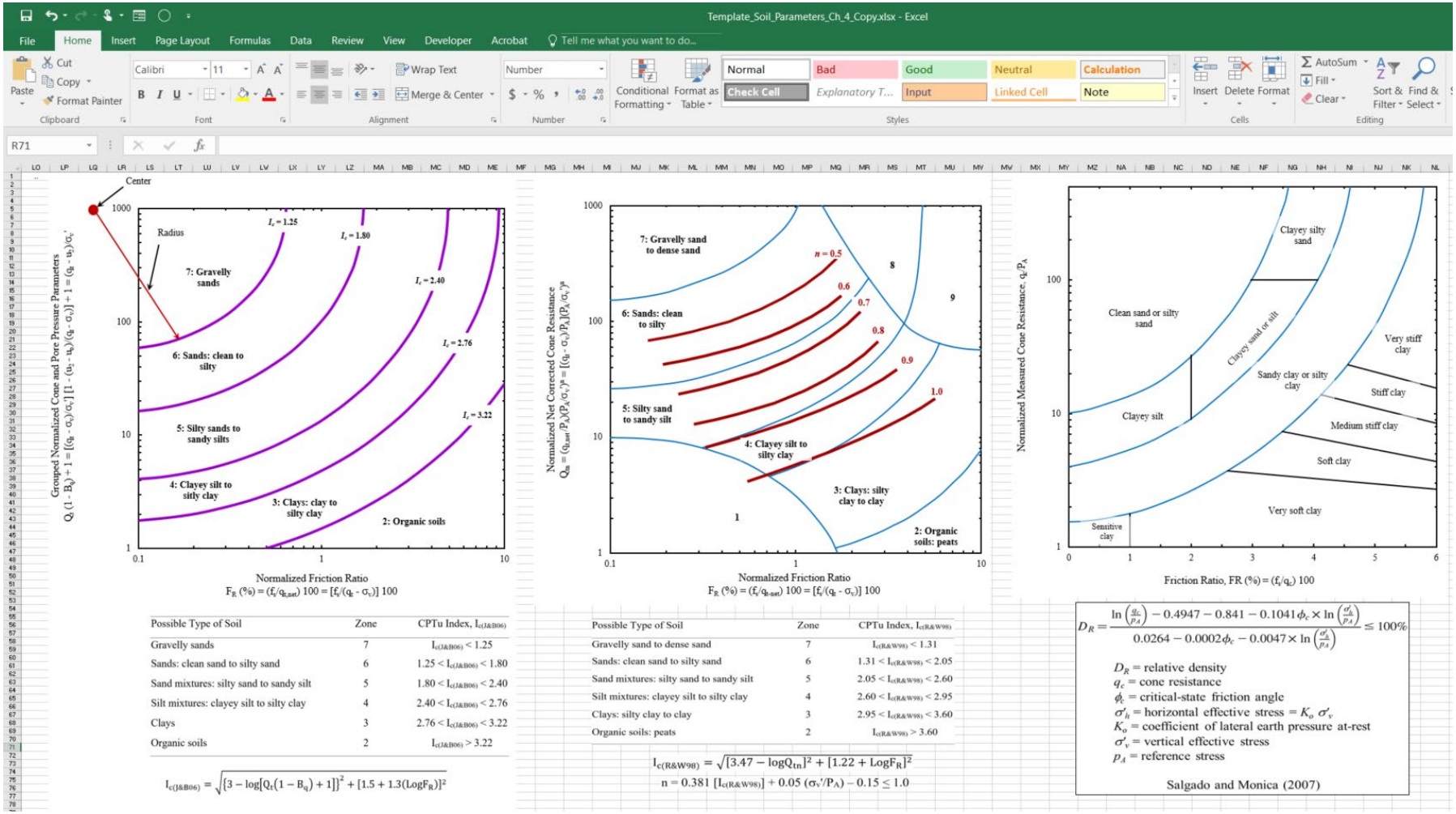

Possible Type of Soil	Zone	CPTu Index, $I_{c(J\&B06)}$
Gravelly sands	7	$I_{c(J\&B06)} < 1.25$
Sands: clean sand to silty sand	6	$1.25 < I_{c(J\&B06)} < 1.80$
Sand mixtures: silty sand to sandy silt	5	$1.80 < I_{c(J\&B06)} < 2.40$
Silt mixtures: clayey silt to silty clay	4	$2.40 < I_{c(J\&B06)} < 2.76$
Clays	3	$2.76 < I_{c(J\&B06)} < 3.22$
Organic soils	2	$I_{c(J\&B06)} > 3.22$

$$I_{c(J\&B06)} = \sqrt{[3 - \log[Q_t(1 - B_q) + 1]]^2 + [1.5 + 1.3(\log F_R)]^2}$$

Possible Type of Soil	Zone	CPTu Index, $I_{c(R\&W98)}$
Gravelly sand to dense sand	7	$I_{c(R\&W98)} < 1.31$
Sands: clean sand to silty sand	6	$1.31 < I_{c(R\&W98)} < 2.05$
Sand mixtures: silty sand to sandy silt	5	$2.05 < I_{c(R\&W98)} < 2.60$
Silt mixtures: clayey silt to silty clay	4	$2.60 < I_{c(R\&W98)} < 2.95$
Clays: silty clay to clay	3	$2.95 < I_{c(R\&W98)} < 3.60$
Organic soils: peats	2	$I_{c(R\&W98)} > 3.60$

$$I_{c(R\&W98)} = \sqrt{[3.47 - \log Q_{tn}]^2 + [1.22 + \text{LogF}_R]^2}$$
$$n = 0.381\,[I_{c(R\&W98)}] + 0.05\,(\sigma_v'/P_A) - 0.15 \le 1.0$$

$$D_R = \frac{\ln\left(\frac{q_c}{p_A}\right) - 0.4947 - 0.841 - 0.1041\phi_c \times \ln\left(\frac{\sigma_h'}{p_A}\right)}{0.0264 - 0.0002\phi_c - 0.0047 \times \ln\left(\frac{\sigma_h'}{p_A}\right)} \le 100\%$$

D_R = relative density
q_c = cone resistance
ϕ_c = critical-state friction angle
σ'_h = horizontal effective stress = $K_o\,\sigma'_v$
K_o = coefficient of lateral earth pressure at-rest
σ'_v = vertical effective stress
p_A = reference stress

Figure B.10 A screen capture of the "Plots & Graphs (Metric)" sheet showing CPT-based SBT classification (continued).

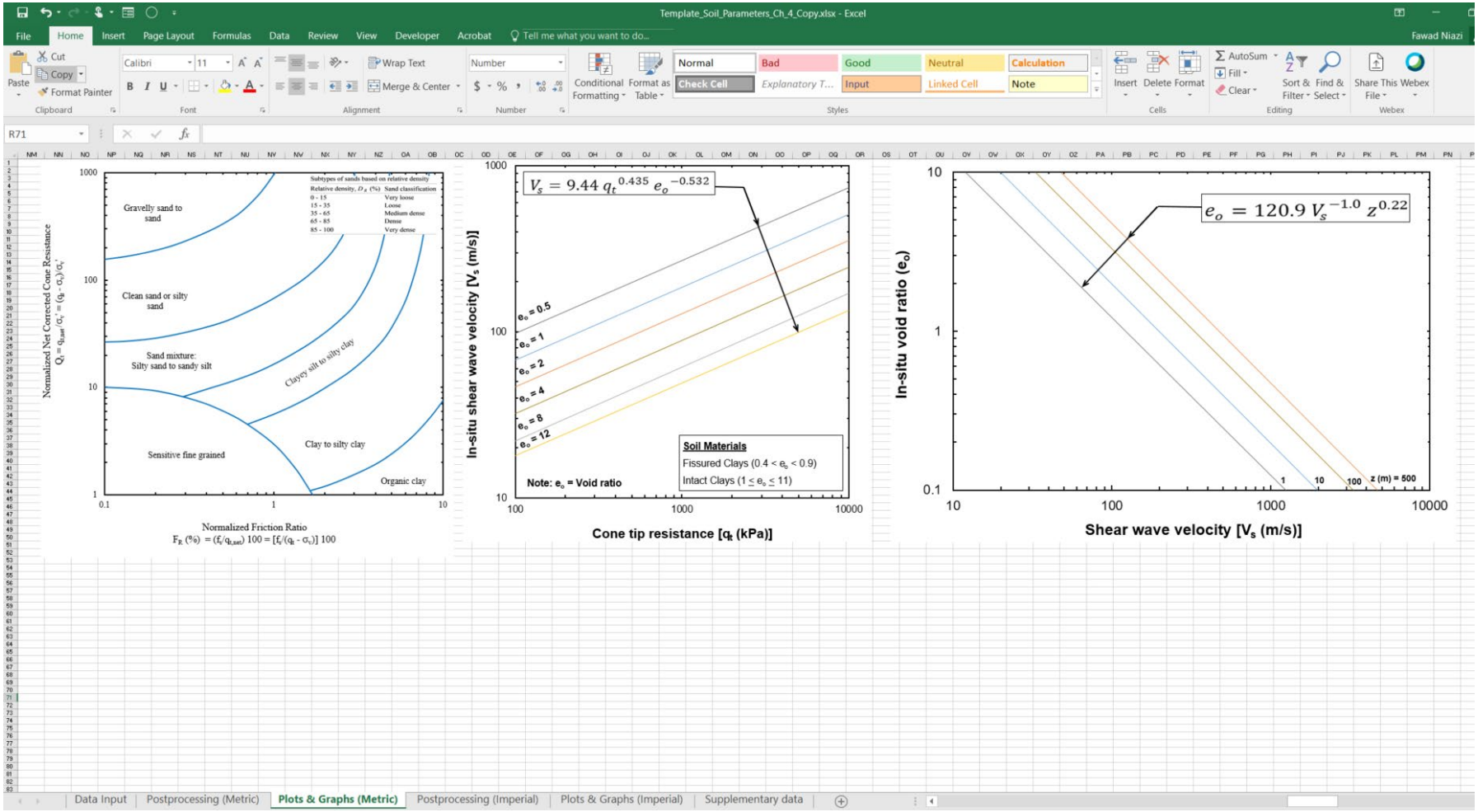

Figure B.11 A screen capture of the "Plots & Graphs (Metric)" sheet showing CPT-based SBT classification and interpreted variables based on CPT data.

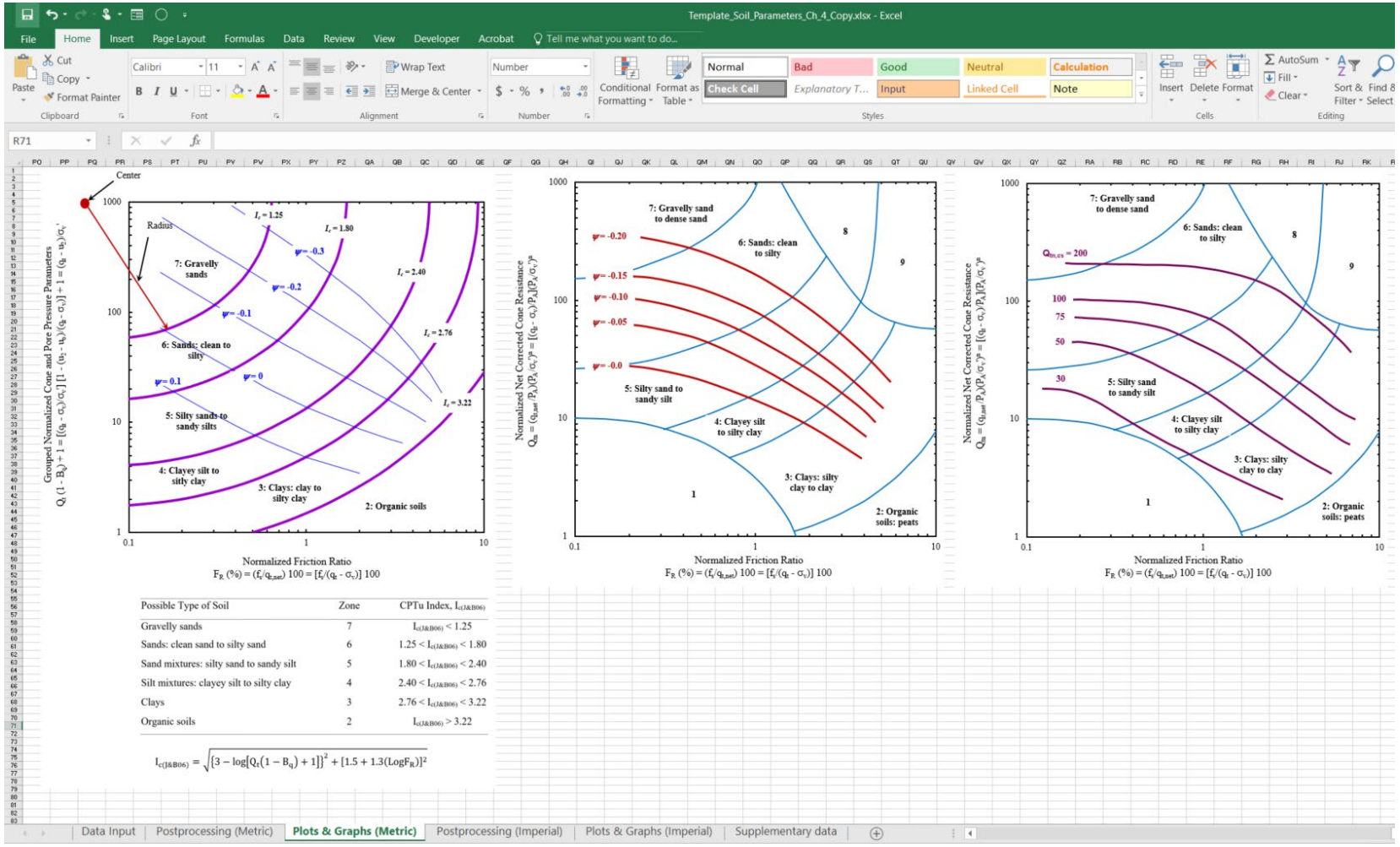

Figure B.12 A screen capture of the "Plots & Graphs (Metric)" sheet showing interpreted variables based on CPT-based SBT classification.

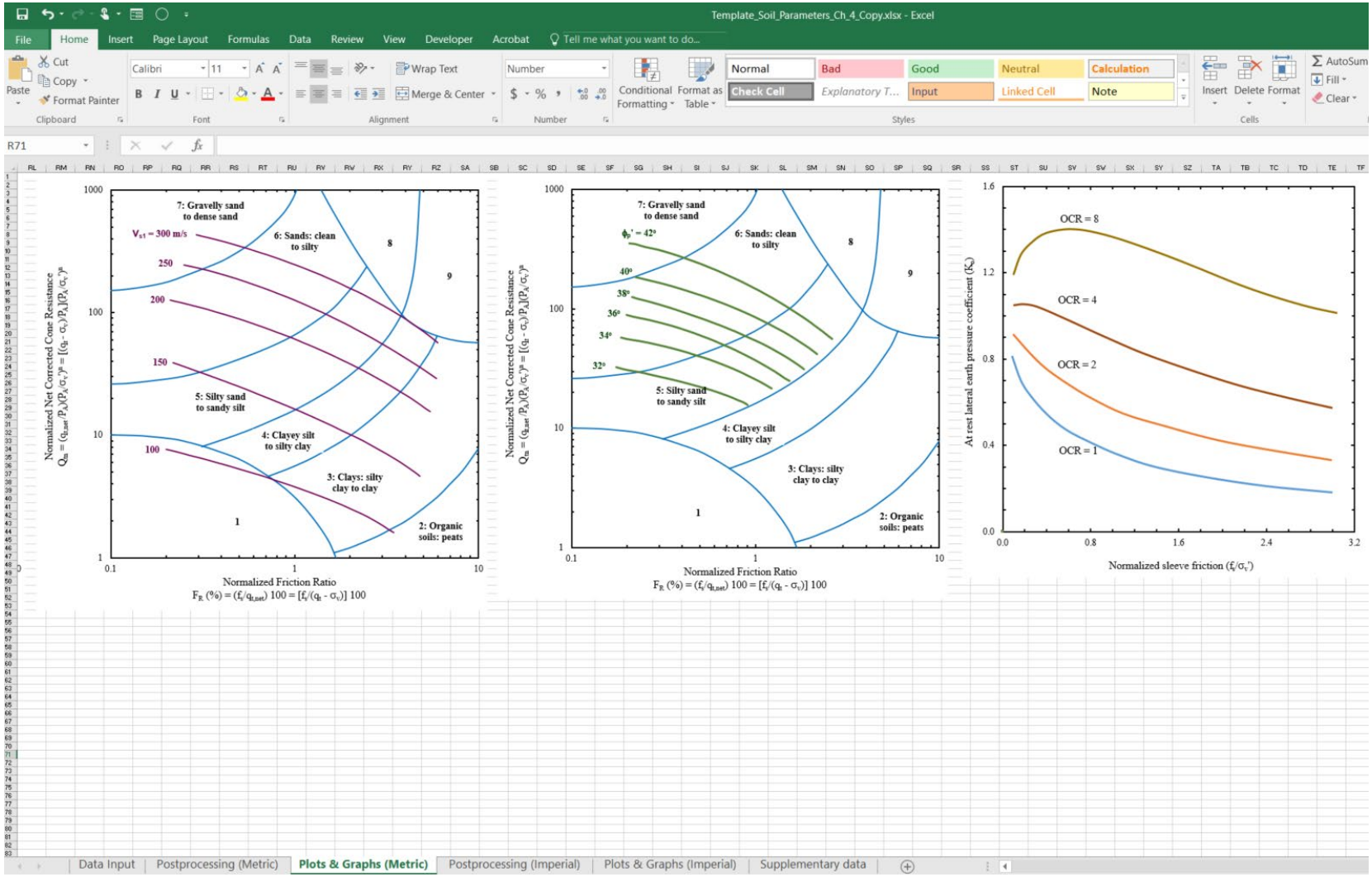

Figure B.12 A screen capture of the "Plots & Graphs (Metric)" sheet showing interpreted variables based on CPT-based SBT classification (continued).

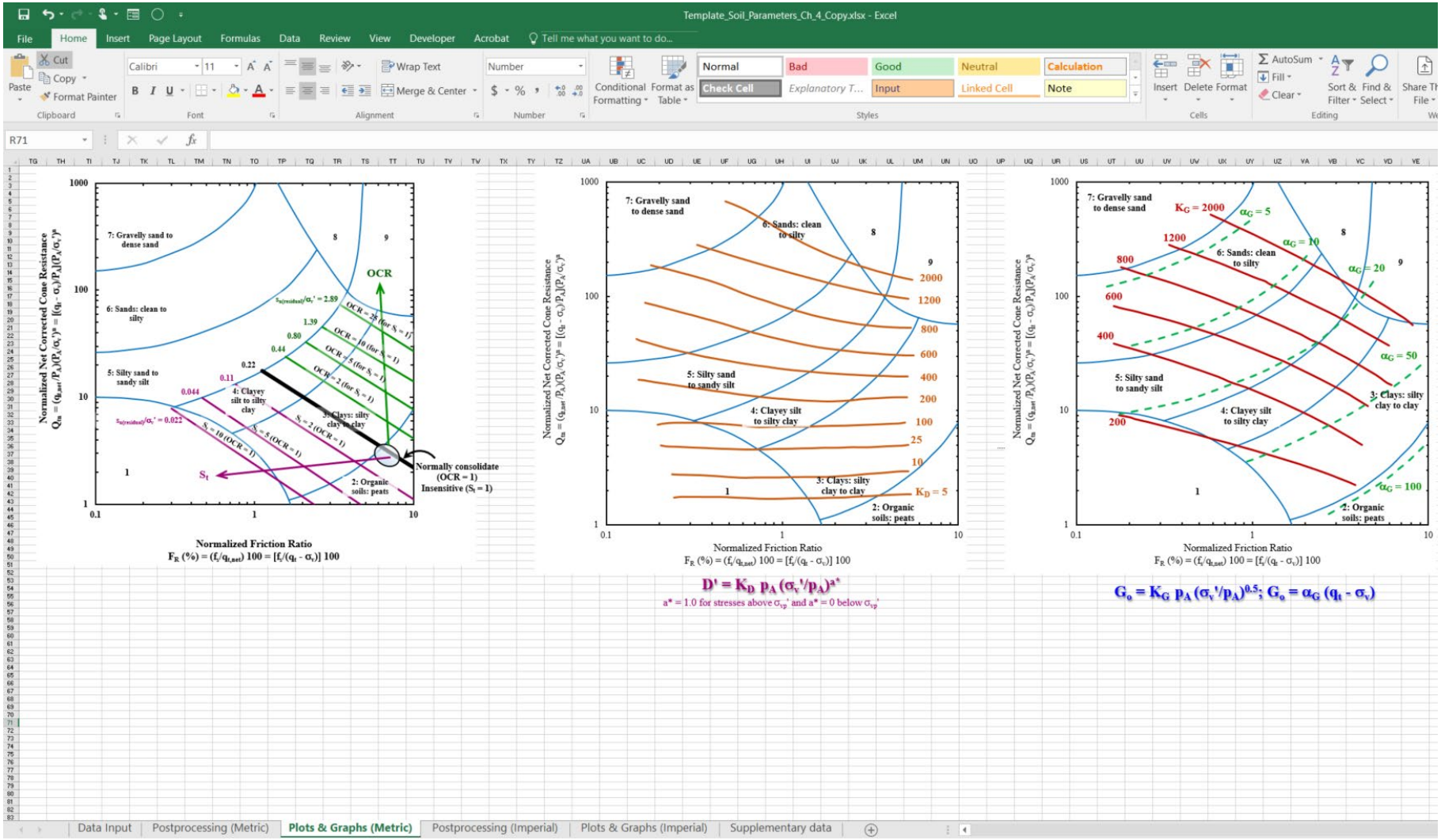

Figure B.12 A screen capture of the "Plots & Graphs (Metric)" sheet showing interpreted variables based on CPT SBT classification (continued).

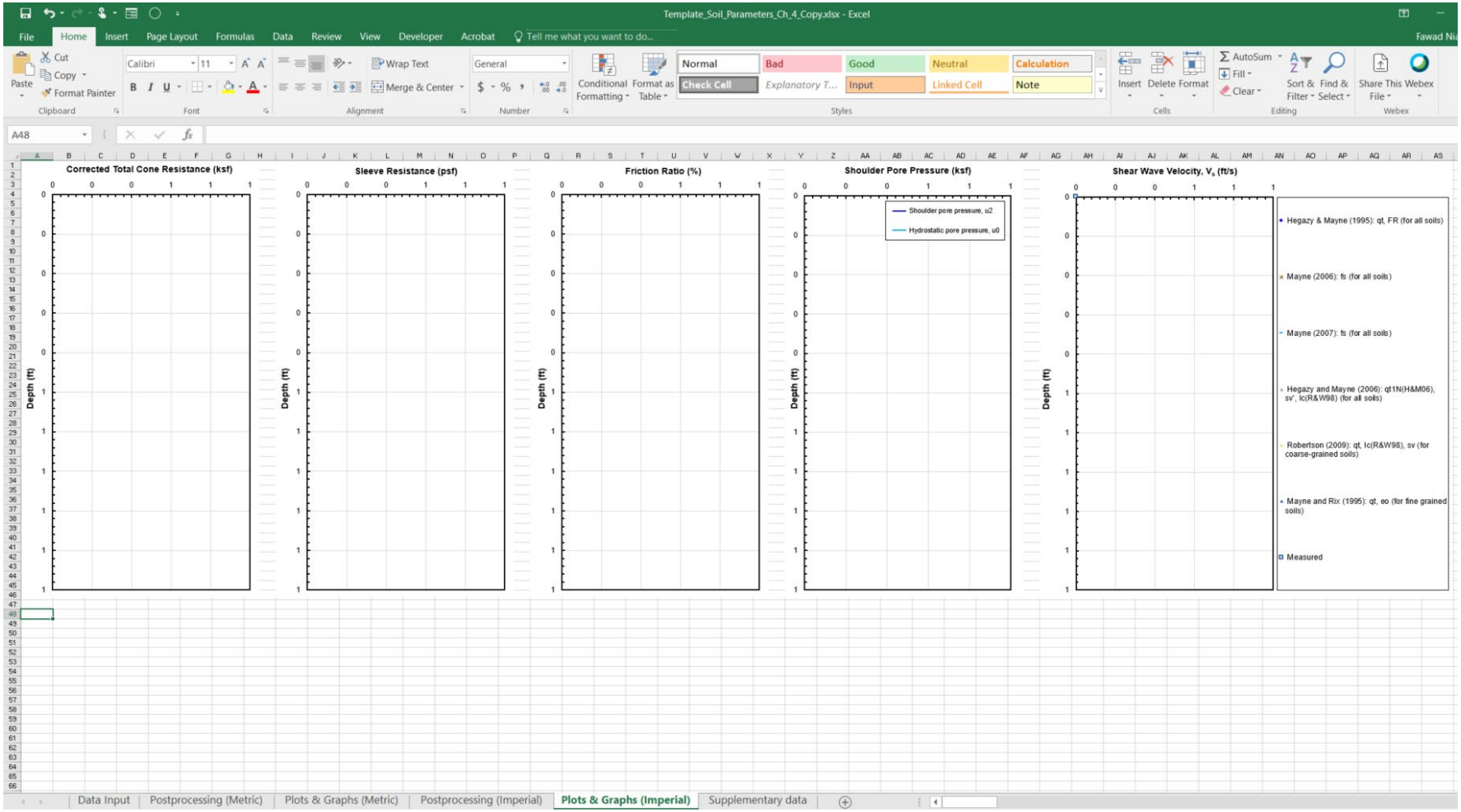

Figure B.13 A screen capture of the "Postprocessing (Imperial)" sheet showing profiles of CPT data.

B.3 Steps for the Use of Template

The sheet titled "Data Input" is the starting point in use of the template for interpretation of the CPT data. The data may be entered in metric or imperial units in the manner explained in this subsection. The simplified steps are listed below, along with explanatory figure for each step.

1. Create a copy the file "Template_Soil_Parameters_Ch_2_Vol._1.xlsx" and rename it according to the site and CPT sounding number.
2. Open the first sheet "Data Input" and enter the data as below (refer to Figure B.3 for cell and column numbers cited below).
    a. Enter the value of net area ratio (a_n) in the cell B1 if available; otherwise leave it blank.
    b. Enter the information of ground water table (GWT) in cell B2 in the units of feet below the ground surface.
    c. Enter the values of depth (in the unit of feet) starting from cell number A6. The depth entries may be copied from source file and pasted into column A, starting with cell number A6 in a single step. The spreadsheet will convert those depth values from feet into meters in corresponding cells of column B. If the depth data are in the unit of meter, leave column A blank and enter depth data in column B, starting from cell B6 down to the maximum recorded depth.
    d. If cone resistance data is available without correction for unequal cone area (i.e., if it is available as q_c instead of q_t) in imperial units of kips per square foot (ksf), enter those in column C, starting from cell number C6. If the units are some different imperial units, convert those to ksf. The spreadsheet will convert q_c from ksf to metric units of Mega Pascals (MPa) in the corresponding cells of column D. If corrected cone resistance (q_t) data is available instead of q_c, leave column C blank, and enter q_t values in column E (titled as "q_t –given") in the units of ksf starting from cell number E6. The spreadsheet will convert q_t from ksf to MPa in the corresponding cells of column F. Lastly, if along with q_c data, the shoulder pore pressure (u_2) data are also available along with the net area ratio (a_n) and those are entered in their respective cells/columns, the spreadsheet will calculate corresponding q_t values in column G (in ksf) and in column H (in MPa), both titled as "q_t – calculated."
    e. Enter sleeve resistance (f_s) data in column I in imperial units of pounds per square foot (psf), starting from cell number I6. The spreadsheet will convert f_s from psf to kPa in the corresponding cells of column J. If the data are available in metric units of kPa, column I should be kept blank and f_s data should be entered in column J, starting from cell number J6.
    f. Enter shoulder pore pressure (u_2) data in the units of ksf in column K, titled "u_2 – measured" starting from cell number K6. The spreadsheet will convert u_2 from ksf to MPa in the corresponding cells of column

L. If the data are available in metric units of MPa, column K should be kept blank and u_2 data should be entered in column L, starting from cell number L6.

g. If the pore pressures are measured via the filter element place at the cone tip (i.e., if u_1 readings are collected) instead of shoulder u_2 readings, columns K and L should be left blank. Enter the apex or midface pore pressure (u_1) data in the units of ksf in column M, titled "u_1 – measured" starting from cell number M6. The spreadsheet will convert u_1 from ksf to MPa in the corresponding cells of column N. If the data are available in metric units of MPa, column M should be kept blank and u_1 data should be entered in column N, starting from cell number N6.

h. The next two columns, O and P of the spreadsheet, calculate and provide hydrostatic pore pressures corresponding to each row of the depth in the imperial unit (psf) and in the metric unit (MPa), respectively. These calculations are based on the unit weight of water (i.e., 62.43 pcf), the information of the GWT entered in cell number B2 and the depth entry in a corresponding row of columns A and B, respectively.

i. If shear wave velocity (V_s) data are available from a SCPT/SCPTu sounding, it should be entered in the unit of feet/second (ft/s) in column Q, starting from cell number Q6. The spreadsheet will convert V_s from ft/s to meter per second (m/s) in the corresponding cells of column R. If the data are available in metric units of m/s, column Q should be kept blank and V_s data should be entered in column R, starting from cell number R6.

j. It may be noted that the V_s data are acquired at a typical interval of 1 m, whereas the penetrometer readings are obtained at a much higher frequency as the CPT probe penetrates into the ground. To handle this discrepancy in the reading's interval, V_s measurements recorded for a certain depth is considered applicable over a one-meter interval with the starting depth half meter above and ending depth half meter below the depth of actual measurement. Where the V_s measurement interval is different than 1 m, the V_s reading may be considered applicable half-way above and half-way below the actual measurement depth with reference to the two adjacent readings (the one above and the one below, respectively). A manual entry and depth assessment is needed for this important step.

k. See example data entered from a SPCTu sounding in Figure B.14, where all 6 sets of readings are available: GWT, depth, q_t, f_s, u_2, and V_s.

3. When the data entry is complete in the "Data Input" sheet, note the total number of rows (say, X) in which data was entered in the above steps.
4. Then, open the next sheet "Postprocessing (Metric)." Here the values of CPT/CPTu/SCPT/SCPTu readings from the row 6 of "Data Input" can be seen

already transferred synchronously in cell number 50 of columns A to Q. Similarly, all the interpretations of different soil variables, parameters and SBT classification indices and soil types can also be seen in cell number 50 of columns R to GF.

5. For the next step, do either of the following to completely populate/fill the desired postprocessed data: (1) select the entire row 50 (i.e., from A50 to GF50), copy these cells and paste in cells A51 to [GF51 + (X – 1)]; or (2) select the entire set of cells (i.e., from cells A50 to [GF51 + (X – 1)]), then click "Home" > "Fill," and choose "Down" (see Figure B.15), or press Ctrl+D. This will transfer complete set of data in the metric units from "Data Input" sheet to "Postprocessing (Metric)" sheet and also transfer the formulas from row 50 down to the row of the maximum depth of CPT sounding in the "Postprocessing (Metric)" sheet.
6. As shown in Figure B.15, row 50 indicates error in the formula. This is because many correlations are based on the Robertson (2009) SBT classification system determined in columns BL to BO, which require circular reference between Q_{tn} (column BL), n (column BM), and $I_{c(R\&W98)}$ (column BN). This necessitates an additional step of refreshing of the formulas in those columns. Therefore, after performing step 5 above, the following should be done.
7. Double click in cell BM50 of "Postprocessing (Metric)" sheet; this will display the formula (see Figure B.16a), and simply press "Enter" for the value of "n" to be displayed. Then do the same for BN50 (see Figure B.16b) for $I_{c(R\&W98)}$ value to be displayed. This will also display the values of Q_{tn}, n, $I_{c(R\&W98)}$, and soil type in cells BL50, BM50, BN50, and BO50, respectively (see Figure B.16c). For these 4 columns, perform the procedure detailed in step 5 above to populate/fill the results in all rows representing the complete depth of CPT sounding (see Figure B.16d).
8. If the laboratory measured/determined values of any of the following variables/parameters are known based on testing of the soil samples obtained from soil borings at the site, those should be entered in the appropriate columns of the sheet "Postprocessing (Metric)," following the approach described for shear wave velocity (V_s) in point 2j above. These column letters are also shown listed below for each parameter.
    a. Soil unit weight, γ_m (column AP)
    b. Void ratio, e_0 (column BT)
    c. Effective friction angle, ϕ' (column CF)
    d. Effective preconsolidation stress, σ_{vp}' (column CT)
    e. Overconsolidation ratio, OCR (column DI)
    f. Relative Density, D_R (column EI)
9. With the implementation of the above steps, the post processing of CPT data in metric units is completed, and all graphs and plots in the sheet "Plots & Graphs (Metric)" will concurrently generate as soon as that sheet is opened (see Figure B.17 to Figure B.21 for sample graphs).

10. For imperial units, the procedure is much straight forward, provided the above steps have been completed. Simply follow the approach described in step 5 above to the sheet “Postprocessing (Imperial).” This will result in complete postprocessing of CPT data for determining the soil variables and parameters in imperial units, and for plotting the graphs and plots in those units in the sheet “Plots & Graphs (Imperial).”

	A	B	C	D	E	F	G	H	I	J	K	L	M	N	O	P	Q	R
1	Net Area Ratio, a_n =																	
2	Ground Watertable, GWT =	9.8	ft	3.00	m													
3	Depth	Depth	q_c	q_c	q_t - given	q_t - given	q_t - calculated	q_t - calculated	f_s - given	f_s	u_2 - measured	u_2 - measured	u_1 - measured	u_1 - measured	u_0	u_0	V_s	V_s
4	(ft)	(m)	(ksf)	(MPa)	(ksf)	(MPa)	(ksf)	(MPa)	(psf)	(kPa)	(ksf)	(MPa)	(ksf)	(MPa)	(psf)	(MPa)	(ft/s)	(m/s)
5																		
6	0.16	0.05			4.87	0.23			20.89	1.00	0.75	0.04			0.00	0.000	393.06	119.80
7	0.33	0.10			5.07	0.24			20.89	1.00	0.76	0.04			0.00	0.000	393.06	119.80
8	0.49	0.15			5.16	0.25			20.89	1.00	0.78	0.04			0.00	0.000	393.06	119.80
9	0.66	0.20			5.58	0.27			28.61	1.37	0.81	0.04			0.00	0.000	393.06	119.80
10	0.82	0.25			13.97	0.67			36.83	1.76	0.89	0.04			0.00	0.000	393.06	119.80
11	0.98	0.30			21.22	1.02			44.38	2.13	0.90	0.04			0.00	0.000	393.06	119.80
12	1.15	0.35			29.79	1.43			66.67	3.19	0.84	0.04			0.00	0.000	393.06	119.80
13	1.31	0.40			44.44	2.13			106.19	5.08	0.80	0.04			0.00	0.000	393.06	119.80
14	1.48	0.45			61.88	2.96			167.08	8.00	0.75	0.04			0.00	0.000	393.06	119.80
15	1.64	0.50			82.53	3.95			232.79	11.15	0.72	0.03			0.00	0.000	393.06	119.80
16	1.80	0.55			104.20	4.99			312.64	14.97	0.68	0.03			0.00	0.000	393.06	119.80
17	1.97	0.60			126.60	6.06			392.49	18.79	0.62	0.03			0.00	0.000	393.06	119.80
18	2.13	0.65			149.27	7.15			472.01	22.60	0.57	0.03			0.00	0.000	393.06	119.80
19	2.30	0.70			172.42	8.26			558.12	26.72	0.52	0.03			0.00	0.000	393.06	119.80
20	2.46	0.75			195.76	9.37			653.55	31.29	0.47	0.02			0.00	0.000	393.06	119.80
21	2.62	0.80			219.00	10.49			753.64	36.08	0.41	0.02			0.00	0.000	393.06	119.80
22	2.79	0.85			241.76	11.58			852.13	40.80	0.33	0.02			0.00	0.000	393.06	119.80
23	2.95	0.90			257.36	12.32			948.04	45.39	0.21	0.01			0.00	0.000	393.06	119.80
24	3.12	0.95			272.48	13.05			1040.58	49.82	0.14	0.01			0.00	0.000	393.06	119.80
25	3.28	1.00			285.02	13.65			1115.44	53.41	0.14	0.01			0.00	0.000	393.06	119.80
26	3.45	1.05			292.47	14.00			1167.34	55.89	0.12	0.01			0.00	0.000	393.06	119.80
27	3.61	1.10			296.03	14.17			1195.93	57.26	0.12	0.01			0.00	0.000	393.06	119.80
28	3.77	1.15			295.71	14.16			1213.77	58.12	0.09	0.00			0.00	0.000	393.06	119.80
29	3.94	1.20			293.19	14.04			1218.75	58.35	0.08	0.00			0.00	0.000	393.06	119.80
30	4.10	1.25			289.11	13.84			1182.12	56.60	0.07	0.00			0.00	0.000	393.06	119.80
31	4.27	1.30			282.86	13.54			1144.20	54.78	0.06	0.00			0.00	0.000	393.06	119.80
32	4.43	1.35			276.54	13.24			1105.00	52.91	0.05	0.00			0.00	0.000	393.06	119.80
33	4.59	1.40			270.37	12.95			1057.93	50.65	0.04	0.00			0.00	0.000	393.06	119.80
34	4.76	1.45			264.71	12.67			1010.69	48.39	0.03	0.00			0.00	0.000	393.06	119.80
35	4.92	1.50			259.29	12.41			957.36	45.84	0.02	0.00			0.00	0.000	393.06	119.80
36	5.09	1.55			254.15	12.17			892.93	42.75	0.02	0.00			0.00	0.000	393.06	119.80
37	5.25	1.60			249.74	11.96			831.08	39.79	0.02	0.00			0.00	0.000	393.06	119.80
38	5.41	1.65			246.09	11.78			776.94	37.20	0.01	0.00			0.00	0.000	393.06	119.80
39	5.58	1.70			242.81	11.63			742.24	35.54	0.01	0.00			0.00	0.000	393.06	119.80
40	5.74	1.75			240.28	11.50			703.36	33.68	0.02	0.00			0.00	0.000	393.06	119.80
41	5.91	1.80			237.47	11.37			669.62	32.06	0.02	0.00			0.00	0.000	393.06	119.80
42	6.07	1.85			235.43	11.27			632.67	30.29	0.02	0.00			0.00	0.000	393.06	119.80
43	6.23	1.90			233.62	11.19			638.61	30.58	0.02	0.00			0.00	0.000	393.06	119.80
44	6.40	1.95			233.14	11.16			643.91	30.83	0.03	0.00			0.00	0.000	393.06	119.80

Data Input | Postprocessing (Metric) | Plots & Graphs (Metric) | Postprocessing (Imperial) | Plots & Graphs (Imperial) | Supplementary data

Figure B.14 Sample data entry in “Data Input” sheet.

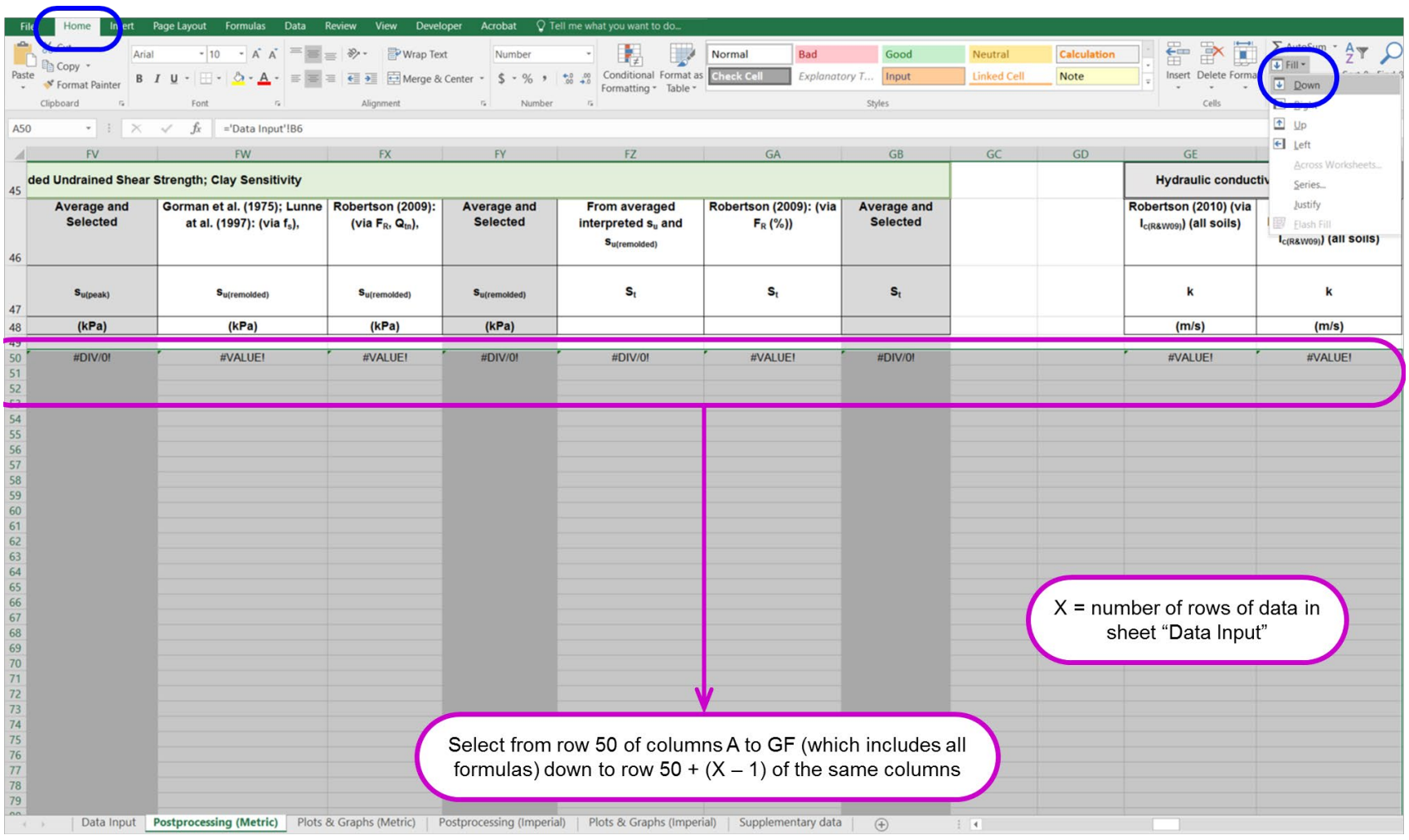

Figure B.15 Steps for reproducing the formulas for the applicable rows of the spreadsheet.

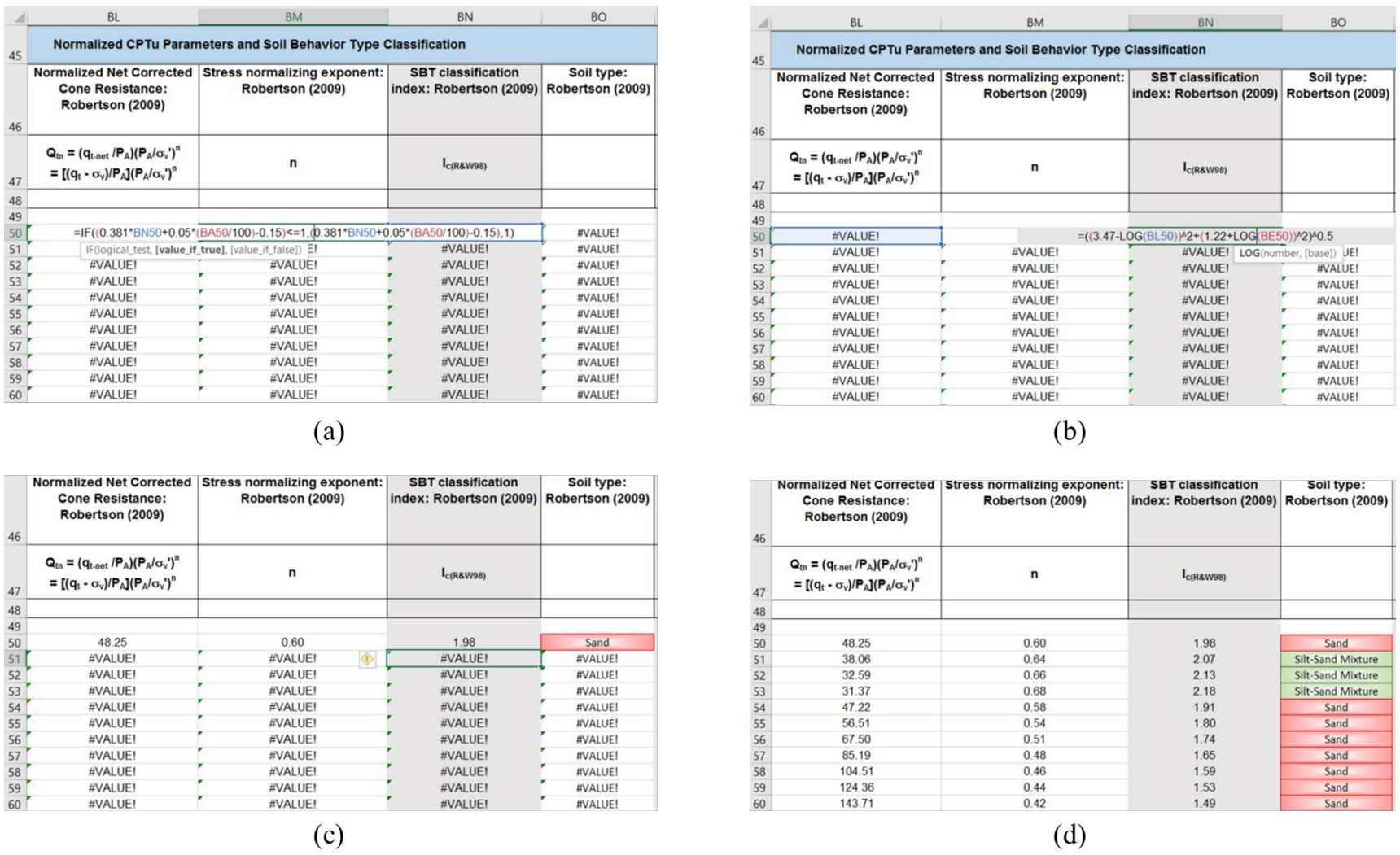

Figure B.16 Steps for generating the Robertson (2009) SBT classification in the "Postprocessing (Metric)" sheet.

Figure B.17 Sample profiles of SCPTu data.

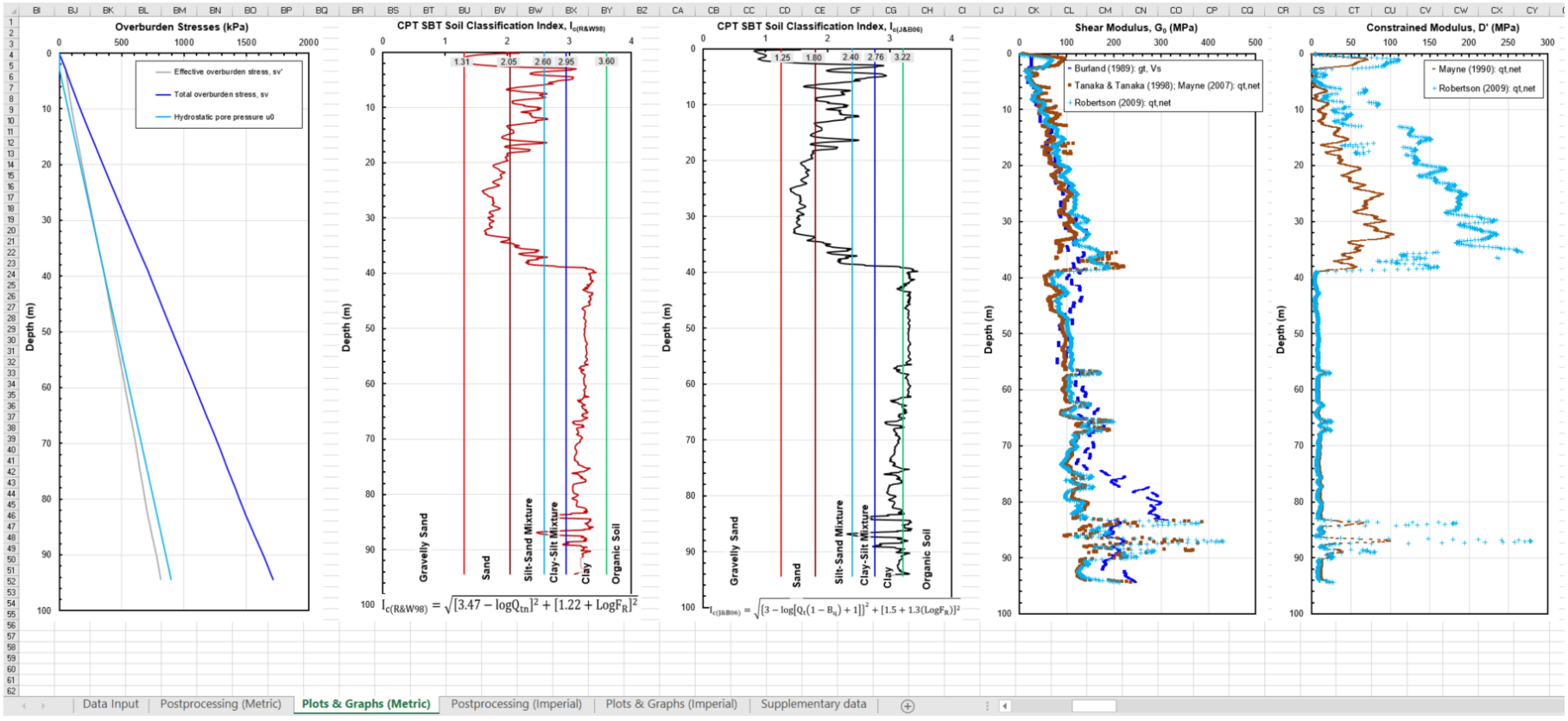

Figure B.18 Sample profiles of soil variables and parameters.

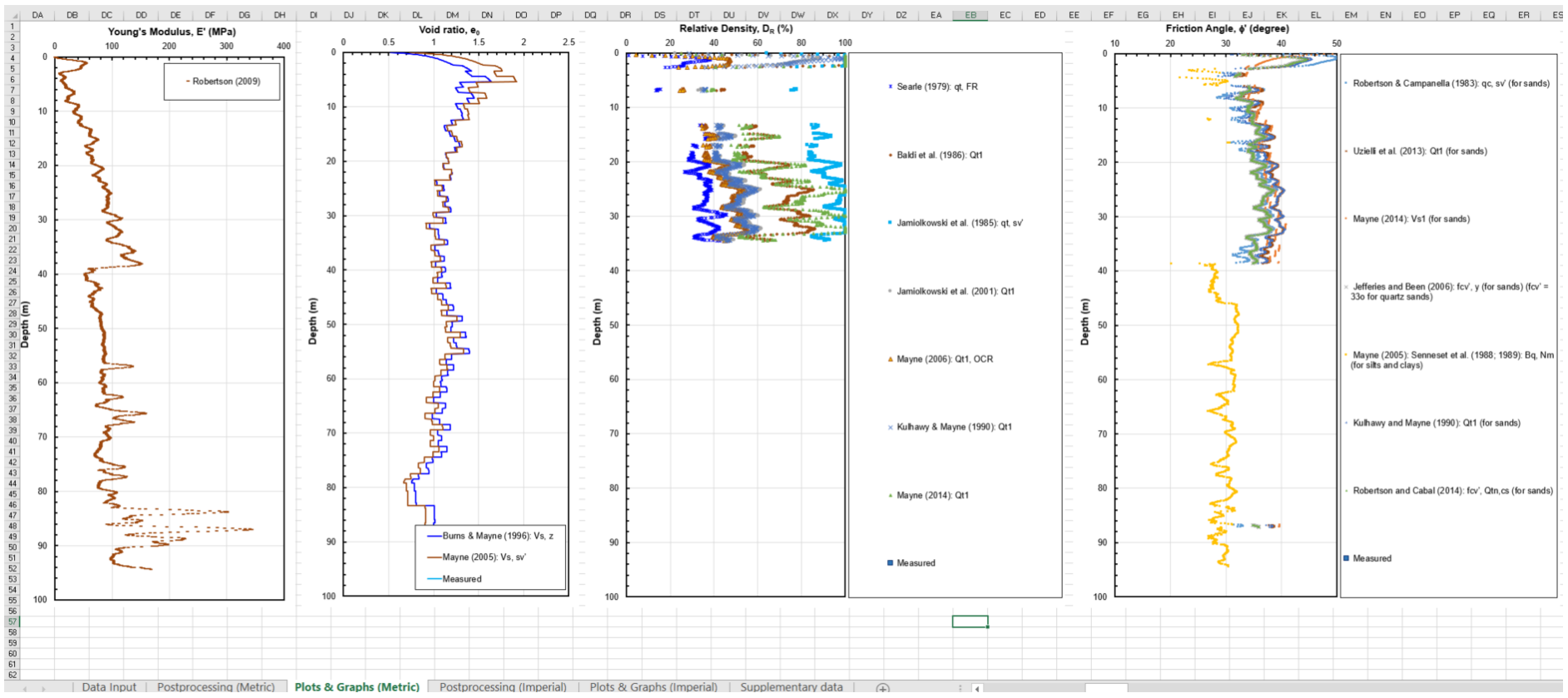

Figure B.19 Sample profiles of soil variables and parameters.

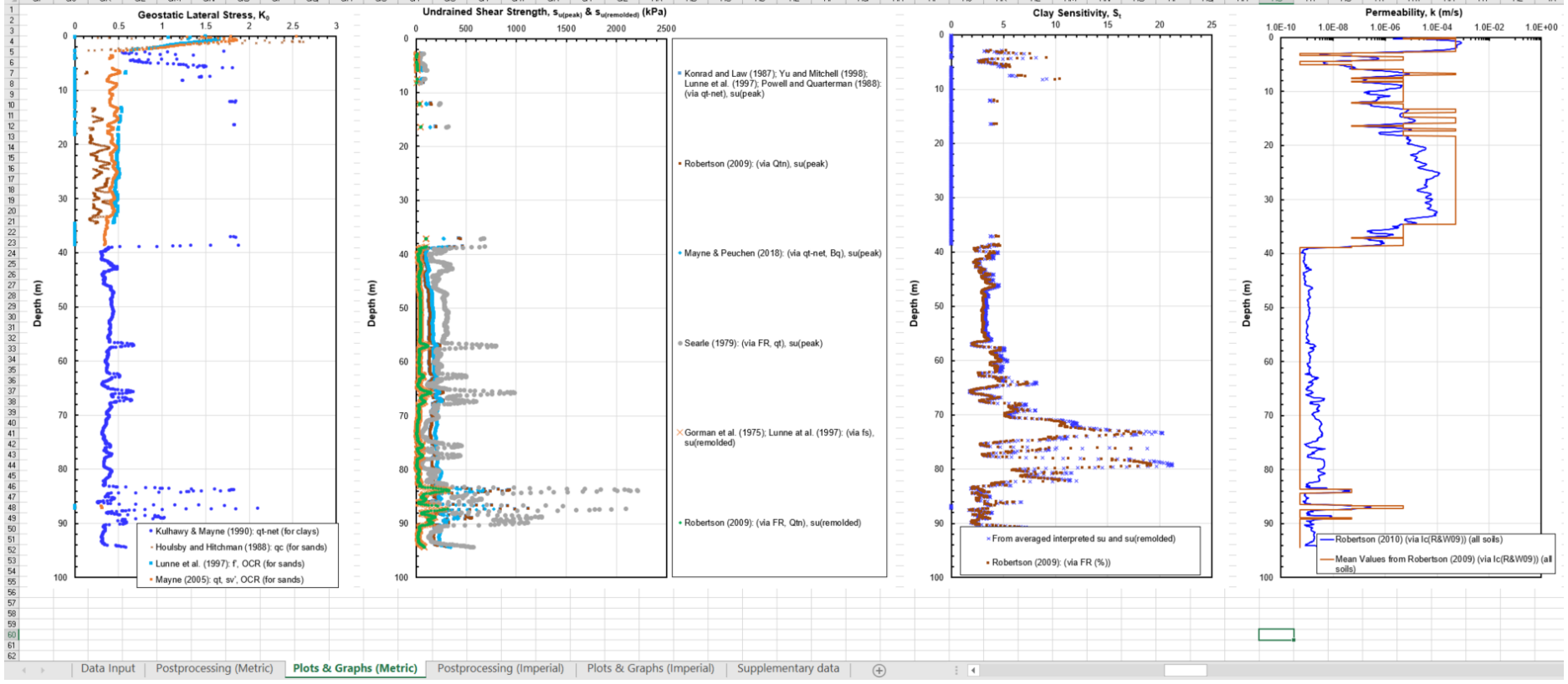

Figure B.20 Sample profiles of soil variables and parameters.

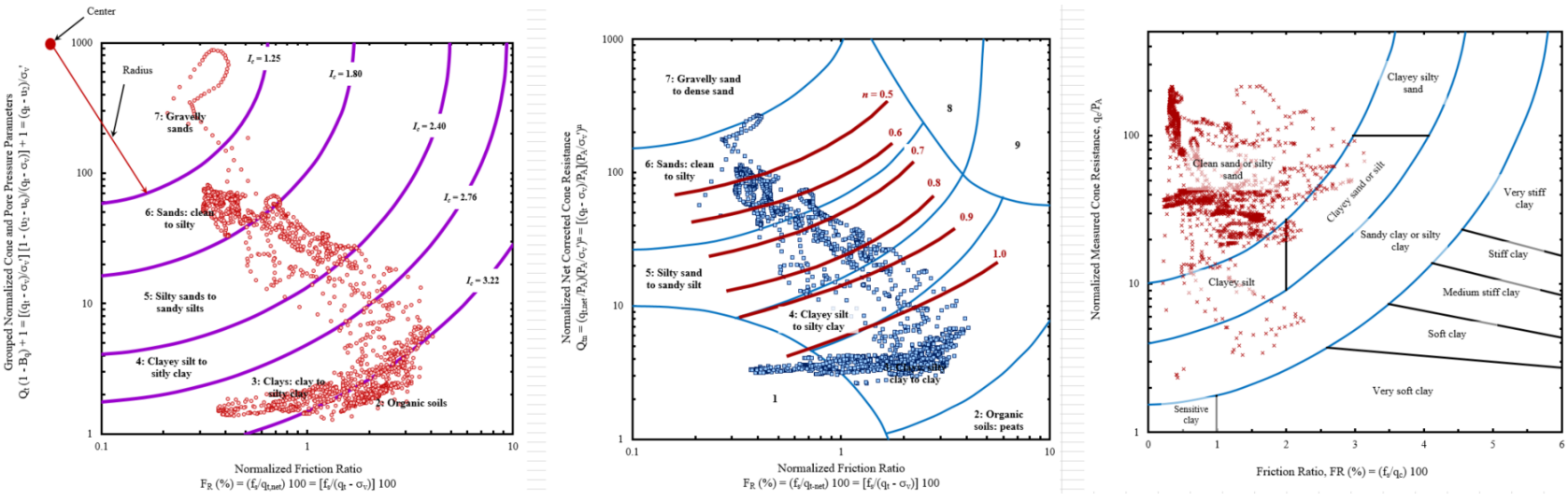

Figure B.21 Sample profiles of soil variables and parameter.

About the Joint Transportation Research Program (JTRP)

On March 11, 1937, the Indiana Legislature passed an act which authorized the Indiana State Highway Commission to cooperate with and assist Purdue University in developing the best methods of improving and maintaining the highways of the state and the respective counties thereof. That collaborative effort was called the Joint Highway Research Project (JHRP). In 1997 the collaborative venture was renamed as the Joint Transportation Research Program (JTRP) to reflect the state and national efforts to integrate the management and operation of various transportation modes.

The first studies of JHRP were concerned with Test Road No. 1—evaluation of the weathering characteristics of stabilized materials. After World War II, the JHRP program grew substantially and was regularly producing technical reports. Over 1,600 technical reports are now available, published as part of the JHRP and subsequently JTRP collaborative venture between Purdue University and what is now the Indiana Department of Transportation.

Free online access to all reports is provided through a unique collaboration between JTRP and Purdue Libraries. These are available at http://docs.lib.purdue.edu/jtrp.

Further information about JTRP and its current research program is available at http://www.purdue.edu/jtrp.

About This Report

An open access version of this publication is available online. See the URL in the citation below.

Niazi, F. (2021). *CPT-based geotechnical design manual, Volume 1: CPT interpretation—Estimation of soil properties* (Joint Transportation Research Program Publication No. FHWA/IN/JTRP-2021/22). West Lafayette, IN: Purdue University. https://doi.org/10.5703/1288284317346